Modelling the Viability of Heat Recovery from Underground Pipes

Deterministic modelling of wastewater temperatures in a 3000 sewer pipe network

Mohamad ABDEL-AAL

Submitted for the Degree of

Doctor of Philosophy

Faculty of Engineering and Informatics

University of Bradford

2015

Abstract

Mohamad Abdel-Aal

Modelling the Viability of Heat Recovery from Underground Pipes

Deterministic modelling of wastewater temperatures in a 3000 sewer pipe network

Keywords: Wastewater temperature, heat recovery, numerical modelling, heat transfer in sewer.

Modelling wastewater temperature variations in a network of 3048 sewer pipes was achieved in this project. Recovering heat from sewers presents attractive options for producing clean energy. However, heat recovery from sewerage may result in wastewater temperature drops which may reduce the influent temperature at the wastewater treatment plant (WWTP). This drop in the WWTP influent temperature may result in the degradation of the biological treatment stage. Therefore, it is vital to predict the impact of recovering heat from sewers on the wastewater temperature. Sewer temperatures along with hydraulic data were measured for up to a year in four different Belgian sites. The measured data was utilised to calibrate a deterministic sewer pipe model that estimates the wastewater temperature variation along the sewer pipe profiles. The latter model was calibrated using data from two sites and then validated using independent data from the other two sites. The sewer pipe model was then further developed to model wastewater temperature variations in a large (3048 pipe) network. The large network model was tested by implementing three different heat recovery scenarios. It was observed that 9 MW may be recovered from the 3048 pipe network, serving a catchment with a population equivalent of 79500 inhabitants, without impacting negatively on the biological processes.

Acknowledgements

All praise and gratitude are due to God ‘Allah’ who made seeking knowledge an act of worship by saying: ‘Read in the name of your Lord, Who created. Created man from a blood clot’ The Quran 96:1-2, for giving me the health and ability to carry out this project.

I would like to thank my principal supervisor Dr Mostafa Mohamed for his continuous help, support and guidance. Special thanks are also due to Prof Simon Tait and to Dr Alma Schellart for their valuable contributions in supervising this project while at Bradford and after they left to Sheffield.

Thanks are also due to the EU Interreg IVB for funding this INNERS project, and to Riet Smits and Dr Kris De Gussem from Aquafin, Belgium for sharing essential data.

I would like also to thank all the lab technicians, in particular Ian Mackay for his dedication and continuous support. Thanks also to my colleagues at Bradford: Alex Ali, Omar Kezza and Ali El-Sheikh for their help with the lab work, to Maxence Carrel from ETH Zurich for his contribution to this project and for translating relevant German text, and to Sara Cipolla from the University of Bologna for her assistance and cooperation.

Thanks to Rob Hillier and David Atkins from ICE Energy who carried out field work which is not included in this thesis.

Thanks to Suliman, Muhammed, Abdelhameeds, Muneer and Mahmood for making our office a pleasant environment to work in.

I would like to thank John McLellan for sharing great bike rides during the writing up of this thesis.

I dedicate this PhD to those who showed true examples of perseverance and resilience around the world, to those who fought and are still fighting for their freedom, to the free Palestinians, Syrians, Libyans and to the Egyptians of R4bia square.

To my dear parents.

To my brothers and sisters.

To Zayd, Yusuf, Safa, Ibrahim and Omar.

Table of Contents

List of Figures

Glossary

Symbol	Explanation	Units
A	Contact surface area	m^2
b	Wastewater free surface width	m
c_p	Specific heat capacity	J/kg.K
D_i	Internal pipe diameter	m
dr	change in radius	m
d_s	Soil penetration depth (Figure 3.6)	m
dT	Change in temperature	K
dt	Change in computational time step	s
dx	Change in the horizontal direction	m
dy	Change in the vertical direction	m
E	Energy	Watts
f_{hwa}	Heat transfer coefficient factor (page 85)	-
h	Convective heat transfer coefficient	$W/m^2.K$
i, i+1, ..	Indicates time step 1, 2 and so on	-
j	Data point number	-
k	Thermal conductivity	W/m.K
K	Kelvin	-
L	Length	m
m, m+1, ..	Location of the measured point on the horizontal axis where m is the first point followed by m+1 and so on	-
$\dot{m}$	Mass flow rate	kg/s
N	Total number of time steps (or data points) in the month	-
N	Number of increments in a sewer pipe	
P	Pipe	-
PDF	Probability Density Function	-
Q	Heat transfer rate	W
q'	Heat transfer per unit length	W/m
Q	Volumetric flow rate	m^3/s
R	Thermal resistivity	m.K/W
r_i and r_o	Inner and outer pipe radii respectively	m
RMSE	Root Mean Squared Error of modelled wastewater temperature at the downstream end of a sewer pipe, given by Equation 5.1	°C
$R_{pipe\text{-}fluid}$	Thermal resistivity between inner pipe wall and fluid in the pipe	m.K/W

$R_{pipe-pipe}$	Thermal resistivity of the pipe wall	m.K/W
$R_{soil-pipe}$	Thermal resistivity between soil and outer pipe wall	m.K/W
R_{total}	Total thermal resistivity	m.K/W
R_{wa}	Thermal resistivity between wastewater and in-sewer air	m.K/W
R_{ws}	Thermal resistivity between wastewater and soil incorporating the effects of pipe wall	m.K/W
T	Temperature	K
T_1	Temperature of a relatively hot surface	K
T_2	Temperature of a relatively cold surface	K
T_∞	Temperatures of the free stream fluid	K
T_m	Mean fluid temperature	K
T	Thickness	m
T_s	Temperatures of the bounded surface	K
u_a	In-sewer air velocity	m/s
u_w	Wastewater velocity	m/s
V	Location of the measured point in the vertical axis	-
wet.p	Wetted perimeter	m
Wp	Wastewater and pipe	-
Ws	Wastewater and soil	-
Wa	Wastewater and in-sewer air	-
WWTP	Wastewater treatment plant	-
ΔL	Increment size of a sewer pipe length	m
ΔT	Difference between modelled and measured wastewater temperatures at downstream ends	°C
$\overline{\Delta T}$	Monthly average difference between modelled and measured wastewater temperatures at downstream ends	°C
A	Thermal diffusivity	m^2/s
ρ	Density	kg/m^3
σ	Population standard deviation for the difference between measured and modelled wastewater temperatures at downstream end of pipes.	°C

1 Introduction

The increasing demand on energy consumption along with tighter EU regulations regarding carbon emissions have boosted the desire for producing energy from alternative low carbon sources to that generated from traditional sources. For example, the UK has set targets to reduce greenhouse gas emissions by 80% or more, from the 1990 baseline, by 2050 (Khan, Wilkes and Prime, 2014). Energy consumption in the UK can be divided into four sectors; transport, domestic, industrial and services. The domestic and transportation sectors are the highest energy consuming, which represented 29% and 36% respectively of the total UK energy consumption in 2013. Industrial and services sectors showed only 16% and 14% respectively while 5% was consumed in non-energy purposes (Khan, Wilkes and Prime, 2014). Despite the growth of utilising renewable energy sources in the last ten years, the majority of UK electricity sources still come from oil, natural gas, coal, and nuclear, while renewable sources, such as wind and hydropower, represent an insignificant part of it (MacLeay, Harris and Annut, 2014). This is also the case for energy consumption in the domestic sector where only 1% of it comes from renewables (Kelly and Thomson, 2012). Most of the domestic energy is consumed on space heating (around 60%) compared with hot water (18%), lighting and appliances (18%), and cooking (3%). Despite the significant improvement in thermal insulation techniques and boiler efficiencies in recent years, the increase in comfort level has caused demands on space heating to remain almost the same to that in the 1970s. For example, average room temperature, which may be considered as a measure for comfort level, has increased from 13.7 to 17.6°C from the 1970s until now (Kelly and Thomson, 2012). One can realise the wish for utilising low carbon emission technologies in order to meet the increasing energy demands while reducing carbon emissions. The high energy consumed in the domestic sector makes it an attractive sector to consider the implementation of alternative technologies to that used for generating energy. It is clear that domestic heating, for hot water and space, has the highest demands and therefore, generating heat by utilising a more sustainable technique, than the conventional methods, is needed. Sustainability in this context refers to low or zero carbon emission. The market for sustainable technologies that are capable of generating heat is vast. Some are applicable to large scale needs, such as combined heat and power system (CHP), while others

may be implemented at small scales such as heat pumps and solar. For the domestic sector, the small scale is more relevant and practical to install. Hence, it is considered in this work. Solar thermal energy is usually used for heating water or for space heating. However, high number of sunshine hours is essential for effective solar thermal technologies whereas a country such as the UK, with around 1400 sunshine hours a year (Met Office, 2014), does not promise a great potential of effective solar thermal energy compared to other places such as southern Egypt and Arizona, USA where sunshine hours reach circa 4000 a year (Osborn, 2014).

Heat pumps extract heat from ground, water or air to heat space and water in a building. Air source heat pumps are usually less efficient than that of ground and water sources, due to less thermal energy in air, as shown by Lohani and Schmidt (2010). A common type of heat pumps is the ground source heat pumps (GSHP) which contain two major parts; the heat pump loop, which is buried underground to collect heat, and the heat pump, which transmits the collected heat to radiators and hot water tank. The heat pump has a similar size to that of a fridge and comprises of an evaporator which contains a refrigerant, a compressor and a condenser. The heat pump loop extracts heat from ground which usually has a higher temperature than that of the ambient air during winter. This heat is then exchanged with the refrigerant in the evaporator and hence, the refrigerant is boiled and converted into a gas. The refrigerant gas is then compressed by the compressor to increase its temperature. Consequently, the compressed gas is then moved to the condenser to exchange heat with the heating distribution system, which transfers the heat to the radiators and hot water system.

Water can also be utilised, instead of the ground, as a heat source where the heat pump loop is replaced by a heat exchanger that is immersed in a lake, pond or wastewater running in sewers. Heat extracted from water is then processed and transformed in a similar manner to that of a ground source heat pump. Temperatures of wastewater are relatively high and were measured by previous studies, in Europe, to reach 22°C (Schilperoort and Clemens, 2009, Abdel-Aal *et al.*, 2014 and Cipolla and Maglionico, 2014), while Hoes *et al.* (2009) found measured in-sewer sewage temperatures to reach 27°C. Hence wastewater may prove to be a viable source of thermal energy. Furthermore, the technology is mature (Schmid, 2008), and there is a great potential of heat recovery from

sewers in European countries. For example, Hanspeter (2008) predicted the Swiss sewerage system has the potential to deliver up to 2 TWh of thermal energy a year. Water is a high energy intensive industry, yet more than 93% of this energy comes from non-renewable sources (Howe, 2009). Therefore, recovering heat from sewerage may prove to be an attractive opportunity for the water industry, to contribute to carbon emission reduction. Energy in the urban water cycle is consumed in different areas that include pumping, treatment and heating for domestic and other usage. In order to estimate the impact of recovering heat on energy usage and carbon emissions in the urban water cycle, an energy balance assessment tool (EBAT) was developed using data from literature and water sectors. The EBAT accounts for energy consumption in the urban water cycle to include abstraction, transportation, water and wastewater treatment, and heating water for domestic usage. According to EBAT, it was found that 94% of energy consumed in the urban water cycle, of a 250,000 UK households catchment, is for heating domestic water.

Although recovering heat from sewers appears to be an attractive option, for reducing carbon emissions, some challenges may appear as barriers to implement this technology. Recovering heat from sewers can impact negatively on the biological process of treating wastewater as shown by Wanner *et al.* (2005) and De Gussem (2013). Recovering heat from sewers may be achieved while overcoming the challenges described above. However, it is imperative to investigate the viability of implementing the technology beforehand, i.e. at the planning stage. Viability is measured by estimating the impact of heat recovery in sewers on the wastewater temperature in the sewer pipes and in the wastewater treatment plant (WWTP) influent.

Therefore the aim and objectives of this study are to;

Aim:

Demonstrate, using computational techniques, the viability of heat recovery from a sewer network.

Objectives

1. Understand the mechanism of heat transfer in sewer pipes.
2. Identify key factors that can be used to investigate the technical viability of recovering heat from sewer pipes.
3. Collect field data related to heat transfer process at catchment scales (e.g. temperatures and hydraulic data) and analyse it to better understand the heat transfer processes in sewer pipes.
4. Develop a deterministic sewer pipe model to estimate the identified factors, mentioned in objective 2, e.g. wastewater temperature, in sewer pipes.
5. Utilise collected data, mentioned in objective 3, to calibrate the developed sewer pipe model.
6. Utilise collected data, mentioned in objective 3, to validate the developed sewer pipe model.
7. Further develop the validated sewer pipe model to model wastewater temperature variation in a sewer network.
8. Present heat recovery scenarios in a real large network and investigate the technical viability of heat recovery from these scenarios.

2 Literature Review

In order to achieve the objectives mentioned in Chapter 1, the literature in the field of modelling wastewater temperature was reviewed in this chapter (Section 2.1). This chapter also discusses previous works and research accomplished in the area of modelling heat transfer in underground pipes (Section 2.2). Critical findings of the literature review are explained in Section 2.3.

2.1 Modelling Wastewater Temperature in the Water Sector

The importance of temperature modelling lies in the fact that biological processes in wastewater treatment are temperature dependent Shammas (1986), Metcalf and Eddy (2004) and Wanner *et al.* (2005), and therefore, estimating lagoon temperatures is crucial for modelling a biological process especially in a temperature changing environment. Modelling the temperature of wastewater at the combined sewer system would ideally consider the effect of wastewater temperatures at the source (rainfall and infiltration) and heat exchanged between soil and sewers (Peters, 2007). Since measuring temperatures at the above sources is usually unfeasible, simpler modelling techniques were implemented by some authors.

Escalas-Cañellas *et al.* (2008) built and calibrated statistical, time series and linear regression, models to estimate the influent temperature of a primary facultative aerated lagoon in a WWTP. Measurement of the influent temperature was achieved by immersing a thermistor 2m deep in the wastewater for 10.5 months with a time step of 8 hours. Escalas-Cañellas *et al.* (2008) model was calibrated with a first of four in-series lagoons used to treat 24,400 m^3/d of combined sewer wastewater. Water supply temperature was excluded when modelling influent temperature as it was assumed that water supply in the modelled area is 100-350m deep and had a stable temperature (Escalas-Cañellas *et al.*, 2008). The latter authors considered ambient temperatures of the same day as well as the few previous days in their model, claiming that ambient temperature does not immediately influence wastewater temperature. The authors have also disregarded ground, water supply and wastewater temperature influences on heat capacity, which slows the variation of wastewater temperature, as it is difficult to express time delay attributed to soil heat capacity.

Instead, wastewater temperature was considered to be mostly influenced by ground temperature due to the continuous contact between sewers and ground

(Escalas-Cañellas *et al.*, 2008). Rainfall can also influence wastewater temperature by mixing with sewage and hence, modelled wastewater temperature is dependent on rainfall of the current day and few previous days. Therefore, Escalas-Cañellas' model relates the amount of rainfall and ambient temperature to the lagoon influent temperature by relying on externally generated inputs. Application of Escalas-Cañellas' model can be used to estimate lagoon and activated sludge influent temperatures which can help with critically evaluating a temperature-dependent biological wastewater treatment process such as nitrification. However, the model should be calibrated locally, as it is site specific, and the initial influent temperature should be known. To eliminate any uncertainties associated with the estimated influent temperature, it is recommended that Escalas-Cañellas' model starts calculations sixty days before targeted period.

2.2 Modelling Heat Transfer in Underground Pipes

Thermal energy in sewers shows a great potential for a clean energy source. Hoes *et al.* (2009) reported sewage having temperatures of up to 27°C in combined sewer system in the Netherlands. Heat, produced from wastewater with temperatures of up to 25°C, has been recovered in some European countries such as Switzerland at scales that ranged from 10kW to few Megawatts (Schmid, 2008). Annual potential of 2TWh was estimated by Hanspeter (2008) to be recovered from Swiss sewers. It was estimated that extracting heat from sewer pipes, with circulating low temperature coolant (e.g. -5°C), delivered by heat pumps results in reducing households thermal energy consumption by 10% and 23% compared with boilers and oil-fired heaters respectively. This was the reason behind several hundred wastewater heat pumps being utilised for more than two decades around the world (Schmid, 2008). However, heat recovery from sewers may result in a large wastewater temperature drop that can impact negatively on the wastewater treatment processes. Therefore, it is crucial to estimate the wastewater temperature variation when heat is recovered from sewers.

Predicting the potential of recovering heat from sewers depends on the phenomena of heat transfer between wastewater and in-sewer air and between the sewer pipe wall material and the surrounding soil. Available published literature in the field of heat transfer modelling in sewers is limited to only a small number of studies such as Dürrenmatt (2006), Dürrenmatt and Wanner (2008 & 2014). The latter authors modelled the longitudinal spatial profile of the wastewater temperature in sewer pipes and developed a code named TEMPEST. Temperature of wastewater in sewer pipes is expected to vary along the pipeline axis due to the heat transfer between wastewater and soil, through convection with the pipe wall, and between wastewater and in-sewer air. Dürrenmatt and Wanner (2008 & 2014) have incorporated these heat transfer phenomena, based on the principles of energy balance, which results in a temperature variation along the sewer pipe profile. Their model (TEMPEST) incorporated the interaction between wastewater, in-sewer air and the surrounding soil by considering mass balance equations, rate expressions of heat transfer and a new empirical model of the heat transfer between the wastewater and the in-sewer air. Figure 2.1 shows a cross section of the sewer pipe and the heat transfer processes that were simulated in the study by Dürrenmatt and Wanner (2008).

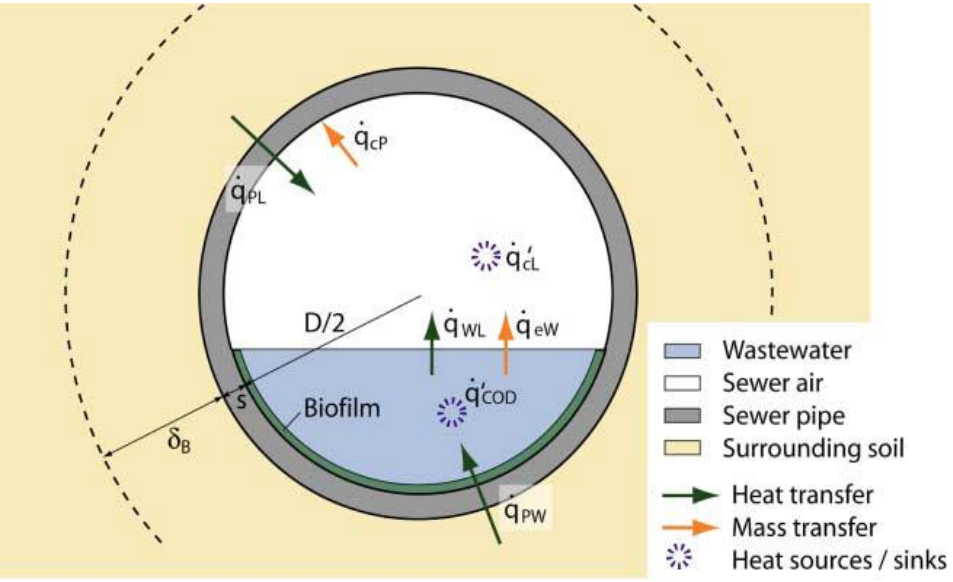

Figure 2.1: Cross-section of a sewer pipe and heat transfer processes as modelled in TEMPEST, $\dot{q}$ is heat transfer rate between; soil and in-sewer air (PL), wastewater and in-sewer air (WL), and soil and wastewater (PW), and mass transfer rate between; in-sewer air and pipe wall (cP), and wastewater and in-sewer air. $\dot{q}_{cL}$ and $\dot{q}_{COD}$ show energy generated in air and by chemical Oxygen demand (COD) respectively. D is pipe diameter, s is pipe thickness and δ_s is penetration depth. Source: Dürrenmatt and Wanner (2008).

The TEMPEST model incorporated several heat transfer processes, and divided the simulated sewers into conduits and nodes to include the effects of different soil and pipe wall characteristics on temperature, wastewater velocity and wastewater depth along the sewer line. The TEMPEST model is a complex one due to the large number of input parameters, such as pipe length and diameter, wall thickness, sewer slope, friction coefficient, Chemical Oxygen Demand (COD) degradation rate, and ambient temperature, that have insignificant effects (less than 0.2%) on the modelled sewer temperature (Dürrenmatt, 2006). Dürrenmatt and Wanner (2014) have calibrated and validated the TMEPEST model on different datasets using data measured over a two day period in March. The overall root mean square error (RMSE) between measured and modelled temperatures was 0.14 and 0.20 °C for calibrated and validated models respectively. Heat transfer in sewers is complicated as the hydraulics of the wastewater in sewer pipes change continuously depending on a number of factors such as stormwater, infiltration rate through sewer pipes and daily water consumption of local residents. Furthermore, thermal convection taking place between wastewater and in-sewer air relies on heat transfer coefficients that

require extensive laboratory work to determine. Hence, little literature was published in the field of heat transfer between wastewater and in-sewer air.

A similar concept to modelling heat transfer in sewers, yet more common, is the ground source heat pump loop (HPL). Unlike the sewer pipes, the HPL consists of fully filled pipes with much smaller diameters. Modelling the heat transfer between HPL and the surrounding soil has been examined by a number of authors such as Piechowski (1998), Esen, Inalli and Esen (2007), Demir, Koyun and Temir (2009), Ngo and Lai (2009), Wu *et al.* (2010) and Mohamed *et al.* (2015). All the models developed by the latter authors were based on the principles of energy balance. Piechowski (1998 & 1999) implemented finite difference (FD) methods, to model theoretical heat and mass transfer between HPL and soil, and consequently estimated the circulating fluid temperature at the outlet. Esen, Inalli and Esen (2007) compared their numerical FD approximation model with experimental results for temperature distribution around the HPL. Assuming constant physical conditions, such as fixed water content in soil around the HPL and uniform ground properties, Esen, Inalli and Esen (2007) have proven a strong correlation between their modelled and experimental data, with a maximum difference of around 1.5 °C (9.4%) in ground temperature between their numerical results and experimental observations. Transient models were developed by some authors such as Esen, Inalli and Esen (2007), Ngo and Lai (2009) and Wu *et al.* (2010). Demir, Koyun and Temir (2009) have validated their numerical model by experimental measurements of ground temperature. The latter authors used an FD method and showed a maximum soil temperature variation between modelled and measured, within 2m horizontal and vertical distances from pipe, of 10%. Esen,Inalli and Esen (2007) and Demir, Koyun and Temir (2009) have neglected the thickness of the HPL when modelling heat transfer between coolant and soil and hence, assumed only conduction was transferring the heat between the soil and coolant. The steady state model developed by Mohamed *et al.* (2015), and validated through experimental work presented a difference of 0.7°C (7.6%) between modelled and measured coolant temperature at the HPL outlet.

2.3 Literature Review Outcomes

The literature has clearly indicated that apart from the model designed by Dürrenmatt and Wanner (2008) and implemented in Dürrenmatt and Wanner (2014) work, no other published models incorporated air in partially filled sewer pipes to estimate wastewater temperature variation along the sewer pipe profiles. The TEMPEST model was calibrated and validated in published literature for only a two day period in February and March respectively. Hence, the model has not shown the behaviour of heat transfer in sewers during other seasons. Moreover, the TEMPEST model is over parameterised which makes it impractical to be implemented as an assessment tool for potential heat recovery from large sewer networks. Hence, there is a gap in developing a computationally efficient model that can estimate the wastewater temperature variations in large sewer networks. Although the model of Escalas-Cañellas *et al.* (2008) can be utilised for some applications such as estimating lagoon and activated sludge influent temperatures to evaluate some wastewater treatment processes such as nitrification, their model needs to be calibrated locally since it is site specific. In an attempt to eliminate any uncertainties associated with the estimated influent temperature, it is recommended that Escalas-Cañellas' model starts calculations sixty days before targeted period. Both local site calibration and the start of modelling two months in advance can clearly cause impracticality for many wastewater utilities, from a logistical as well as economy point of view. Furthermore, other input parameters, required by Escalas-Cañellas' model such as gas-phase coefficient and the overall vapour pressure driving force, may not be easily available to wastewater utilities.

Principles of energy balance were implemented when modelling heat transfer in heat pump loop (HPL), in sewer pipes and in other areas in the water industry mentioned in this chapter. Therefore, and since the process of heat transfer in sewers is a complex one, the same principle (energy balance), will be implemented in this project. The most similar heat transfer models, which are common in published literature, to that of sewer pipes is the heat transfer models for fully filled pipes (e.g. HPL). Therefore, it is necessary to understand the modelling methods implemented in fully filled pipes (e.g. HPL) and adapt that to meet the demands of modelling heat transfer in sewer pipes. This would ultimately enable the modelling of wastewater temperature variation along sewer

pipe profiles. Numerical modelling allows for integrating more complexities to the system, such as the parameters associated with heat transfer in partially filled pipes. Therefore, numerical methods will be considered for estimating the wastewater temperature variation in sewers.

Conduction alone was assumed to take place when modelling heat transfer, from HPL radially and vertically in soil, by authors such as Esen, Inalli and Esen, (2007) and Demir, Koyun and Temir (2009). However, accuracy of the latter authors' models, which varied from 5 to 10%, did not vary much with those who incorporated convection between coolant fluid and pipe surface such as Wu *et al.* (2010) who obtained model accuracy of around 10%. This finding was also confirmed by Piechowski (1999). The different assumptions made by different authors, regarding the consideration of different heat transfer processes, suggest that some processes may have insignificant impacts on the modelling accuracy and hence, these processes may be excluded. Therefore, focusing on the key heat transfer parameters that dominate the estimation of wastewater temperature variation in sewer pipes is crucial for developing a computationally efficient model capable of implementation on large sewer networks

Although Wu *et al.* (2010) implemented a 3D model using sophisticated modelling software (CFD Fluent), their model's accuracy was almost as or less accurate than simpler (2D) models developed by Demir, Koyun and Temir (2009) and Esen,Inalli and Esen (2007). Therefore, it is worth considering the implementation of simpler modelling techniques (e.g. 1D or 2D) in order to develop an efficient yet accurate model that estimates wastewater temperature variation along sewer pipe profiles. Previous authors of heat transfer modelling in sewer pipes as well as in heat pump loops agreed on basic parameters required for modelling, these are; thermal conductivity of soil (and pipe wall in case of sewers), pipe dimensions, soil temperature, thermo-physical properties of soil surrounding the pipe, fluid volumetric flow rate and temperature of the fluids running in the pipe. The range of soil thermal conductivity values, which is a key parameter in modelling heat transfer in soil, vary from 0.24 to 2.5 W/m.K and may differ from calculated values by +/- 25%, as proven by Piechowski (1998).

In order to realise the great potential, described in Chapter 1 and in this chapter, for recovering heat from sewers, it is crucial to develop a reliable heat transfer model to estimate the wastewater temperature variation in a sewer pipe and its

surroundings. This model can be further developed, in this work, to account for estimating wastewater temperature variation in large sewer networks. The ultimate aim of the sewer network model is to observe the impact of recovering heat from a large sewer network on the temperature of wastewater in sewers and the temperature of the WWTP influent. Thus, the next chapter explains how modelling the wastewater temperature variation in sewer networks can be developed.

3 Method

As concluded from Chapter 2, the principles of energy balance were implemented to model heat transfer in heat pump loops (HPL) and sewer pipes. Therefore, Section 3.1 of this chapter explains the energy balance principles and describes the basics behind heat transfer processes. Section 3.2 describes different modelling techniques and methods for selecting the most appropriate technique for modelling wastewater temperature variations in large sewer networks. The most common models of heat transfer in pipes were found in literature to be that of fully filled pipes, as explained in Chapter 2. Therefore, Section 3.3 shows how the mechanism of heat transfer in fully filled pipes model can be adapted to model heat transfer in partially filled sewer pipes. This is then utilised to develop a model for heat transfer in a sewer network that can model wastewater temperature variations in large sewer networks.

3.1 Energy Balance and Basic Heat Transfer Phenomena

The first law of thermodynamics states that energy in any system is conserved, which means that the amount of energy in a system can only change if energy crosses the system's boundaries. Therefore, Equation 3.1 can be used to describe the energy stored in a closed system, i.e. a region of fixed mass.

$$E_{stored} = E_{in} - E_{out} + E_{generated} \quad (3.1)$$ (Incropera *et al.*, 2007)

E is energy, in = gained, out= lost.

Equation 3.1 can also be applied for control volume systems; where a mass passes in a region of space bounded by a control surface. The first law of thermodynamics demonstrates that heat transferred through a system boundary results in energy increase (gain) or decrease (loss). Understanding the heat transfer phenomena of conduction and convection is necessary to apply the energy balance equations and ultimately enables the modelling of fluid temperature variations in pipes.

Thermal conduction is the transfer of heat from relatively warm to relatively cold surfaces within an object or between two objects that are in contact with each other. The process is dependent on the atomic and molecular structure of the object. The rate of thermal conduction (q) is given by Equation 3.2.

$$q_{conduction} = kA\frac{dT}{dx} = kA\frac{T_2 - T_1}{t} \qquad (3.2)\ \text{(Incropera } et\ al.\text{, 2007)}$$

$q_{conduction}$= Thermal conduction rate (W), across a material with a contact surface area of A (m^2) and t thickness (m). k= thermal conductivity (W/m.K), T_2 & T_1 are temperatures of relatively hot and cold surfaces respectively (K).

Thermal convection is the heat transfer between a moving fluid and a boundary surface. The direction of heat transfer is from relatively hot to relatively cold objects. Convective heat is transferred through the random molecular and macroscopic motion of the fluid in the presence of temperature differences. In this work the focus will be on the forced convective heat transfer between a flowing fluid and a bounded surface with a different temperature. The term 'forced convection' indicates that the fluid is forced to flow by external means. Convective heat transfer is expressed by Equation 3.3.

$$q_{convection} = hA(T_s - T_\infty) \qquad (3.3)\ \text{(Incropera } et\ al.\text{, 2007)}$$

$q_{convection}$ is thermal convection rate (W), between a moving fluid and a material with a contact surface area of A (m^2), h is the convective heat transfer coefficient ($W/m^2.K$) which is dependent on fluid type and velocity, T_s & T_∞ are temperatures of the bounded surface and the fluid respectively (K).

Thermal conductivity and the convective heat transfer coefficient may be expressed by thermal resistivity. Heat transfer can then be expressed as a function of thermal resistivity as shown by Equation 3.4.

$$q = \frac{1}{R}(T_2 - T_1) \times L \qquad (3.4)\ \text{(Incropera } et\ al.\text{, 2007)}$$

q is heat transfer rate through conduction or convection (W), R is thermal resistivity (m.K/W), T_2 & T_1 are temperatures of relatively hot and relatively cold surfaces respectively and L is length (m).

The concept of thermal resistivity is similar to electrical resistance, which is a function of the electrical conductivity. In heat transfer thermal resistivity is a function of thermal conductivity and convective heat transfer coefficient in cases of conduction and convection respectively. Using Equation 3.4 and rearranging Equations 3.2 and 3.3, thermal resistivity can be expressed by Equations 3.5 and 3.6 for thermal conduction and convection respectively.

$$R_{conduction} = \frac{T_2 - T_1}{q_{conduction}} \times L = \frac{t}{kL} \quad (3.5)$$ (Incropera *et al.*, 2007)

$$R_{convection} = \frac{T_s - T_f}{q_{convection}} \times L = \frac{1}{hL} \quad (3.6)$$ (Incropera *et al.*, 2007)

q is heat transfer rate through conduction or convection (W), L is Length (m), k & h are thermal conductivity (W/m.K) and heat transfer coefficient (W/m^2.K) respectively. T_s & T_∞ are temperatures of the bounded surface and the fluid respectively (K).

Thermal conduction for a cylindrical geometry can be expressed by Equation 3.7.

$$q_{conduction} = kA\frac{dT}{dr} = 2\pi krL\frac{dT}{dr} \quad (3.7)$$ (Incropera *et al.*, 2007)

dT and dr are change in temperature and change in radius respectively while L is cylinder length.

Integrating Equation 3.7, and assuming T_2 and T_1 are temperatures of outer and inner cylinder radii respectively (i.e. the outer surface has a higher temperature than the inner surface), yields to Equation 3.8.

$$q_{conduction} = 2\pi kL\frac{T_2 - T_1}{ln(r_o/r_i)} \quad (3.8)$$

r_o & r_i are outer and inner radii respectively.

Rearranging Equation 3.8, and implementing the same principle used in Equation 3.5, to express thermal resistivity for heat transfer in a cylindrical body is shown by Equation 3.9

$$\mathrm{R_{conduction}} = \frac{\ln(\mathrm{r_o}/\mathrm{r_i})}{2\pi \mathrm{kL}} \quad (3.9)$$

Thermal energy can be advected by the mass of a moving fluid that crosses the boundaries of a closed system. Neglecting kinetic and potential energy, Equation 3.10 can be used to compute thermal energy variation for a flowing incompressible liquid with constant specific heat capacity.

$$q_{advected\ by\ mass} = \dot{m} c_p (T_{out} - T_{in}) \quad (3.10)$$ (Incropera *et al.*, 2007)

$q_{advected\ by\ mass}$ is thermal energy advected by mass (W), $\dot{m}$=mass flow rate (kg/s), c_p= specific heat capacity (J/kg.K). T_{in} & T_{out} are temperatures of the inflow and the outflow respectively (K).

3.2 Modelling Techniques

This section is dedicated to describing some of the modelling techniques that can be implemented to estimate the wastewater temperature variation in underground pipes. These techniques are mainly based on numerical methods for solving one dimensional (1D) and two dimensional (2D) problems under transient and steady state conditions. A three dimensional (3D) model is not required in this work since the ultimate aim of modelling is only to estimate fluid temperature variation along a pipe profile. Furthermore, a 3D model requires high computational time which is undesired for the main aim of this work. The finite element and finite volume methods are commonly used for irregular geometries, which is not the case in the sewer pipes. The finite element methods are also suitable for mesh refinement, yet this was proven to have insignificant impact as will be proven later in Chapter 5 (Table 5.5). Numerical methods have the advantage of adding more complicity in the system that can yield to a fair approximation to the solution. The decision-making process of selecting the most appropriate modelling technique, to estimate wastewater temperature variation in a large sewer network, is explained in Section 3.2.1. The latter section ends by showing the selected modelling technique.

Complex heat transfer problems, require the consideration of the heat transferred in multi-coordinates systems. Solving multi-dimensional heat transfer problems is achieved by exact solution or approximate methods techniques. Consider a steady state system (time independent) where thermal conduction is taking place in the x and y directions of a long solid object as shown by Figure 3.1.

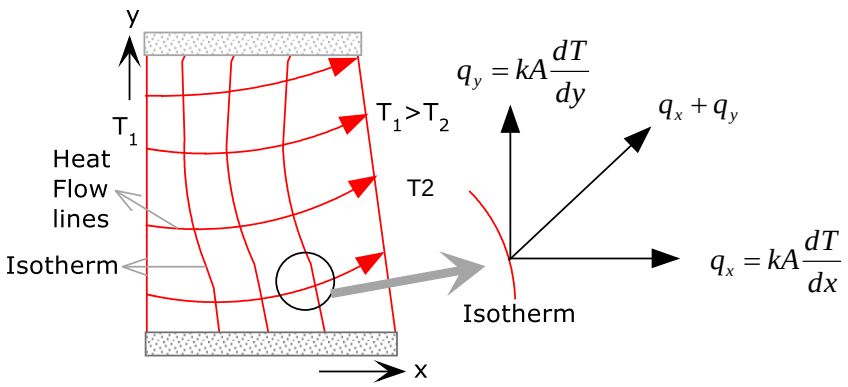

Figure 3.1: Thermal conduction in two dimensional coordinates

Assuming the two surfaces (hatched in Figure 3.1) are thermally insulated, heat is transferred from warm (T_1) to cold (T_2) sides of the solid. Heat flow lines, shown in Figure 3.1, indicate the direction at which heat is transferred. These lines, according to Fourier's law, are vectors perpendicular to lines of constant temperatures, known as therms. Values of these vectors are equal to the resultant of heat transferred in x and y directions. Equation 3.11 can be used to compute temperature variation in x and y directions for steady state conditions with no energy generated and constant thermal conductivity.

$$\frac{d^2T}{dx^2} + \frac{d^2T}{dy^2} = 0 \qquad (3.11)$$ (Incropera *et al.*, 2007)

Equation 3.11 can be solved through analytical or numerical methods. A less common technique for solving Equation 3.11 is the graphical approach which would be impractical for the applications described in this work, and hence will be avoided. The numerical method offers the ability to add more complicities in the modelling of heat transfer in sewers compared with the analytical method. Therefore, and since heat transfer in sewers is a complex process as explained in Section 2.2, the numerical method is considered for modelling heat transfer in sewer pipes.

The finite difference method is a numerical technique based on replacing the derivative of the differential equations by differences assuming that the errors are small when the differences are taken over small enough distances. This can be done by implementing the principles of energy balance. For simplification purposes and to focus on explaining the modelling techniques, consider

temperature variation in a rod, which has similar geometry to that of a pipe, as a function of length x as shown by Figure 3.2.

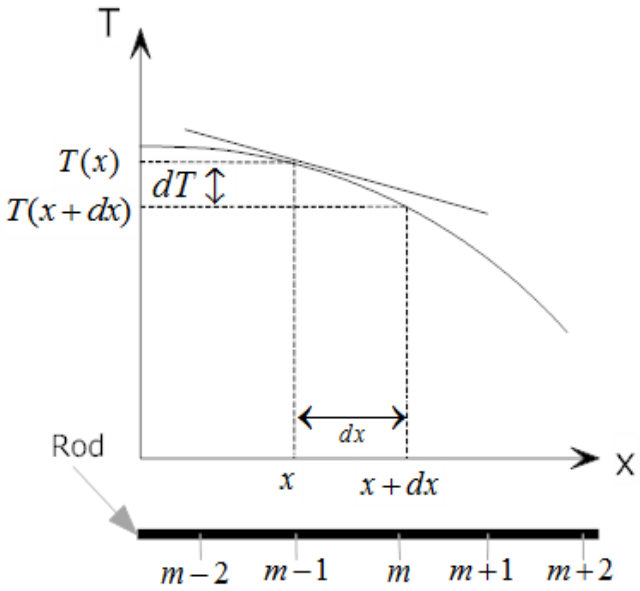

Figure 3.2: Temperature variation along a rod in one dimension.

The slope of a point in the curve of Figure 3.2 is the first derivative of T(x) which is the ratio of change in temperature (dT) to the change of length increment (dx) as presented by Equation 3.12.

$$\frac{dT}{dx} = \frac{T(x+dx)-T(x)}{dx} \tag{3.12}$$

Equation 3.12 can also be expressed in a nodal form, where nodes are points on the object distributed at equal spacing of dx, as shown in Figure 3.2. The nodal expression of the temperature variation, at two adjacent points that are midway between m and m-1 ($m-\frac{1}{2}$) and midway between m and m+1 ($m+\frac{1}{2}$), in the rod of Figure 3.2, is shown by Equations 3.13.

$$\left.\frac{dT}{dx}\right|_{m-\frac{1}{2}} = \frac{T_m - T_{m-1}}{dx}, \quad \left.\frac{dT}{dx}\right|_{m+\frac{1}{2}} = \frac{T_{m+1}-T_m}{dx} \tag{3.13}$$

One can realise that the finite difference equations, such as 3.13, are only valid at nodes. The finite difference method assumes that temperature varies linearly between nodes which is not true in cases where energy is generated in the system. Therefore, the finite difference method is considered to be an approximation technique (Cengel, 2003).

Solving a two-dimensional problem, similar to that described in Figure 3.1, can also be achieved by using the differential method. Nodes used for solving the

two-dimensional problem is shown by Figure 3.3, where m refers to nodes in the horizontal (x) direction while v represents the nodes in the vertical (y) direction.

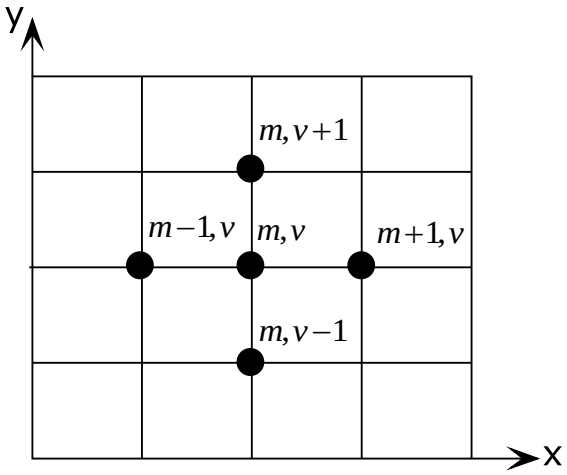

Figure 3.3: Nodes in a two-dimensional heat transfer problem described by Figure 3.1.

Equation 3.11 is the derivative of Equation 3.13 plus the second derivative of temperature variation along the y direction. Using the same techniques implemented to solve Equations 3.13, Equation 3.14 can be developed to solve the second derivative of temperature variation along the x axis of the example described by Figure 3.2.

$$\left.\frac{d^2T}{dx^2}\right|_m = \frac{\left.\frac{dT}{dx}\right|_{m+\frac{1}{2}} - \left.\frac{dT}{dx}\right|_{m-\frac{1}{2}}}{dx} = \frac{\frac{T_{m+1}-T_m}{dx} - \frac{T_m-T_{m-1}}{dx}}{dx} = \frac{T_{m+1}-2T_m+T_{m-1}}{dx^2} \qquad (3.14)$$

In a similar manner, second derivative of temperature variation with respect to the y direction, in reference to Figure 3.3, can be obtained by Equation 3.15.

$$\left.\frac{d^2T}{dy^2}\right|_n = \frac{\frac{T_{v+1}-T_v}{dy} - \frac{T_v-T_{v-1}}{dy}}{dy} = \frac{T_{v+1}-2T_v+T_{v-1}}{dy^2} \qquad (3.15)$$

Therefore, Equation 3.11 can be solved, by combining Equations 3.14 and 3.15, for the temperature at middle point (m,v) of Figure 3.3.

$$\frac{T_{m+1}-2T_m+T_{m-1}}{dx^2} + \frac{T_{v+1}-2T_v+T_{v-1}}{dy^2} = 0 \qquad (3.16)$$

Transient heat transfer can also be solved numerically using the finite difference method in a similar manner to that of steady state systems described above, yet the temperature in transient systems varies with respect to both time and spatial coordinates. Applying energy balance for one dimensional coordinate, described by Equation 3.1, and assuming no energy generation with constant thermal conductivity, Equation 3.17 may be developed.

$$\frac{dT}{dt} = \alpha \frac{d^2T}{dx^2} \qquad \text{(3.17) (Incropera } et\ al.\text{, 2007)}$$

Where α is thermal diffusivity, *dt is the change in computational time step.*

The transient system described by Equation 3.17 has an important stability criterion which is dependent on the value of Fourier number (Fo). This Fo number, shown by Equation 3.18, shall be greater than 0.5 to meet the stability criterion.

$$Fo = \frac{\alpha\ \mathrm{dt}}{\mathrm{dx}^2} \qquad \text{(3.18) (Incropera et al., 2007)}$$

A transient one dimensional heat transfer problem can be represented using nodes as shown by Figure 3.4. Variation in time of the transient heat transfer case, illustrated by Figure 3.4, is represented by i, where first time step is denoted by i, second time step is denoted by i+1 and so on.

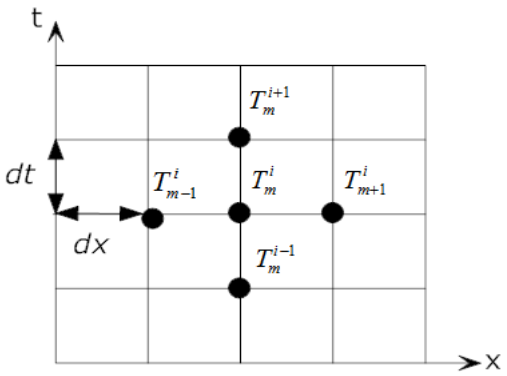

Figure 3.4: Transient temperature variation in one-dimensional system.

Referring to Figure 3.4, Equation 3.17 can be solved by explicit and implicit finite difference methods as shown by Equations 3.19 and 3.20 respectively (Ozisik, 1994).

$$\frac{T_m^{i+1} - T_m^i}{dt} = \alpha \frac{T_{m+1}^i - 2T_m^i + T_{m-1}^i}{dx^2} \qquad (3.19)$$

$$\frac{T_m^{i+1} - T_m^i}{dt} = \alpha \frac{T_{m+1}^{i+1} - 2T_m^{i+1} + T_{m-1}^{i+1}}{dx^2} \qquad (3.20)$$

Where α is thermal diffusivity.

3.2.1 Selecting the appropriate modelling technique

It is clear from the previous section that there is a variety of modelling techniques that can be implemented to estimate temperature variation in an object. This section is dedicated to select the most appropriate modelling technique for estimating wastewater temperature variation in a large sewer network.

The main criteria for assessing the suitability of a modelling technique are: the computation time, the accuracy of the model and the number of input parameters.

Computation time is considered to be the most important criterion in the modelling process. Fast computation can clearly save time, cut costs and minimise efforts to ultimately provide a computationally efficient model. This is specifically crucial for estimating wastewater temperature variation in a large sewer network with a large number of pipes. Model accuracy is the key for a reliable prediction. The purpose of this model is to estimate the impact of recovering heat on the wastewater temperature especially of that at the WWTP influent, where wastewater treatment processes are sensitive to temperature, as explained in Section 2.3. Hence, the job of the developed model is to estimate the significance of wastewater temperature drop, in sewer pipes and at the WWTP influent, as a result of a heat recovery application. This estimate of wastewater temperature drop may then be compared with the usual case where there is no heat recovery taking place in the sewer network. Therefore, modelling accuracy was weighted the second highest when deciding on selecting the appropriate modelling technique. The least number of measurable input parameters, i.e. parameters that define the boundary conditions, is required to develop a practical model. Requesting many input parameters, most of which are unlikely to be known by the model end user, may result in too many assumptions that may consequently show uncertain results. Table 3.1 shows how the three criteria mentioned above (computation time, modelling accuracy and the number of input parameters) that weighted from 1 to 3, where 3 is the most important criterion. The impact of each modelling technique (i.e. transient, steady state, 1D and 2D) on each criterion was scaled from 1 to 5, where 5 shows the most positive impact on the relevant criterion as shown by Table 3.1.

Table 3.1: Interpretation of weight and impact values used for decision making matrix shown by Table 3.2.

Value (criteria)	**Weight**	**Value (modelling techniques)**	**Impact**
3	Very important	4 to 5	Positive
2	Important	2 to 3	Average
1	Preferred	1 to 2	Negative

Table 3.2 shows the decision making matrix of selecting the appropriate modelling technique for modelling wastewater temperature variation in sewer networks. The decision matrix (Table 3.2) was developed by obtaining a score for each modelling technique. This score is the multiplication product of the weight and impact values, given by Table 3.1, on each criterion. The decision matrix shows four combinations, or options, of modelling techniques, these are: transient & 1D, transient & 2D, steady state & 2D and SS & 1D. The total score of each option is the summation of the scores obtained for each modelling technique. For example, the total score for SS and 1D combination is equal to the score of SS plus that of 1D, i.e. 24 (for SS) + 26 (for 1D) = 50.

Table 3.2: Decision matrix for selecting the most appropriate modelling technique for estimating the wastewater temperature variation in a large sewer network. SS, 1D & 2D denote for steady state, one and two dimensional respectively.

Criteria considered	**Weight**	**Transient**	**Steady state (SS)**	**2D**	**1D**
		Score = weight x impact (refer to Table 3.1)			
Computation time	3	3 x 1	3 x 5	3 x 3	3 x 5
Modelling accuracy	2	2 x 4	2 x 3	2 x 4	2 x 3
Number of input parameters	1	1 x 1	1 x 3	1 x 2	1 x 5
	Score	12	24	19	26
	Options	Transient & 1D	Transient & 2D	SS & 2D	SS & 1D
	Total score	38	31	43	50

It is clear from Table 3.2 that a steady state one dimensional model is the most appropriate since it showed the highest total score. Therefore, a 1D steady state model is considered for modelling wastewater temperature variation in large sewer networks. However, the model will incorporate the impact of heat transfer to the surroundings, in the radial (in-sewer air) and the lateral (soil) directions, on the modelled wastewater temperatures. Nevertheless, the 1D steady state model would provide computation results for one (horizontal) dimension.

3.3 Applications of Heat Transfer

Section 3.1 addressed the basics of heat transfer processes and explained how conduction and convection can be combined with the principles of energy balance to model heat transfer in an object. This section is specifically concerned with heat transfer in fully filled pipes (Section 3.3.1). This is then utilised to explain how modelling heat transfer in sewer pipes may be developed on the basis of that in fully filled pipes (Section 3.3.2). The modelling of heat transfer in sewer pipes is further developed to estimate wastewater temperature variation in a network of sewer pipes (Section 3.3.3). The modelling technique to be implemented, in the three heat transfer applications of this section, is the 1D steady state as concluded from Section 3.2.1.

3.3.1 Heat Transfer in Fully Filled Pipes

This section is dedicated to developing a deterministic model for estimating the fluid temperature at the outlet of a fully filled pipe based on the relevant heat transfer mechanisms. Modelling heat transfer between a flowing fluid in a fully filled pipe and the surroundings is based on energy balance, thermal energy advected by the mass of the fluid, thermal convection between the fluid and the inner pipe wall and thermal conduction within the pipe wall and its surroundings. It is important to determine the system boundaries when modelling temperature distribution in a medium. The boundary conditions identify the temperature, or the state of heat transfer, at the boundaries of the studied region. Considering a similar case to sewer pipes, heat pump loops (HPL) is used in this section as an example of fully filled pipes. For a fluid flowing at a mass flow rate ($\dot{m}$), through a pipe buried in soil, with inlet temperature (T_{in}) lower than that of the outlet (T_{out}), the heat transfer mechanism can be illustrated by Figure 3.5.

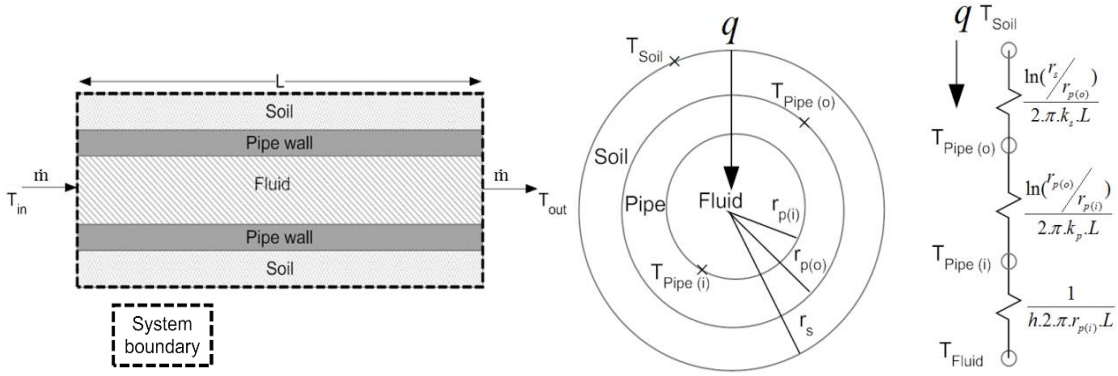

Figure 3.5: Longitudinal (left) and radial (middle) profiles of heat transfer in a fully filled pipe buried in soil. At the right is thermal resistivity associated with heat transfer from soil to the flowing fluid in the pipe. q is heat transfer rate (W), r is radius (m), k is thermal conductivity (W/m.K), h is the convective heat transfer coefficient (W/m^2.K) while s, p, o & i denote for soil, pipe, outer and inner properties respectively.

Modelling the temperature variation along the profile of a fully filled pipe can be achieved by applying the principle of energy balance described by Equation 3.1. Assuming steady state conditions, i.e. time independent heat and mass transfer processes, and no heat is generated or stored within the system's boundaries, Equation 3.1 is reduced to Equation 3.21.

$$E_{in}=E_{out} \tag{3.21}$$

Equation 3.21 can be expressed, by Equation 3.22, to reflect E_{in} 'Energy in' and E_{out} 'Energy out' in a fully filled pipe buried in soil. Considering heat transfers per unit length, E_{in} is the heat conducted through soil to the pipe wall ($q'_{soil-pipe}$) and heat conducted through pipe wall ($q'_{pipe-pipe}$) in addition to heat convected between the inner pipe wall and the fluid flowing in the pipe ($q'_{pipe-fluid}$). E_{out} is measured by the temperature difference between the inlet and the outlet and is defined as the energy advected by mass per unit length ($q'_{advected\ by\ mass}$).

$$q'_{soil-pipe} + q'_{pipe-pipe} + q'_{soil-fluid} = q'_{advected\ by\ mass} \tag{3.22}$$

Equation 3.22 can be solved, for a pipe with length L (m), by considering the relevant temperatures and the values of thermal resistivity as shown by Equation 3.23.

$$\frac{1}{R_{soil-pipe}}\left(T_s - T_{p(o)}\right) + \frac{1}{R_{pip-pipe}}\left(T_{p(o)} - T_{p(i)}\right) + \frac{1}{R_{pip-fluid}}\left(T_{p(i)} - T_f\right) = \frac{\dot{m}c_p(T_{out} - T_{in})}{L} \tag{3.23}$$

Referring to Figure 3.5, while considering heat transfer processes per unit length, thermal resistivity between the soil and the fluid flowing in the fully filled pipe is given by the R values shown by Equations 3.24.

$$R_{soil-pipe} = \frac{ln(^{r_s}/_{r_{p(o)}})}{2\pi k_s},\ R_{pipe-pipe} = \frac{ln(^{r_{p(o)}}/_{r_{p(i)}})}{2\pi k_p},\ R_{pipe-fluid} = \frac{1}{h2\pi r_{p(i)}} \qquad (3.24)$$

r is radius (m), k is thermal conductivity (W/m.K), h is the convective heat transfer coefficient (W/m^2.K) while s, p, f, o & i denote properties for soil, pipe, fluid, outer and inner respectively.

Rearranging Equation 3.23 and substituting R values obtained from Equations 3.24, Equation 3.25 can be developed to estimate the fluid temperature at the outlet (T_{out}) of a fluid flowing in a fully filled pipe buried in soil.

$$T_{out} = T_{in} - \left(\frac{\frac{1}{R_{soil-pipe}} \times (T_s - T_{p(o)}) + \frac{1}{R_{pip-pipe}} \times (T_{p(o)} - T_{p(i)}) + \frac{1}{R_{pip-fluid}} \times (T_{p(i)} - T_f)}{\dot{m} \times c_p} \times L \right) \qquad (3.25)$$

Equation 3.25 can be used to estimate the fluid temperature variation along the fully filled pipe profile by dividing the pipe into increments. Therefore, the fluid outlet temperature would be the temperature of the fluid inlet at the next increment. More details of modelling fluid temperature variation along the pipe profile is discussed in the next section where a model is developed for estimating wastewater temperature along a sewer pipe profile.

3.3.2 Heat Transfer in Sewer Pipes (Sewer Pipe Model)

The aim of this section is to develop a deterministic model for wastewater temperature variation along sewer pipe profiles. The developed model in this section is named the sewer pipe model. Sewer pipes can be described as partially filled pipes where wastewater flows at the pipe invert level, with a depth of d_w, while in-sewer air flows in the gap between the wastewater top surface and the crown of the sewer pipe. Figure 3.6 demonstrates the radial (left) and longitudinal (right) illustrations of wastewater flowing in a sewer pipe buried in soil.

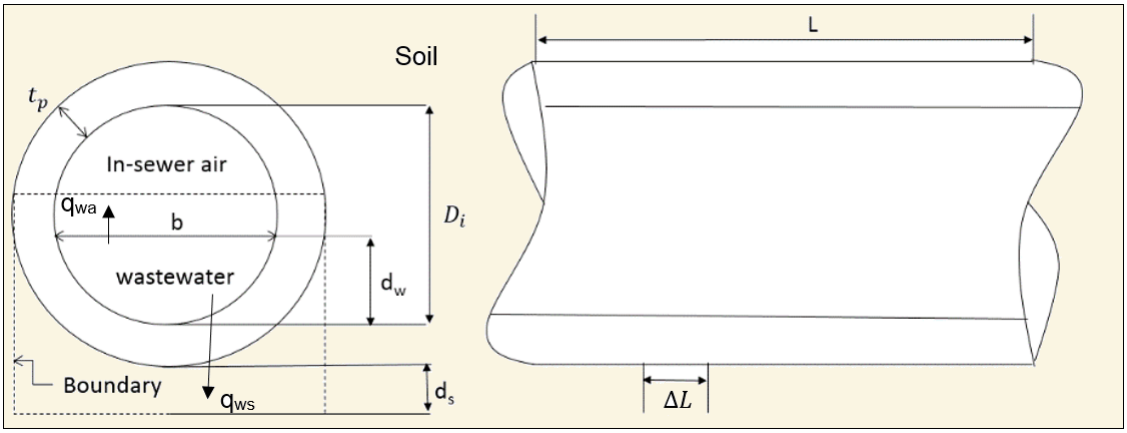

Figure 3.6: Cross and longitudinal sections of a sewer pipe.

In a similar approach to that used for modelling fluid temperature in fully filled pipes, estimating the wastewater temperature variation along the profile of a sewer pipe can also be achieved by applying the principles of energy balance described by Equation 3.1. Assuming steady state conditions, i.e. time independent heat and mass transfer processes, and no heat is generated or stored within the system's boundaries, the same equation used for fully filled pipes (Equation 3.21) can also be modified and implemented here.

Since the sewer pipes are partially filled, the fully filled pipe model developed in Section 3.3.1 needs to be adapted for the case of sewer pipes. During dry weather in combined sewer systems wastewater in sewer pipes usually flows at much smaller depths than their relevant sewer pipe diameters. This was observed through Infoworks CS data from a real sewer pipe network in Belgium as shown by Figure 3.7. The latter figure illustrates the ratio of average wastewater depth to the sewer pipe diameter for a randomly chosen period between 1st April 2012 and 1st June 2012.

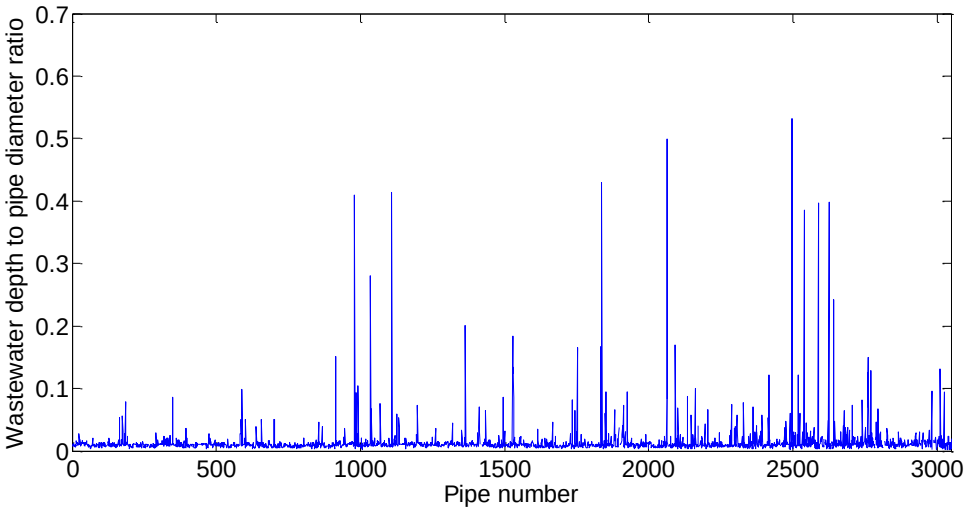

Figure 3.7: Ratio of average wastewater depths to their relevant sewer pipe diameters in a Belgian large sewer network. Wastewater depths were obtained from Infoworks CS data for the period between 1/04/2012 to 1/06/2012.

It is clear from Figure 3.7 that the depth of wastewater is usually much lower in value than the pipe diameter. Moreover, the sewer pipes are not fully confined pipes due to the existence of the manholes which result in air flowing through the sewer pipes. Therefore, the transfer of heat in sewer pipes is assumed to be close to that of heat transfer of fluid flowing over a flat plate. Hence, and for simplification purposes it was assumed that wastewater flowing in sewer pipes is similar to the case of a fluid flowing over a flat plate.

Applying energy balance equations (i.e. Equation 3.21) and accounting for heat transfer per unit length in wastewater flowing at a constant mass flow rate, Equations 3.26 can be developed.

$$q'_{wa} = \frac{1}{R_{wa}} \times (T_w - T_a), \quad q'_{ws} = \frac{1}{R_{ws}} \times (T_w - T_{soil}) \tag{3.26}$$

q' is heat transfer per unit length (W/m) while T is temperature (K). w, a & s denote for wastewater, air and soil respectively.

Referring to Figure 3.6, the pipe is divided into streamwise increments with a length of ΔL each. Applying Equation 3.6 while accounting for heat transfer per unit length, overall thermal resistivity between wastewater and air (R_{wa}) and between wastewater and soil (R_{ws}) can be defined by Equation 3.27 and 3.28 respectively.

$$R_{wa} = \frac{1}{h_{wa} \times b} \quad (3.27)$$

$$R_{ws} = \frac{1}{h_{wp} \times wet.p} + \frac{t_p}{k_p \times wet.p} + \frac{d_s}{k_s \times wet.p} \quad (3.28)$$

R is thermal resistivity (m.K/W). w, a, p & s denote for wastewater, air, pipe and soil respectively, t_p is the pipe wall thickness (m), d_s is the soil penetration depth (m), h_{wp} is the convective heat transfer coefficient between wastewater and pipe (W/m^2.K), b is the surface width of wastewater running in a sewer pipe (m), wet.p is the sewer pipe wetted perimeter (m), ΔL is mesh size or increment length (m), k is thermal conductivity (W/m.K).

Soil penetration depth (d_s) is the distance from the sewer pipe external pipe wall (invert level), shown by Figure 3.6, at which soil temperature is independent of the heat transfer process between wastewater and soil. Velocity of wastewater flowing in sewer pipes was assumed to have gradual reduction (vertical wise) to reach zero at the pipe invert level (no-slip condition). Therefore, it is assumed that convection between the wastewater and the inner pipe wall is neglected. Hence, conduction takes place between the wastewater and the surrounding soil through the pipe wall without convection.

Hence, Equation 3.28 is reduced to express conduction in pipe wall and surrounding soil, which is shown by Equation 3.29.

$$R_{ws} = \frac{t_p}{k_p \times wet.p} + \frac{d_s}{k_s \times wet.p} \quad (3.29)$$

The heat transfer coefficient between water and air can be only estimated. It was found, by Flinspach (1973), to be a function of water velocity relative to that of surrounding air. This expression, shown by Equation 3.30, was used by previous authors for modelling heat transfer in sewer pipes such as Dürrenmatt and Wanner (2008 & 2014) and Abdel-Aal, *et al.* (2014).

$$h_{wa} = 5.85 \times \sqrt{u_{wa}} \quad (3.30) \text{ (Flinspach, 1973)}$$

h_{wa} is the convective heat transfer coefficient (W/m^2.K) between wastewater (w) and in-sewer air (a). u_{wa} is the relative wastewater velocity to that of in-sewer air (m/s).

Applying the principle of energy balance described by Equation 3.1, accounting for thermal energy advected by mass, as explained by Equation 3.10, and by expressing thermal convection and conduction shown by Equation 3.4, Equation 3.31 was developed based on heat transfers per unit length. Equation 3.31 is

applied in sequence, starting from upstream wastewater temperature (T_m) to compute temperature variation along the sewer pipe (T_{m+1}, T_{m+2}, ...) and finally calculates the wastewater temperature at the downstream of the sewer pipe (T_{m+n}).

$$T_{m+1} = T_m - \left(\frac{\frac{1}{R_{wa}} \times (T_m - T_{air}) + \frac{1}{R_{ws}} \times (T_m - T_{soil})}{\rho \times Q \times c_p} \times \Delta L \right) \qquad (3.31)$$

T is temperature (K), R is thermal resistivity (m.K/W), wa and ws denote for wastewater and in-sewer air and wastewater and soil respectively, ΔL is the increment length (m), ρ is the wastewater density (kg/m^3), Q is the wastewater volumetric flow rate (m^3/s) and c_p is the specific heat capacity for wastewater (J/kg.K).

It is worth noting that Equation 3.31 is valid for temperatures measured in Celsius (°C) which is likely to be the case for many modelling applications. This is because temperature in Kelvin (K) is equal to that of Celsius plus 273.15 which means that a rise of 1 degree Celsius is equal to 1 degree Kelvin.

Equation 3.31 is used for the sewer pipe model and will be implemented in the sewer network model as will be explained in Section 3.3.3.

3.3.3 Heat Transfer in a Sewer Network (Sewer Network Model)

This section shows the methodology followed to develop a model that estimates wastewater temperature variations in a sewer network, it is named the sewer network model. Modelling wastewater temperature variation in a sewer network can be achieved using the same principles implemented in a single sewer pipe explained in Section 3.3.2. However, there are some differences, between a single pipe and a network of pipes, caused by the multiple pipes connections at manholes. This section shows how these differences shall be taken into account. The process of modelling wastewater temperature variation in a sewer network can be summarised in Figure 3.8 which is followed by more detailed steps.

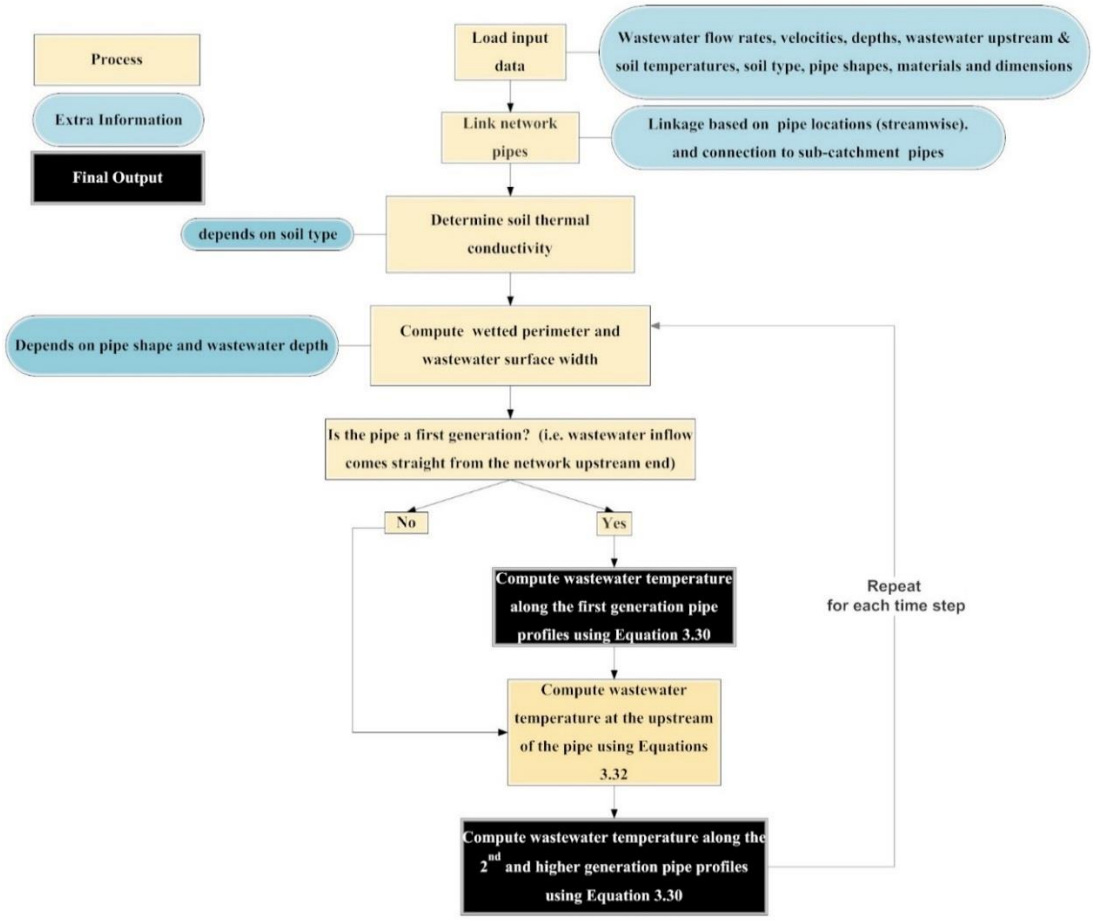

Figure 3.8: Process of modelling wastewater temperature variation in a sewer network.

A sewer network consists of sewer pipes that are located at different generations numbered from 1 to as many generations as required to describe the streamwise development in the network. Each generation represents the location of the sewer pipe in the network streamwise direction, where generation 1 contains the most upstream pipes in the network at which wastewater is discharged directly from the source (e.g. from residential homes, factories etc.). Wastewater of the first generation pipes is discharged to the second generation pipes and so on. Therefore, Equation 3.31 is implemented for each pipe in the sewer network. The sewer network model consists of input parameters that define boundary conditions, algorithms and outputs. Steady state conditions were applied in the sewer network model which is also the case for the sewer pipe model. However, the sewer network model can be implemented under different time steps, where the model estimates the wastewater temperature variation for each time step. The required input parameters are shown in Table 3.3. The final output of sewer network model is the wastewater temperature at the downstream end of each sewer pipe in the network.

Table 3.3: Input parameters for modelling wastewater temperature variations in a sewer network.

Category	**Input parameter (boundary conditions)**	**Notes /assumptions**
Temperatures	Upstream wastewater temperature of the first generation pipes	Required for each time step
	In-sewer air temperature	Applies for partially filled pipes. Required for each time step
Hydraulic data in each pipe	Wastewater flow rate	Required for each time step
	Wastewater velocity	Required for each time step
	Wastewater depth	Required for each time step
Specifications of each pipe	Pipe shapes	e.g. Circle
	Pipe materials	e.g. Concrete
	Pipe lengths, diameters and wall thicknesses	
Soil details	Soil type surrounding each sewer pipe	e.g. sandy sand
	Soil temperature in the region	Required for each time step
Pipe linkages	Pipe headers linking pipes, in the network, that define their generations	

The algorithms used for the network model can be divided into the following steps in this order:

1. Calculate the geometric dimensions (surface width and wetted perimeter) of wastewater flowing in the network pipes.
   Heat transfer in pipes depends on thermal resistivity which is influenced by the wastewater dimensions, these are wetted perimeter and width of wastewater surface, as explained in Section 3.3.2 and used in Equations 3.27 and 3.29.

2. Compute thermal resistivity values.
   Equations 3.27 and 3.29 can be implemented to compute thermal resistivity between wastewater and in-sewer air and between the wastewater and soil, (R_{wa} and R_{ws} respectively), for each pipe in the network.

3. Account for hydraulic data.
   This includes wastewater flow rate, depth, and velocity in each pipe of the network. The flow of each pipe in the network is fed to the next pipe in the streamwise direction.

4. Compute the wastewater temperature variation along each 1st generation pipe.
   This is done by computing the variation of the wastewater temperature along the first generation pipes using Equation 3.31, by utilising the given wastewater upstream values (T_m) which is identified as an input parameter in Table 3.3.

5. Compute the wastewater temperature variation along the 2nd and higher generation pipes. A sewer network consists of a number of upstream (1st generation) pipes connected to downstream (higher generation pipes) in a similar way shown by Figure 3.9. The wastewater temperature in the upstream end of the higher generation pipe (i.e. generation 2 and above) was assumed to be a function of pipe flows and wastewater temperatures at downstream ends of lower generation pipes.

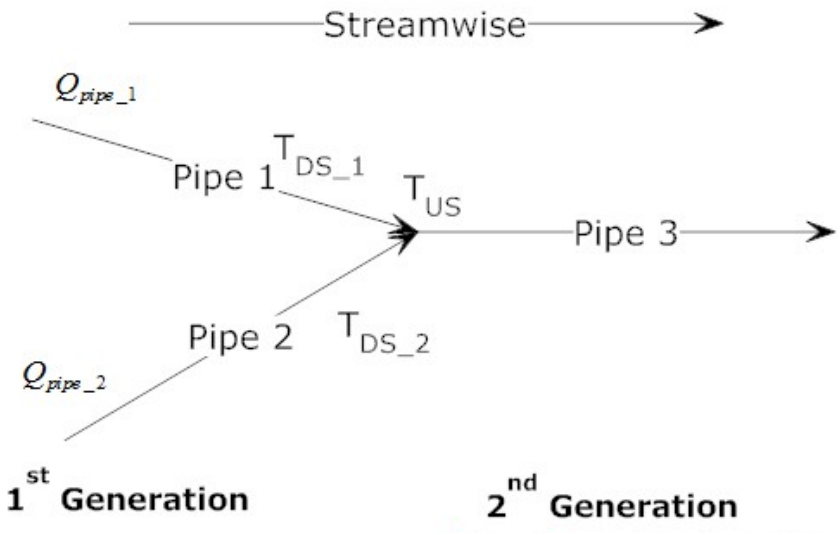

Figure 3.9: Multiple pipes connection in a sewer network.

Equations 3.32 and 3.33 show how upstream wastewater temperatures in 2nd and higher generation pipes can be computed in a sewer network.

$$Q_{Multiple\ pipes} = Q_{pipe\_1} + Q_{pipe\_2} + Q_{pipe\_np} \quad (3.32)$$

$$T_{US} = \frac{T_{DS\_1} \times Q_{pipe\_1} + T_{DS\_2} \times Q_{pipe\_2} + T_{DS\_np} \times Q_{DS\_np}}{Q_{Multiple\ pipes}} \quad (3.33)$$

T is the temperature of wastewater (°C) and Q is wastewater volumetric flow rate (m^3/s). US and DS denote for upstream and downstream ends of a pipe respectively, np is the number of connected pipes.

Once the upstream wastewater temperature of 2nd and higher generation pipes is computed, wastewater temperature variation along the sewer pipe is calculated using Equation 3.31. Therefore, T_m in Equation 3.31 is replaced by T_{US}.

4 Data Collection

The aim of the measurement campaign in the combined sewer pipes is to collect data to gain an understanding of the temperature variation in sewer pipes and to use that understanding to model wastewater temperature variation along sewer pipe profiles. Modelling in this context involves calibrating key heat transfer parameters in the equations that describe heat transfers within and to sewer pipes. Therefore, the selection of sewer pipes for measurements was based on the sewer pipe characteristics to reflect the nature of a sewer network where it includes both “urban” and “large sewers”. In this study “urban sewers” are defined as pipes in the upstream part of the combined sewer network, draining dense urban areas. Large sewers are defined as downstream collector sewers, collecting sewage from a number of areas. The average measured dry weather flow (DWF) for urban sewers is around 0.01 m^3/s or $36m^3/hour$, while the large sewers’ average DWF is between 0.09 m^3/s and 0.36 m^3/s or 330 $m^3/hour$ and 1300 $m^3/hour$. Two sewer sites of each type (i.e. urban and large) were selected for the measurement campaign so one can be utilised for calibration while the other can be used for validation for each sewer type as will be discussed in chapter 5.

The measured data was provided by a Belgian wastewater company named Aquafin (http://www.aquafin.be/). The author collaborated with Aquafin to specify the required site characteristics along with the required type of measurements while Aquafin installed the sensors, collected the readings and managed the measurement campaign in general. Figure 4.1 shows the locations of the sewer pipes used in this measurement campaign, while Table 4.1 shows the details of the urban and large sites used for the measurement campaign.

Figure 4.1: Locations of sewer sites used for measuring wastewater, in-sewer air and soil temperatures in Sites 1 (urban), 2 (urban), 3 (large) and 4 (large). Soil temperatures 1, 2 & 3 are soil temperature stations. Obtained using Google Earth.

Table 4.1: Urban and large sewer sites used for the measurement campaign.

Site	Type	Average DWF across all periods		Pipe length	Pipe depth		Pipe thickness	Pipe internal diameter	Pipe material	Shape
					Upstream	Downstream				
		(m^3/s)	(m^3/h)	(m)	(m)	(m)	(m)	(m)		
1	Urban	0.008	28	464	2.4	3	0.14	1.2	Concrete	Circle
2	Urban	0.01	39	232	3	4	0.14	1.2	Concrete	Circle
3	Large	0.36	1300	1031	3.5	3	0.14	1.2	Concrete	Circle
4	Large	0.09	330	749	3	2.8	0.12	0.7	Concrete	Circle

Studying the heat transfer processes and the energy balance in partially filled pipes (Section 3.3.2), led to the conclusion that the key heat transfer parameters in partially filled pipes can be divided into thermal resistivity, wastewater volumetric flow rate and wastewater and in-sewer air temperatures. Thermal resistivity comprises of resistivity between wastewater and soil R_{ws} and between wastewater and in-sewer air R_{wa}. Each thermal resistivity component involves some parameters that were measured, computed using measured data, calibrated or retrieved from previous works and published literature. Figure 4.2 shows the structure of the key heat transfer parameters that are crucial for modelling wastewater temperature variation along sewer pipe profiles. Some key parameters, stated in Figure 4.2, were impractical and costly to measure onsite, these are soil and pipe thermal conductivities, in-sewer air velocity and heat transfer coefficient between wastewater and in-sewer air. However, the pipe materials were known, as shown by Table 4.1, and therefore the relevant pipe thermal conductivity can be found from literature. The measured data in this work are temperatures, wastewater hydraulic data and sewer pipe dimensions. Measured temperatures comprise of soil temperatures, wastewater temperatures at up and down streams (Tw_{US} and Tw_{DS} respectively) and in-sewer air temperature at up and downstream ends (Ta_{US} and Ta_{DS} respectively). Soil temperatures were measured at 1.5m and 3.75m underground near the urban sewer sites and at 3.7m depth near the large sewer sites. There were three soil temperature stations located 1.8 km from Site 1, 1.4 km from Site 2, 2.8 km from Site 3 and 0.5 km from Site 4. Measured hydraulic data are the wastewater velocity (u_w) and wastewater depth (d_w), while wastewater flow rate (Q) is calculated by the sensor on the basis of measured u_w and d_w data. Pipe internal diameter and wall thickness were recorded for the sewer pipes as shown in Table 4.1.

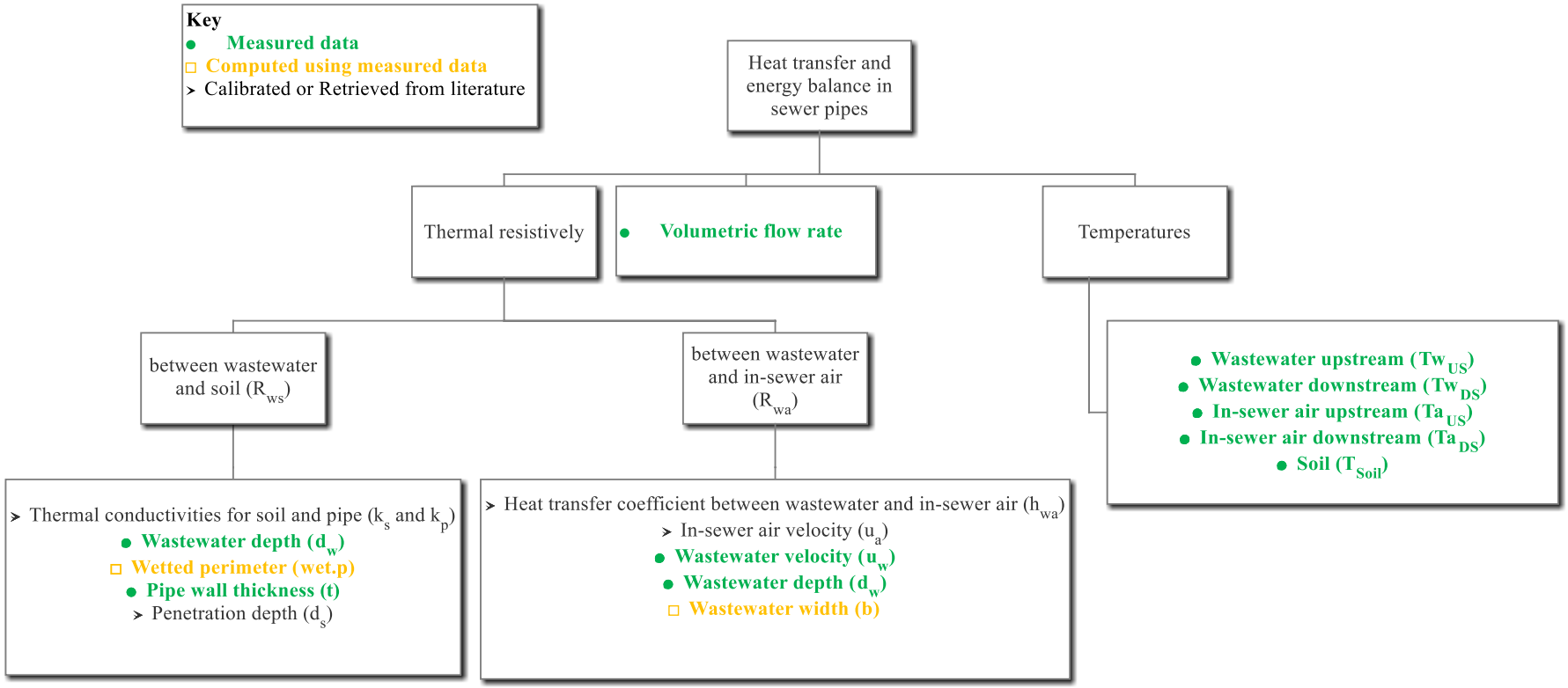

Figure 4.2: Illustration of the key heat transfer parameters required for modelling wastewater temperature variation along sewer pipe profiles.

4.1 Measured Temperatures

This section shows wastewater, in-sewer air and soil temperatures in Sites 1, 2, 3 and 4. Measured temperature data was smoothed by implementing the moving average technique in order to present clear readable data plots. Temperatures in urban sewer sites were recorded every 20 minutes and were plotted in this work by averaging the measured data over 24 hours (72 points). Temperatures in the large sewer sites, and that of ambient and influent were recorded every 15 minutes and were plotted by averaging the data over 24 hours (96 points).

Temperatures of wastewater and in-sewer air in urban sewer sites were measured using Tinytag (PBRF-5006-5m) with Radio logger of TGRF-3022-A sensors that have an accuracy of +/-0.06°C and better than 0.05°C resolution. This accuracy was based on the standard deviation values. Large sewer sites used PT100 10 m sensors with MM3P loggers supplied by Bar Instruments to measure temperatures of wastewater, in-sewer air and soil (shown by 'Soil Temperature 3' in Figure 4.1). These PT100 10 m sensors have +/-0.1°C accuracy. The sensors used for measuring in-sewer air temperatures were installed 1m below the sewer manhole cover while the wastewater temperature sensors were mounted just above the sewer pipe invert level. Thermocouples of EJB 378 K type were used for measuring soil temperatures near the urban sewers (referred to as 'Soil Temperatures 1 & 2' in Figure 4.1) and were calibrated by BERCU EJB. The EJB 378 K type thermocouples have measurement accuracy of +/- 0.7°C. A summary of sensor accuracies and the measurement periods for the four sites is shown by Table 4.2 (Section 4.2).

Ambient air temperature was measured by Antwerp council in a nearby area which is located within 12 km from the urban and large sewer sites, shown as 'Ambient Temperature' in Figure 4.1. Variation of ambient air temperature during the year 2012 is shown by Figure 4.3.

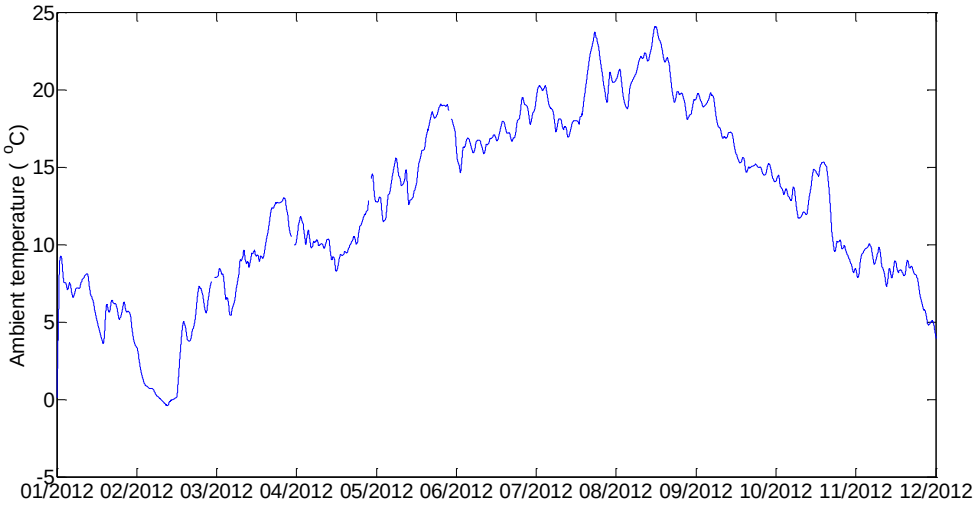

Figure 4.3: Ambient temperature variation, during the year 2012, located within 12km from the urban and large sewer sites. Data was averaged over 24 hours (96 points). Gaps in the plot indicates missing data.

In order to assess the quality of the measured data, daily wastewater temperature variations in urban sites were plotted in winter and in summer. These plots were then utilised to relate to the daily water consumption in residential homes. Understanding the pattern of daily wastewater temperature variation may be enhanced by observing the flow variation during the day to reflect the water consumption in the local area. Avoiding rainfall events and observing the changes in a typical day helps in understanding and analysing the measured data. Therefore, working days in winter and in summer that showed dry weather flow (DWF) conditions were chosen. Measured data in urban sewers were considered in this observation since they are influenced by the local water consumption. Hence, wastewater temperatures at upstream ends in Sites 1 and 2 were plotted along with wastewater flow rates on Monday 27th February and Friday 1st June all in 2012 as shown by Figure 4.4 and Figure 4.5 respectively. Data plotted in these days was averaged over 3 points for temperature to show variation every 1 hour. Since flow rate was measured every 2 minutes, flow data was averaged

over 30 points to illustrate hourly variation. The moving average technique was implemented in all plots shown in this chapter.

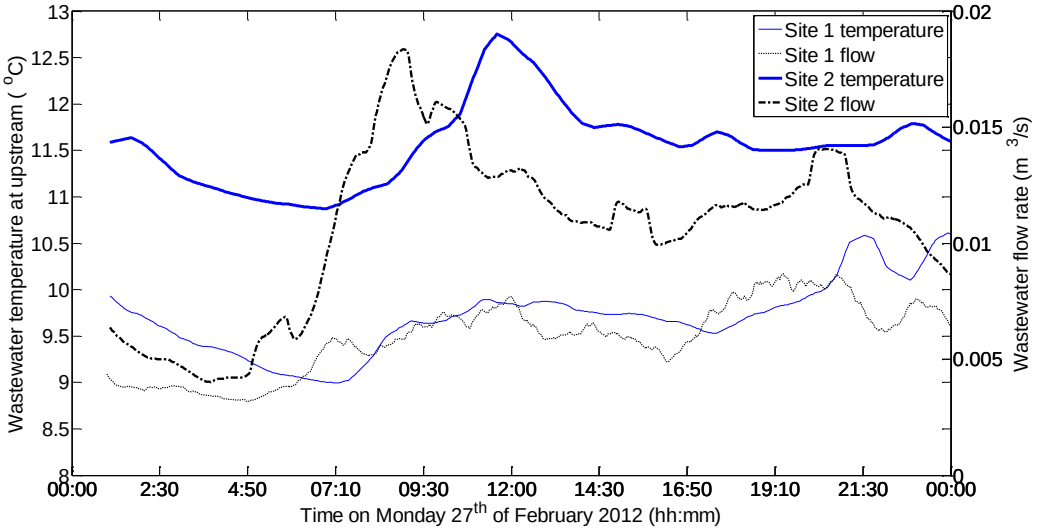

Figure 4.4: Wastewater temperature and flow rate variations in Sites 1 and 2 during Monday 27th February 2012. Data was averaged over one hour, (3 points for temperature and 30 points for flow rate).

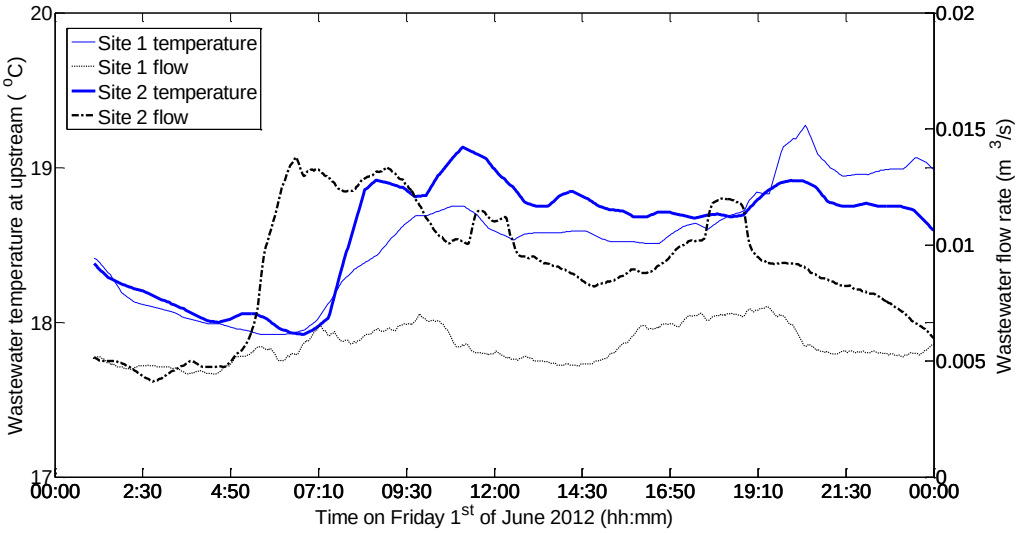

Figure 4.5: Wastewater temperature and flow rate variations in Sites 1 and 2 during Friday 1st June 2012. Data was averaged over one hour, (3 points for temperature and 30 points for flow rate).

Variations of wastewater and in-sewer air temperatures in Sites 1 and 2 at upstream and downstream ends are shown by Figure 4.6 and Figure 4.7 respectively. Measurement period in Sites 1 and 2 was from 1st February 2012 to 31st January 2013.

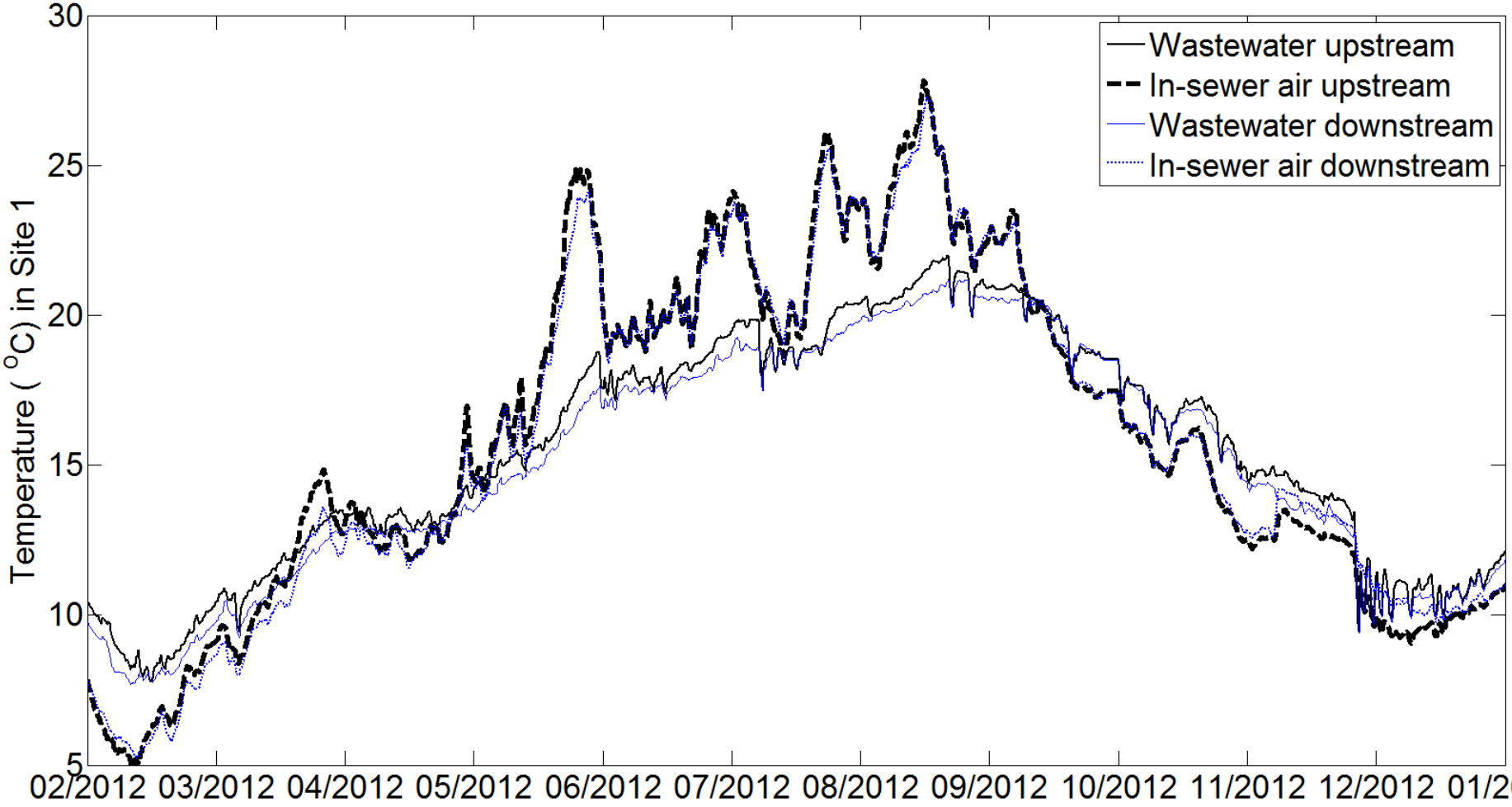

Figure 4.6: Measured wastewater and in-sewer air temperatures in Site 1 at upstream and downstream ends, during the period between 1st February 2012 and 31st January 2013. Data was averaged over 24 hours (72 points).

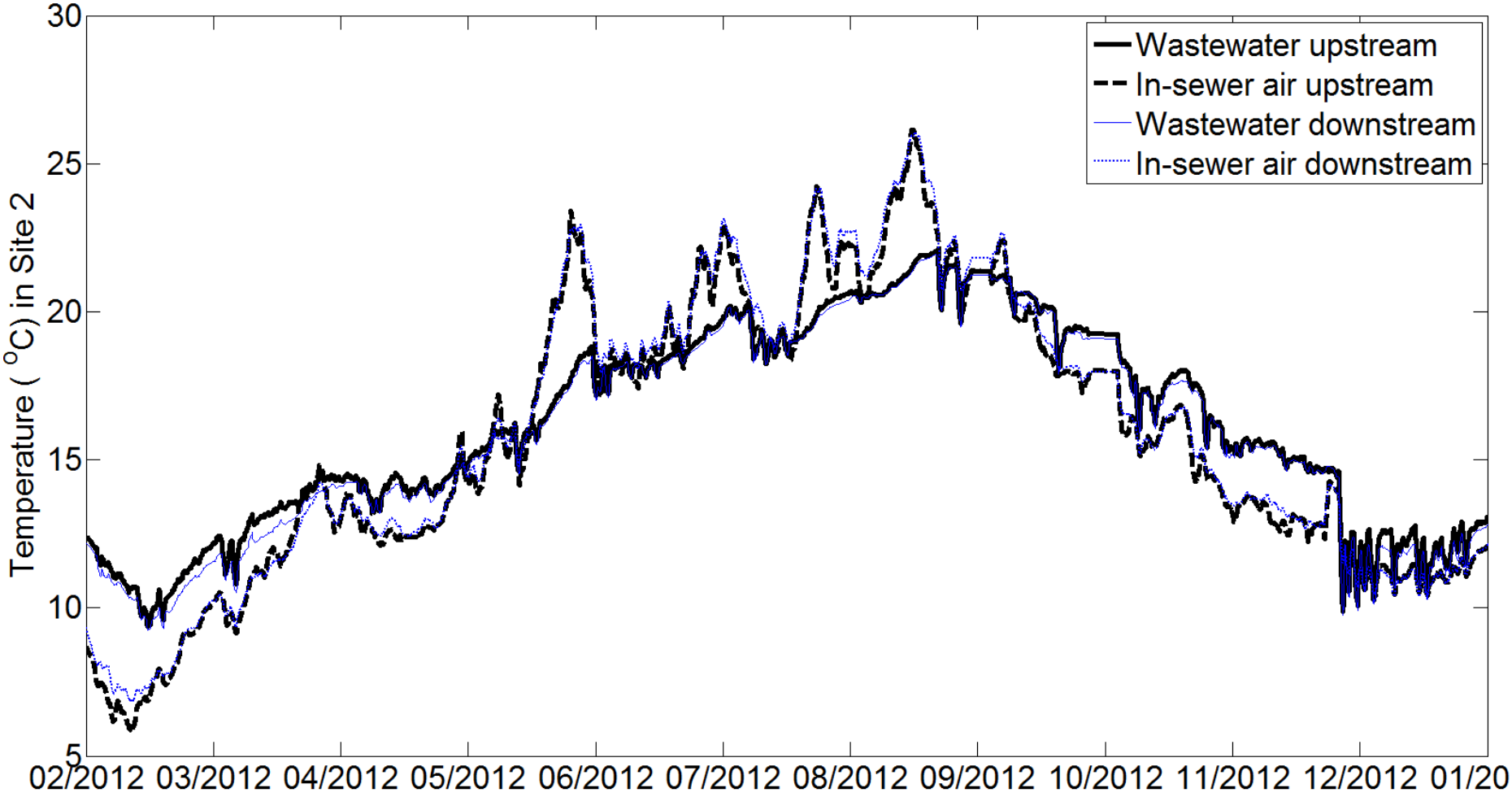

Figure 4.7: Measured wastewater and in-sewer air temperatures in Site 2 at upstream and downstream ends, during the period between 1st February 2012 and 31st January 2013. Data was averaged over 24 hours (72 points).

Wastewater and in-sewer air temperatures in Sites 3 and 4 at upstream and downstream ends are shown in Figure 4.8 and Figure 4.9 respectively. Measurement period in Sites 3 and 4 was from 1st March 2013 to the 28th February 2014. Temperatures measured in Site 4 between September 2013 and December 2013 were unavailable due to technical issues.

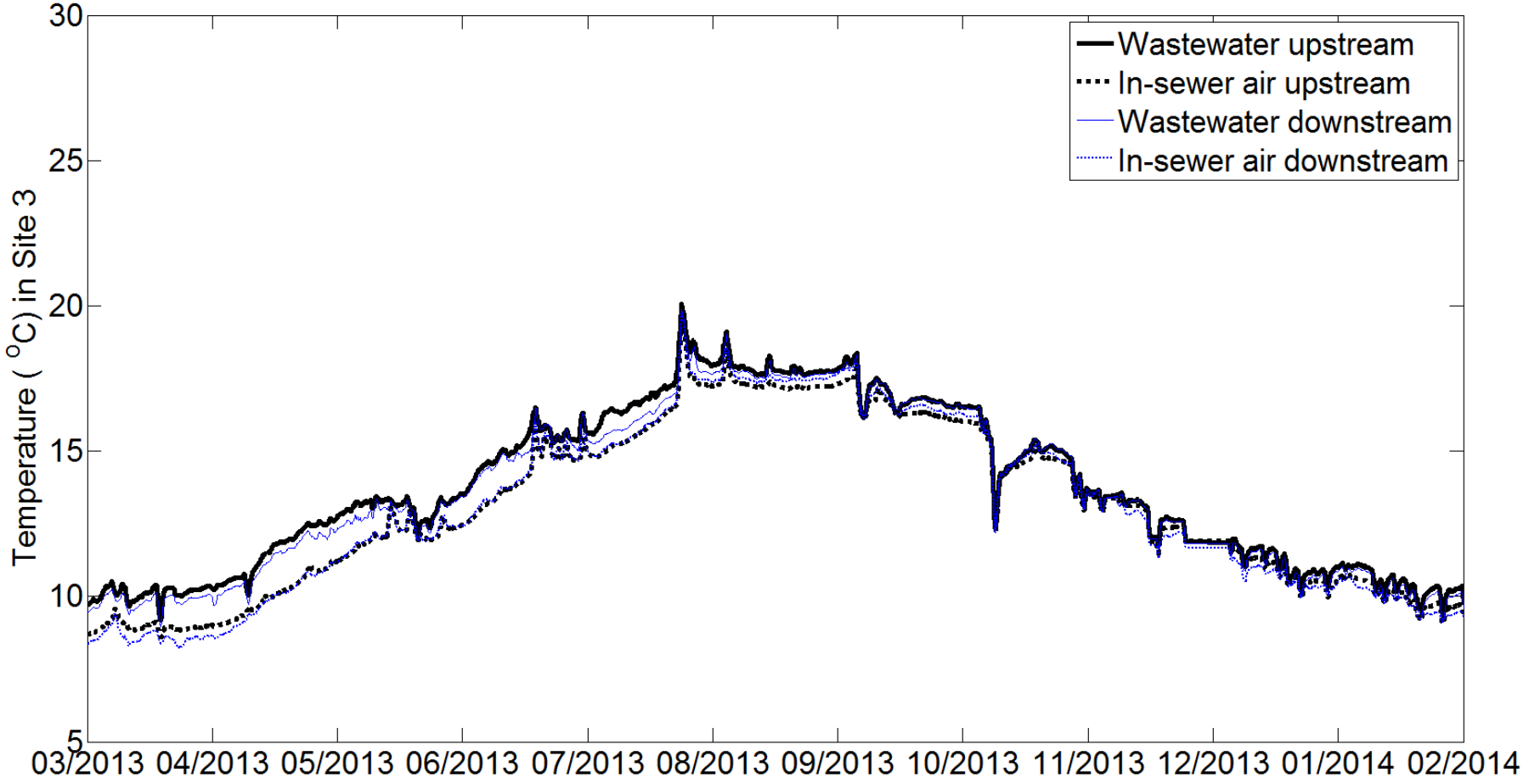

Figure 4.8: Measured wastewater and in-sewer air temperatures in Site 3 at upstream and downstream ends, during the period between 1st March 2013 and 28th February 2014. Data was averaged over 24 hours (96 points).

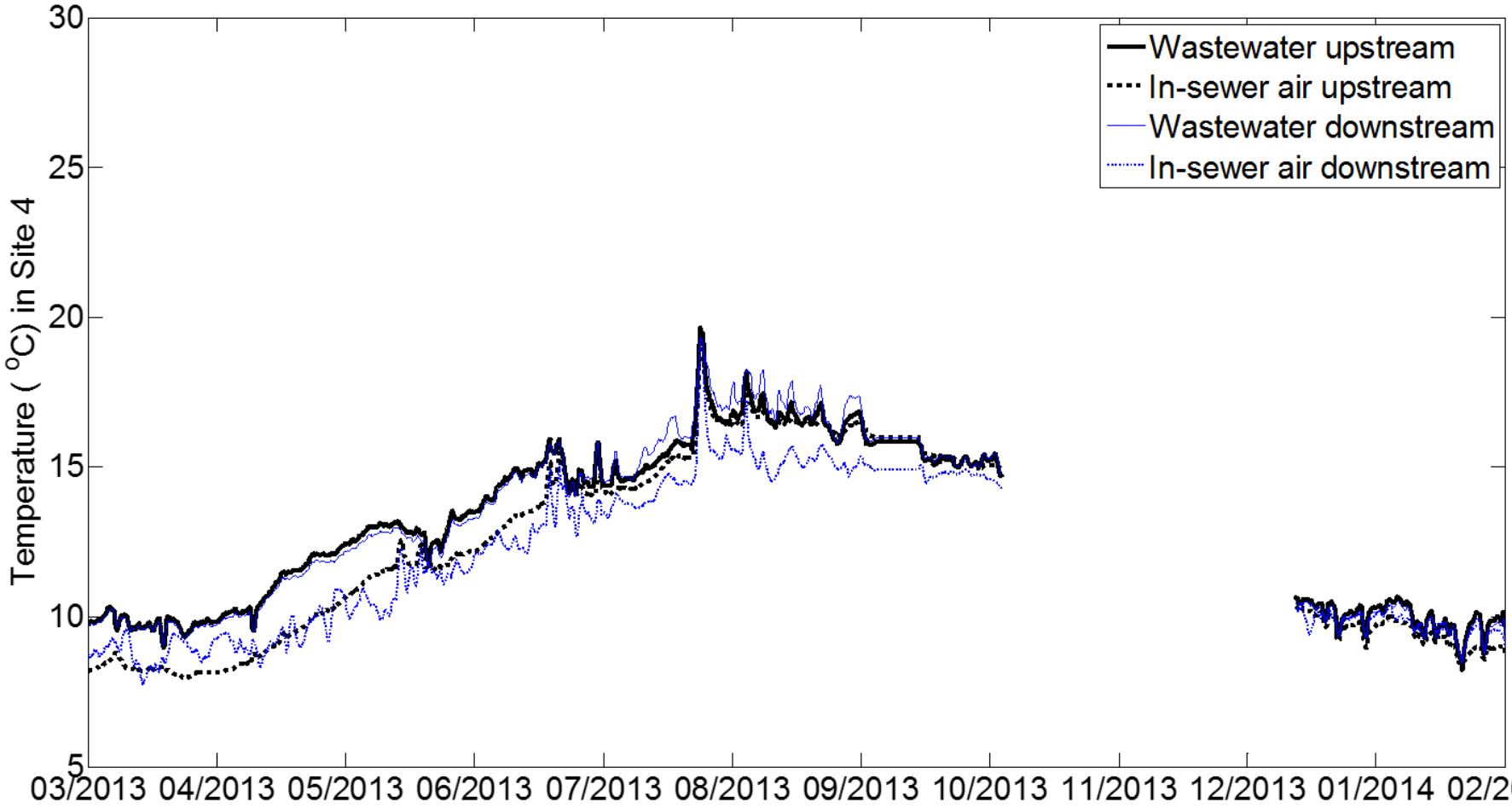

Figure 4.9: Measured wastewater and in-sewer air temperatures in Site 4 at upstream and downstream ends, during the period between 1st March 2013 and 28th February 2014. Data was averaged over 24 hours (96 points). The gap in the plot indicates missing data.

Temperatures of soil were measured at three stations; two of them were near to the urban sewers (within 2km) while the third was close to the large sewers (within 2.8km). Figure 4.10 shows soil temperatures at 1.5m and 3.7m depths near Site 1, referred to as 'Soil Temperature 1' in Figure 4.1. Soil temperatures at similar depths near Site 2 (referred to as 'Soil Temperature 2' in Figure 4.1) are shown in Figure 4.11. Temperatures of soil, at both depths, near Site 1 and 2 were measured from 1st March 2012 to 31st July 2012.

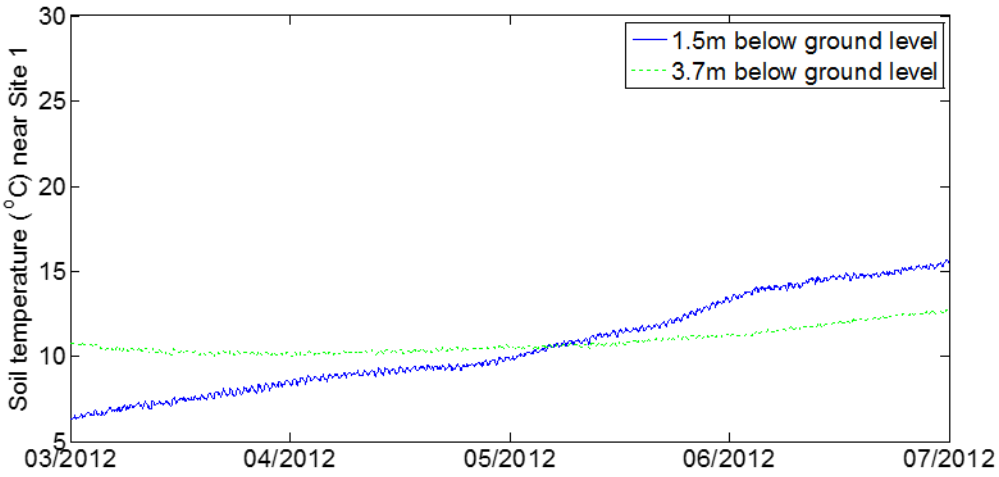

Figure 4.10: Soil temperatures measured 1.8km from Site 1, measurement station is referred to as 'Soil Temperature 1' in Figure 4.1. Data was averaged over 24 hours (72 points).Measurement period is from 1st March 2012 to 31st July 2012.

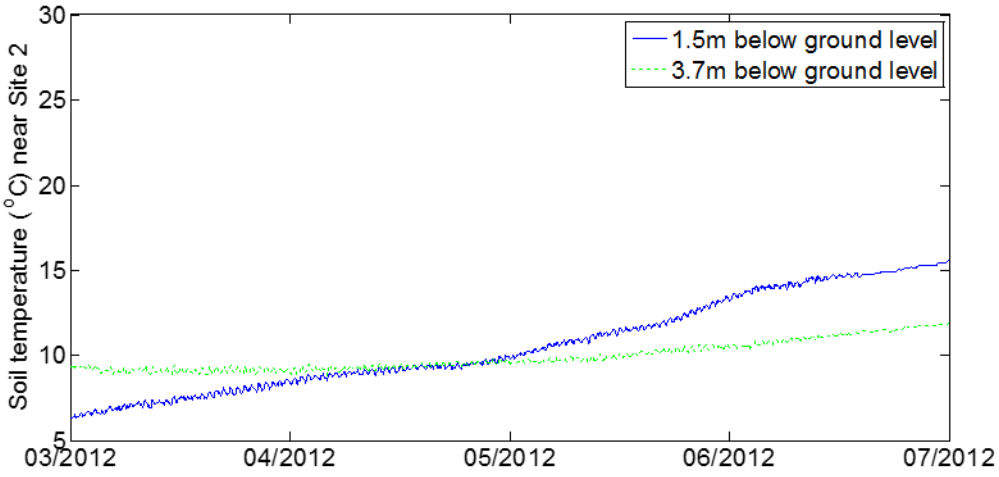

Figure 4.11: Soil temperatures measured 1.4km from Site 2, measurement station is referred to as 'Soil Temperature 2' in Figure 4.1. Data was averaged over 24 hours (72 points). Measurement period is from 1st March 2012 to 31st July 2012.

Since Site 1 showed an average sewer depth of 2.7m, soil temperature near Site 1 was considered to be the average of that at 1.5m and 3.7m depths. On the other hand, soil temperature for Site 2 was that measured near it at 3.7m depth since Site 2 sewer average depth was 3.5m. Figure 4.12 shows the considered soil temperatures for urban sewer sites that will be utilised for model calibration and validation in Chapter 5.

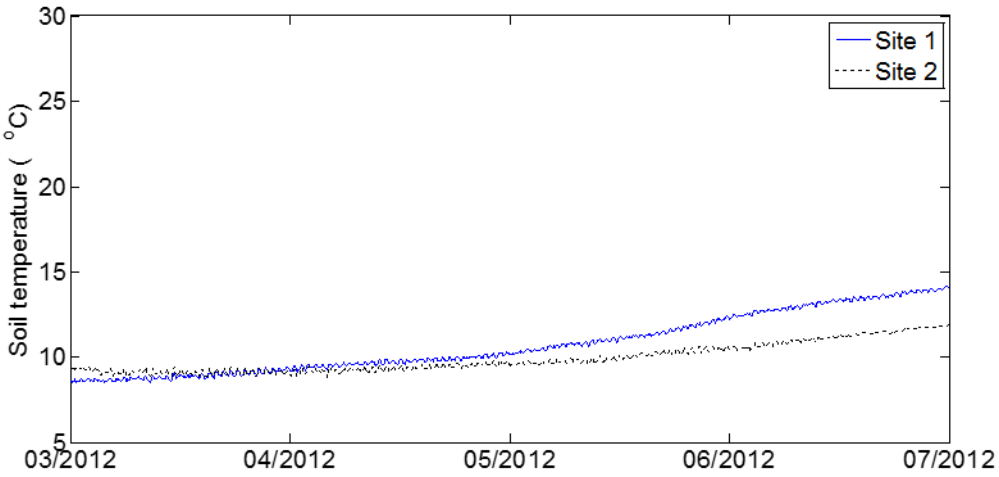

Figure 4.12: Soil temperatures considered for model calibration and validation for Sites 1 and 2. Measurement period is from 1st March 2012 to 31st July 2012. Data was averaged over 24 hours (72 points).

Soil temperatures near the large sewer sites were measured from 1st March 2013 to 28th February 2014. Figure 4.13 shows soil temperatures considered for large sewer sites, i.e. Sites 3 and 4.

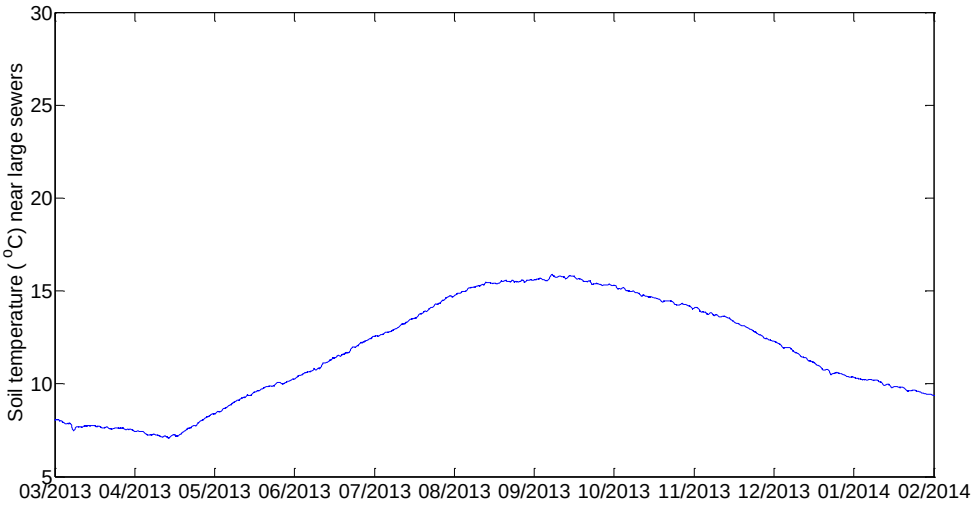

Figure 4.13: Measured soil temperatures 2.8km from Site 3 and 0.5km from Site 4 at 3.75m below ground. Measurement station is referred to as 'Soil Temperature 3' in Figure 4.1. Data was averaged over 24 hours (96 points). Measurement period is from 1st March 2013 to 28th February 2014.

Influent temperature was measured at Antwerp North Wastewater Treatment Plant (WWTP), which is located 1.3km from Site 4 as shown in Figure 4.1. Measured WWTP influent temperature, for Antwerp North, was for the period between 1st March 2013 and 28th February 2014 as shown by Figure 4.14

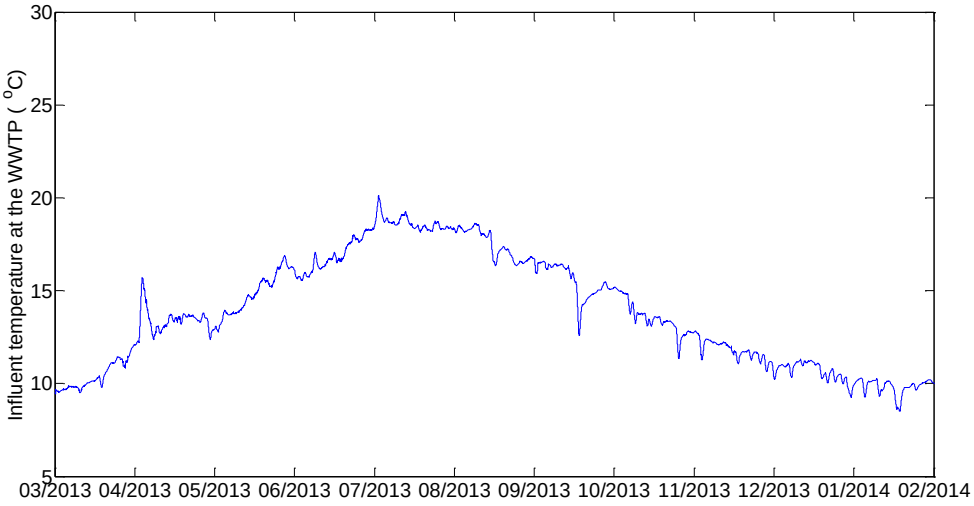

Figure 4.14: Influent temperature in Antwerp North WWTP between 1st March 2013 and 28th February 2014. Data was averaged over 24 hours (96 points).

The measured temperatures illustrated in this section have generally shown expected variations. The daily variation of wastewater temperatures and flow

rates in Sites 1 and 2 (Figure 4.4 and Figure 4.5) reflect the expected daily water consumption. Wastewater temperatures in Sites 1, 2, 3 and 4 presented a similar pattern to that of ambient temperature. It was observed from Figure 4.6 and Figure 4.7 that both urban sewer sites (1 and 2) showed similar scales of temperature variations. This was also the case in large sewers where Sites 3 and 4 showed close temperature variations (Figure 4.8 and Figure 4.9). This suggests that sewer pipes of similar scales provide similar data. Soil temperatures measured near the ground surface were more influenced by the ambient temperature than those measured at deeper depths, which was expected. The anticipated patterns of temperature variations in this section suggest that data collected in this work is likely to be similar in other sewers of similar sizes and climate. More details about the measured temperatures is discussed in Section 4.3.

4.2 Hydraulic Data

This section shows the data of wastewater flow rates, measured wastewater velocities and wastewater depths at Sites 1, 2, 3, and 4. Measured hydraulic data was smoothed by implementing the moving average technique, in a similar manner to that of Section 4.1, for the purpose of presenting clear readable data plots. Hydraulic data in all the four sites were recorded every 2 minutes and was plotted in this section by averaging the data over 1 hour intervals (30 points) as will be shown later.

Wastewater flow rates in urban and large sewer sites were monitored by Isco 2150 area velocity type meters that were calibrated onsite by Studiebureau Patrick Casier, Belgium. The flow meters were visited on a weekly basis where both the wastewater velocity and depth were checked and the sensors were cleared from any obstructing particles if necessary. The flow meters measure wastewater depths, from 0.01 to 3.05m, through submerged pressure transducers with +/- 0.003m accuracy. Wastewater velocity was also measured using the Isco 2150 area velocity type meter through the Doppler ultrasonic method with 500 kHz frequency which requires 0.025m minimum wastewater depth. The Isco 2150 meter has velocity measurement accuracy of +/-0.03m/s. A summary of sensor accuracies and the measurement periods for the four sites is shown in Table 4.2. Wastewater hydraulic data was measured during the period between 1st March 2012 and 31st July 2012 in urban sewers (Sites 1 & 2) and

between 1st February 2013 and 31st May 2013 in large sewers (Sites 3 & 4). Measured wastewater flow rate in Site 1 was plotted in Figure 4.15 at all conditions in the top plot (i.e. including rainfall events) and during days of dry weather flow (DWF) in the bottom plot. A typical flow rate for a dry weather flow condition was observed, through data plotting (Figure 4.15 and Figure 4.16), to be between 0.007 and 0.016 m^3/s in Sites 1 and 2. Therefore, in order to obtain the variation of DWF, data was filtered using Matlab to avoid rainfall events. All hydraulic data (wastewater flow rate, velocity and depth) at urban and large sites were measured every 2 minutes. In order to smooth the plotted data, the hydraulic readings were averaged over one hour (30 points).

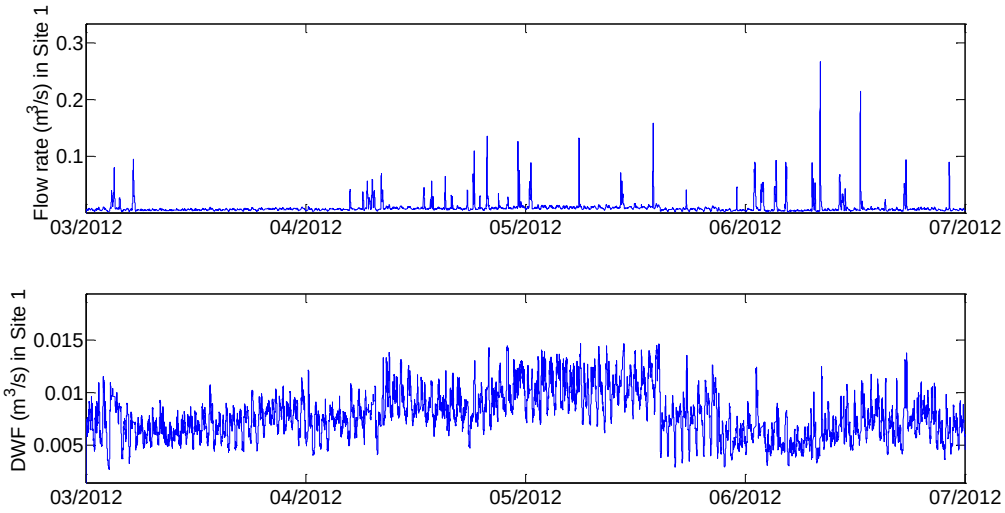

Figure 4.15: Measured wastewater flow rate from 1st March 2012 to 31st July 2012, in Site 1, at all conditions (top) and during dry weather flow (DWF) days (bottom). Data was averaged over 1 hour (30 points).

Measured wastewater flow rate in Site 2 was plotted in Figure 4.16 at all conditions (top plot) and during DWF (bottom plot).

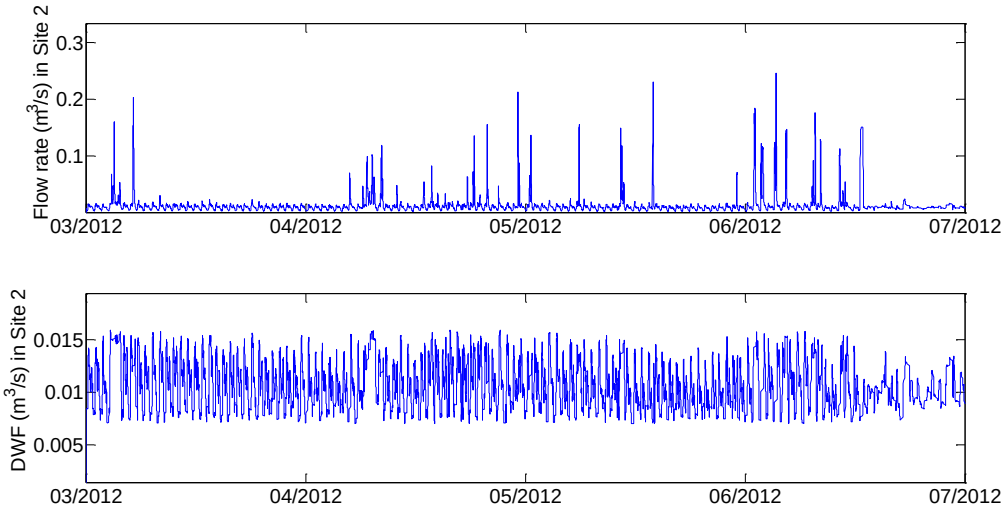

Figure 4.16: Measured wastewater flow rate from 1st March 2012 to 31st July 2012, in Site 2, at all conditions (top) and during dry weather flow (DWF) days (bottom). Data was averaged over 1 hour (30 points).

A typical dry weather flow day shows a wastewater flow range between 0.03 and 0.65 m^3/s in Site 3 and between 0.07 and 0.14 m^3/s in Site 4. This was obtained through Matlab by filtering data of rainfall events observed from Figure 4.17 and Figure 4.18.

Measured wastewater flow rate in Site 3 is shown by Figure 4.17 at all conditions (top plot) and during DWF (bottom plot).

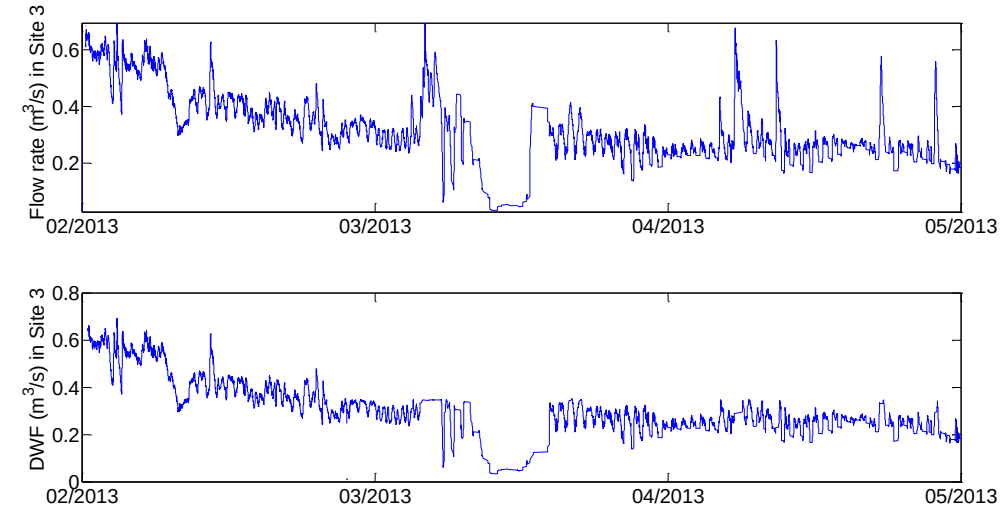

Figure 4.17: Measured wastewater flow rate from 1st February 2013 to 31st May 2013, in Site 3, at all conditions (top) and during dry weather flow (DWF) days (bottom). Data was averaged over 1 hour (30 points).

Measured wastewater flow rate in Site 4 is shown by Figure 4.18 at all conditions (top plot) and during DWF (bottom plot).

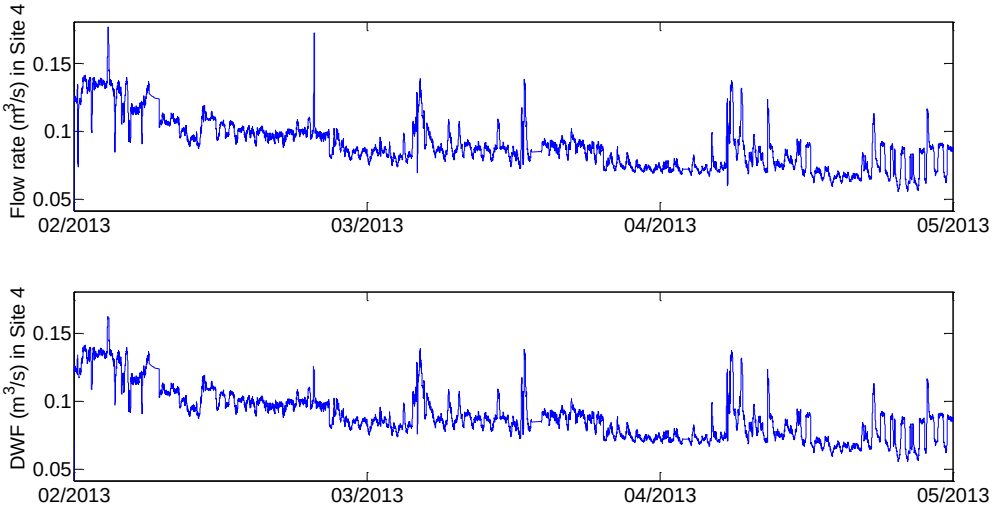

Figure 4.18: Measured wastewater flow rate from 1st February 2013 to 31st May 2013, in Site 4, at all conditions (top) and during dry weather flow (DWF) days (bottom). Data was averaged over 1 hour (30 points).

Measured wastewater velocities in Sites 1 and 2 are shown by Figure 4.19 and Figure 4.20 respectively.

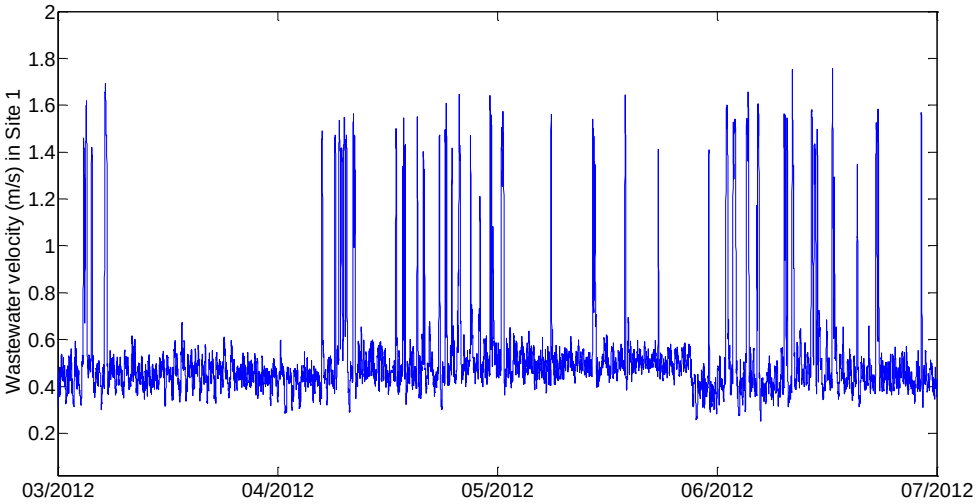

Figure 4.19: Measured wastewater velocity from 1st March 2012 to 31st July 2012, in Site 1. Data was averaged over 1 hour (30 points).

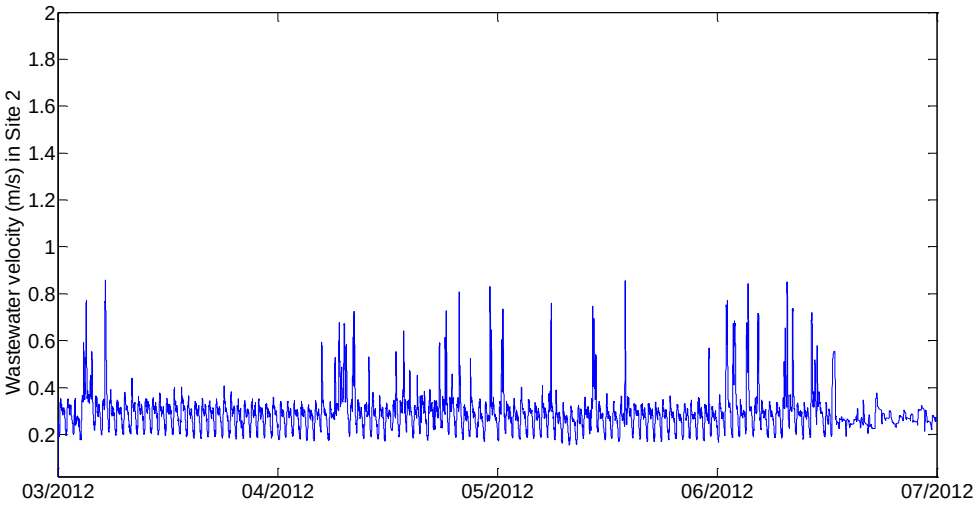

Figure 4.20 Measured wastewater velocity from 1st March 2012 to 31st July 2012, in Site 2. Data was averaged over 1 hour (30 points).

Measured wastewater velocities in Sites 3 and 4 are shown by Figure 4.21 and Figure 4.22 respectively.

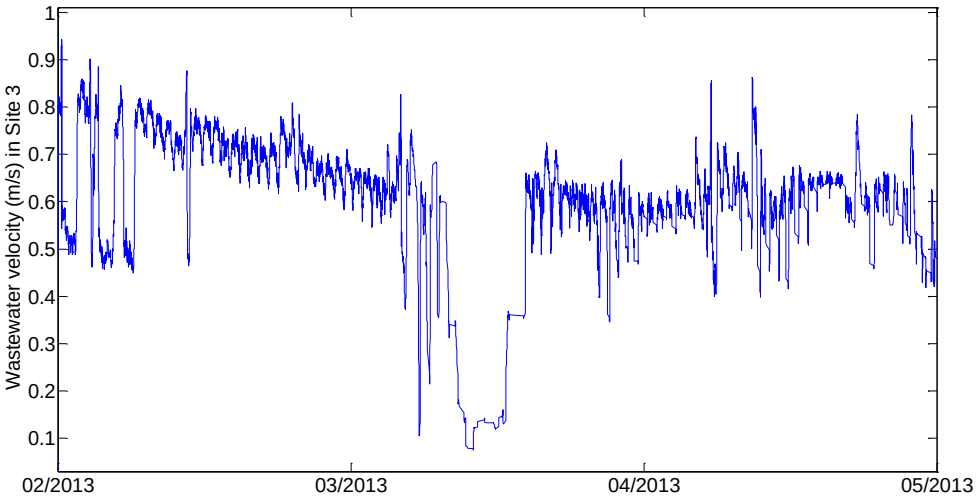

Figure 4.21: Measured wastewater velocity from 1st February 2013 to 31st May 2013, in Site 3. Data was averaged over 1 hour (30 points).

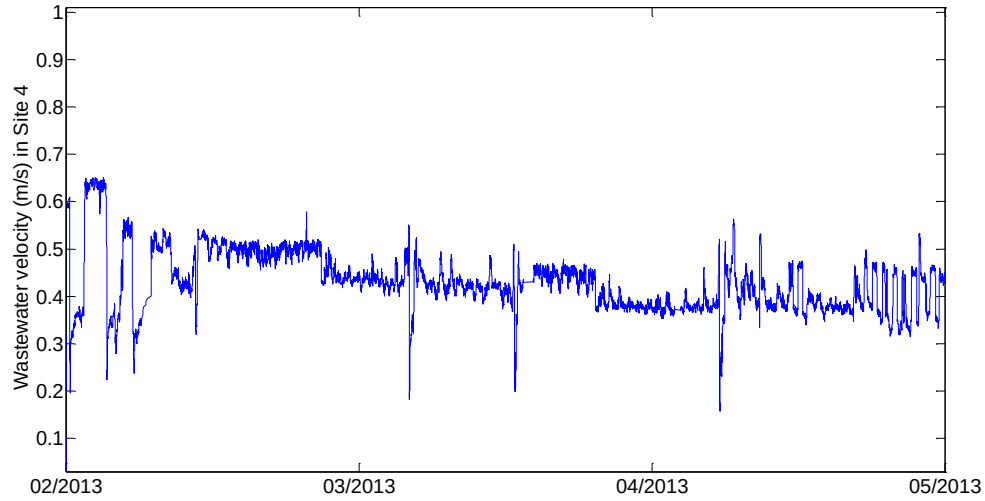

Figure 4.22: Measured wastewater velocity from 1st February 2013 to 31st May 2013, in Site 4. Data was averaged over 1 hour (30 points).

Measured wastewater depths in Sites 1 and 2 are shown by Figure 4.23 and Figure 4.24 respectively.

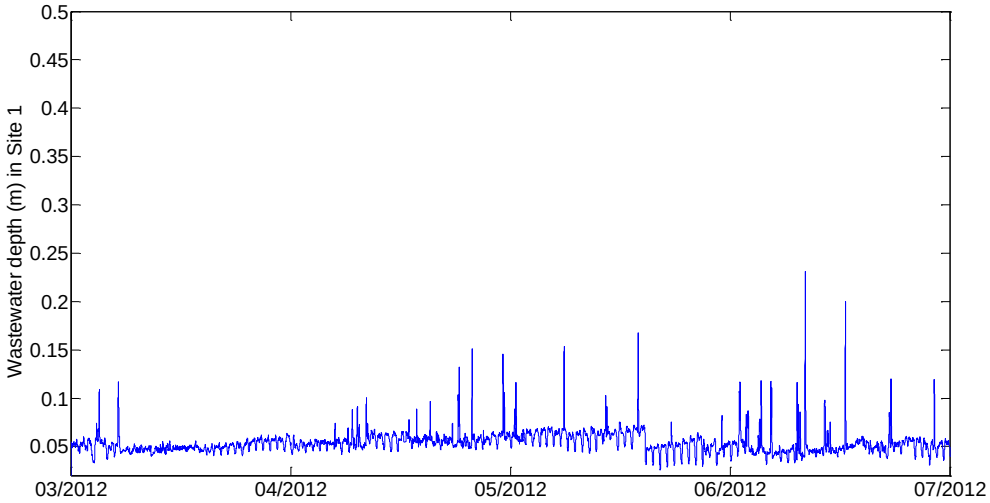

Figure 4.23: Wastewater depth in Site 1 from 1st March 2012 to 31st July 2012. Data was averaged over 1 hour (30 points). Site 1 internal pipe diameter is 1.2m.

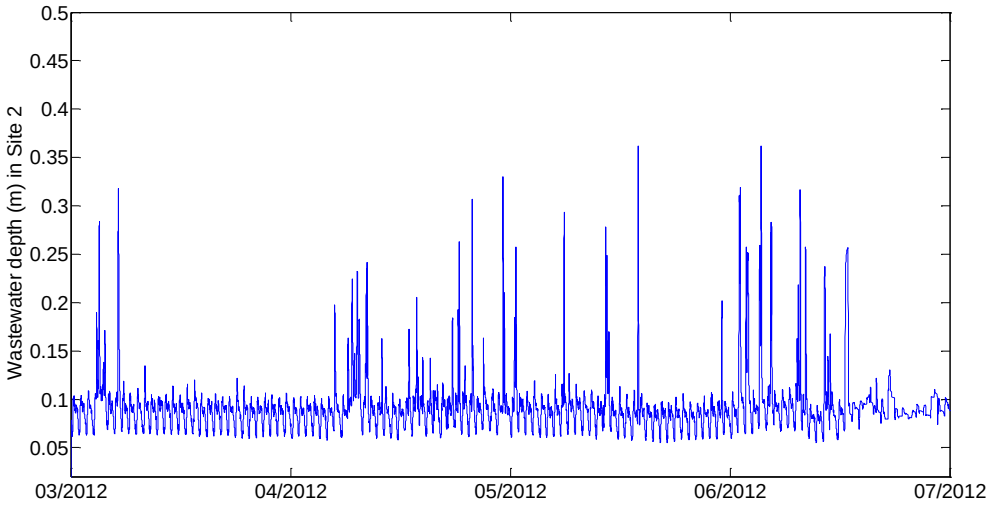

Figure 4.24: Wastewater depth in Site 2 from 1st March 2012 to 31st July 2012. Data was averaged over 1 hour (30 points). Site 2 internal pipe diameter is 1.2m.

Measured wastewater depths in Sites 3 and 4 are shown by Figure 4.25 and Figure 4.26 respectively. Since the sensors measuring wastewater depths, in Site 3 and 4, were placed in the manhole, some wastewater depths in these sites were obtained to be higher than the sewer pipe diameter. Therefore, wastewater depth values higher than the corresponding pipe diameters in Site 3 and 4 were filtered (deleted) in Figure 4.25 and Figure 4.26.

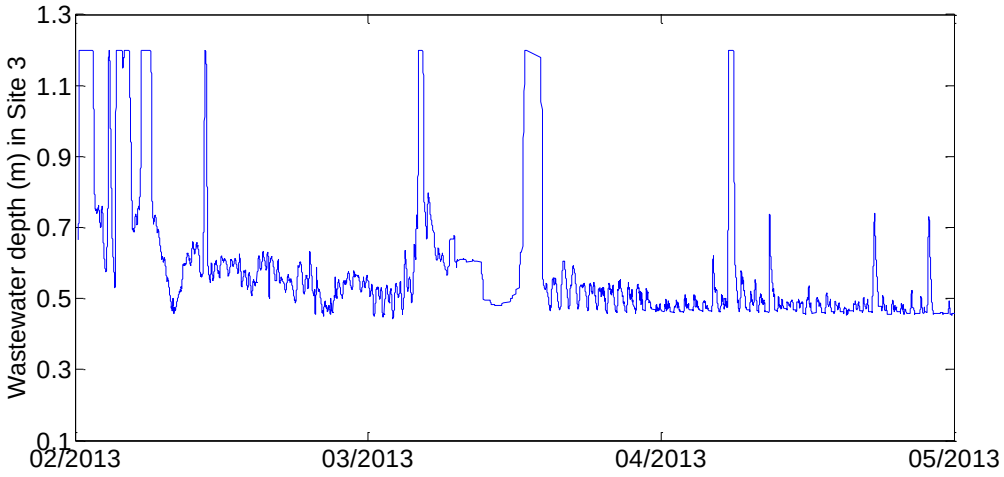

Figure 4.25: Wastewater depth in Site 3 from 1st February 2013 to 31st May 2013. Data was averaged over 1 hour (30 points). Wastewater depth values above Site 3 internal pipe diameter (1.2m) were filtered.

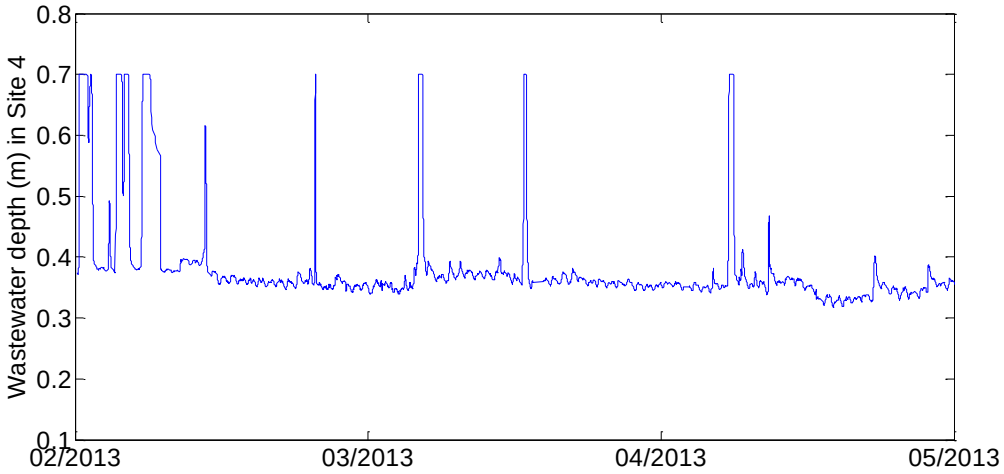

Figure 4.26: Wastewater depth in Site 4 from 1st February 2013 to 31st May 2013. Data was averaged over 1 hour (30 points). Wastewater depth values above Site 4 internal pipe diameter (0.7m) were filtered.

Urban sewers showed similar patterns and scales of wastewater flow, velocity and depth variations. The large sewers have also shown similarity in terms of scale and hydraulic data variations. Dry weather flow was observed to be the common case in both urban and large sewer sites which is expected in a western European climate. These expected patterns of hydraulic data variations indicate that the measured wastewater flow rates, velocities and depths data is likely to be similar to other sites of similar characteristics and climates.

Table 4.2 shows a summary of sensor accuracies and the measurement periods for the four sites.

Table 4.2: Summary of the sensor accuracies for the measured parameters and their relevant measurement periods.

Measured parameter	Sites	Sensor accuracy	Unit	Measurement period
Wastewater temperature	1 and 2	+/-0.06	°C	1st February 2012 to 31st January 2013
In-sewer air temperature	1 and 2	+/-0.06	°C	1st February 2012 to 31st January 2013
Soil temperature	1 and 2	+/-0.7	°C	1st March 2012 to 31st July 2012
Wastewater temperature	3 and 4	+/-0.1	°C	1st March 2013 to 28th February 2014
In-sewer air temperature	3 and 4	+/-0.1	°C	1st March 2013 to 28th February 2014
Soil temperature	3 and 4	+/-0.1	°C	1st March 2013 to 28th February 2014
Wastewater depth	1 and 2	+/- 0.003	m	1st March 2012 to 31st July 2012
Wastewater velocity	1 and 2	+/-0.03	m/s	1st March 2012 to 31st July 2012
Wastewater depth	3 and 4	+/- 0.003	m	1st February 2013 to 31st May 2013
Wastewater velocity	3 and 4	+/-0.03	m/s	1st February 2013 to 31st May 2013

4.3 Discussion of the Measured Data in Sewer Pipes

Ambient air temperature within 12km from Sites 1, 2, 3, and 4 varied between -0.7 and 25°C in the year 2012 as shown by Figure 4.3. This variation of ambient air temperature, obtained by Antwerp Council, presented a similar pattern to that of wastewater and in-sewer air temperature variations. However, the ambient temperature range was higher than that of the wastewater where the latter was between 7 and 22°C in both urban and large sites as shown by Figures 4.6 to 4.9. The daily upstream wastewater temperature and flow rate variations in urban sewer sites, during Monday 27th February 2012, reflect the behaviour of domestic hot water consumption by the local residents as illustrated by Figure 4.4. The latter figure considers dry weather flow rate. The characteristic of Site 1 plot in Figure 4.4 illustrates a natural drop in wastewater flow rate after midnight, which then starts to increase at around 6:00 AM when local residents begin to consume domestic hot water. This increase in wastewater flow rate causes an increase in wastewater temperatures an hour later (07:00 AM) which then lasts for around two hours (i.e. until around 09:00 AM). Apart from some short flow peaks during the day (27th February 2012) in Site 1, a noticeable increase in wastewater flow rate occurs in the evening (around 17:00) where demand on domestic hot water increases again by the local area. This is also followed by wastewater temperature increase, at Site 1, in a similar manner to that during the morning of the same day. Sites 1 and 2 showed similar patterns of wastewater flow and temperature variations during Monday 27th February 2012 as shown by Figure 4.4 , yet it is clear that Site 2 presented larger wastewater flow rates than that of Site 1. This is likely to be due to Site 2 collecting wastewater from a different catchment type to that of Site 1, which may involve industrial and or small businesses wastewater discharges.

The variation of wastewater flow rate and upstream temperatures in urban sewers during a summer day (Friday 1st June 2012) showed similar pattern to that of a winter day (Monday 27th February 2012) as shown by Figure 4.5. This is expected since both cases reflect consumption of domestic hot water during working days.

Large sewers have presented lower wastewater temperatures than those of urban sewers where Sites 3 and 4 showed a temperature range varying between 8°C and 20°C, as shown by Figure 4.8 and Figure 4.9 .

Measured wastewater temperatures in all sites are within the range found by Schilperoort and Clemens (2009), Hoes *et al.* (2009), and Cipolla and Maglionico (2014) who carried out their measurements in the Netherlands and Italy. It was observed that overall in-sewer air temperatures were lower than that of wastewater between the months of September and May in urban sewers. On the other hand, the large sewers have shown that in-sewer air temperatures were generally lower than that of wastewater throughout the year. This is likely due to the urban sewers being close to urban buildings and hence, influenced by the higher temperatures of foul discharges while the large sewers are far from the urban areas as shown by Figure 4.1. Heat transfer was taking place in all sewer pipes, proven by the temperature difference between wastewater temperatures at upstream and downstream ends. However, Site 4 has experienced the least average wastewater temperature variation along the sewer pipe profile showing a negligible difference, between wastewater temperatures at upstream and downstream ends. Temperature variation streamwise at Sites 1, 2 and 3 presented average wastewater temperature differences between upstream and downstream ends of 0.44, 0.20 and 0.19°C respectively. This shows that these three sites experienced an overall wastewater temperature drop streamwise. However, sewer pipe lengths differ and therefore one shall account for the corresponding pipe length when comparing wastewater temperature variation along sewer pipes. Hence, wastewater temperature variations per kilometre along sewer pipes were computed to be 0.95, 0.86, 0.18 and -0.01 all in °C/km for Sites 1, 2, 3 and 4 respectively. It is worth illustrating the probability density function (PDF) of the wastewater temperature variations per kilometre along Site 1, 2, 3 and 4 sewer pipes. Figure 4.27 shows the PDF of wastewater temperature variation streamwise (upstream minus downstream) per kilometre in Sites 1, 2, 3 and 4 for their measurement periods.

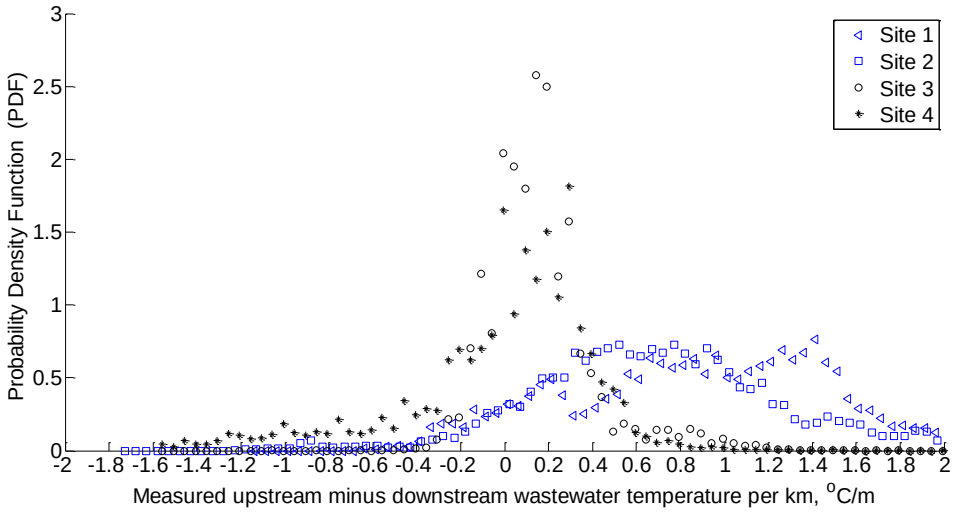

Figure 4.27: Probability distribution function (PDF) of measured wastewater temperature variation streamwise per kilometre for Sites 1, 2, 3 and 4.

It is clear from Figure 4.27 that wastewater temperature variation along the large sewer pipe profiles was different to that for the urban sewer. One can observe that the large sewers (Sites 3 and 4) presented higher probability for wastewater temperature drop between 0.1 and 0.2°C/km than those of urban sewers. On the other hand the urban sewers (Sites 1 and 2) have shown left skewed PDF, indicating higher probability for larger wastewater temperature drops per kilometre than that of large sewers. This suggests that the heat transfer process in sewer pipes differ depending on the scale of the wastewater flow rate. The variation of wastewater temperatures in the four sites was noticed to be influenced by the in-sewer air temperature. The local measured soil temperatures were generally within a close range to that of the wastewater, which also suggests that wastewater temperature is affected by the temperature of the local soil. Measured soil temperatures at 3.75m depth, in stations near Sites 1 and 2, have shown less variation (6.5°C to 16.5°C) than those measured at 1.5m depth in the same location (9.5°C to 13°C). This was expected as the soil temperature at 1.5m depth is more sensitive to ambient temperature than that at 3.7m depth. Soil temperatures measured near the large sewer at 3.7m depth showed a close range, of 7°C to 15.7°C, to that near the urban sewers measured at the same depth. Figure 4.13 shows that minimum (7°C) and maximum (15.7°C) soil temperatures occur in April 2013 and September 2013 respectively. This suggests that soil temperature at such depth (i.e. 3.7m) may be independent of

ambient temperature (Figure 4.3), assuming that years 2012 and 2013 show similar ambient temperature variations.

Influent temperature at the Antwerp WWTP, shown in Figure 4.1 was above 9°C and below 19°C. Despite the different measurement times, this range is close to that obtained in Sites 3 and 4 since the WWTP is few kilometres from these sites.

Urban sewers showed a similar pattern of wastewater flow rate variation that reflects the rainfall events in the region. The rainfall events, in urban sewers, were found to be occurring only 10% of the measurement time. This was found by quantifying the number of data points of both rainfall events and DWF. The scale of DWF in the large sewers was also close to that of large sewers where rainfall events in the latter were also occurring around 10% of the flow measurement time. Average DWF in Site 3 was almost 3 times that of Site 4, yet both sites experienced relatively high flow rates to reflect the nature of main sewer collectors. A large drop in Site 3 wastewater flow rate was noticed, shown by Figure 4.17, to take place between 16th and 23rd March 2013. This was unusual interruption to the flow pattern shown in Site 3 by Figure 4.17. This may be due to some issues with the flow sensor during this period. It was also noticed from Figure 4.17 and Figure 4.18 that the large sewers (Site 3 and 4) have presented larger wastewater flow rates in February 2013 than that in other months. This might be due to snow being melted at a low rate. Wastewater depths in urban and large sewer sites reflect the rainfall events in a similar pattern to that of flow rates as shown by the depth peaks in Figure 4.23, Figure 4.24, Figure 4.25 and Figure 4.26 for Sites 1, 2, 3 and 4 respectively. The large sewers presented some peak depths that are mostly wider, in terms of timescale (horizontal axes), than that of urban sewers. The larger widths of these peak depths, shown by Figure 4.25 and Figure 4.26 for Sites 3 and 4 respectively, are likely due to the time taken for the large sewers to discharge the rainfall runoff. It was noticed that February 2013, in Sites 3 and 4, has usually presented longer time (2 days) to discharge the large sewers than other months that required around 1 day to discharge the rainfall runoff. This may also be due to snow melting in the local area as mentioned earlier.

Wastewater temperature sensors with an accuracy of up to +/-0.1 °C, were found to be reasonable for implementation in such field work conditions. Onsite checking of the hydraulic sensors (Isco 2150 area velocity type meter) adds the

advantage of enhancing the accuracy of flow, velocity and depth measurements. More details on the impact of sensor accuracy on the modelled wastewater temperature is discussed in Section 5.4. The measured wastewater temperatures and flow rates presented realistic values, proven by the patterns of wastewater flow rates and temperatures in winter and summer days that match the expected daily water consumption in the local areas. The measured wastewater temperatures for longer periods (yearly basis) illustrated similar patterns to those measured by Antwerp council which also reconfirms the validity of the measured temperatures in sewers. Measured wastewater temperatures were also close to those found in literature. Therefore, measured data shown in this chapter is reliable enough to be utilised for calibration and validation as will be explained in Chapter 5. The minimum influent temperature of 9°C suggests that heat recovery from sewers may be viable as long as the influent temperature does not drop below 9°C. Measured data in urban and large sewers presented different heat transfer behaviours, proven by lower temperature variations along pipe profiles in large sewers. Hence, this shall be considered when calibrating the sewer pipe model as will be explained in Chapter 5.

5 Calibration and Validation of the Sewer Pipe Model

This chapter is dedicated to calibrating some of the key unmeasured heat transfer parameters in sewers. Key parameters are identified through a sensitivity analysis of the unmeasured parameters involved in the sewer pipe model. The chapter also utilises independent datasets to validate the calibrated model.

Heat transfer in sewers is a complex process as it involves a number of different physical processes that can be described by several equations and requires a number of parameters that may prove challenging to measure or find in published literature. These parameters include heat transfer coefficient between wastewater and in-sewer air (h_{wa}), soil penetration depth (d_s), thermal conductivities of sewer pipe materials (k_p) and the surrounding soil (k_s). To the best of the author's knowledge, the available technical literature contains a limited amount of research work on the values of these parameters for wastewater in sewerage applications. Dürrenmatt (2006) and Dürrenmatt and Wanner (2008 & 2014) implemented information obtained from a study done by Flinspach (1973) to estimate h_{wa} as a function of the relative wastewater to in-sewer air velocity multiplied by a factor of 5.85 as shown in Equation 3.30. In order to enhance the accuracy of the sewer pipe model developed in Section 3.3.2, unmeasured model parameters need to be calibrated. The abundancy of measured data in this study that includes wastewater flow rates and temperatures of soil, in-sewer air and wastewater, strengthens the calibration quality and enables the validation of calibrated parameters. Two methods were implemented to calibrate the parameters mentioned above, these are a Matlab optimisation function and an optimisation by division method utilising Matlab 'for loop' codes.

This chapter shows the process followed for calibrating the heat transfer parameters used in this work for both urban and large sewers at different periods as will be illustrated in Section 5.1. The chapter then identifies the key heat transfer parameters to be considered for calibration through a sensitivity analysis, which forms part of the calibration process (Section 5.1). Results obtained from both optimisation methods are explained in Section 5.2 showing relevant probability density functions (PDFs) for modelling errors (measured minus modelled values), contour plots of root mean square error (RMSE) and standard deviation values. The calibrated parameter values are shown in Section 5.2.3, along with a summary of all RMSE and standard deviation values for calibrated

and validated models. The findings of calibration and validation are discussed in Section 5.3.

5.1 Process of Calibrating and Validating the Sewer Pipe Model for Urban and Large Sewers

Calibrating and validating the sewer pipe model was based on the mechanism of heat transfer in sewer pipes (Section 3.3.2) which is described by Equation 3.31. Measured data, shown in Chapter 4, was utilised for implementing Equation 3.31, while T_{air} in the equation above was assumed to be the average of upstream and downstream in-sewer air temperatures. The steps followed to calibrate and validate the sewer pipe model can be summarised below, while Figure 5.1 illustrates the process followed. More details of each step is provided afterwards (Sections 5.1.1 to 5.1.8) with the aid of figures.

1. Identify the most relevant calibrating parameters.
2. Investigate the impact of varying the number of mesh points and the size of time step on calibration results. Impact, in this context, is measured through the root mean square error (RMSE) of the difference between measured and modelled downstream wastewater temperatures. Equation 5.1 was implemented to compute RMSE for temperatures in one pipe at N time steps.

$$RMSE = \sqrt{\sum_{j=1}^{j=N} \frac{(T_{Measured\ DS\ \ j} - T_{Modelled\ DS\ \ j})^2}{N}} \quad (5.1)$$

T is the wastewater temperature (°C) while DS stands for Downstream. N is the total number of time steps (or data points), j is data point number.

3. Determine a range for each calibrating parameter.
4. Apply Matlab optimization functions (fminsearch, fmincon and fminunc) for optimising the calibrating parameters using the identified range in the step above where applicable. Use the most appropriate optimisation function for the sewer pipe model. The optimisation target is to minimise the difference between measured and modelled wastewater temperatures. Therefore, interpreting this target through Matlab optimisation function can be achieved by minimising the absolute norm of temperature difference between

measured and modelled downstream wastewater temperatures (V), which can be expressed by Equation 5.2.

$$|V| = 0 \tag{5.2}$$

Where

$$\{V\} = \{Measured_{DS_{WW}} - Modelled_{DS_{WW}}\} \tag{5.3}$$

DS denotes for downstream while WW stands for wastewater.

5. Plot probability density functions (PDF) of the difference between measured and modelled downstream wastewater temperatures for each site at each month.
6. Obtain the root mean square errors (RMSE) of modelled wastewater temperature at the downstream end, using Equation 5.1.
7. Obtain the population standard deviation (σ) values, using Equation 5.4, for each site and month.

$$\sigma = \sqrt{\frac{1}{N}\sum_{j=1}^{N}(\Delta T_i - \overline{\Delta T})^2} \tag{5.4}$$

σ is population standard deviation for the difference between measured and modelled wastewater temperatures at the downstream ends of pipes (°C), N is total number of time steps (or data points) in the month, j is data point number, ΔT is difference between modelled and measured wastewater temperatures at downstream ends (°C). $\overline{\Delta T}$ is the monthly average difference between modelled and measured wastewater temperatures at the downstream ends (°C).

8. Implement the method of optimisation by division, to investigate the potential of improving the RMSE obtained through Matlab optimisation functions, in step 4 (page 65), using the same range identified in step 3 (page 65).
9. Compare calibration results achieved through Matlab optimisation function with that carried out by implementing the 'optimisation by division' method.

Before explaining the steps followed to calibrate the parameters associated with the partially filled pipe model, it is worth mentioning that the model can be calibrated using data from urban sewers (DWF between 0.008 and 0.01 m^3/s or 28 and 39 m^3/hour) and large sewers (DWF greater than 0.09 m^3/s or 330 m^3/hour). The heat transfer mechanism may prove to be different in urban to that in large sewers, as concluded from Chapter 4, and hence calibrating parameters may show different values for each sewer type. The different heat transfer mechanism for urban sewer to that of large sewers was also the findings from a predictive model developed by Abdel-Aal *et al.* (2015), who used abductive networks to predict wastewater temperatures in urban and large sewers. Hence, calibration was carried out for urban and large sewers separately using the same methodology. Therefore, one site was selected randomly from each category (i.e. urban and large) while the other is utilised for validation. Referring back to Chapter 4, Site 2 data will be utilised for calibrating the sewer pipe model for urban sewers, which leaves Site 1 data for validating the calibrated parameters using urban sewers as shown by Table 5.1. The large sewer data in Site 3 will be used for calibrating the sewer pipe model for large sewers while Site 4 data will be employed for validating the large sewer calibrated parameters. Sites 1, 2, 3 and 4 details are shown in Table 5.1 while Figure 5.1 illustrates the process followed for calibrating the sewer pipe model.

Table 5.1: Urban and large sewer sites used for calibrating the sewer pipe model. Highlighted rows indicate site data used for calibration while site data from the other rows used for validation.

Site	Used for	Type	Data availability from to (inclusive)	Average DWF across all periods (m^3/s)	(m^3/hour)	Pipe length (m)	Pipe thickness (m)	Pipe diameter (m)	Material	Shape
1	Validation	Urban	March to July 2012	0.008	28	464	0.14	1.2	Concrete	Circle
2	Calibration	Urban		0.01	39	232	0.14	1.2	Concrete	Circle
3	Calibration	Large	February to May 2013	0.36	1300	1031	0.14	1.2	Concrete	Circle
4	Validation	Large		0.09	330	749	0.12	0.7	Concrete	Circle

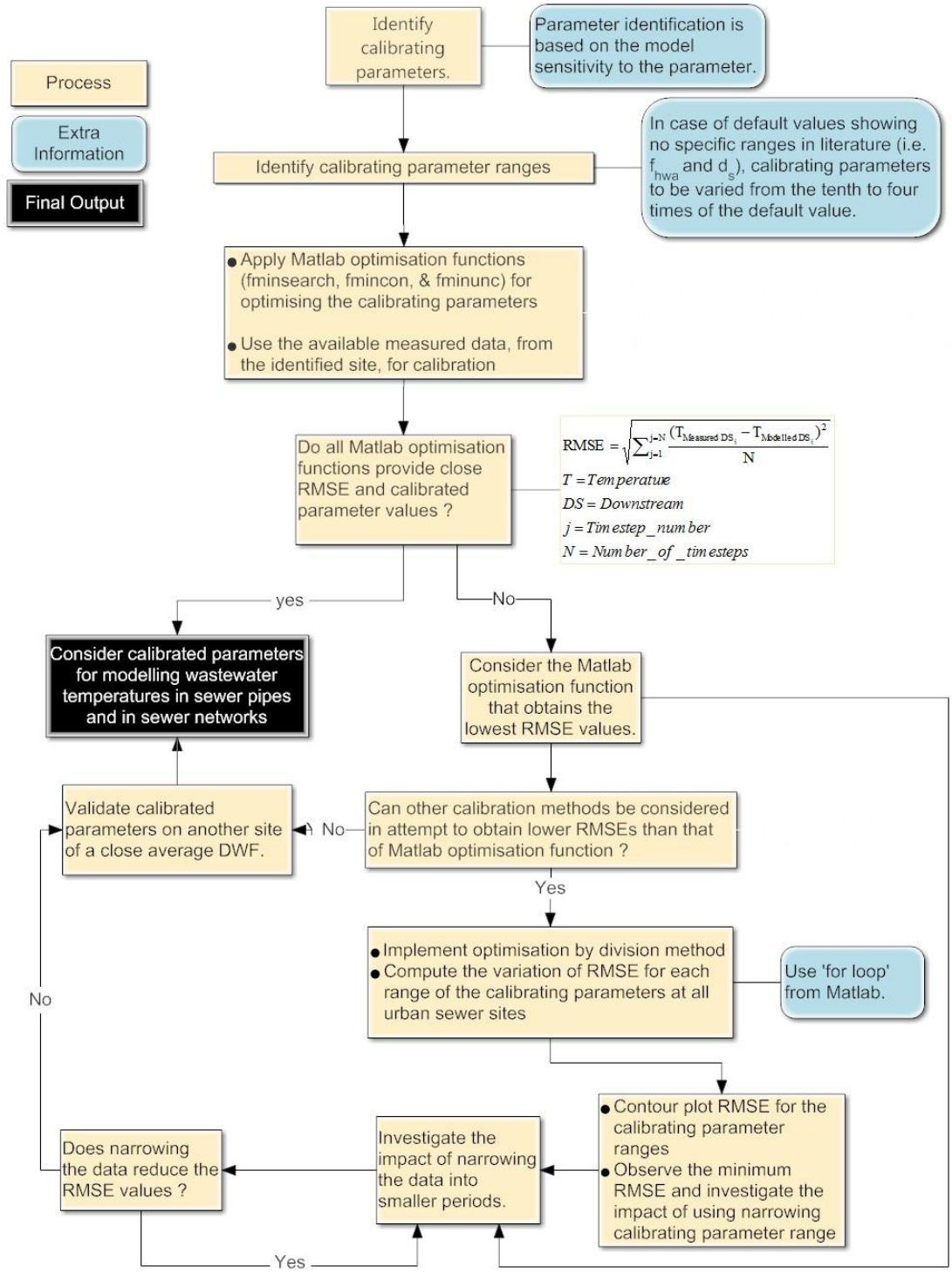

Figure 5.1: Illustration of the process followed for calibrating the sewer pipe model.

The steps followed for calibrating the sewer pipe model are explained in more details in Sections 5.1.1 to 5.1.8.

5.1.1 Identify the Most Relevant Calibrating Parameters.

Method: This is based on examining the model sensitivity to a parameter and the ability to measure it. Referring to Equation 3.31, one can realise that the predicted wastewater temperature variation along a sewer pipe profile can be expressed as a function of pipe and soil thermal conductivities, the convective heat transfer coefficient between wastewater and in-sewer air, sewer temperature, and wastewater flow rate, as shown by Equations 5.5 to 5.8. All notations for these equations are described in Table 5.2.

$$T_{m+n} = f\left(R_{wa}, T_{air}, R_{ws}, T_{soil}, \rho, Q, c_p\right) \quad (5.5)$$

$$R_{wa} = f(h_{wa}, b), h_{wa} = f(f_{hwa}, u_{wa}) \quad (5.6)$$

$$u_{wa} = f(u_w, u_a) \quad (5.7)$$

$$R_{ws} = f\left(k_p, t_p, k_s, d_s, wet.p\right) \quad (5.8)$$

Table 5.2: Explanation of notations shown in Equations 5.5, 5.6, 5.7 and 5.8.

Symbol	Unit	Description
B	m	Wastewater free surface width
c_p	J/kg.K	Specific heat capacity
d_s	m	Soil penetration depth.
f_{hwa}	-	Heat transfer coefficient factor. More details is explained later in this section (page 85)
H	W/m^2.K	Convective heat transfer coefficient
K	W/m.K	Thermal conductivity
N	-	Number of increments in a sewer pipe
P	-	Pipe
Q	m^3/s	Volumetric flow rate
R	m.K/W	Thermal resistivity
S	-	Soil
T	K	Temperature
t_p	m	Pipe wall thickness
T_m	K	Wastewater temperature at the upstream end of a sewer pipe
u_a	m/s	In-sewer air velocity
u_w	m/s	Wastewater velocity
u_{wa}	m/s	Relative wastewater velocity to that of in-sewer air
wa	-	Wastewater and in-sewer air
wet.p	m	Wetted perimeter
ws	-	Wastewater and soil
P	kg/m^3	Wastewater density

Soil temperature (T_{soil}), wastewater volumetric flow rate (Q), wastewater velocity (u_w) and wastewater depth (d_w) were measured while in-sewer air temperature (T_{air}) is the average of measured upstream and downstream in-sewer air temperatures. Values of wastewater free surface width (b) and wetted perimeter (wet.p) were computed based on wastewater depths and pipe diameters. Therefore, the parameters that were not measured or calculated are wastewater density (ρ), specific heat capacity for wastewater (c_p), convective heat transfer coefficient between wastewater and in-sewer air (f_{hwa}), pipe and soil thermal conductivities (k_p & k_s) and soil penetration depth (d_s). In order to identify the calibrating parameters, a sensitivity analysis was carried out on all unmeasured parameters of the sewer pipe model. The specific heat capacity for wastewater (c_p) and wastewater density are constant values and hence were excluded from the sensitivity analysis. Wastewater density was assumed to be that of water (1000kg/m^3) as in Metcalf and Eddy (2004). The value of c_p for wastewater was also assumed to be that of water (41800 to 4200 J/kg.K) which was used in previous studies (e.g. Shizas and Bagley (2004)). The sensitivity analysis was achieved by varying each unmeasured parameter within its range found in literature or in case the parameter has no specific range, i.e. penetration depth (d_s) and heat transfer coefficient factor (f_{hwa}), sensitivity of the model was tested against a range from 0.1 to 4 times their default values retrieved from published literature. The range from 0.1 to 4 was chosen arbitrarily to reflect the impact of low and high values for d_s and f_{hwa}. Since in-sewer air flow direction is influenced by atmospheric pressure, in-sewer air was assumed to be able to travel in both directions. Therefore, u_{wa} in Equation 3.30, which is the relative wastewater velocity (u_w) to that of in-sewer air (u_a), can be given by either Equation 5.9 or Equation 5.10 for in-sewer air flowing streamwise or in opposite directions respectively.

$$u_{wa} = u_w - u_a \tag{5.9}$$

$$u_{wa} = u_w - (-u_a) \tag{5.10}$$

Table 5.3 shows the ranges used for each calibrating parameter.

Table 5.3: Parameter ranges used for the sensitivity analysis (SA).

Parameter	Values in literature	Default	Range used for SA	Unit	Notes / References
f_{hwa}	5.85	5.85	0.58 : 23.40	-	Assumed to vary from 0.1 to 4 times default value from Dürrenmatt and Wanner (2014). More details is explained in Section 5.12 (page 85).
u_a	0.00 : 0.50	0.25	-0.50 : 0.50	m/s	Default range from Parker and Ryan (2001), and Madsen, Hvitved-Jacobsen and Vollertsen (2006). u_a was considered for air flowing in similar and opposite directions to that of wastewater.
k_s	0.24 : 2.50	1.37	0.24 : 2.50	W/m.K	(Mitchell and Soga, 1993).
k_p	0.60 : 1.40	1.00	0.60 : 1.40	W/m.K	(Incropera *et al.*, 2007).
d_s	0.01:1.00	0.50	0.04:2.00	m	Assumed to vary from 0.1 to 4 times default value from (Dürrenmatt and Wanner, 2014).

Each parameter shown in Table 5.3 was varied, within its range, while all other parameters were fixed at their default values. Temperature of wastewater at the downstream end was computed and compared with that estimated using the default values. Theses default values are referred to as 'Default' in Table 5.3 and relate to $T_{Default}$ in Equation 5.11. The sensitivity of the model was measured by the difference between the computed wastewater temperatures, using the identified parameter ranges in Table 5.3 ($T_{parameter\ range}$), and that computed using the default values as shown by Equation 5.11.

$$Impact\ on\ T = \sum_{j=1}^{j=N} \frac{T_{parameter\ range_j} - T_{Default_j}}{N} \quad (5.11)$$

T is wastewater temperature at the downstream end (°C). j is data point number for each time step. N is the total number of time steps (or data points), which was around 720 for a day based on data measurement frequency of 2 minutes. $T_{parameter\ range_j}$ *is the modelled downstream wastewater temperature (°C), at each data point (j), using the identified parameter ranges, named 'Range used for SA' in Table 5.3.* $T_{Default}$ *is the modelled wastewater temperature (°C) at the downstream end, using the identified default parameters for each data point (j).*

Matlab software was implemented using the 'for loop' code to vary each parameter within its range identified in Table 5.3. Heat transfer in urban sewers may behave differently from large sewers, which was concluded from Chapter 4 and by Abdel-Aal *et al.* (2015) using their predictive method to predict wastewater temperatures in urban and large sewers. Therefore, this sensitivity analysis was carried out on urban and large sewers independently using data from early March and late May to reflect cold and warmer climates using the available data, as shown by Table 5.1. Data from working days (Monday to Friday) with dry weather flow (DWF) was selected for the sensitivity analysis. The measured wastewater flow rate data, illustrated in Section 4.2, showed that dry weather flows (DWF) events occur most of the measurement period (around 90% of the time), yet the large sewers have experienced less DWF days (around 40% of the time) in May 2013. Therefore, it was difficult to find DWF data during May 2013 in the large sewers.

The sensitivity analysis carried out using urban sewer data (Site 1) on 1st March 2012 is shown by Figure 5.2. The top plot of Figure 5.2 illustrates sensitivity for parameters with assumed ranges, i.e. f_{hwa} and d_s, as they have no specific ranges available in published literature, while the bottom plot of Figure 5.2 shows the sensitivity of k_s, u_a and k_p using the ranges retrieved from literature. This approach of plotting provides a fair like to like comparison and was followed for Sites 1 and 3 data during March and May.

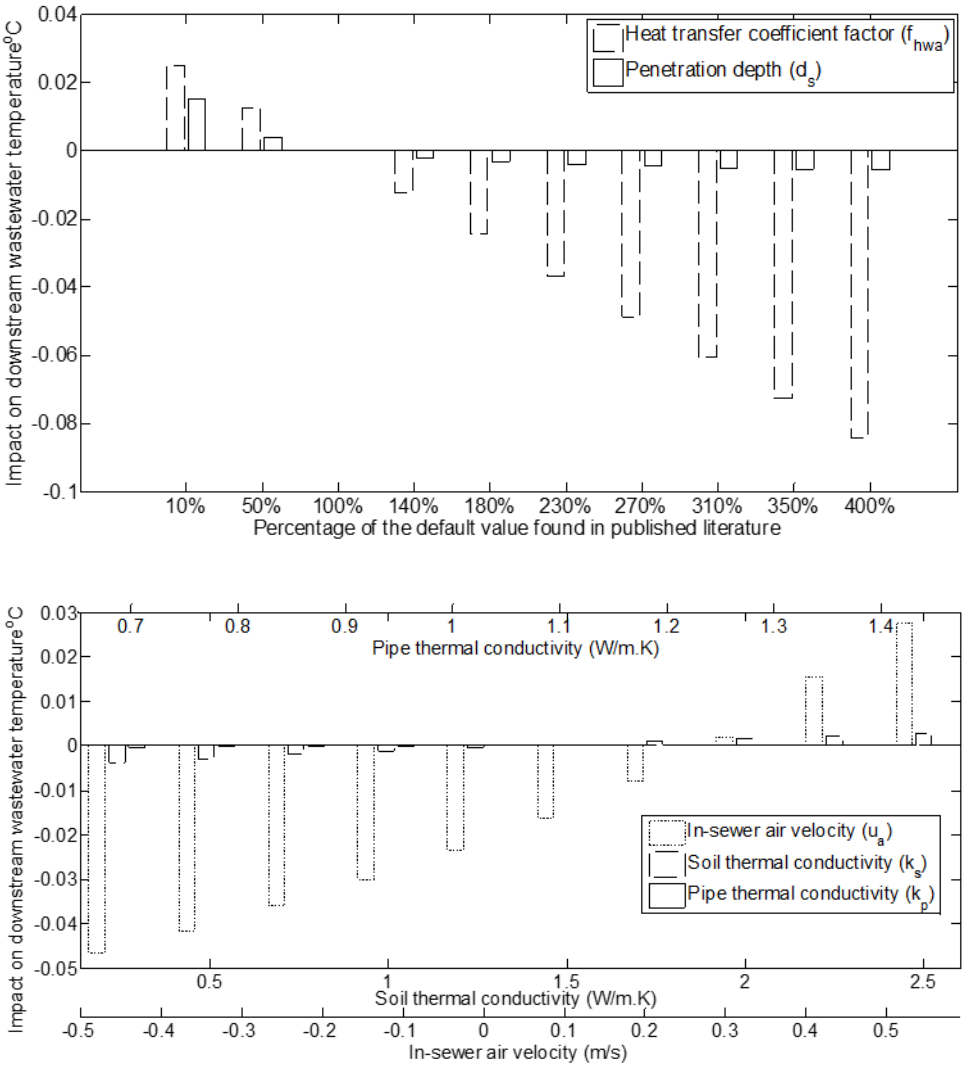

Figure 5.2: Sensitivity analysis, using urban sewer (Site 1) data on 1st March 2012, for the unmeasured parameters in the sewer pipe model. Top plot shows the impact of varying f_{hwa} and d_s using their assumed ranges while the bottom plot illustrates the impact of varying u_a, k_s and k_p within their default ranges found in literature. All parameter ranges are shown in Table 5.3.

One can notice, from Figure 5.2, that the pipe thermal conductivity proved to have the smallest impact on the modelled downstream wastewater temperatures, in the urban sewer, during 1st March 2012.

The sensitivity analysis was also carried out on data from warmer weather using urban sewer data (Site 1) obtained on the 31st May 2012 as shown by Figure 5.3. The top plot of Figure 5.3 illustrates sensitivity for parameters with assumed ranges, i.e. f_{hwa} and d_s, as they have no specific ranges available in published literature, while the bottom plot of Figure 5.3 shows the sensitivity of k_s, u_a and k_p using the ranges retrieved from literature.

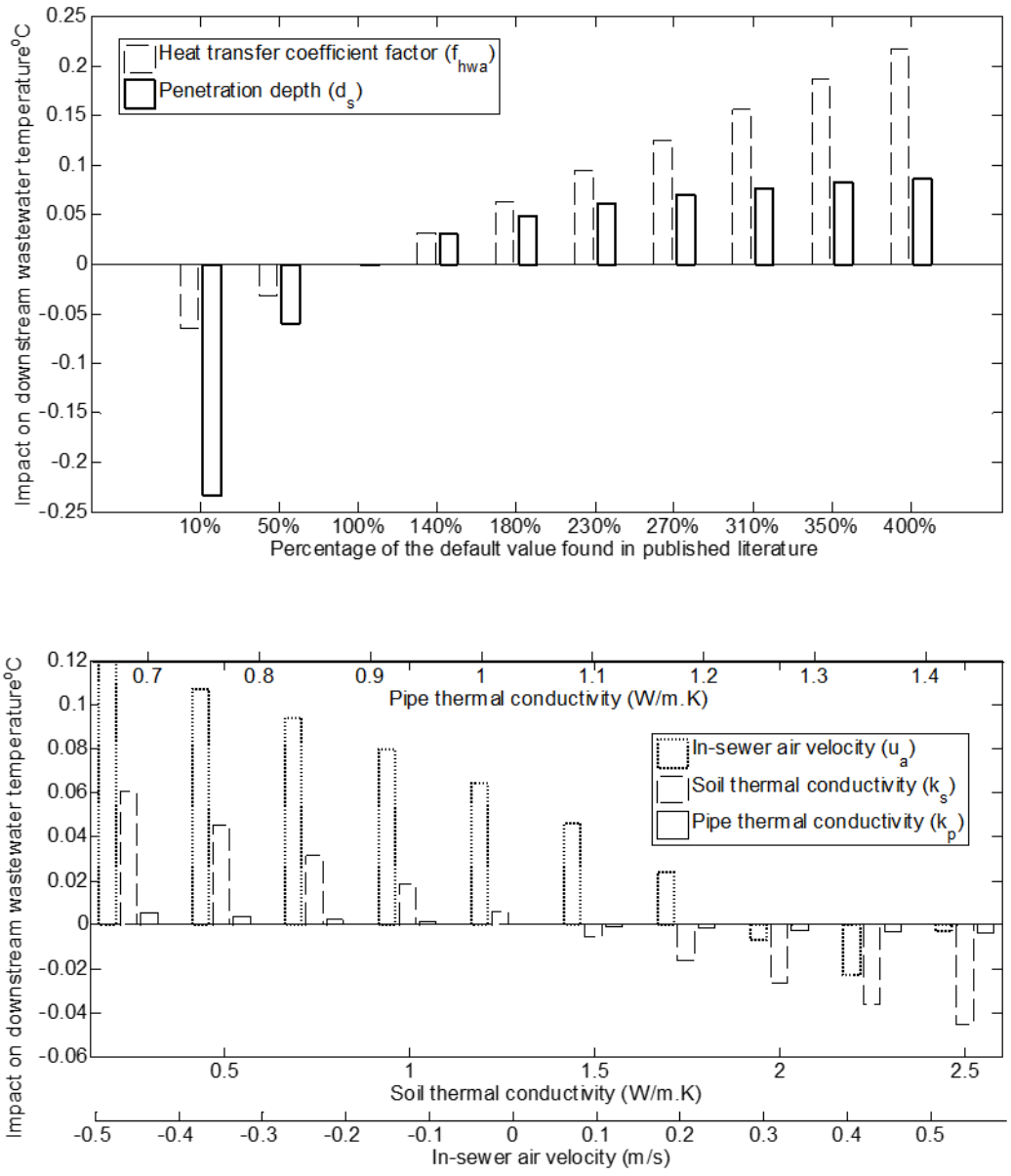

Figure 5.3: Sensitivity analysis, using urban sewer (Site 1) data on the 31st May 2012, for the unmeasured parameters in the sewer pipe model. Top plot shows the impact of varying f_{hwa} and d_s using their assumed ranges while the bottom plot illustrates the impact of varying u_a, k_s and k_p within their default ranges found in literature. All parameter ranges are shown in Table 5.3.

Pipe thermal conductivity was also proven to have the smallest impact on the modelled downstream wastewater temperatures, in the urban sewer, during the 31st May 2012 as shown by Figure 5.3. However, the impacts of penetration depth (d_s) and soil thermal conductivity (k_s) on the downstream wastewater temperatures was different in March to that in late May at the urban sewer. In order to investigate the impact of using longer periods of data (more data points)

on the modelled wastewater temperature, the sensitivity analysis was carried out over the last week of May 2012 using the urban sewer data (Site 1), as shown by Figure 5.4.

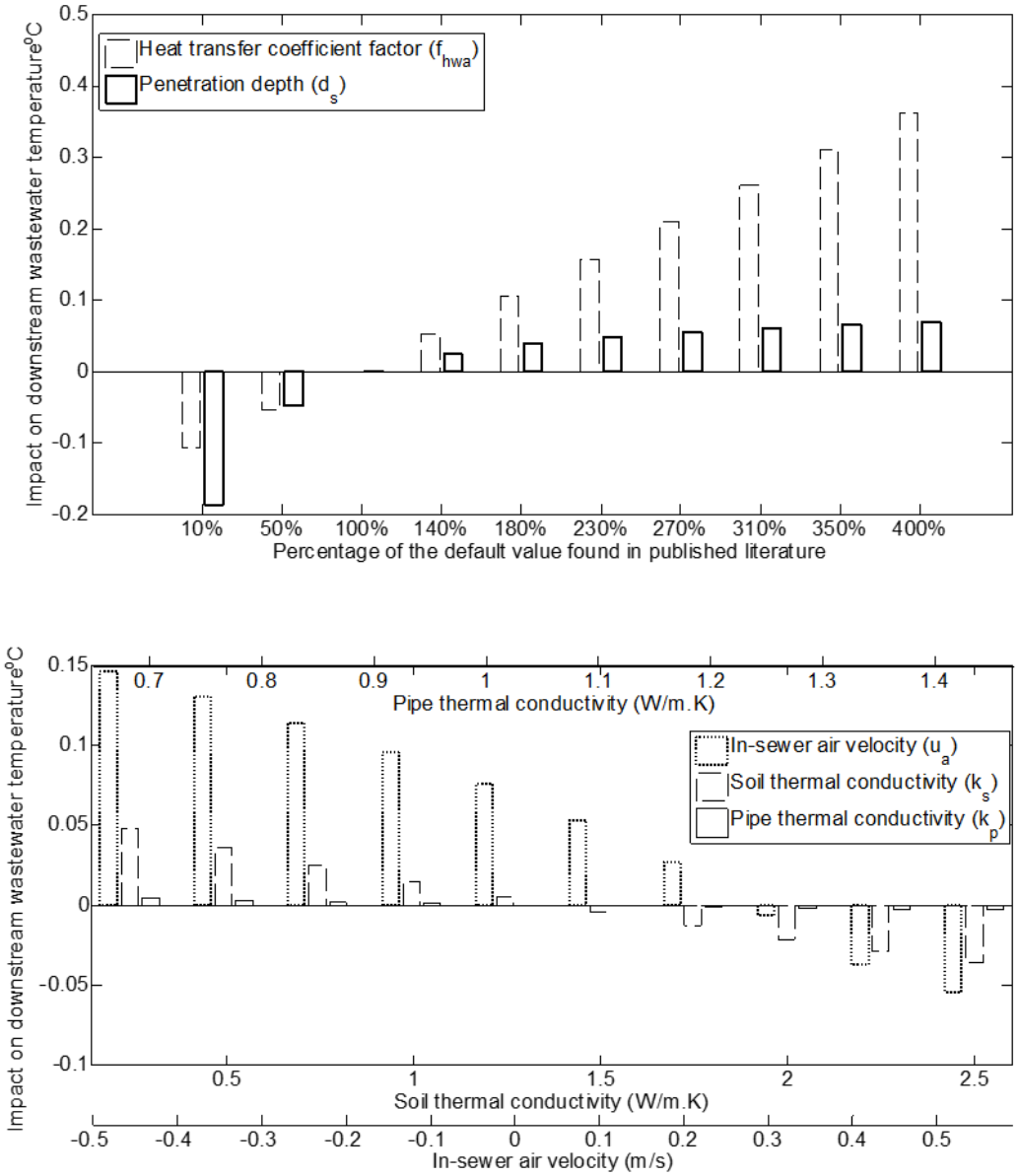

Figure 5.4: Sensitivity analysis, using urban sewer (Site 1) data on the last week of May 2012, for the unmeasured parameters in the sewer pipe model. Top plot shows the impact of varying f_{hwa} and d_s using their assumed ranges while bottom plot illustrates the impact of varying u_a, k_s and k_p within their default ranges found in literature. All parameter ranges are shown in Table 5.3.

The last week of May 2012 in urban sewers provided close sensitivity analysis results to that of 31st May 2012 which can be observed from Figure 5.3 (31st May)

and Figure 5.4 (last week of May). Therefore, datasets recorded on one day periods, at different Months, were considered for the sensitivity analysis.

Sensitivity analysis was also carried out using the large sewer data in a similar manner to that achieved for urban sewers. Figure 5.5 shows the sensitivity analysis performed using data from the large sewers (Site 3) obtained on 1st March 2013. The top plot of Figure 5.5 illustrates the sensitivity for parameters with assumed ranges, i.e. f_{hwa} and d_s, while the bottom plot of Figure 5.3 shows the sensitivity of k_s, u_a and k_p using the ranges retrieved from literature.

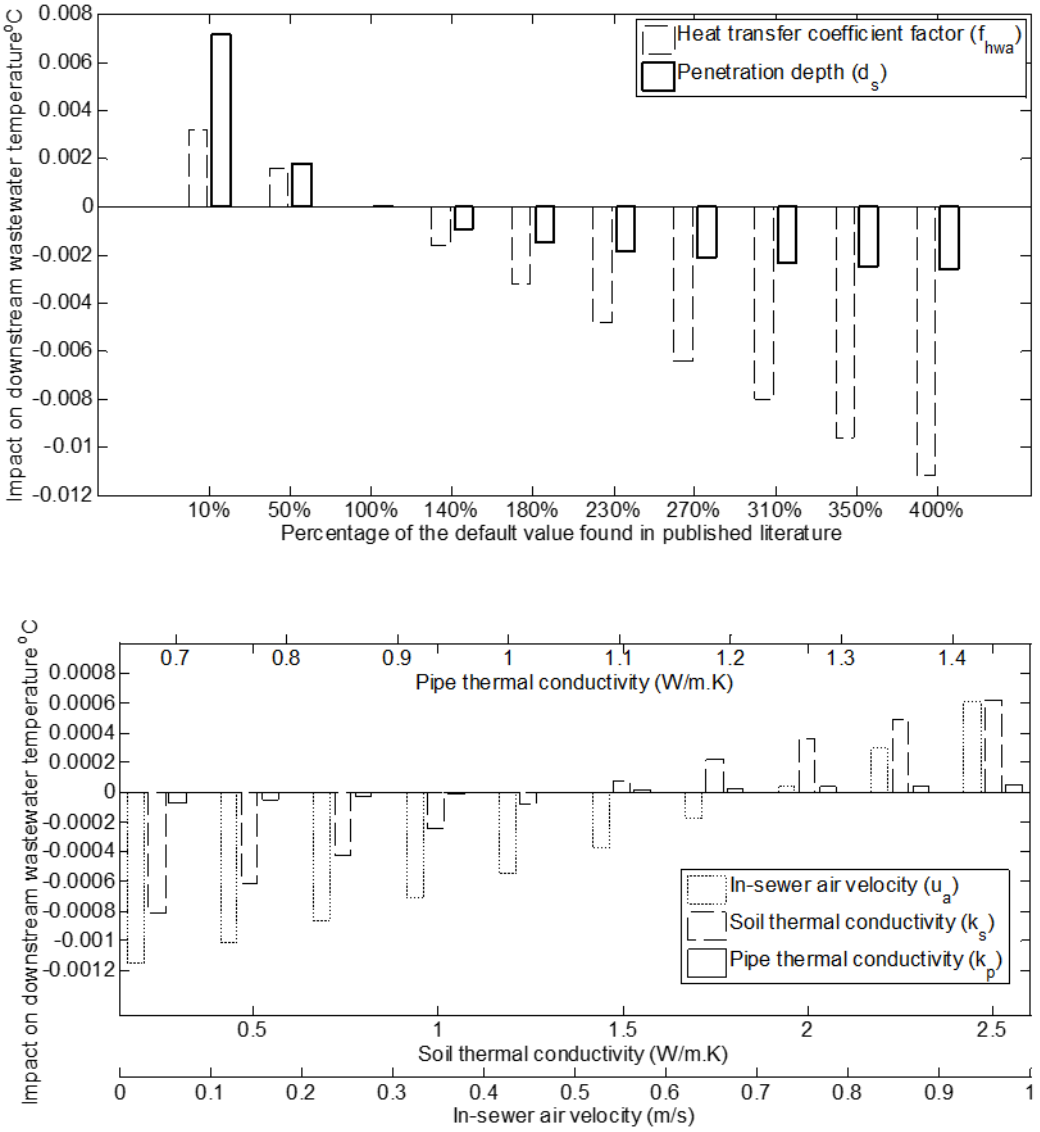

Figure 5.5: Sensitivity analysis, using large sewer (Site 3) data on 1st March 2013, for the unmeasured parameters in the sewer pipe model. Top plot shows the impact of varying f_{hwa} and d_s using their assumed ranges while the bottom plot illustrates the impact of varying u_a, k_s and k_p within their default ranges found in literature. All parameter ranges are shown in Table 5.3.

Figure 5.6 shows the sensitivity analysis carried out using data from the large sewers (Site 3) obtained on the 31st May 2013. The top plot of Figure 5.6 illustrates the sensitivity for parameters with assumed ranges, i.e. f_{hwa} and d_s, while the bottom plot of Figure 5.6 shows the sensitivity of k_s, u_a and k_p using the ranges retrieved from literature.

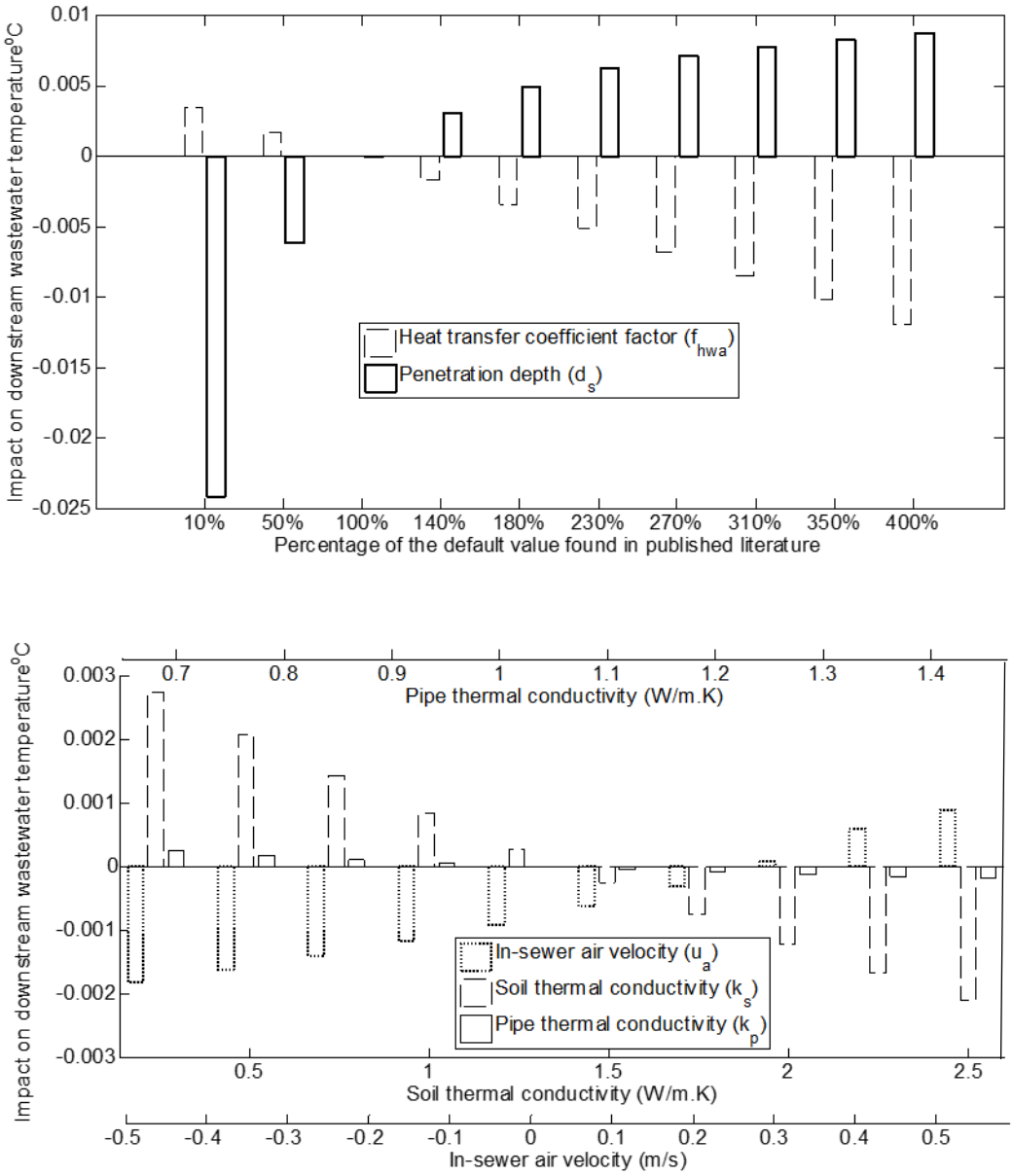

Figure 5.6: Sensitivity analysis, using large sewer (Site 3) data on the 31st May 2013, for the unmeasured parameters in the sewer pipe model. Top plot shows the impact of varying f_{hwa} and d_s using their assumed ranges while the bottom plot illustrates the impact of varying u_a, k_s and k_p within their default ranges found in literature. All parameter ranges are shown in Table 5.3.

Observing the characteristics of the sensitivity analysis plots for urban (Site 1) and large (Site 3) sewers, the pipe thermal conductivity proved to have the smallest impact on the modelled downstream wastewater temperatures, in urban and large sewers as shown by Figures 5.2, 5.3, 5.5 and 5.6. The impacts of penetration depth (d_s) and soil thermal conductivity (k_s) on the modelled downstream wastewater temperatures were different in March to that in late May in the urban and large sewers. This is likely due to the change in wastewater and soil temperatures at different months. Heat transfer coefficient factor (f_{hwa}) and in-sewer air velocity (u_a) had also shown different impacts on modelled wastewater temperatures in urban sewers during March and May periods as shown by Figure 5.2 and Figure 5.3. Therefore, in order to understand the impacts of d_s, k_s, f_{hwa} and u_a on the modelled downstream wastewater temperatures, during different months, it is worth demonstrating temperature differences between wastewater and soil and between wastewater and in-sewer air in urban and large sewers during March and May periods. Figure 5.7 shows the temperature differences between wastewater and in-sewer air and between wastewater and soil, for urban sewers during 1st and 2nd March 2012.

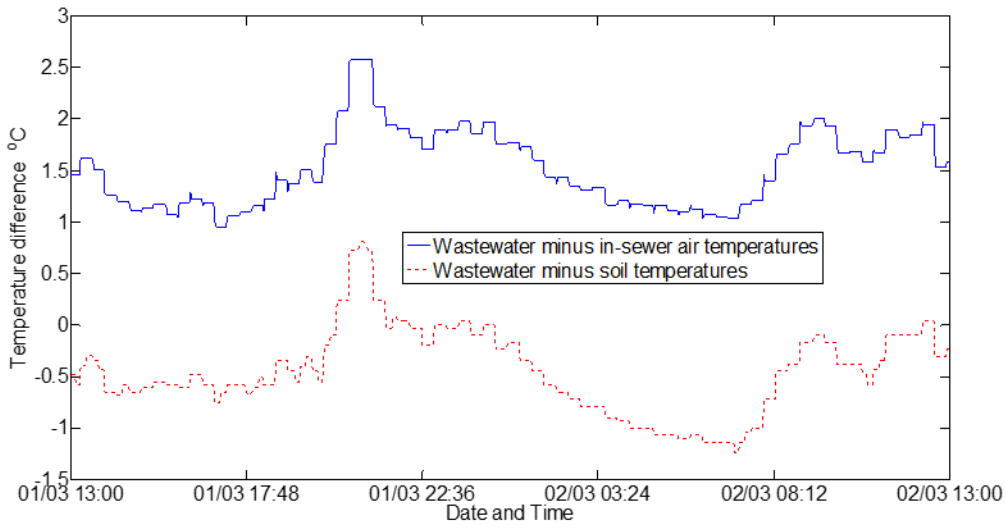

Figure 5.7: Temperature differences in the urban sewer (Site 1) recorded on 1st and the 2nd March 2012. This data was used for the sensitivity analysis.

Figure 5.8 shows the temperature differences between wastewater and that of in-sewer air and soil, for the urban sewer (Site 1) on late May 2013 and early June 2012.

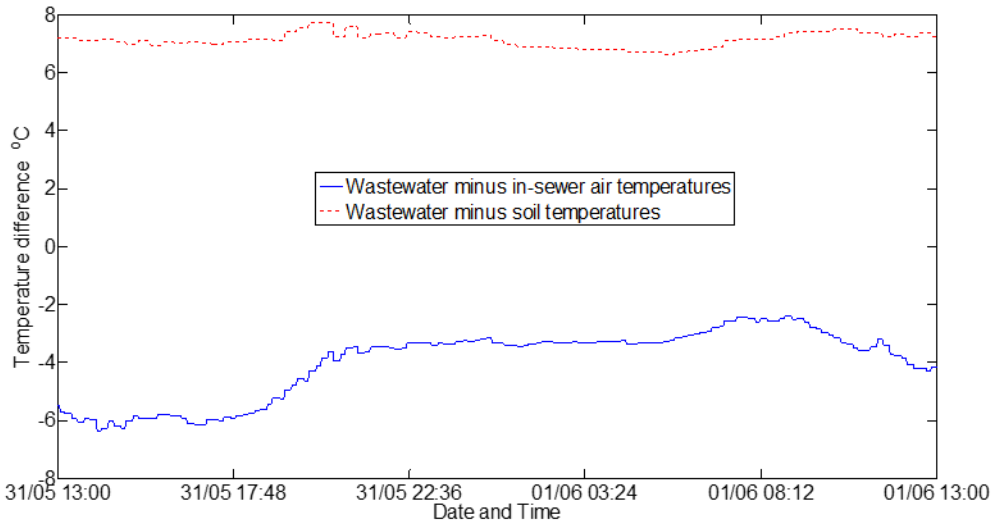

Figure 5.8: Temperature differences in the urban sewer (Site 1) recorded on 31st May 2012 and 1st June 2012. This data was used for the sensitivity analysis.

It is clear from Figure 5.7 and Figure 5.8 that Site 1 temperature differences between wastewater and in-sewer air and between wastewater and soil were different during 1st March 2012 to those obtained for 31st May 2012 period. The temperature differences between wastewater and soil and between wastewater and in-sewer air were also plotted for the large sewers. Figure 5.9 shows these temperature differences during 1st and 2nd March 2013 in the large sewer (Site 3).

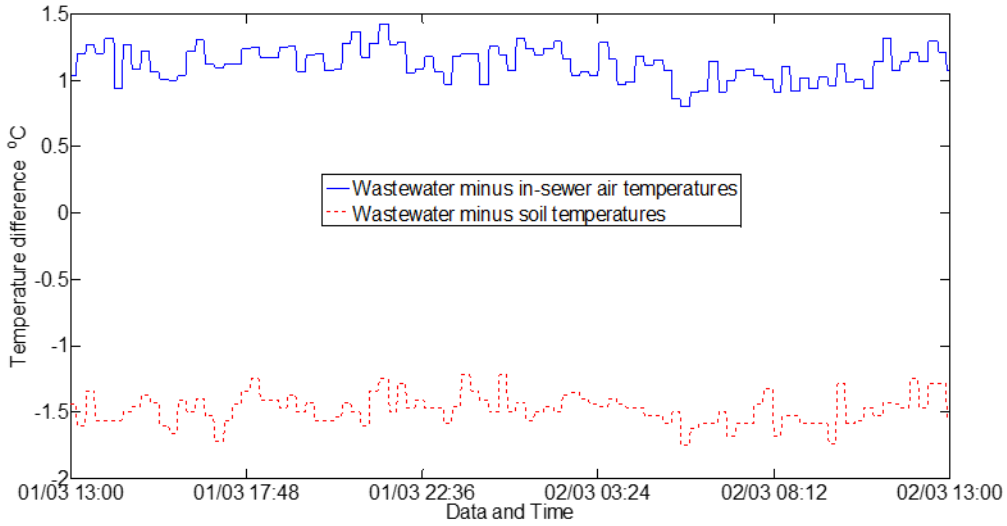

Figure 5.9: Temperature differences in the large sewer (Site 3) recorded on 1st and 2nd March 2013. This data was used for the sensitivity analysis.

Figure 4.10 shows the temperature differences between wastewater and soil and between wastewater and in-sewer air during late May 2013 and early June 2013 in the large sewer (Site 3).

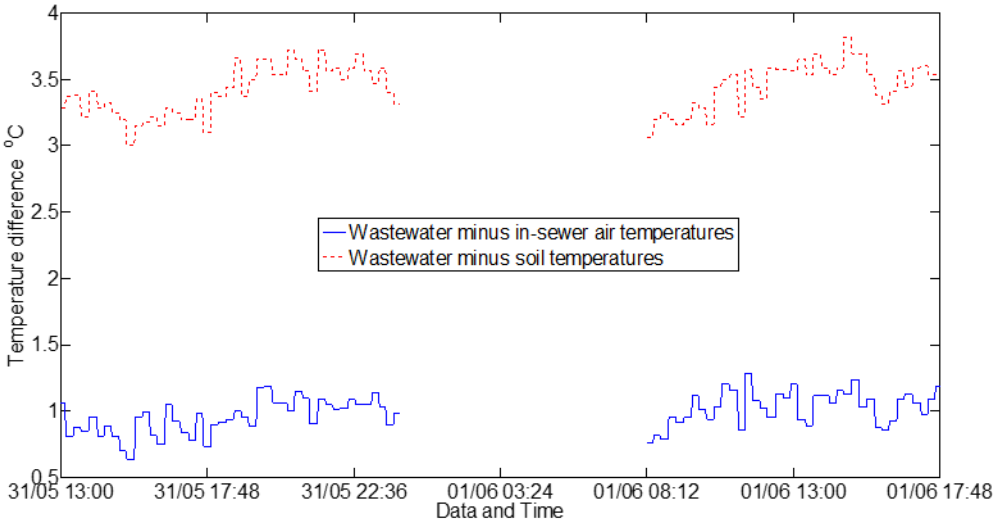

Figure 5.10: Temperature differences in the large sewer (Site 3) on 31st May 2013 and 1st June 2013. This data was used for the sensitivity analysis. The gap in the plot means missing data.

As previously observed from the temperature differences in the urban sewer during March 2012 and May 2012 (Figure 5.7 and Figure 5.8), the large sewer (Site 3) has also presented a similar case, where the temperature differences between wastewater and soil and between wastewater and in-sewer air in March (Figure 5.9) are different to those obtained from May data (Figure 4.10). These different behaviours in both large and urban sewers are expected as they reflect the measured soil, in-sewer air and ambient temperature in March and May (Section 4.1). The impact of these variations on the modelled downstream wastewater temperature in March and May, using the urban and large sewers' data, is discussed further in the next part of this section.

Discussion of the sensitivity analysis

It can be observed form Figures 5.7, 5.8, 5.9 and 5.10 that the differences between wastewater and soil temperatures change from negative values in March to positive values in May, for both site types (i.e. urban and large). This means that heat is transferred from soil to wastewater in March and from wastewater to soil in May. The differences between wastewater and in-sewer air temperatures, in the urban sewer, have also changed signs from positive in

March (Figure 5.7) to negative in May (Figure 5.8). Hence, the impact of varying the unmeasured parameters on modelled wastewater temperature was different in different sites and months. For example, in the urban sewer (Site 1), when wastewater temperature was higher than that of in-sewer air during March, the increase in f_{hwa} values at the sensitivity analysis enhanced the transfer of heat from the wastewater to the in-sewer air. Therefore, modelled wastewater temperature using the f_{hwa} range, identified in Table 5.3, drops below the modelled one using the default parameter values as demonstrated by Figure 5.2. An opposite case would be in Site 1 during May when measured wastewater temperature was lower than that of in-sewer air, and hence impacts of varying f_{hwa} on the modelled wastewater temperatures were different in Site 1 during March and May as shown by Figure 5.2 and Figure 5.3 respectively. A comprehensive explanation of the different sensitivity behaviours in the urban and large sites during March and May is shown in Table 5.4.

The sensitivity analysis has therefore shown that boundary conditions influence the behaviour of the sewer pipe model's sensitivity. However, the magnitude of the impact caused by varying the identified unmeasured parameters is almost independent of the boundary condition variations. One exception of this is the soil thermal conductivity where it showed lower impact in the urban sewer in March 2012 (Figure 5.2) than that in May 2012 (Figure 5.3).

Table 5.4: Explanation of the sensitivity analysis (SA) findings. T_{ww}, T_{air} and T_{soil} are measured temperatures of wastewater, in-sewer air and soil respectively.

Observation	Meaning	Situation [Site (Month)]	Explanation of SA figures
$T_{ww} > T_{air}$	Heat is transferred from wastewater to in-sewer air	[1 & 3 (March)], [3 (May)]	The increase in heat transfer coefficient (i.e. f_{hwa} increases or u_a decreases) results in wastewater dissipating more heat to in-sewer air and hence wastewater temperature, obtained from SA parameter ranges, drops below the modelled one using the default values.
$T_{ww} < T_{soil}$	Heat is transferred from soil to wastewater	[1 & 3 (March)]	The increase in soil thermal conductivity (k_s) results in wastewater gaining more heat from soil and hence wastewater temperature, obtained from SA, becomes higher than that modelled using the default values. The same applies when d_s decreases as thermal resistivity increases when d_s decreases.
$T_{ww} < T_{air}$	Heat is transferred from in-sewer air to wastewater	[1 (May)]	The increase in heat transfer coefficient (i.e. f_{hwa} increases or u_a decreases) results in wastewater gaining more heat from in-sewer air and hence wastewater temperature, obtained from SA, becomes higher than that modelled using the default values.
$T_{ww} > T_{soil}$	Heat is transferred from wastewater to soil	[1 & 3 (May)]	The increase in soil thermal conductivity results in wastewater dissipating more heat to the soil and hence wastewater temperature, obtained from SA, drops below the modelled one using the default values. The same applies when d_s decreases as thermal resistivity increases when d_s decreases.

The sewer pipe model utilising urban sewer data was generally more sensitive to the identified unmeasured parameters, stated in Table 5.3, than that utilising large sewer data. This is expected since wastewater temperature variation along the large sewer pipe was much less (around the fifth) than that in urban sewers as discussed in Section 4.3. Therefore, the scale of heat transfer rate in large sewers is less than that in urban sewers and hence, varying a heat transfer parameter results in less impact on the modelled wastewater temperature. Nevertheless, the sensitivity analysis for the 31st March 2013 data in the large sewers showed considerably lower impacts on the modelled wastewater temperatures compared to that for the 31st May 2013. This requires further investigations and analyses, to fully understand how different months impact on the magnitude of the sewer pipe model sensitivity.

The sensitivity analysis, carried out in this section using urban and large sewer data, showed that influential heat transfer parameters in the sewer pipe model, can be identified as follows; the heat transfer coefficient factor (f_{hwa}), penetration depth (d_s), in-sewer air velocity (u_a) and soil thermal conductivity (k_s). The heat transfer coefficient between water and air is usually estimated empirically and is difficult to determine its value in a sewer pipe. This has led Flinspach (1973) to estimate heat transfer coefficient between water and air to be a function of the relative water velocity to that of air as shown by Equation 3.30. The latter Equation can be expressed in the form shown by Equation 5.12.

$$h_{wa} = f_{hwa} \times \sqrt{|u_{wa}|} \qquad (5.12)$$ Flinspach (1973)

f_{hwa} is the heat transfer coefficient factor, which has a default value of 5.85 in Equation 3.30 when implemented by Dürrenmatt and Wanner (2014). Keeping this relation in place, the relevant calibrating parameter is therefore f_{hwa} and is now named ‘heat transfer coefficient calibrating parameter’. Calibrating f_{hwa} may improve the accuracy of the modelled results significantly as it is very influential parameter shown by the sensitivity analysis in most occasions. Therefore and since f_{hwa} cannot be measured, it was calibrated in this work. It is worth noting that in-sewer air velocity is directly associated with f_{hwa}, as shown by Equation 3.30. Previous authors found that determination of in-sewer air velocity was challenging as the amount of air flowing into and out of the sewer system is uncontrolled (Edwini-Bonsu and Steffler, 2006). Hence, in-sewer air velocity was also calibrated. Soil penetration depth (d_s), shown in Figure 3.6, may prove to be

a difficult parameter to determine for heat transfer in sewer pipes. A practical, yet costly technique to estimate d_s is to measure the temperature profile, for a few meters away from the external pipe wall at the invert side. Such measurements were not available in this project and may prove to be impractical for similar works. Therefore, d_s was considered to be one of the calibrating parameters. Soil thermal conductivity is influenced by its moisture levels and is stated to be between 0.24 and 2.5 W/m.K by Mitchell and Soga (1993), which is close to those measured by Mohamed *et al.* (2015), in laboratory under dry (0.31 W/m.K) and 75% saturated (2.2W/m.K) conditions. Therefore, measuring the soil thermal conductivity is ideally required to be achieved continuously over a long period of time, i.e. six or more months to reflect the seasonal changes. Retrieving correspondent values for thermal conductivities at the different climatic conditions is challenging. Therefore, it is impractical to determine the soil thermal conductivity within the vicinity of a sewer pipe, which demands its calibration. This was also the findings of Dürrenmatt and Wanner (2014) who calibrated soil thermal conductivity in their wastewater temperature estimation model (TEMPEST).

Result: Based on the sensitivity analysis of the sewer pipe model on the unmeasured model parameters, it was decided that heat transfer coefficient calibrating parameter (f_{hwa}), in-sewer air velocity (u_a), soil penetration depth (d_s) and soil thermal conductivity (k_s) are the parameters to be calibrated for the sewer pipe model.

5.1.2 Investigate the impact of varying the number of mesh points and the size of time step on calibration results.

Method: The impact of varying the number of mesh points (increment size as shown by ΔL in Figure 3.5) and the size of time steps is measured by the root mean square error (RMSE) of the modelled downstream wastewater temperature. This is done by comparing modelled and measured temperatures as shown by Equation 5.1.

Two months were selected, from the available measured data of the sites shown in Table 5.1, in urban and large sewers, to reflect cold (March) and warm (May) temperatures. In order to attain a high level of modelling accuracy and to compare results effectively, the values of RMSE obtained in March and May were rounded to the nearest hundredth °C. An arbitrary mesh size of 10 points (i.e. dividing the

sewer pipe into 10 increments) was initially selected for the sewer pipe model to predict wastewater temperatures along the pipe profiles. The mesh size was then varied from 10, to 200 and then to 1000 in order to observe the impact of this variation on RMSE of the modelled wastewater downstream temperatures. In a similar manner, the impact of varying the time step sizes was carried out. The minimum default time step of 2 minutes, available from the measured data, was increased to 20 minutes, 1 hour, 5 hours, and then to 1 day while RMSE for modelled wastewater downstream temperature was observed for each time step size. Table 5.5 shows the impact of varying the number of mesh points and time step sizes using monthly datasets. This impact was translated by the RMSE values based on the difference between modelled and measured downstream wastewater temperatures (Equation 5.1).

Table 5.5: Impact of varying the number of mesh points and the time step size on the sewer pipe model.

Parameter	**Value**	**Unit**	**RMSE (°C) in March**		**RMSE (°C) in May**	
			Urban (Site 2)	**Large** (Site 3)	**Urban** (Site 2)	**Large** (Site 3)
Mesh size	10	Points	0.68	0.27	0.35	0.18
	200		0.68	0.27	0.35	0.18
	1000		0.68	0.27	0.35	0.18
Time steps	2	Minutes	0.68	0.27	0.35	0.18
	20	Minutes	0.70	0.28	0.36	0.18
	1	Hour	0.70	0.29	0.36	0.18
	5	Hours	0.72	0.29	0.38	0.19
	1	Day	0.81	0.32	0.40	0.20

Enlarging the number of mesh points from 10 to 200 and then to 1000 did not change the RMSE values as shown by Table 5.5. Therefore, the mesh size in this work was decided to be 10 points. A noticeable change was observed in Sites 2 and 3 when the time step size was larger than two minutes as demonstrated by Table 5.5. Therefore, using time steps of 20 minutes or more may result in higher RMSE of modelled wastewater downstream temperature.

Result: A mesh size of 10 points and time step size of 2 minutes were considered for calibrating the sewer pipe model.

5.1.3 Determine a Range for Each Calibrating Parameter.

Method: Heat transfer calibrating parameter (f_{hwa}) was set to be within an arbitrary range as there is no clear range found in literature. Since the model is highly sensitive to f_{hwa}, the modelling accuracy can be enhanced through good calibration of f_{hwa}. Therefore, a wide range of 0.1 to 1000 for f_{hwa} was initially set to observe its effect on RMSE values with the intention to narrow the range should that result in reducing the value of RMSE. Since there is no abundancy of published literature showing ranges of in-sewer air velocities, the range found in Madsen, Hvitved-Jacobsen and Vollertsen (2006), i.e. 0.05 to 0.22m/s, was combined with that obtained from Parker and Ryan (2001), which was 0.06 to 0.5 m/s, to form the same range used in the sensitivity analysis which is -0.5 to 0.5 m/s. The negative signs indicate that air may be flowing both streamwise and opposite directions as explained earlier through Equations 5.9 and 5.10. Penetration depth of soil had no specific values in literature, however it was considered to be 0.01 and 1m in Dürrenmatt and Wanner (2014) work. This range was extended to be between 0.01 and 10m in this work in a similar manner to that followed for obtaining f_{hwa} range where both parameters are difficult to quantify. The range of soil thermal conductivity was also set to be similar to that in the sensitivity analysis, which was obtained from Mitchell and Soga (1993) to be between 0.24 and 2.5 W/m.K.

Result: All calibrating parameter ranges are identified as shown in Table 5.6.

Table 5.6: Calibrating parameter ranges used to calibrate the sewer pipe model using urban and large sewer data.

Parameter	Range used for calibration	Unit
f_{hwa}	0.1 : 1000	-
u_a	-0.5 : 0.5	m/s
k_s	0.24 : 2.5	W/m.K
d_s	0.1:10	m

5.1.4 Apply Matlab Optimization Functions (fminsearch, fminunc and fmincon) for Optimising the Calibrating Parameters.

Method: Applying the above optimisation functions is achieved by minimising optimisation target, which is the difference between measured and modelled downstream wastewater temperatures at all time steps. Obtaining the minimum difference between measured and modelled values can be achieved effectively by minimising the modulus of the norm of the vector ($|V|$) consisting of the differences between modelled and measured downstream temperatures at all time steps. This is represented by Equations 5.2 and 5.3.

Since the derivative information of the temperature variation function (Equation 3.31) is not available, a Matlab derivative-free optimisation method was utilised. This method can be implemented using 'fminsearch' code in Matlab which is based on Nelder-Mead simplex direct search technique. Nevertheless, the 'fminsearch' code showed unrealistic values. The Matlab 'fminunc' also presented similar problems to that of 'fminsearch'. For example, penetration depth and soil thermal conductivity were obtained to be negative values while other calibrating parameters were found to be too large (e.g. a magnitude of 10^3 m/s for in-sewer air velocity). Therefore, applying limits on the calibrating parameters may provide realistic values for the calibrating parameters. Hence, 'fmincon' code in Matlab was implemented where the upper and lower boundaries of each calibrating parameter were set to be within the range determined in Table 5.6. The 'fmincon' code is specific for non-linear functions and is also known as constrained nonlinear programming. The fmincon is run by setting an initial point for each calibrating parameter and then the function uses an iterative gradient-based approach to minimise the specified function which is in this case ($|V|$) as

shown by Equations 5.2 and 5.3. The number of steps it takes depends on the convergence of those steps along with the specified tolerances. More details on the fmincon function used in this section can be found in the Matlab R2013a documentation.

Result: Implement Matlab optimisation function 'fmincon' also known as the 'constrained nonlinear programming' method to calibrate the sewer pipe model using urban and large sewer data. The identified calibrating parameter ranges, used for this calibration, are shown in Table 5.6.

5.1.5 Plot Probability Density Functions (PDF) of the Difference between Measured and Modelled Downstream Wastewater Temperatures for Each Site at Each Month.

Method: Apply Equation 5.13 with the aid of Matlab.

$$PDF\ of\ model\ error = \frac{Histogram\ count\ of\ model\ error}{N \times Bandwidth} \quad (5.13)$$

Model error is the measured minus modelled wastewater temperatures at downstream ends, N is the total number of data points (around 720 for one month) and Bandwidth is the increment size at which model error was divided to, which was 0.05 °C.

Result: Plots of PDF are shown in section 5.2.

5.1.6 Obtain Root Mean Square Error (RMSE) Values for Each Site and Month.

Method: Apply Equation 5.1, which is the RMSE for modelled downstream wastewater temperature, for each site and month.

Result: Obtained RMSE values are shown in Section 5.2 and summarised in Section 5.2.3.

5.1.7 Obtain the Population Standard Deviation (σ) for Each Site and Month.

Method: Implement Equation 5.4.

Result: Obtained population standard deviation values are shown in Section 5.2 and summarised in Section 5.2.3.

5.1.8 Implement the Method of Optimisation by Division.

This is to investigate the potential of improving the RMSE (Equation 5.1) obtained through Matlab optimisation functions (Section 5.1.4), using the same ranges identified in Table 5.6.

Method: Vary each calibrating parameter, independently from the optimisation functions in Matlab and compute the relevant root mean square error (RMSE) values. This allows the observation of RMSE variation under the four calibrating parameter ranges. The following steps were therefore followed.

a. Start with the full range of calibrating parameters identified in Table 5.6.
b. Divide the specified calibrating parameter ranges into eleven points.
c. Vary all calibrating parameters (i.e. heat transfer calibrating parameter f_{hwa}, in-sewer air velocity u_a, penetration depth d_s and soil thermal conductivity k_{soil}) together so each of the eleven points in the calibrating parameter range is tested against the other three calibrating parameters' eleven points. Matlab software was implemented to perform this process using the 'for loop' code. However, due to the limited computation capability, variation of the more sensitive parameters (f_{hwa}, u_a & d_s) was achieved by implementing three Matlab 'for loop' codes, one for each calibrating parameter. Soil thermal conductivity, which was usually less sensitive than the other three parameters, was assumed to be the average found in literature (i.e. 1.37W/m.K)
d. Compute RMSEs at each value (point) of the calibrating parameter range using the available data for each site. Values of RMSE were obtained through Equation 5.1.
e. Contour plot RMSE for the three most sensitive calibrating parameters (i.e. f_{hwa}, u_a & d_s) ranges. Matlab contour code was implemented for RMSE illustration of heat transfer calibrating parameter (f_{hwa}) and in-sewer air velocity (u_a) at different penetration depths (d_s). Therefore, and due to the capability of Matlab 'contour' code, each contour figure consists of the RMSE from f_{hwa} and u_a contour plots at different d_s values.
f. Find the minimum RMSE and consider the corresponding calibrating parameter values to be the optimum values. Matlab 'find' code was utilised to find the absolute minimum.
g. Vary the range of soil thermal conductivity against the optimum calibrating parameters obtained from the step above. Observe the minimum RMSE and consider its corresponding k_s value to be the optimum soil thermal conductivity.

h. Narrow the range of the calibrating parameters, should this provide lower RMSE values.
i. Use probability density functions (Equation 5.13) to illustrate the modelling error for each site.
j. Repeat steps a to i for each calendar month in large and urban sewers.

Result: Implement the 'optimisation by division' method to calibrate the sewer pipe model using urban and large sewer data through Matlab 'for loop' code. This is to investigate the improvement (minimisation) of the RMSE values. The identified calibrating parameter ranges in Table 5.6 was used for this calibration. Contour plots of RMSE, obtained from varying the most three sensitive calibrating parameters (f_{hwa}, u_a and d_s) are shown in Section (5.2). Impact of varying soil thermal conductivity against RMSE, using the optimum f_{hwa}, u_a and d_s obtained from the contour plots or through 'find' code, was plotted in Section 5.2.

5.1.9 Compare Calibration Results Achieved through Matlab 'fmincon' Code with that carried out by Implementing 'Optimisation by Division' Method.

Method: Comparison is mainly based on RMSE values, while accounting for the standard deviations and calibrated parameter values. Calibrating parameters showing lower RMSE and lower standard deviation values will be considered for implementation in the sewer pipe and the sewer network models. Consistency of the RMSE values among all sites is another factor to be accounted for when selecting the calibrated parameters for modelling. Consistency in this context implies that values of RMSE obtained, using data from Site 2 (used for calibrating the urban sewer parameters), shall be close to those obtained using Site 1 (used for validating the urban sewer parameters). In a similar manner, consistency of large sewer RMSE values means that RMSE from Site 3 data (used for calibrating the large sewer parameters) are close to those of Site 4 (used for validating the large sewer parameters).

Result: The comparison between both calibration methods is discussed in Section 5.3.

5.2 Calibration and Validation Results for the Sewer Pipe Model

The results of calibration using the Matlab optimisation function 'fmincon' are shown in Section 5.2.1, while the optimisation by division method results are

shown in Section 5.2.2. Probability distribution function (PDF) plots for the modelling error obtained using the calibrated parameters from Matlab optimisation function 'fmincon' (explained in Section 5.1.5) are illustrated in Section 5.2.1 for urban and large sewers. Contour plots of RMSE obtained by varying h_{wa} and u_a at different d_s values (step e of Section 5.1.8) are shown in Section 5.2.2 for the optimisation by division method. Also in Section 5.2.2 are the plots for soil thermal conductivity variation against RMSE to obtain k_s with minimum corresponding RMSE (explained by step g of Section 5.1.8). Plots of PDF for the modelling error using the calibrated parameters obtained from the optimisation by division method (step i of Section 5.1.8) are shown in Section 5.2.2. The modelling error is the measured minus the modelled wastewater temperatures at the downstream ends of the sewer pipes. Dividing the calibration data into smaller periods (i.e. two weeks) obtained similar or larger RMSE calibrating parameter values than that for the full months. An example of this is shown for March 2012, under both calibration methods for the urban sewers, in Sections 5.2.1 and 5.2.2. Therefore, calibration was achieved by considering monthly data for both calibration methods. Urban sewer data was available for the period between March 2012 and July 2012 inclusive, while data for the large sewers was available between February 2013 and May 2013 inclusive, as shown by Table 5.1.

Values of calibrated parameters using both calibration methods are tabulated, along with their corresponding RMSE and standard deviation values, in Section 5.2.3. The calibrated sewer pipe model using the urban sewer data will be referred to as the 'urban sewer model' while the calibrated sewer pipe model using the large sewer data will be known as the 'large sewer model'.

5.2.1 Matlab 'fmincon' Optimisation Function (optimisation by constrained nonlinear programming)

This section shows the results obtained from the Matlab optimisation function 'fmincon' using urban and large sewers. Results in this section consists of RMSE of modelled wastewater temperatures at the downstream end of the sewer pipe using the calibrated parameters (Equation 5.1), standard deviation values (Equation 5.4) and plots of probability density function (PDF) of model error (Equation 5.13). Values of calibrated parameters obtained from the Matlab 'fmincon' code are shown in Section 5.2.3 and discussed further in Section 5.3.

This section is divided into urban and large sewers and each type shows the relevant monthly results.

Urban sewers

Figure 5.11 shows the probability density function (PDF), of the modelling error (measured minus modelled wastewater temperatures at downstream ends), obtained from the Matlab optimisation function 'fmincon' for Site 1 (used for validation) and Site 2 (used for calibration) data in March 2012. The RMSE for March 2012 was found to be 0.55 °C for Site 1, which is slightly higher than that obtained for Site 2 (0.52°C). Data from the last two weeks of March was utilised for calibrating and validating the urban sewer model to observe the impact of varying the calibration period on RMSE. This has shown that two weeks data provides RMSE of 0.62 and 0.55 for Sites 1 and 2 respectively which are clearly higher than those obtained using the full month (March) data. Therefore, the rest of the calibration process, using 'fmincon' code is carried out using Monthly data. Population standard deviation for March 2012 has presented values of 0.43°C and 0.49°C for Sites 1 and 2 respectively. This indicates that the calibrated urban sewer model has similar performance for Sites 1 and 2 data recorded in March 2012. However, Figure 5.11 shows slight skewness to the right for Site 1 since its data was used to validate the urban sewer model.

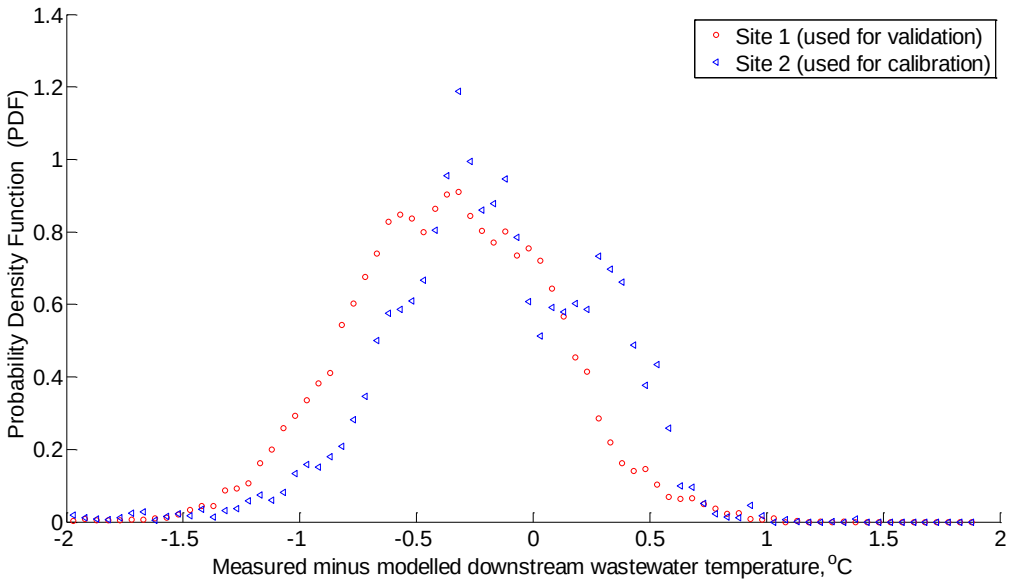

Figure 5.11: PDF of model errors, using the calibrated parameters obtained from Matlab optimisation function, for the urban sewer sites in March 2012.

The PDF of model error, obtained from the Matlab optimisation function 'fmincon' using April 2012 data, is shown in Figure 5.12 for Site 1 (used for validation) and Site 2 (used for calibration). While the RMSE for April 2012 was found to be 0.48°C and 0.33°C for Sites 1 and 2 respectively, the population standard deviation values were 0.48°C for Site 1 and 0.33°C for Site 2. The lower RMSE and standard deviation values, of April 2012, obtained using Site 2 data were lower than those obtained from Site 1, as data from the latter was utilised for calibration. This is also reflected in the PDF file obtained from both urban sites (Figure 5.12), where using Site 1 data provided a PDF that is almost symmetric around zero model error.

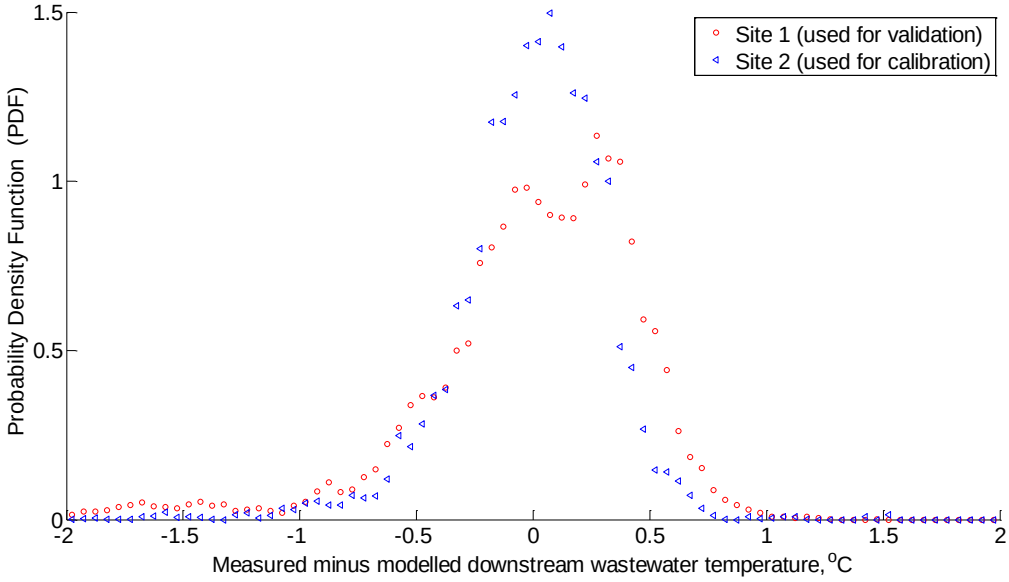

Figure 5.12: PDF of model errors, using the calibrated parameters obtained from Matlab optimisation function, for the urban sewer sites in April 2012.

The PDF showing the distribution of model error, obtained from the Matlab optimisation function 'fmincon' using May 2012 data, is shown by Figure 5.13 for Site 1 (used for validation) and Site 2 (used for calibration). While the RMSE for May 2012 was found to be 0.72°C and 0.33°C for Sites 1 and 2 respectively, the population standard deviation values were 0.36°C for Site 1 and 0.32°C for Site 2. A higher RMSE for May 2012 was obtained for data used for validation (Site 1) which is also interpreted by the PDF of Site 1 data. This can be noticed from Figure 5.13, where PDF for Site 1 data is skewed to the right.

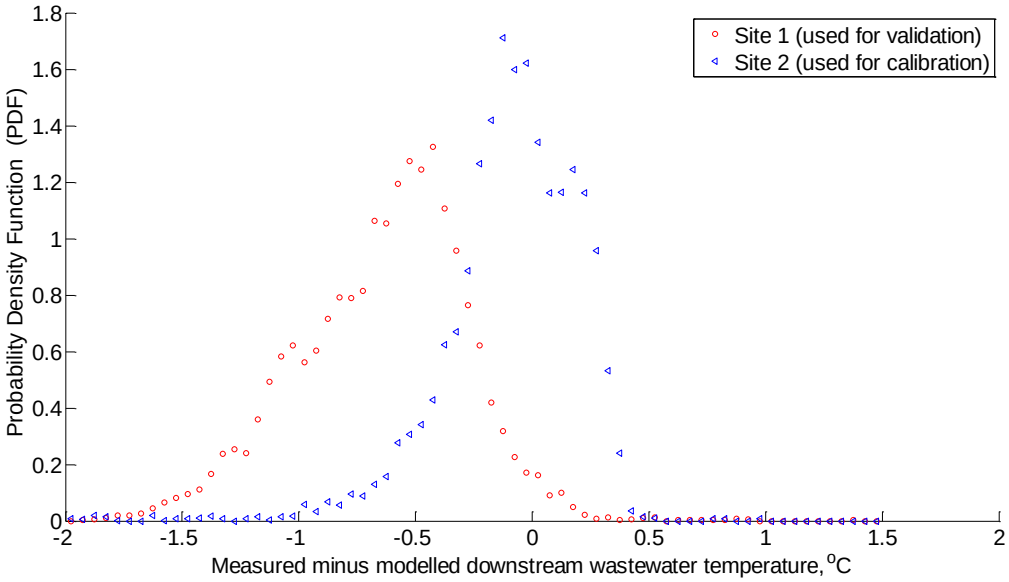

Figure 5.13: PDF of model errors, using the calibrated parameters obtained from Matlab optimisation function, for the urban sewer sites in May 2012.

The PDF of model error, obtained from the Matlab optimisation function 'fmincon' using June 2012 data, is shown in Figure 5.14 for Site 1 (used for validation) and Site 2 (used for calibration). The RMSE for June 2012 was found to be 0.36°C and 0.27°C for Sites 1 and 2 respectively, while the population standard deviation values were 0.30°C for Site 1 and 0.27°C for Site 2. June 2012 data used for calibration (from Site 2) showed slightly lower RMSE and standard deviation values than that of Site 1. This means that the calibrated urban sewer model performance is very close in Sites 1 and 2 during June 2012, which is also reflected in the PDF variation (Figure 5.14).

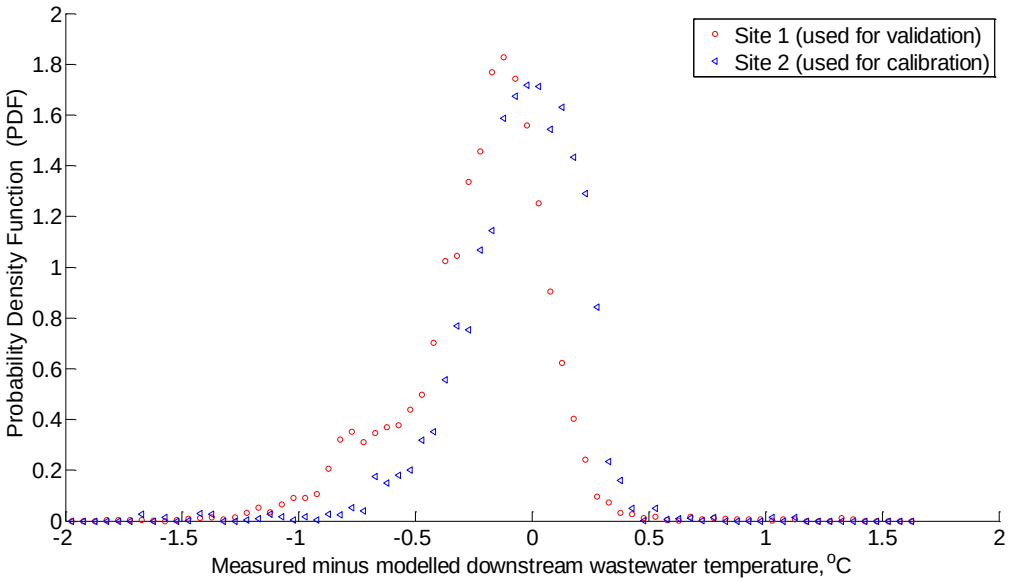

Figure 5.14: PDF of model errors, using the calibrated parameters obtained from Matlab optimisation function, for the urban sewer sites in June 2012.

The PDF of model error, obtained from the Matlab optimisation function 'fmincon' using July 2012 data, is shown by Figure 5.15 for Site 1 (used for validation) and Site 2 (used for calibration). The RMSE for July 2012 was found to be 0.31°C and 0.22°C for Sites 1 and 2 respectively, and the population standard deviation values were 0.30°C for Site 1 and 0.22°C for Site 2. Lower RMSE and standard deviation, in July 2012, were also noticed to be obtained for Site 2 data as it was used for calibration. This also explains the fact that PDF obtained using Site 2 data was more symmetric than that of Site 1 as shown by Figure 5.15.

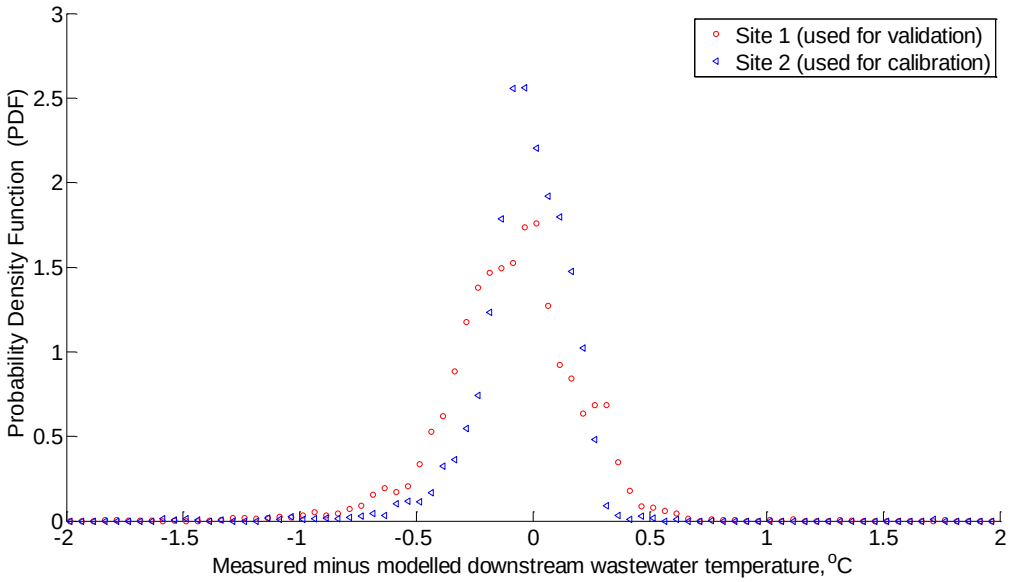

Figure 5.15: PDF of model errors, using the calibrated parameters obtained from Matlab optimisation function, for the urban sewer sites in July 2012.

Large sewers

Figure 5.16 shows the probability density function (PDF) of the model error obtained from the Matlab optimisation function 'fmincon' in Site 3 (used for calibration) and Site 4 (used for validation) in February 2013. The RMSE for February 2013 data was found to be 0.15 °C and 0.35°C for Sites 3 and 4 respectively. A population standard deviation of 0.13°C was obtained for Site 3 and 0.14 °C for Site 4 in February 2013. Lower RMSE of Site 3 than that of Site 4 in February 2013 was expected since Site 3 data was utilised for calibrating the large sewer model. This fact was also reflected in the PDF of Site 3 showing a near symmetry around a lower model error value compared to that of Site 4 (Figure 5.16).

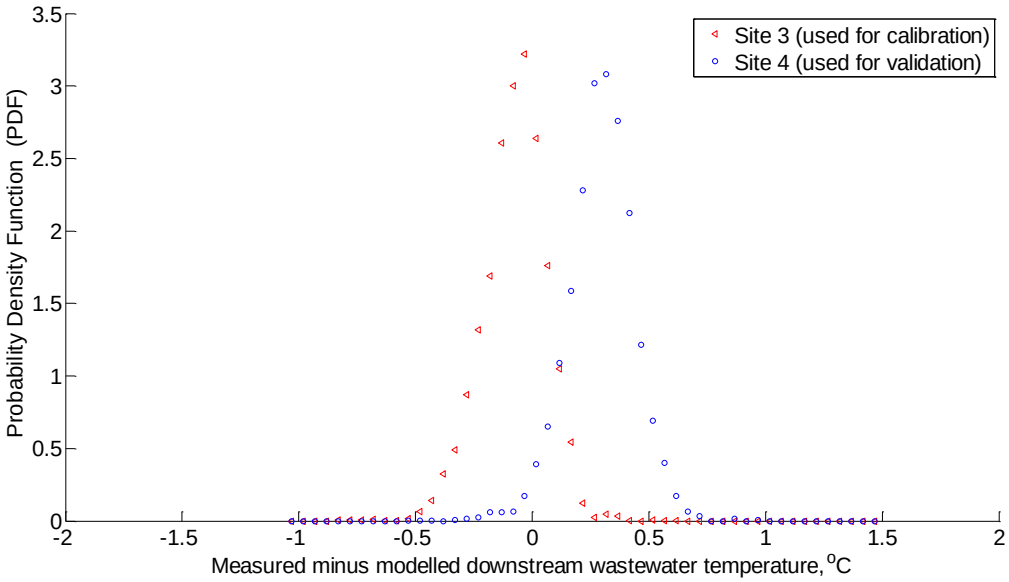

Figure 5.16: PDF of model errors, using the calibrated parameters obtained from Matlab optimisation function, for the large sewer sites in February 2013.

The PDF distribution of the model error obtained from the Matlab optimisation function 'fmincon' using Site 3 (used for calibration) and Site 4 (used for validation) data in March 2013 is illustrated in Figure 5.17. The March 2013 RMSE was found to be 0.12 °C and 0.33°C for Sites 3 and 4 respectively. The population standard deviation values were found to be 0.11°C and 0.15°C for Sites 3 and 4 respectively in March 2013. In a similar case to February 2013, RMSE for the site used for calibration in March 2013 (Site 3), is lower than that of the site used for validation (Site 4). As expected and also in a similar case to February 2013, Site 3 showed symmetry around a lower model error than that of Site 4 (Figure 5.17), since Site 3 data was utilised for calibration.

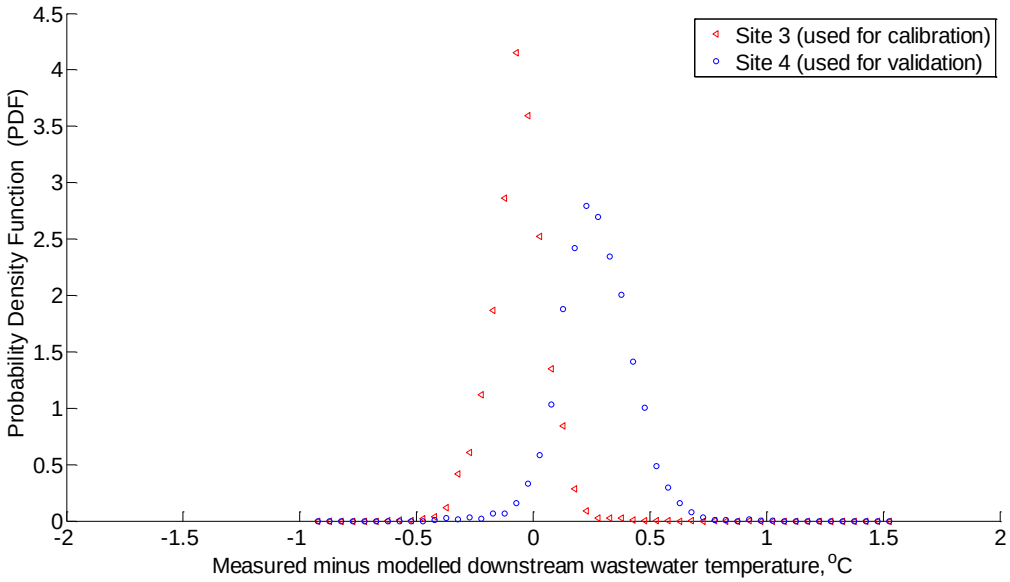

Figure 5.17: PDF of model errors, using the calibrated parameters obtained from Matlab optimisation function, for the large sewer sites in March 2013.

The PDF of the model error obtained from the Matlab optimisation function 'fmincon' in Site 3 (used for calibration) and Site 4 (used for validation) in April 2013 is shown by Figure 5.18. The RMSE for April 2013 was found to be 0.13 °C and 0.29°C for Sites 3 and 4 respectively. The population standard deviation values were found to be of 0.13°C and 0.15°C for Sites 3 and 4 respectively in April 2013. As previously mentioned, data used for calibration (from Site 3) was expected to provide more accurate model results. This is reflected by Site 3 lower RMSE and standard deviation values, and explains why the PDF being symmetric around lower model error in Site 3 than that in Site 4.

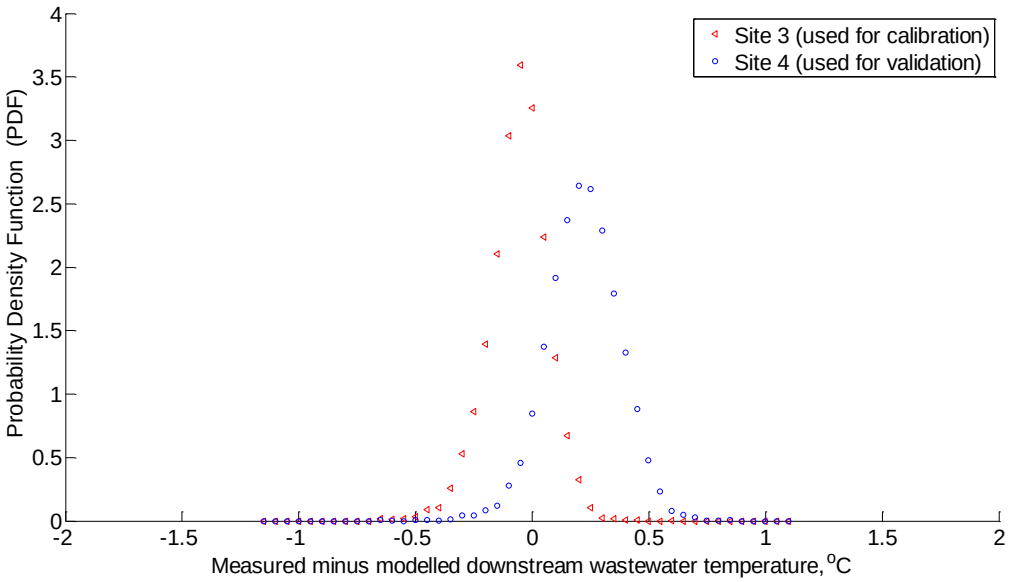

Figure 5.18: PDF of model errors, using the calibrated parameters obtained from Matlab optimisation function, for the large sewer sites in April 2013.

The PDF of the model error obtained from the Matlab optimisation function 'fmincon' in Site 3 (used for calibration) and Site 4 (used for validation) for May 2013 is shown by Figure 5.19. The RMSE for May 2013 was found to be 0.14 °C and 0.16°C for Sites 3 and 4 respectively. The population standard deviation values were found to be of 0.14°C and 0.16°C for Sites 3 and 4 respectively for May 2013. The close RMSE values and also similar PDF patterns for both large sewer sites suggest that the large sewer calibrated model has similar performance using the calibration and validation data for May 2013.

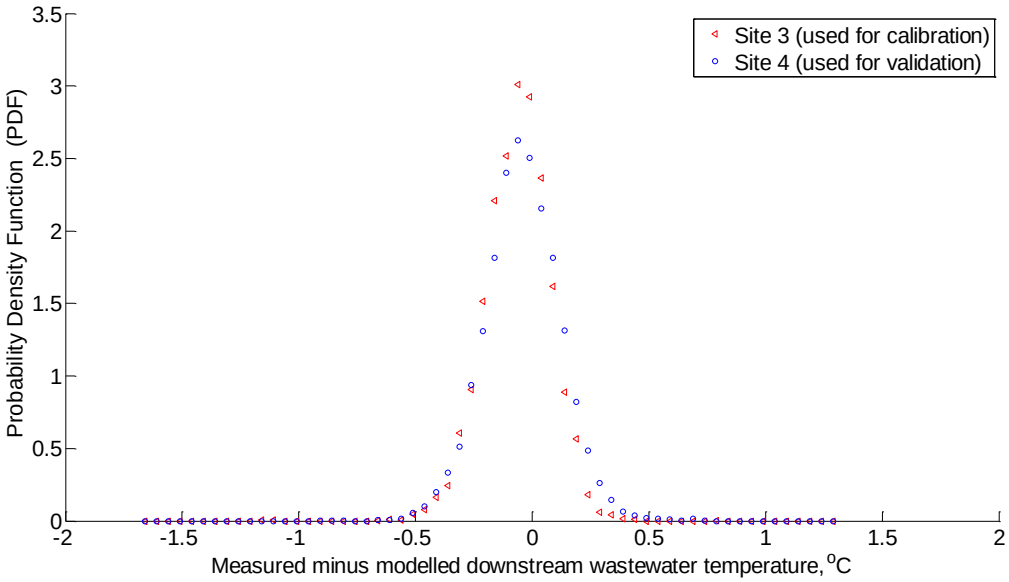

Figure 5.19: PDF of model errors, using the calibrated parameters obtained from Matlab optimisation function, for the large sewer sites in May 2013.

Summary of findings from applying the Matlab optimisation function 'fmincon'

It was observed that values of RMSE and standard deviation, obtained from 'fmincon' code were in the same order during all months in the four sites. It was clear that data used for calibration, using the above code, obtained lower RMSE and standard deviation values than that used for validation. Calibrating and validating the large sewer model has generally shown lower RMSE values and demonstrated more symmetric PDF plots than those obtained from the urban sewer model. The values of calibrated parameters are shown in Section 5.2.3, while the findings from calibrating the sewer pipe model using the Matlab 'fmincon' method is discussed further in Section 5.3.

5.2.2 Optimisation by Division

This section shows the results obtained from the optimisation by division method using the urban and large sewers. Results in this section consists of contour plots of RMSE obtained from using different calibrating parameter values (Table 5.6), RMSE of modelled wastewater temperatures at the downstream end of the sewer pipe using the calibrated parameters (Equation 5.1), standard deviation values (Equation 5.4) and plots of probability density function (PDF) of model error (Equation 5.13). Values of calibrated parameters obtained from the optimisation by division method are presented in Section 5.2.3 and discussed further in Section 5.3. Urban sewer data was recorded between the beginning of March

2012 and end of July 2012, while the large sewer data was logged between the start of February 2013 and end of May 2013. This section is divided into urban and large sewers and each section shows the relevant monthly results.

Urban sewers

The contour plots of Site 2 RMSE, obtained from the optimisation by division method, were initially plotted at soil penetration depths of 10, 1 and 0.1m in March 2012 as shown by Figure 5.20, Figure 5.21 and Figure 5.22 respectively.

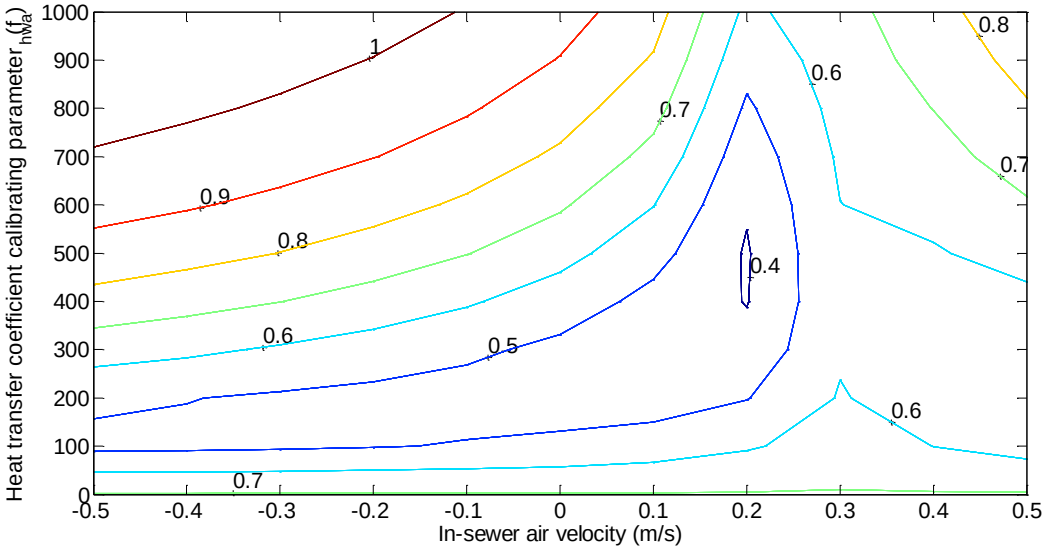

Figure 5.20: Contour plots of RMSE obtained from varying heat transfer coefficient calibrating parameter (f_{hwa}) and in-sewer air velocity (u_a), at soil penetration depth (d_s) of 10m. Urban sewer data from Site 2, recorded in March 2012, was utilised. Values of RMSE are shown on the contour lines.

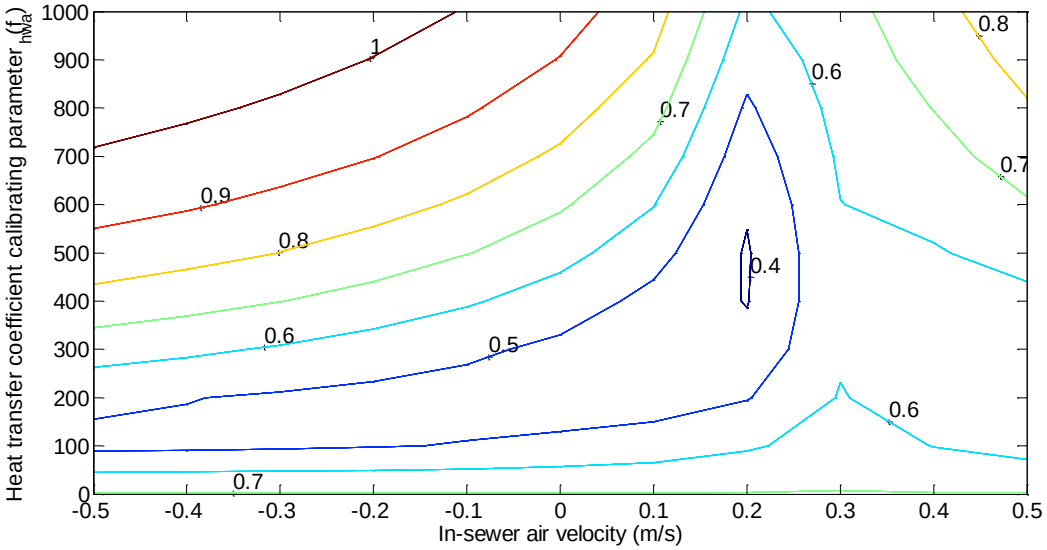

Figure 5.21: Contour plots of RMSE obtained from varying heat transfer coefficient f_{hwa} and in-sewer air velocity (u_a), at soil penetration depth (d_s) of 1m. Urban sewer data from Site 2, recorded in March 2012, was utilised. Values of RMSE are shown on the contour lines.

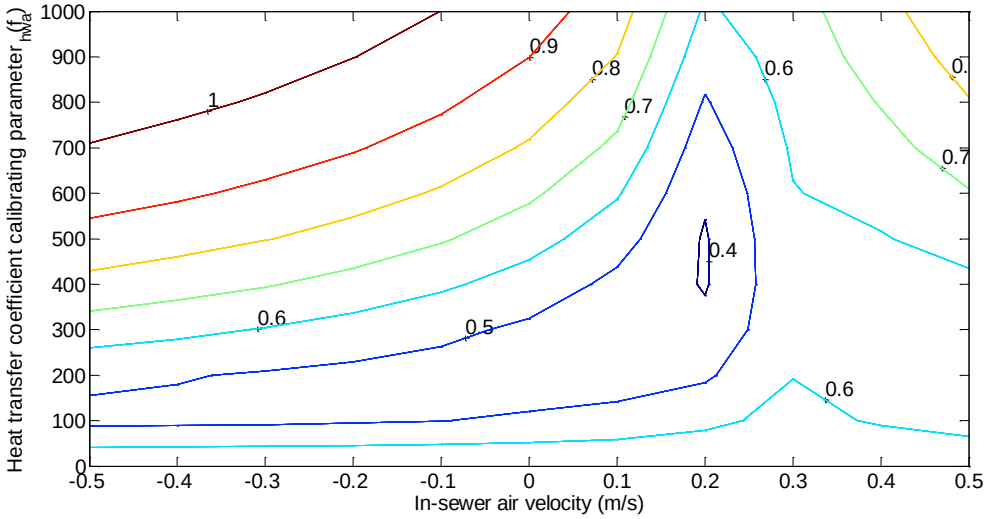

Figure 5.22: Contour plots of RMSE obtained from varying f_{hwa} and in-sewer air velocity (u_a), at soil penetration depth (d_s) of 0.1m. Urban sewer data from Site 2, recorded in March 2012, was utilised. Values of RMSE are shown on the contour lines.

It is clear from Figures 5.20 to 5.22 that varying the penetration depth (d_s) causes negligible impact on the shape of the contour plots. Therefore, for a more effective way of illustrating the contour plots, it was decided to combine the contour plots of different penetration depths into one plot that shows the variation of RMSE by changing both heat transfer calibrating parameter (f_{hwa}) and in-sewer air velocity (u_a) at different penetration depths (d_s). The minimum RMSE value and its

corresponding f_{hwa}, ua and d_s were found through the utilisation of 'find' code in Matlab.

Figure 5.23 shows the contour plots for Site 2 RMSE, obtained from the optimisation by division method, at various penetration depths for March 2012.

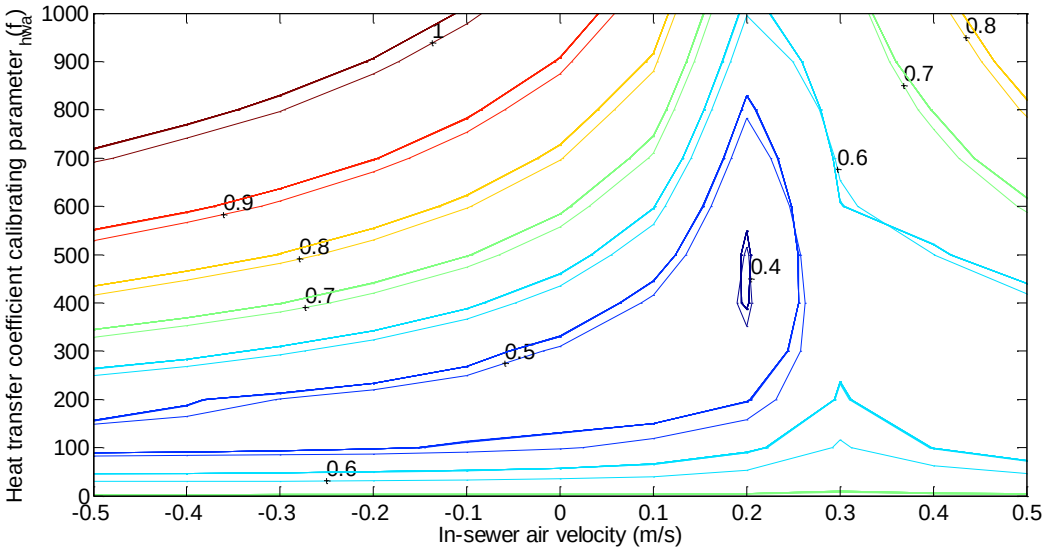

Figure 5.23: Contour plots of RMSE obtained from varying f_{hwa} and in-sewer air velocity (u_a), at 0.1, 1 and 10m penetration depths (d_s). Urban sewer data from Site 2, recorded in March 2012, was utilised. Values of RMSE are shown on the contour lines.

The data obtained in March 2012, for urban sewers, was divided into fortnight periods (first two weeks of March) to investigate the impact this may cause on the obtained RMSE values as shown in Figure 5.24.

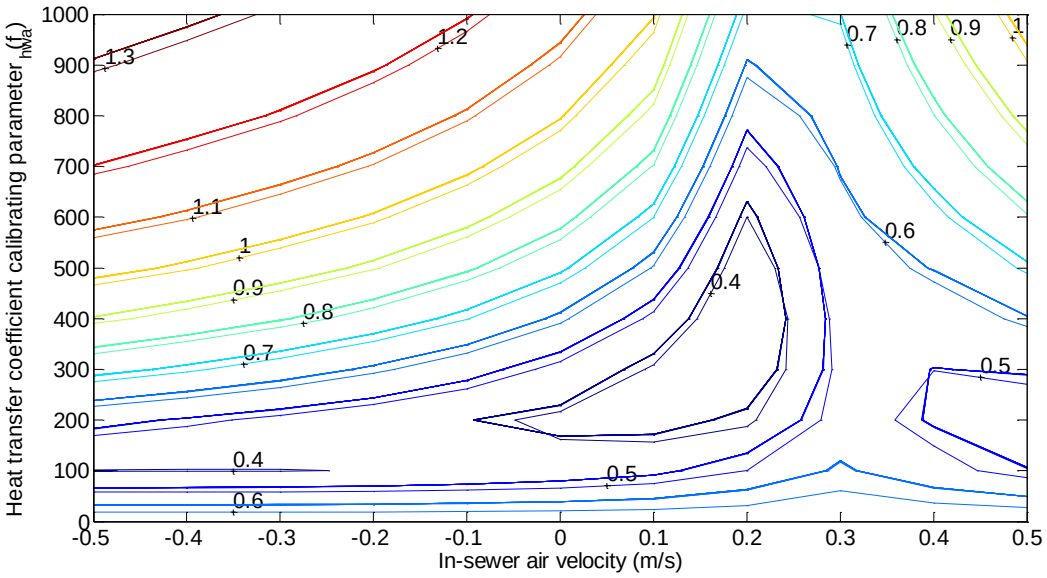

Figure 5.24: Contour plots of RMSE, for the first two weeks of March 2012, obtained from varying f_{hwa} and in-sewer air velocity (u_a) at different penetration depths (d_s). Urban sewer data from Site 2 was utilised. Values of RMSE are shown on the contour lines.

Figure 5.24 showed the impact of dividing the data obtained very close relevant RMSE values. Therefore, the rest of the calibration is carried on the basis of monthly data.

The impact of varying the soil thermal conductivity while assuming optimum calibrated parameter values obtained from Figure 5.23, on the RMSE for Site 2 in March 2012, is shown in Figure 5.25.

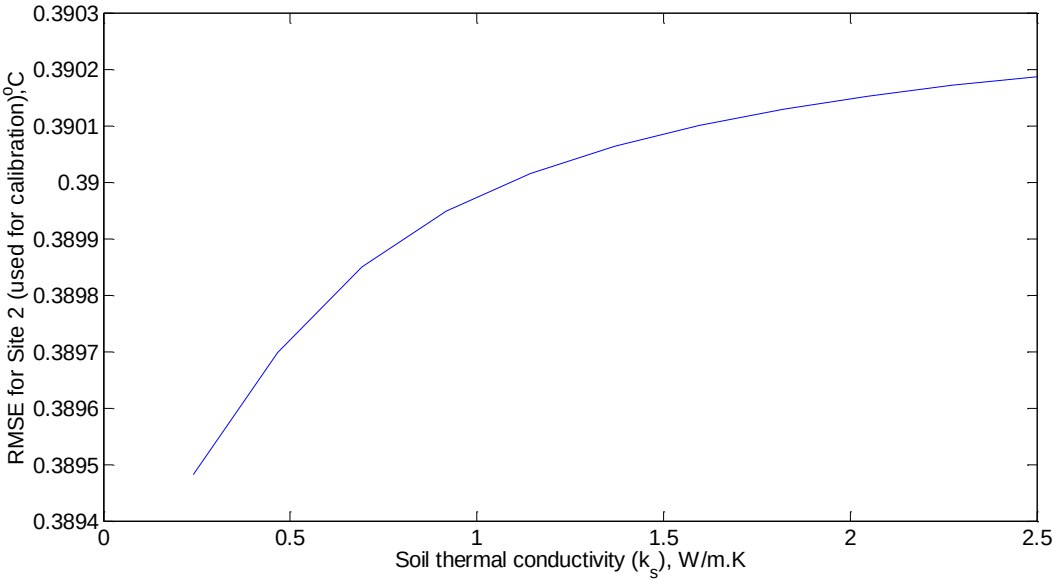

Figure 5.25: Values of RMSE obtained from varying the soil thermal conductivity (k_s) using data from Site 2, recorded in March 2012 (full month data). Optimum f_{hwa}, u_a and d_s, for March 2012, were considered in this plot.

Impact of varying k_s on RMSE was found, from Figure 5.25, to be insignificant when using Site 2 data recorded in March 2012, which means that k_s value can vary within the range shown in Figure 5.25. However, the same procedure described in Section 5.1 was followed. Therefore, considering the soil thermal conductivity value that obtained the minimum RMSE in Figure 5.25, and narrowing the range of calibrating parameters in March 2012 for Site 2, Figure 5.26 was plotted to illustrate optimum calibrating parameters.

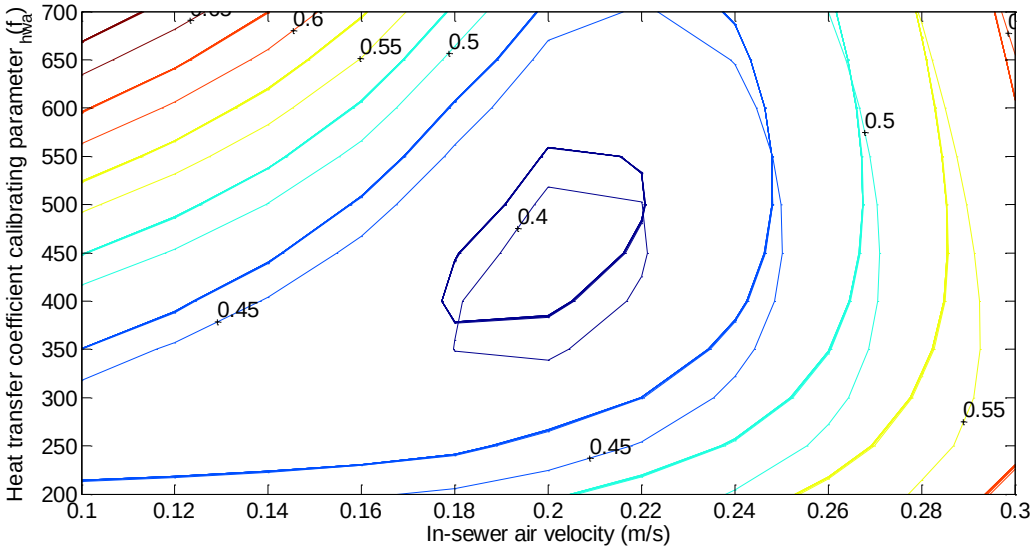

Figure 5.26: Replotting of March 2012 (full month data) contour plot for RMSE obtained from varying f_{hwa} and in-sewer air velocity (u_a) at different penetration depths (ds). Narrower calibrating parameter ranges were used while k_s showing minimum RMSE was assumed using urban sewer data from Site 2. Values of RMSE are shown on the contour lines.

The PDF of model error, obtained from the optimisation by division method using March 2012 data from Site 1 (used for validation) and Site 2 (used for calibration) is shown by Figure 5.27. The RMSE values, in March 2012, were 0.83°C and 0.39°C for Sites 1 and 2 respectively, while the population standard deviations were 0.77 °C for Site 1 and 0.39°C for Site 2. As expected, the site data used for validation (Site 1) sowed PDF skewness while PDF for Site 2 model error was almost symmetric around zero since its data was utilised for calibrating the urban sewer model.

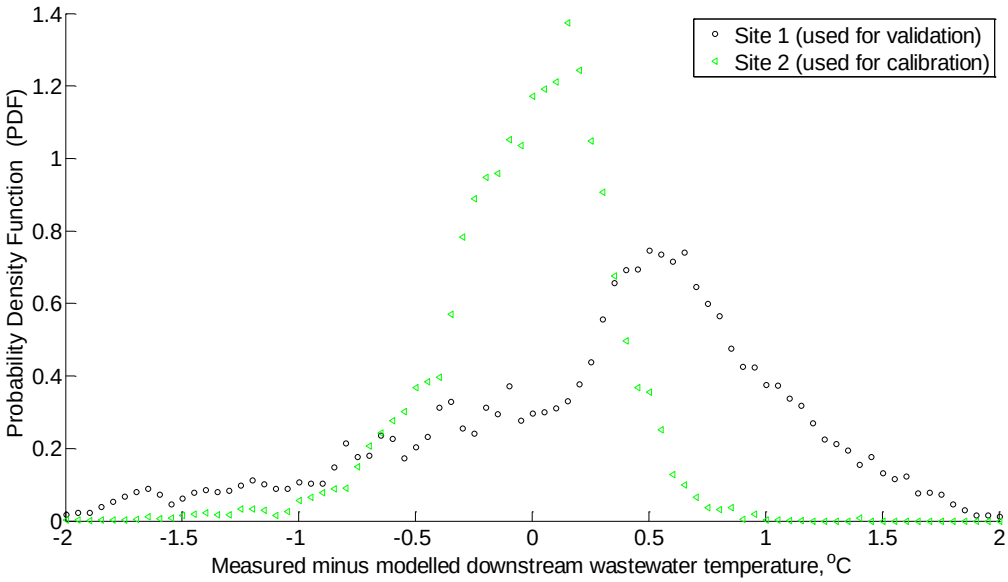

Figure 5.27: PDF of model errors, using the calibrated parameters obtained from the optimisation by division method, for the urban sewer sites in March 2012 (full month data).

The same procedure of implementing the calibration by division method on monthly basis for March 2012 was followed in other months. The contour plots of Site 2 RMSE, obtained from the optimisation by division method, were created at various penetration depths for April 2012 as shown in Figure 5.28.

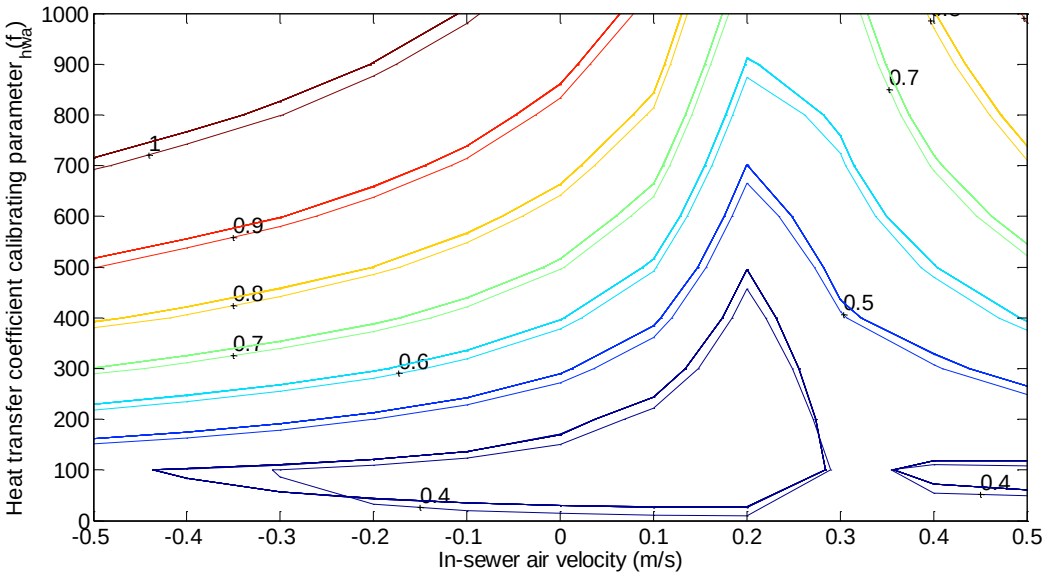

Figure 5.28: Contour plots of RMSE obtained from varying f_{hwa} and in-sewer air velocity (u_a) at different penetration depths (d_s). Urban sewer data from Site 2, recorded in April 2012, was utilised. Values of RMSE are shown on the contour lines.

The impact of varying the soil thermal conductivity, on the RMSE for Site 2 in April 2012, is shown by Figure 5.29.

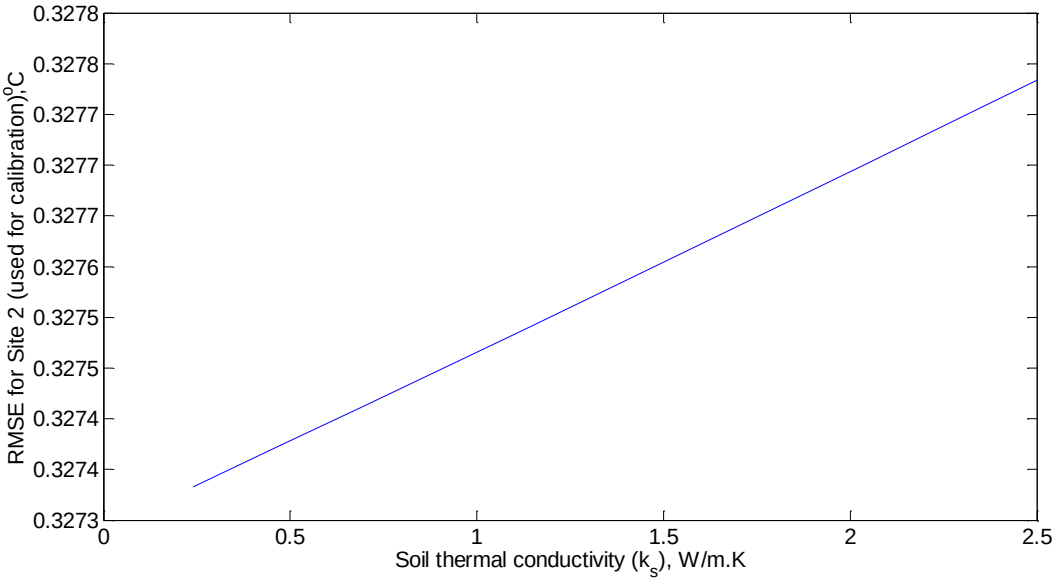

Figure 5.29: Values of RMSE obtained from varying the soil thermal conductivity (k_s) using data from Site 2, recorded in April 2012. Optimum f_{hwa}, u_a and d_s, for April, were considered in this plot.

In a similar case to March 2012, the urban sewer model has shown insignificant sensitivity to the soil thermal conductivity in April 2012, which indicates any k_s

value with the range shown in Figure 5.29 may be selected. Nevertheless, the same procedure described in Section 5.1 was followed. Therefore, considering the soil thermal conductivity value that obtained the minimum RMSE in Figure 5.29, and narrowing the range of calibrating parameters in April 2012 for Site 2, Figure 5.30 was plotted to illustrate optimum calibrating parameters.

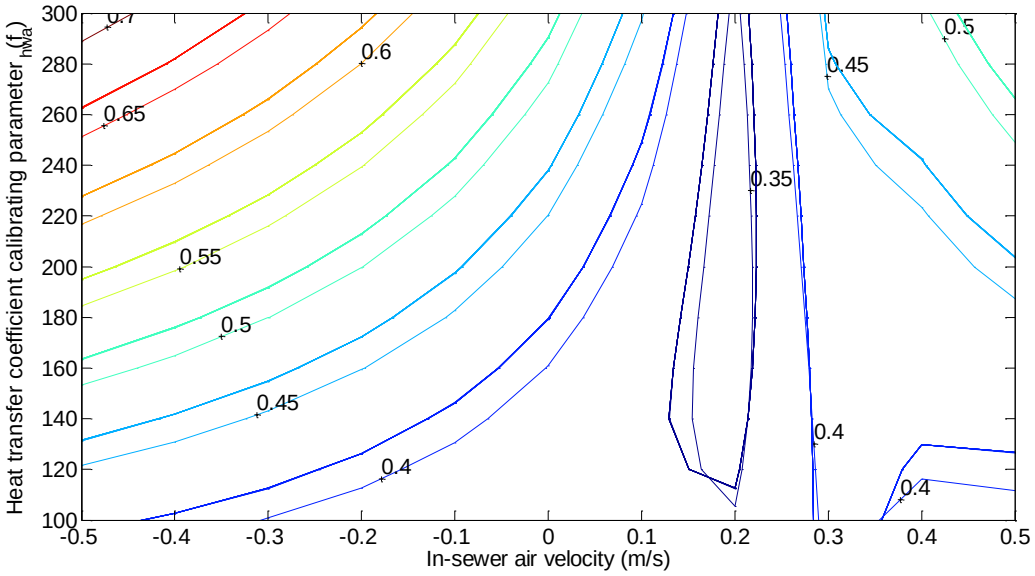

Figure 5.30: Replotting of April 2012 contour plot for RMSE obtained from varying f_{hwa} and in-sewer air velocity (u_a) at different penetration depths (d_s). Narrower calibrating parameter ranges were used while k_s showing minimum RMSE was assumed using urban sewer data from Site 2. Values of RMSE are shown on the contour lines.

The PDF of model error, obtained from the optimisation by division method using April 2012 data from Site 1 (used for validation) and Site 2 (used for calibration) is shown by Figure 5.31. The RMSE values, for April 2012, were 0.48°C and 0.33°C for Sites 1 and 2 respectively, while the population standard deviations were 0.48 °C for Site 1 and 0.33°C for Site 2. The PDF for April 2012 using Site 1 data was close to that of Site 2. This was different in March 2012 where the data used for calibration (Site 2) was more symmetric than that of Site 1 (used for validation).

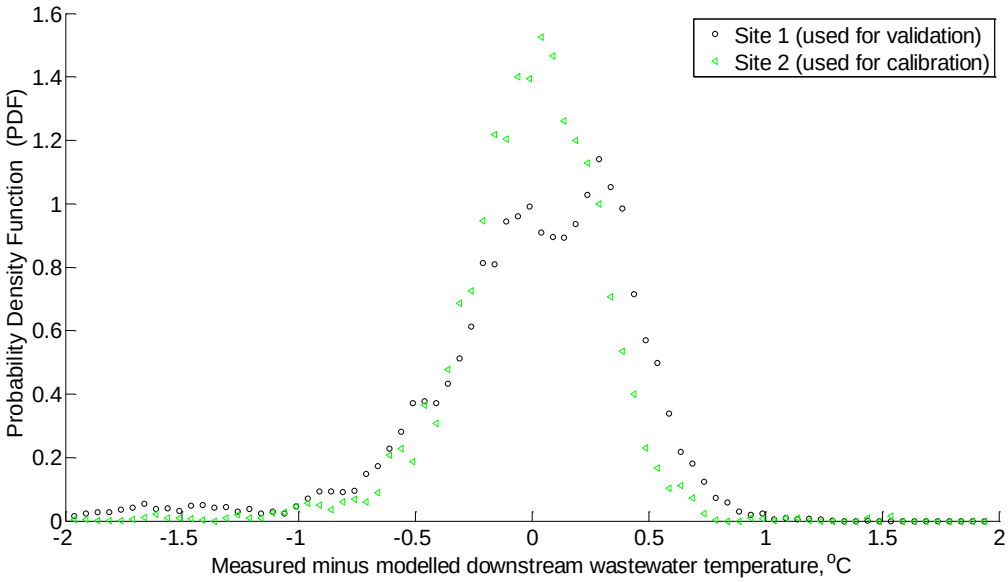

Figure 5.31: PDF of model errors, using the calibrated parameters obtained from the optimisation by division method, for the urban sewer sites in April 2012.

The contour plots of Site 2 RMSE, obtained from the optimisation by division method, were created at various penetration depths for May 2012 as shown by Figure 5.32.

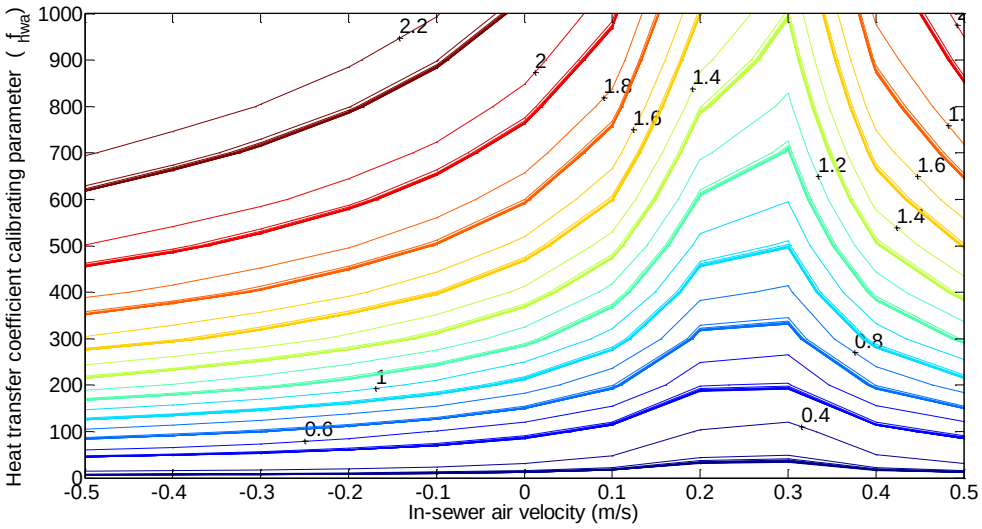

Figure 5.32: Contour plots of RMSE obtained from varying f_{hwa} and in-sewer air velocity (u_a) at different penetration depths (d_s). Urban sewer data from Site 2, recorded in May 2012, was utilised. Values of RMSE are shown on the contour lines.

The impact of varying the soil thermal conductivity, on the RMSE for Site 2 in May 2012, is shown by Figure 5.33.

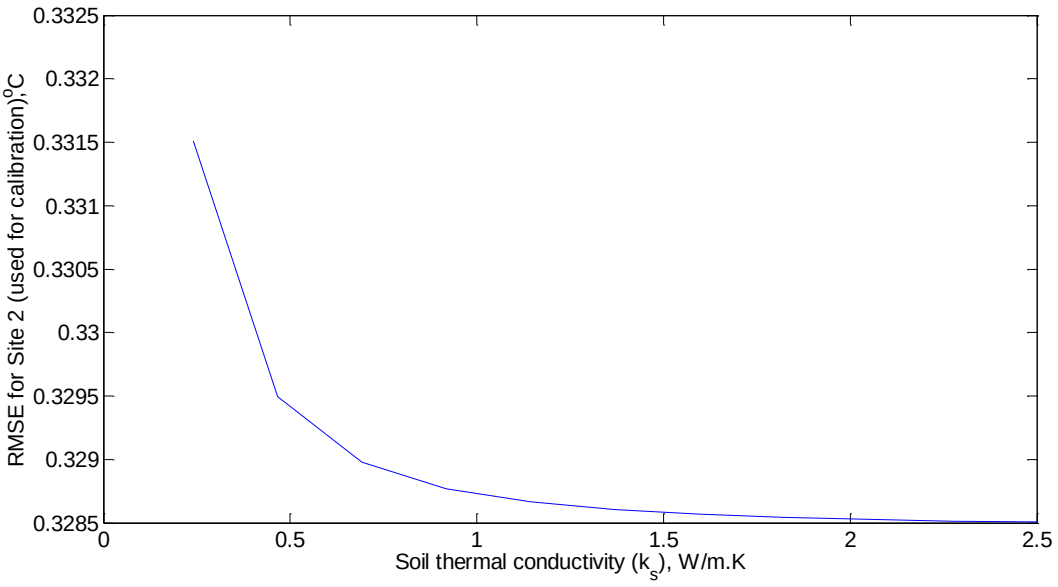

Figure 5.33: Values of RMSE obtained from varying the soil thermal conductivity (k_s) using data from Site 2, recorded in May 2012. Optimum f_{hwa}, u_a and d_s, for May, were considered in this plot.

It can be noticed, from Figure 5.32, that varying the calibrating parameters (f_{hwa}, u_a, d_s and k_s) causes insignificant impacts on the RMSE obtained from the urban sewer model. Therefore, considering the soil thermal conductivity value that obtained the minimum RMSE in Figure 5.33, and narrowing the range of calibrating parameters in May 2012 for Site 2, Figure 5.34 was plotted to illustrate the optimum calibrating parameters.

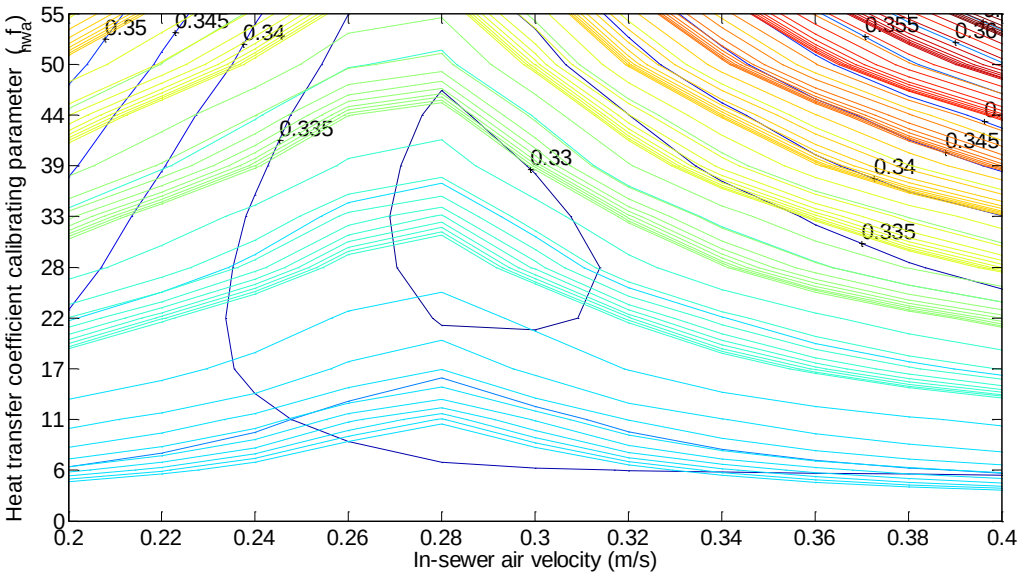

Figure 5.34: Replotting of May 2012 contour plot for RMSE obtained from varying f_{hwa} and in-sewer air velocity (u_a) at different penetration depths (d_s). Narrower calibrating parameter ranges were used while k_s showing minimum RMSE was assumed using urban sewer data from Site 2. Values of RMSE are shown on the contour lines.

It was noticed, from Figure 5.34, that the variation of penetration depth (d_s) changes the shape of the contour plot which is unusual in the urban and large sewers. However, minimum RMSE and its corresponding calibrating parameters (i.e. f_{hwa}, u_a and d_s) were found through the Matlab 'find' code and are shown in Section 5.2.3.

The PDF of model error, obtained from the optimisation by division method using May 2012 data from Site 1 (used for validation) and Site 2 (used for calibration) is shown by Figure 5.35. The RMSE values, in May 2012, were 0.74°C and 0.33°C for Sites 1 and 2 respectively, while the population standard deviations were 0.40 °C for Site 1 and 0.33°C for Site 2. The PDF of model error obtained, using the optimisation by division method, in urban sewers using May 2012 data was found to be similar to that obtained for May 2012 using the 'fmincon' method. This can be noticed from Figure 5.13 (fmincon) and Figure 5.35 (optimisation by division) where the site data used for validation (Site 1) showed PDF of model errors that are skewed to the right.

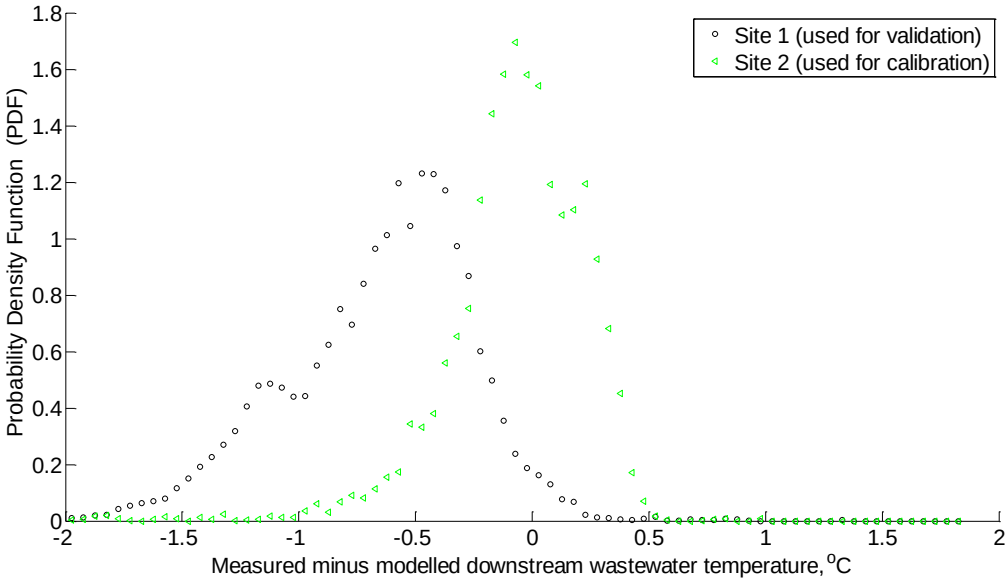

Figure 5.35: PDF of model errors, using the calibrated parameters obtained from the optimisation by division method, for the urban sewer sites in May 2012.

The contour plots of Site 2 RMSE, obtained from the optimisation by division method, were created at various penetration depths in June 2012 as shown by Figure 5.36.

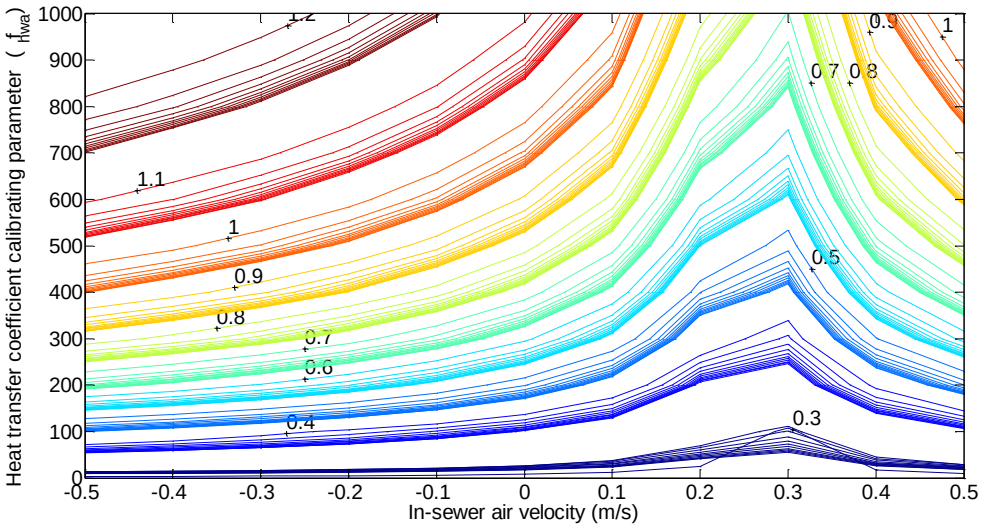

Figure 5.36: Contour plots of RMSE obtained from varying f_{hwa} and in-sewer air velocity (u_a) at different penetration depths (d_s). Default soil thermal conductivity was assumed while urban sewer data from Site 2, recorded in June 2012, was utilised. Values of RMSE are shown on the contour lines.

The impact of varying the soil thermal conductivity, on the RMSE for Site 2 in June 2012, is shown by Figure 5.37.

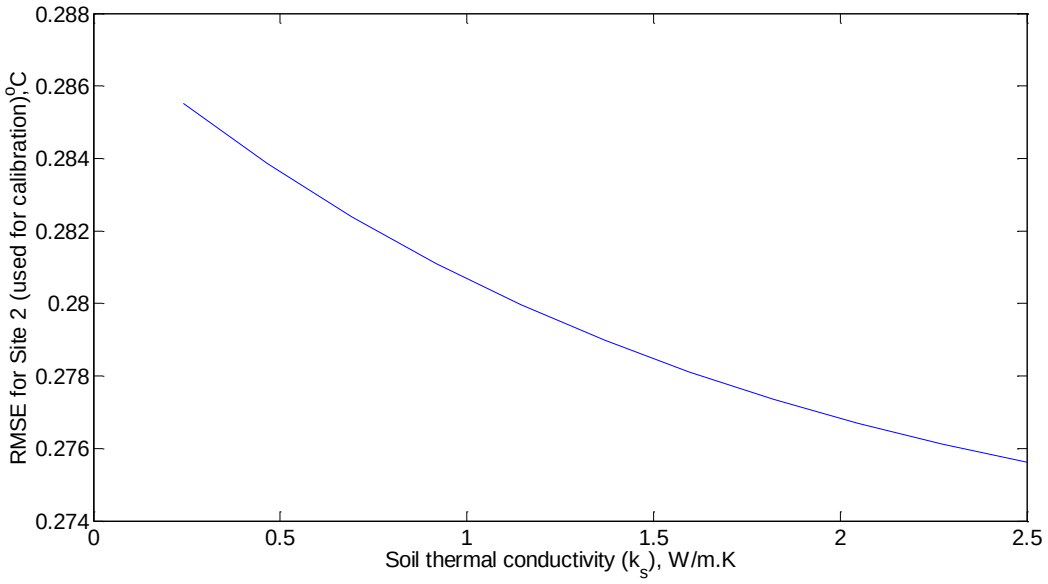

Figure 5.37: Values of RMSE obtained from varying the soil thermal conductivity (k_s) using data from Site 2, recorded in June 2012. Optimum f_{hwa}, u_a and d_s, for June, were considered in this plot.

In a similar case to May 2012 in the urban sewer, the contour lines in June 2012 has demonstrated that the impact of varying calibrating parameters (f_{hwa}, u_a, d_s and k_s) causes insignificant impacts on the RMSE obtained from the urban sewer model. Therefore, Figure 5.38 was plotted in an attempt to observe minimum RMSE value while considering the k_s value that corresponds to the minimum RMSE obtained from Figure 5.37, and by narrowing the range of calibrating parameters in June 2012 for Site 2,

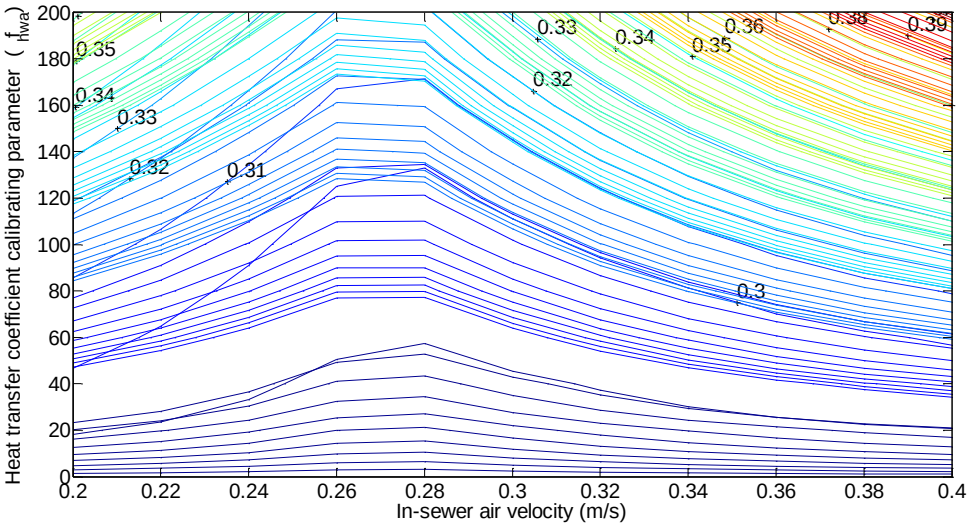

Figure 5.38: Replotting of June 2012 contour plot for RMSE obtained from varying f_{hwa} and in-sewer air velocity (u_a) at different penetration depths (d_s). Narrower calibrating parameter ranges were used while k_s showing minimum RMSE was assumed using urban sewer data from Site 2. Values of RMSE are shown on the contour lines.

The PDF of model error, obtained from the optimisation by division method in June 2012, for Site 1 (used for validation) and Site 2 (used for calibration) is shown by Figure 5.39. The RMSE values, in June 2012, were 0.40°C and 0.28°C for Sites 1 and 2 respectively, while the population standard deviations were 0.31 °C for Site 1 and 0.27°C for Site 2. The model errors from both urban sites in June 2012 obtained close patterns of PDF, yet Site 1 data was slightly more skewed than that of Site 2 since Site 1 data was used for validation.

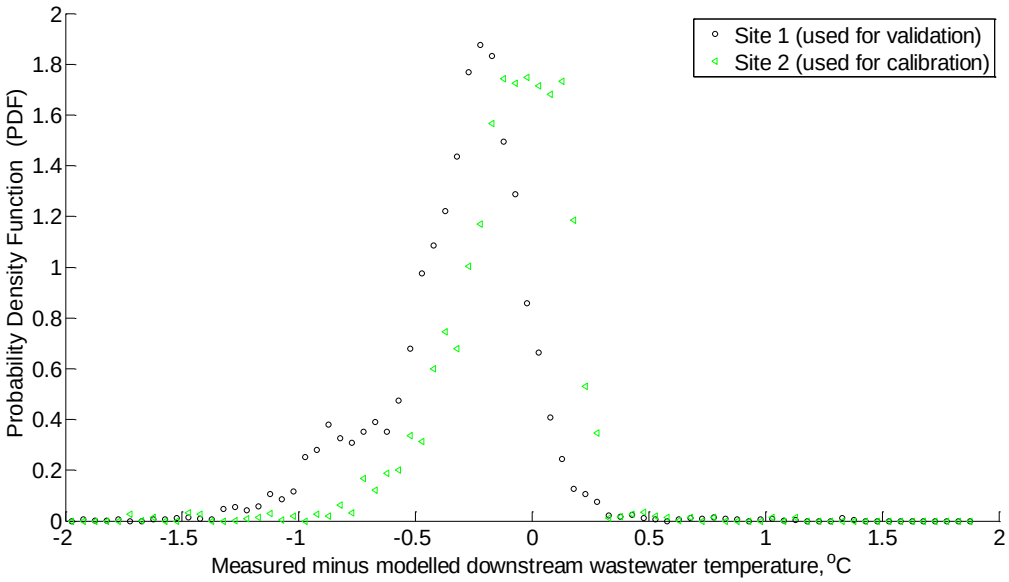

Figure 5.39: PDF of model errors, using the calibrated parameters obtained from the optimisation by division method, for the urban sewer sites in June 2012

The contour plots of Site 2 RMSE, obtained from the optimisation by division method, were created at various penetration depths in July 2012 as shown by Figure 5.40.

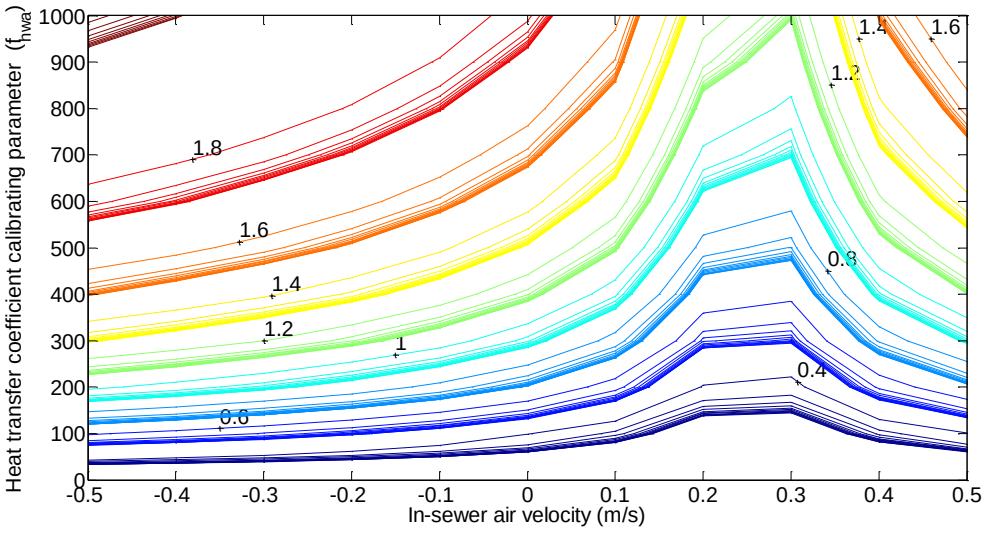

Figure 5.40: Contour plots of RMSE obtained from varying f_{hwa} and in-sewer air velocity (u_a) at different penetration depths (d_s). Urban sewer data from Site 2, recorded in July 2012, was utilised. Values of RMSE are shown on the contour lines.

The impact of varying the soil thermal conductivity, on the RMSE for Site 2 in July 2012, is shown by Figure 5.41.

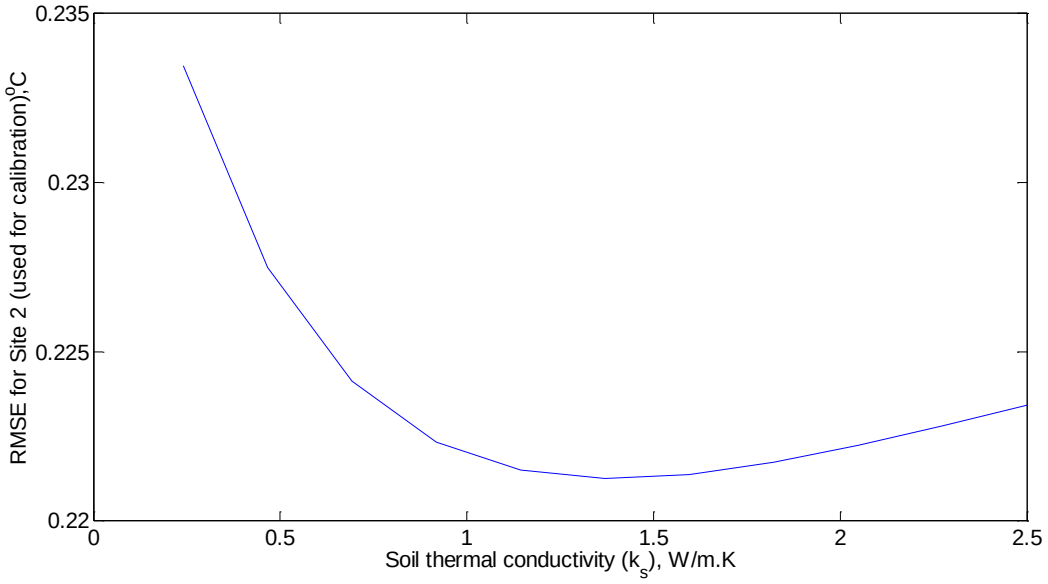

Figure 5.41: Values of RMSE obtained from varying the soil thermal conductivity (k_s) using data from Site 2, recorded in July 2012. Optimum f_{hwa}, u_a and d_s, for July, were considered in this plot.

Figure 5.42 was plotted to illustrate optimum calibrating parameters. This was achieved by considering the soil thermal conductivity value that obtained the minimum RMSE in Figure 5.41 while narrowing the range of calibrating parameters in July 2012 for Site 2.

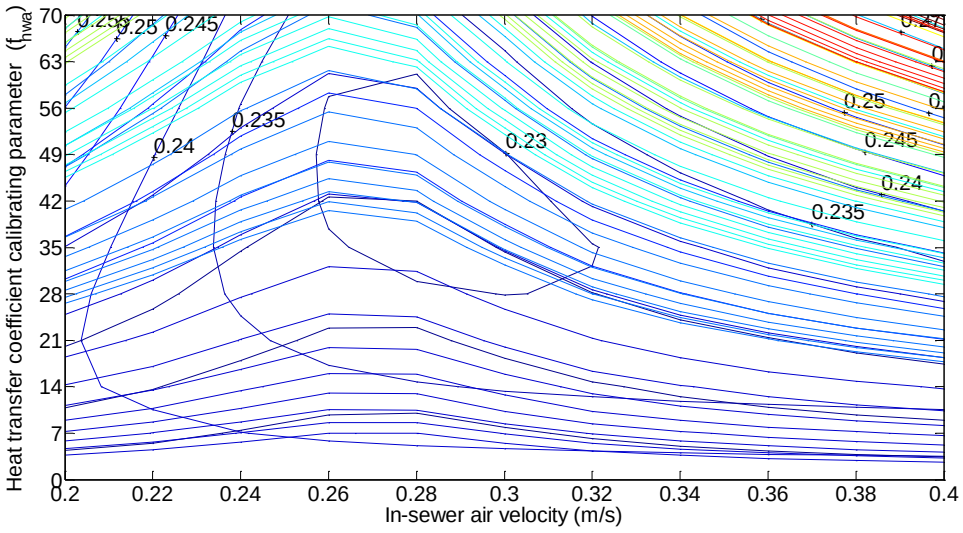

Figure 5.42: Replotting of July 2012 contour plot for RMSE obtained from varying f_{hwa} and in-sewer air velocity (u_a) at different penetration depths (d_s). Narrower calibrating parameter ranges were used while k_s showing the minimum RMSE was assumed using urban sewer data from Site 2. Values of RMSE are shown on the contour lines.

The variation of penetration depth (d_s) in Figure 5.42 changes the shape of the contour plot, yet minimum RMSE and its corresponding calibrating parameters (i.e. f_{hwa}, u_a and d_s) were found through the Matlab 'find' code as mentioned earlier in this section. Values of the calibrated parameters for all months are shown in Section 5.2.3. The PDF of model error, obtained from the optimisation by division method in July 2012, for Site 1 (used for validation) and Site 2 (used for calibration) is shown by Figure 5.43. The RMSE values, in July 2012, were 0.31°C and 0.22°C for Sites 1 and 2 respectively, while the population standard deviations were 0.30°C for Site 1 and 0.22°C for Site 2. The sewer pipe model showed similar performance when using Sites 1 and 2 data in July 2012 as can be noticed from Figure 5.43. However, Site 1 data showed more skewness since it was used for validation.

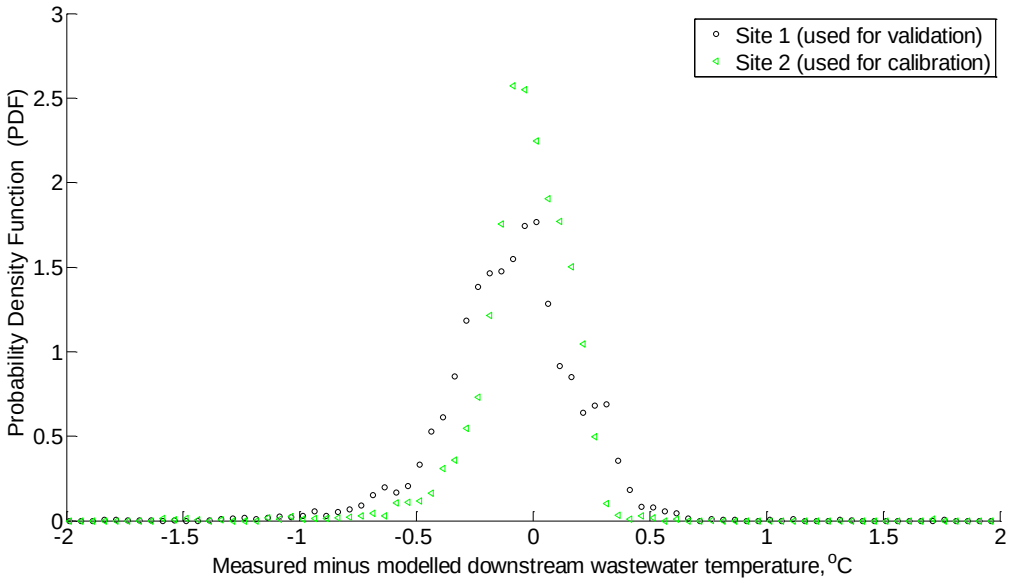

Figure 5.43: PDF of model errors, using the calibrated parameters obtained from the optimisation by division method, for the urban sewer sites in July 2012.

Large sewers

The contour plots of Site 3 RMSE, obtained from the optimisation by division method, were created at various penetration depths in February 2013 as shown by Figure 5.44.

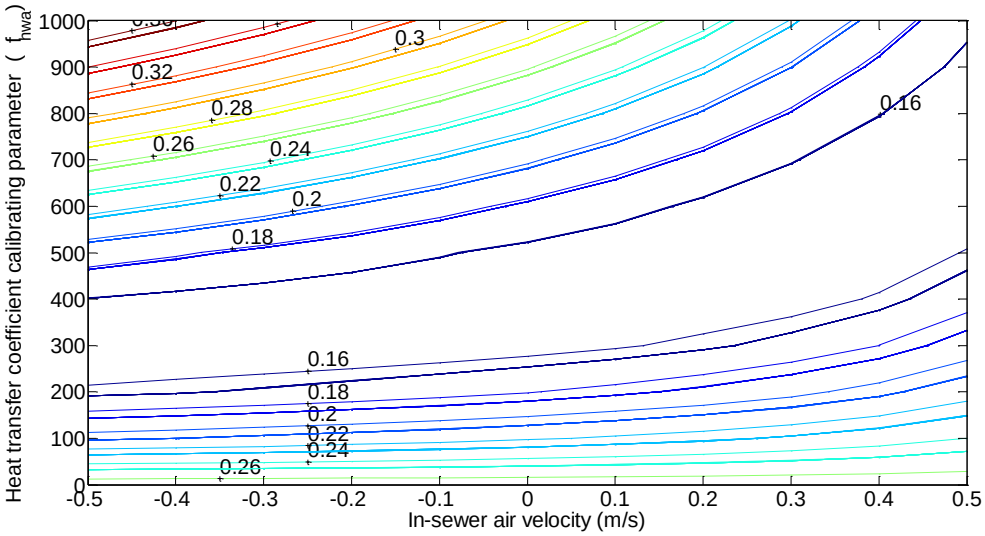

Figure 5.44: Contour plots of RMSE obtained from varying f_{hwa} and in-sewer air velocity (u_a) at different penetration depths (d_s). Large sewer data from Site 3, recorded in February 2013, was utilised.

The impact of varying the soil thermal conductivity, on the RMSE for Site 3 in February 2013, is shown by Figure 5.45.

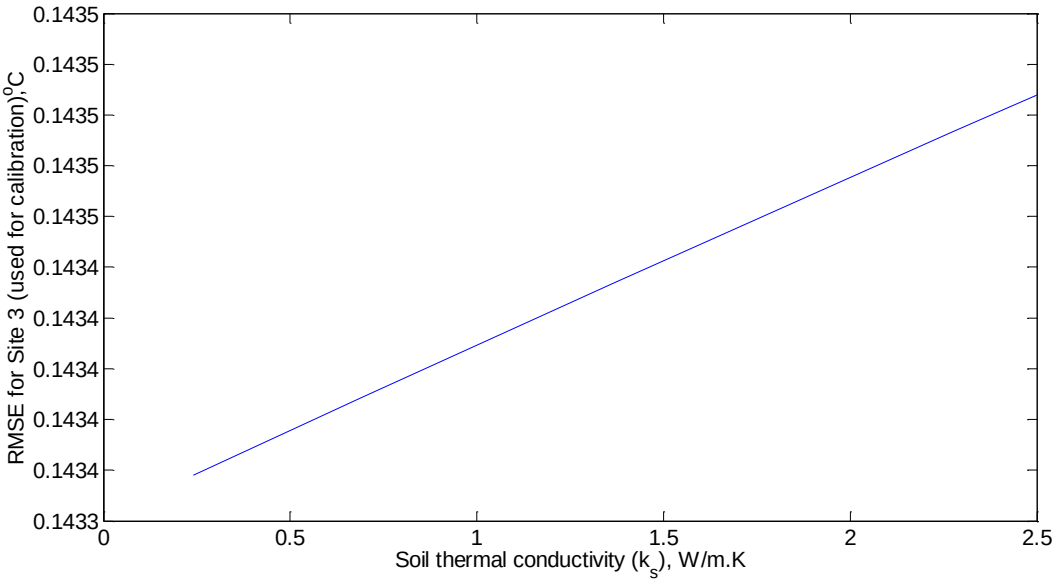

Figure 5.45: Values of RMSE obtained from varying the soil thermal conductivity (k_s) using data from Site 3, recorded in February 2013. Optimum f_{hwa}, u_a and d_s, for February, were considered in this plot.

Impact of varying the soil thermal conductivity on RMSE values was insignificant using the large sewer model for February 2013 data as shown by Figure 5.45. This indicates that the sewer pipe model is insensitive to soil thermal conductivity and hence, any value of k_s within the range shown in Figure 5.45 may be considered. However, the steps described in Section 5.1 were followed. Therefore, considering the soil thermal conductivity value that obtained the minimum RMSE in Figure 5.45, and narrowing the range of calibrating parameters in February 2013 for Site 3, Figure 5.46 was plotted to illustrate optimum calibrating parameters.

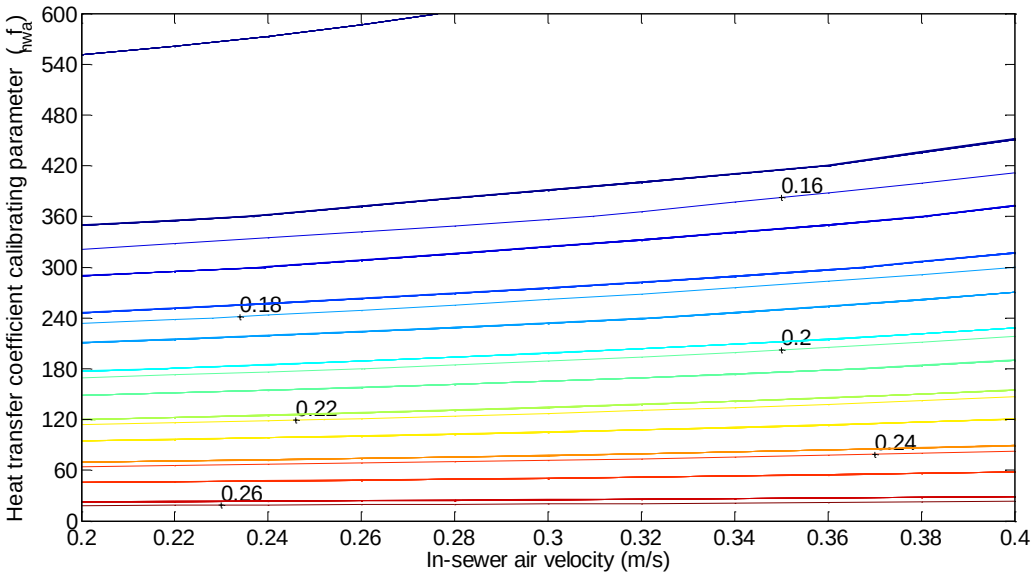

Figure 5.46: Replotting of February 2013 contour plot for RMSE obtained from varying f_{hwa} and in-sewer air velocity (u_a) at different penetration depths (d_s). Narrower calibrating parameter ranges were used while k_s showing minimum RMSE was assumed using large sewer data from Site 3. Values of RMSE are shown on the contour lines.

Replotting of the contour lines for the RMSE of large sewer model in February 2013 has not demonstrated an absolute RMSE minimum, instead almost straight lines were shown by Figure 5.46. This means that the large sewer model was insensitive to the calibrating parameter (f_{hwa}, u_a and d_s). The PDF of model error, obtained from the optimisation by division method for February 2013 data from Site 3 (used for calibration) and Site 4 (used for validation) is shown by Figure 5.47. The RMSE values, in February 2013, were 0.14°C and 0.28°C for Sites 3 and 4 respectively, while the population standard deviation was 0.14°C for each of Site 3 and Site 4. The PDF in Figure 5.46 showed the expected pattern where the site data used for calibration (Site 3) provided a symmetry around a lower model error than that used for validation (Site 4).

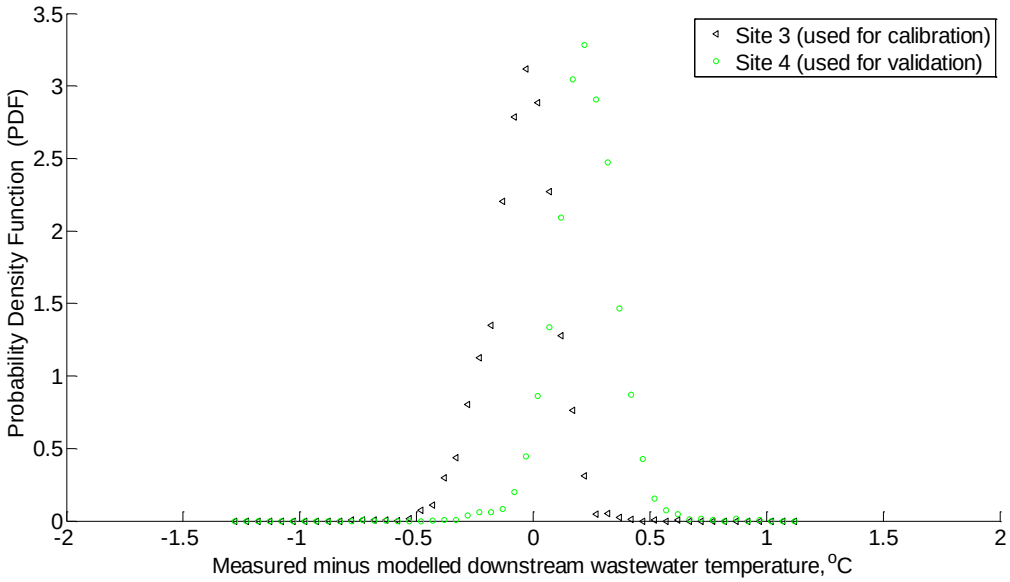

Figure 5.47: PDF of model errors, using the calibrated parameters obtained from the optimisation by division method, for the large sewer sites in February 2013.

The contour plots of Site 3 RMSE, obtained from the optimisation by division method, were created at various penetration depths for March 2013 data as shown by Figure 5.48.

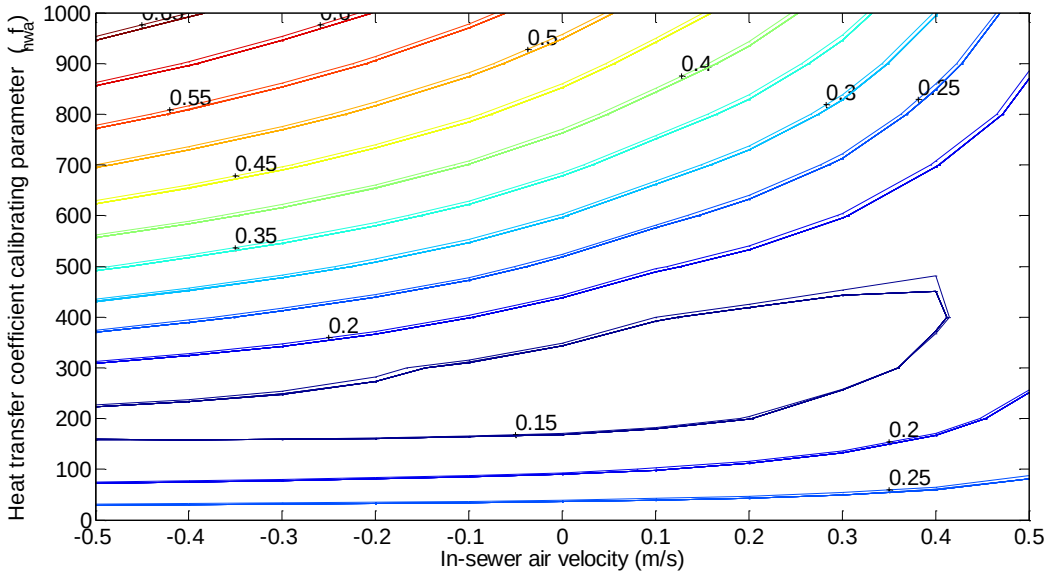

Figure 5.48: Contour plots of RMSE obtained from varying f_{hwa} and in-sewer air velocity (u_a) at different penetration depths (d_s). Large sewer data from Site 3, recorded in March 2013, was utilised. Values of RMSE are shown on the contour lines.

The impact of varying the soil thermal conductivity, on the RMSE for Site 3 using March 2013 data, is shown by Figure 5.49.

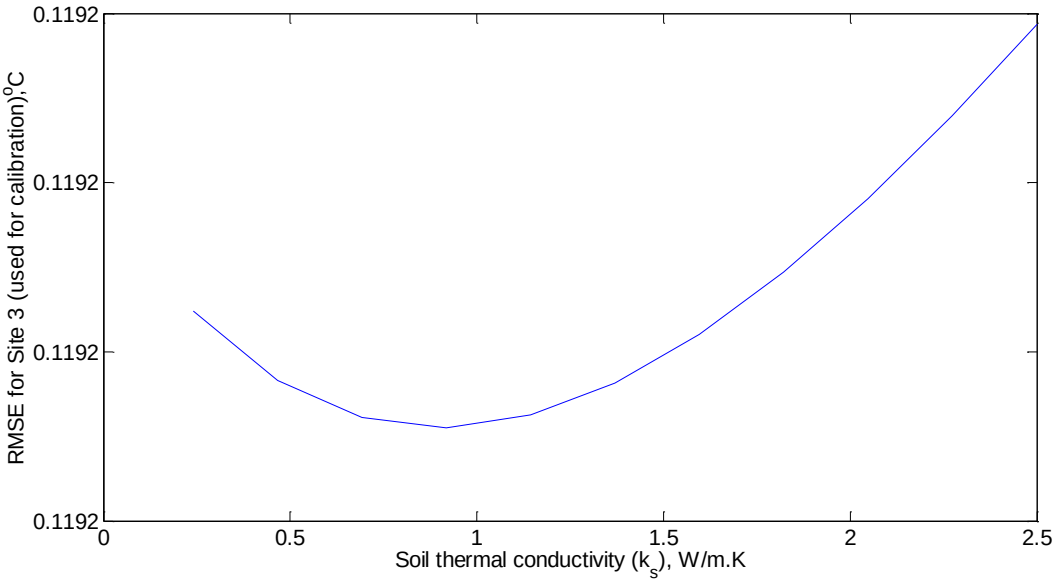

Figure 5.49: Values of RMSE obtained from varying the soil thermal conductivity (k_s) using data from Site 3, recorded in March 2013. Optimum f_{hwa}, u_a and d_s, for March, were considered in this plot.

As in February 2013 case, the variation of k_s presented an insignificant impact on the RMSE obtained for March 2013. This suggests that considering any k_s value within the range shown in Figure 5.49 shall yield to similar modelling results. Yet, the procedure explained in Section 5.1 was followed. Hence, considering the soil thermal conductivity value that obtained the minimum RMSE in Figure 5.49, and narrowing the range of calibrating parameters in March 2013 for Site 3, Figure 5.50 was plotted to illustrate optimum calibrating parameters.

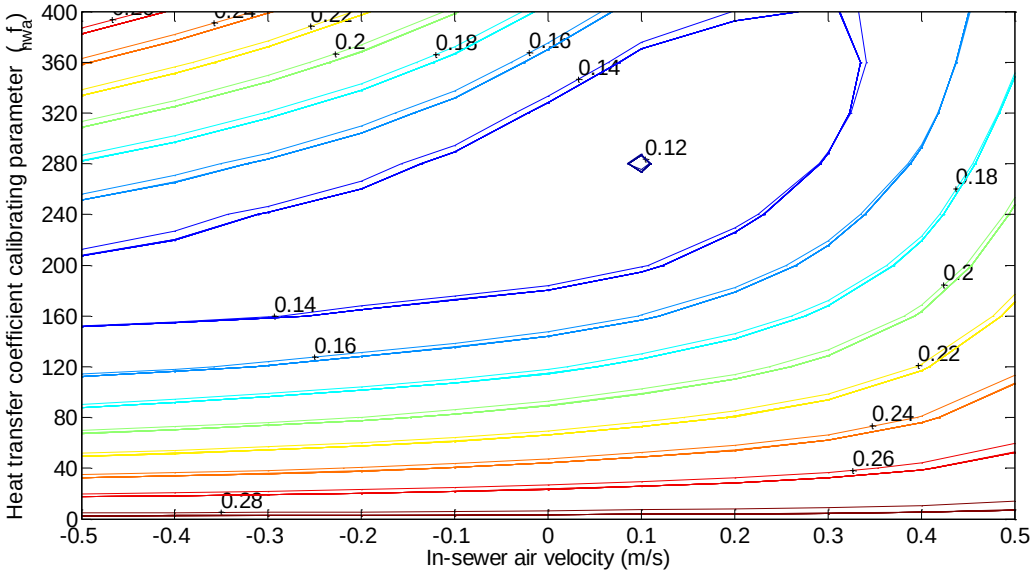

Figure 5.50: Replotting of March 2013 contour plot for RMSE obtained from varying f_{hwa} and in-sewer air velocity (u_a) at different penetration depths (d_s). Narrower calibrating parameter ranges were used while k_s showing minimum RMSE was assumed using large sewer data from Site 3. Values of RMSE are shown on the contour lines.

The PDF of model error, obtained from the optimisation by division method using March 2013 data from Site 3 (used for calibration) and Site 4 (used for validation), is shown by Figure 5.51. The RMSE values, in March 2013, were 0.12°C and 0.25°C for Sites 3 and 4 respectively, while the population standard deviations were 0.12°C for Site 3 and 0.15 °C Site 4. Distribution of model error for March 2013 shown by Figure 5.51 is very close to that obtained from large sewers in February 2013.

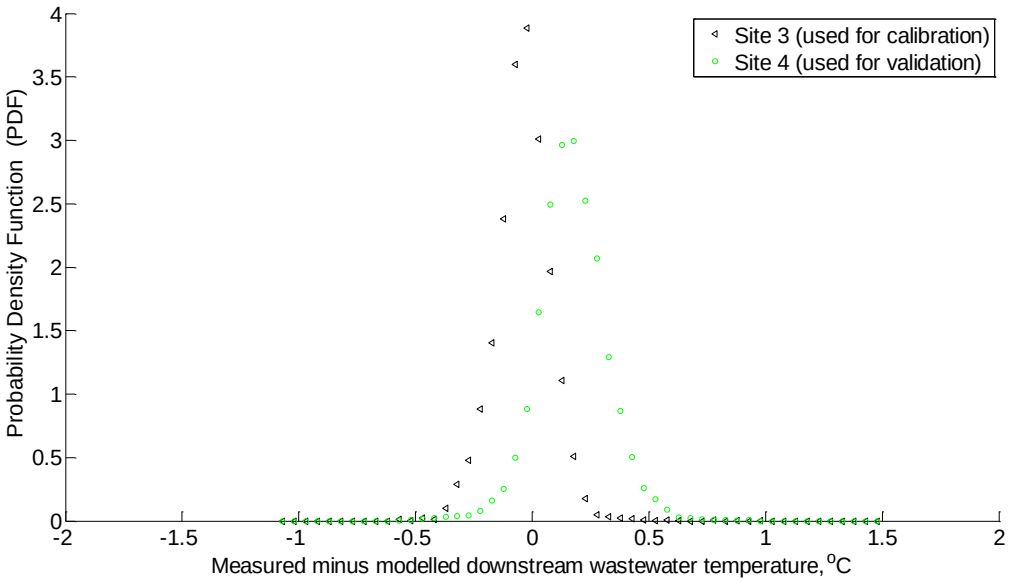

Figure 5.51: PDF of model errors, using the calibrated parameters obtained from the optimisation by division method, for the large sewer sites in March 2013.

The contour plots of Site 3 RMSE, obtained from the optimisation by division method, were created at various penetration depths in April 2013 as shown by Figure 5.52.

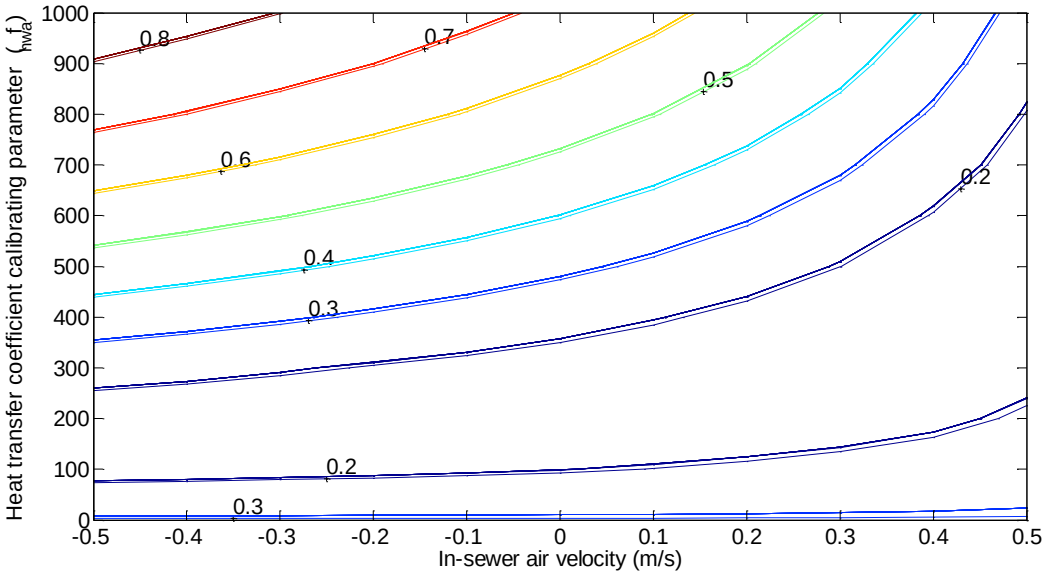

Figure 5.52: Contour plots of RMSE obtained from varying f_{hwa} and in-sewer air velocity (u_a) at different penetration depths (d_s). Large sewer data from Site 3, recorded in April 2013, was utilised.

The impact of varying the soil thermal conductivity, on the RMSE for Site 3 in April 2013, is shown by Figure 5.53.

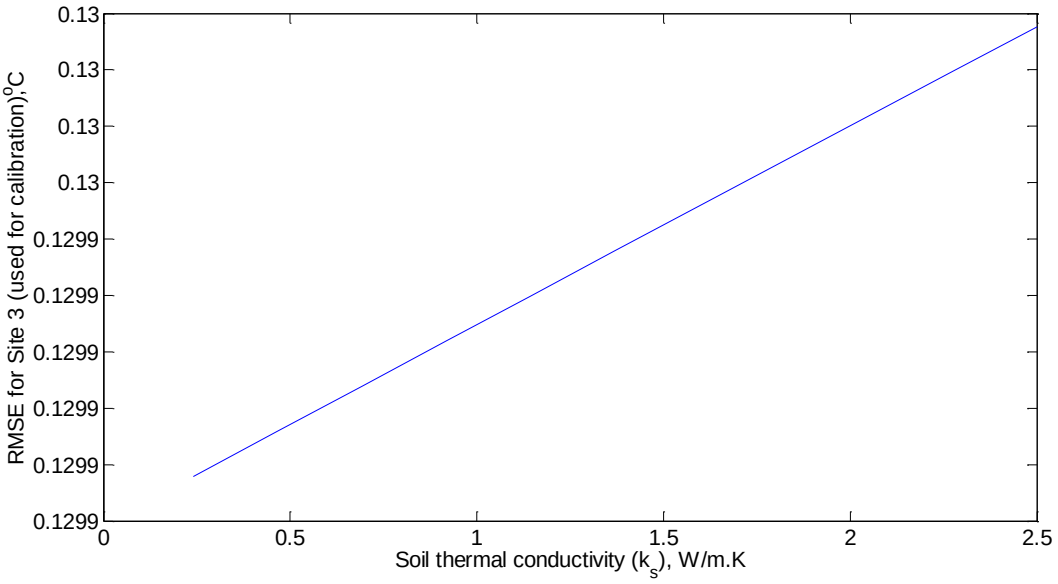

Figure 5.53: Values of RMSE obtained from varying the soil thermal conductivity (k_s) using data from Site 3, recorded in April 2013. Optimum f_{hwa}, u_a and d_s, for April, were considered in this plot.

Figure 5.52 and Figure 5.53 indicate that the large sewer model may prove insensitive to the four calibrating parameters (f_{hwa}, u_a, d_s and k_s). Therefore, considering the soil thermal conductivity value that yielded the minimum RMSE in Figure 5.53, and narrowing the range of calibrating parameters in April 2013 for Site 3, Figure 5.54 was plotted to illustrate optimum calibrating parameters.

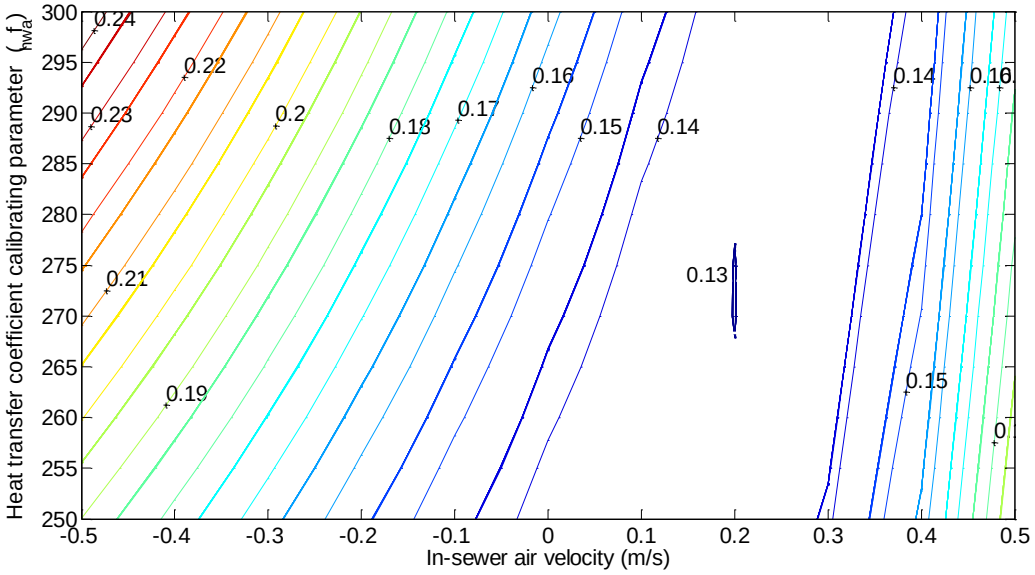

Figure 5.54: Replotting of April 2013 contour plot for RMSE obtained from varying f_{hwa} and in-sewer air velocity (u_a) at different penetration depths (d_s). Narrower calibrating parameter ranges were used while k_s showing minimum RMSE was assumed using large sewer data from Site 3. Values of RMSE are shown on the contour lines.

The PDF of model error, obtained from the optimisation by division method in April 2013, at Site 3 (used for calibration) and Site 4 (used for validation) is shown by Figure 5.55. The RMSE values, in April 2013, were 0.13°C and 0.20°C for Sites 3 and 4 respectively, while the population standard deviations were 0.13°C for Site 3 and 0.15 °C for Site 4. The characteristic of the PDF presented by Figure 5.55 is very similar to that obtained from large sewer model using February 2013 data.

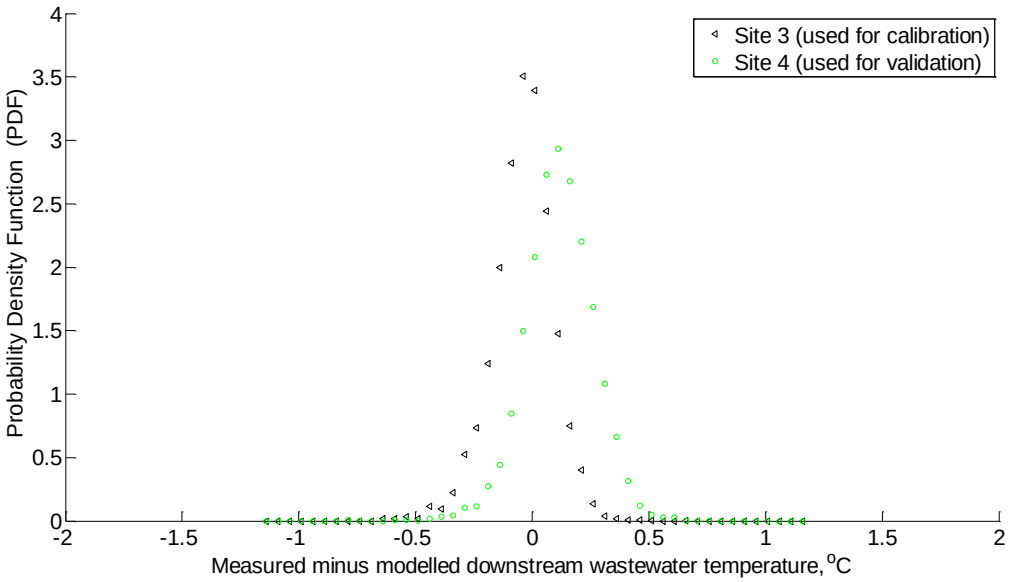

Figure 5.55: PDF of model errors, using the calibrated parameters obtained from the optimisation by division method, for the large sewer sites in in April 2013.

The contour plots of Site 3 RMSE, obtained from the optimisation by division method, were created at various penetration depths in May 2013 as shown by Figure 5.56.

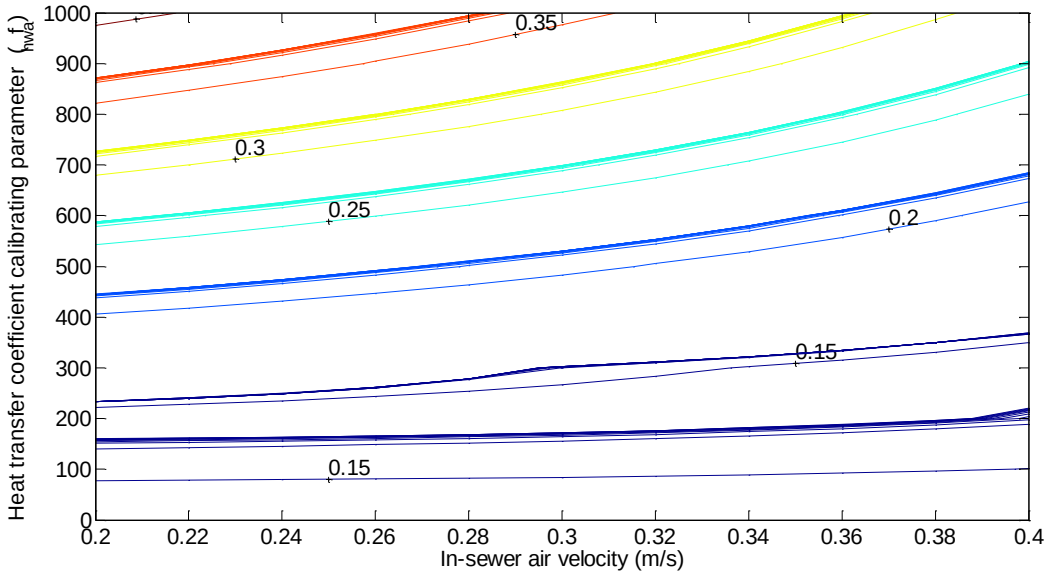

Figure 5.56: Contour plots of RMSE obtained from varying f_{hwa} and in-sewer air velocity (u_a) at different penetration depths (d_s). Large sewer data from Site 3, recorded in May 2013, was utilised.

The impact of varying the soil thermal conductivity, on the RMSE for Site 3 in May 2013, is shown by Figure 5.57.

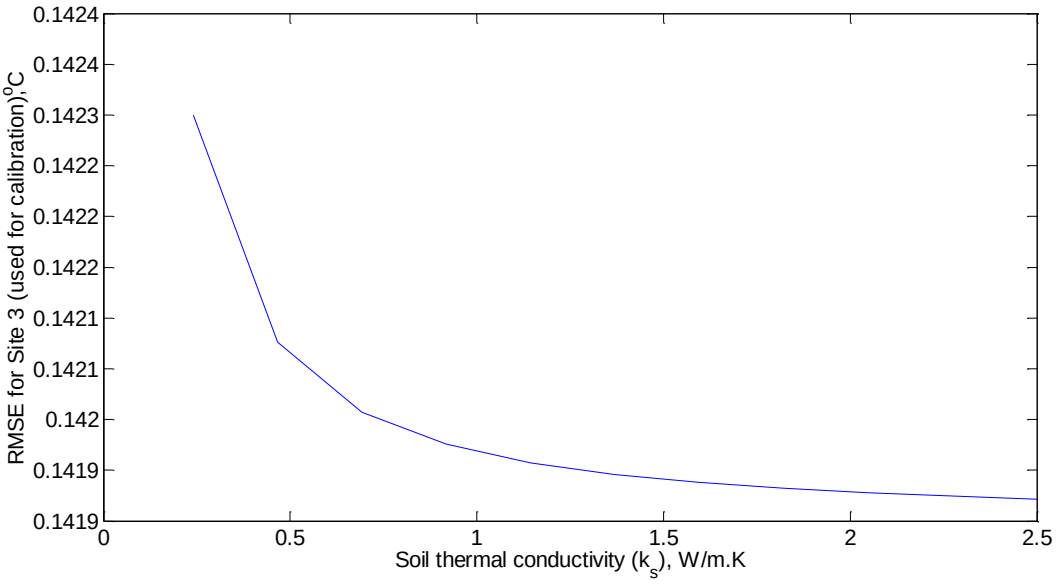

Figure 5.57: Values of RMSE obtained from varying the soil thermal conductivity (k_s) using data from Site 3, recorded in May 2013. Optimum f_{hwa}, u_a and d_s, for May, were considered in this plot.

In a similar case to that of April 2013 in large sewers, Figure 5.56 and Figure 5.57 indicate that the large sewer model is insensitive to the four calibrating parameters in May 2013, yet the procedure explained in Section 5.1 was followed. Hence, Figure 5.56 was replotted by considering the soil thermal conductivity value that obtained the minimum RMSE in Figure 5.57, and by narrowing the range of calibrating parameters in May 2013 for Site 3. Figure 5.58 shows the replotting of Figure 5.56 to illustrate the optimum calibrating parameters.

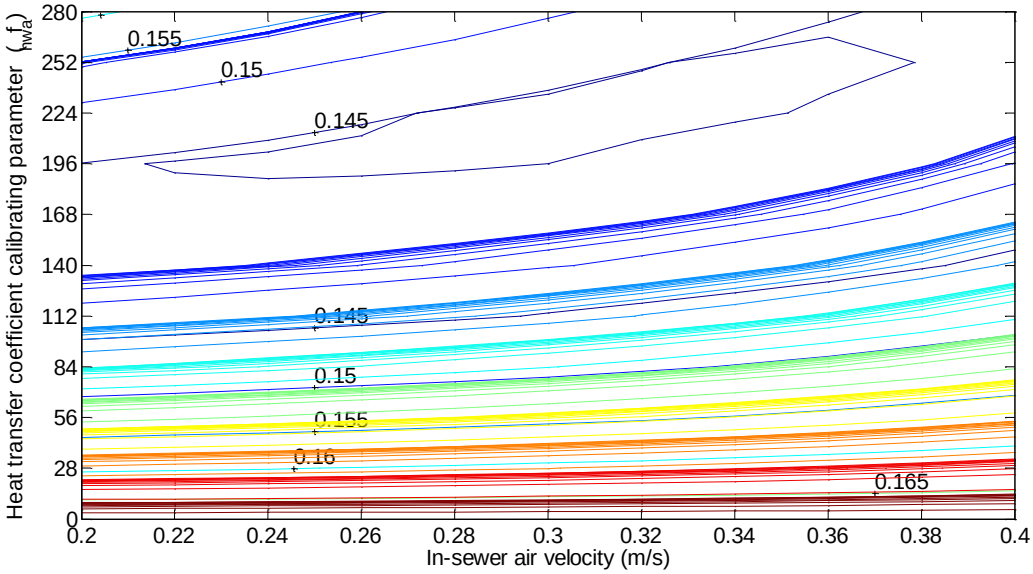

Figure 5.58: Replotting of May 2013 contour plot for RMSE obtained from varying f_{hwa} and in-sewer air velocity (u_a) at different penetration depths (d_s). Narrower calibrating parameter ranges were used while k_s showing minimum RMSE was assumed using large sewer data from Site 3. Values of RMSE are shown on the contour lines.

The PDF of model error, obtained from the optimisation by division method in May 2013, at Site 3 (used for calibration) and Site 4 (used for validation) is shown by Figure 5.59. The RMSE values, in May 2013, were 0.14°C and 0.15°C for Sites 3 and 4 respectively, while the population standard deviations were 0.14°C for Site 3 and 0.15°C Site 4. Figure 5.59 shows that the large sewer model presents good symmetry around a near zero model error for data from Sites 3 and 4 in May 2013.

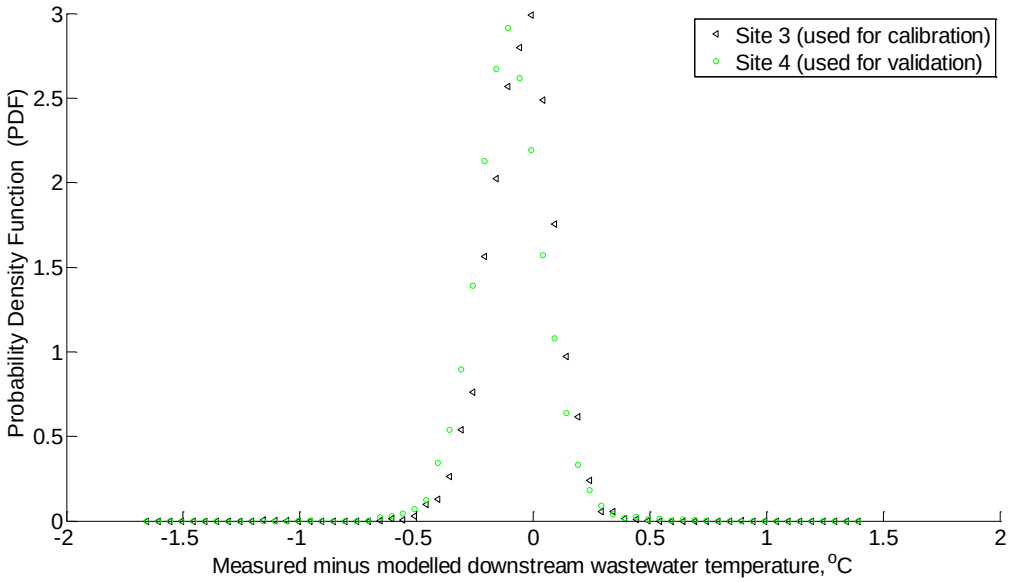

Figure 5.59: PDF of model errors, using the calibrated parameters obtained from the optimisation by division method, for the large sewer sites in May 2013.

Summary of findings from implementing the optimisation by division method

The large sewer model has generally shown lower RMSE and standard deviation values than that of the urban sewer model using the optimisation by division method. Overall, the RMSE and standard deviation values, in this section, were in the same order, while the urban and large sewers' data used for calibration (Sites 2 and 3) obtained lower RMSEs than those obtained from validation data (Sites 1 and 4). The PDF plots, obtained from implementing the optimisation by division method, showed that the large sewer model using the calibration data from Site 3 showed close distribution of the model error to that when the model used the validation data from Site 4. In general the optimisation by division method showed that the large sewer model provides more accurate results than that of the urban sewer model which is interpreted by the RMSEs, standard deviations and PDF plots. The next section shows the values of calibrated parameters obtained from the contour plots in this section. Results and findings from the optimisation by division method is discussed further in Section 5.3.

5.2.3 Values of Calibrated Parameters, RMSE and Standard Deviation

Values of calibrated parameters, RMSE and population standard deviation obtained from using both calibration methods, for all sites are shown in this section. Table 5.7 and Table 5.8 are dedicated for showing RMSE and population standard deviation values in urban sewers using the Matlab optimisation function 'fmincon' code and the optimisation by division methods respectively, while Table 5.9 and Table 5.10 show the same values for large sewers using Matlab optimisation function and optimisation by division methods respectively.

Table 5.7: Values of calibrated parameters, using the Matlab optimisation function 'fmincon' code, and their relevant RMSE and population standard deviation values for urban sewers in the periods between March 2012 and July 2012. Highlighted rows indicate site data used for calibration.

Parameter	**Unit**	**March**	**April**	**May**	**June**	**July**
Heat transfer calibrated parameter, f_{hwa}	-	118	199	25	0.10	0.10
In-sewer air velocity, u_a	m/s	0.50	0.19	0.28	0.28	0.50
Penetration depth, d_s	m	0.01	10.00	0.10	0.48	0.20
Soil thermal conductivity, k_s	W/m.K	2.50	0.24	2.50	2.49	1.27
Site				**RMSE**		
1 (used for validation)	°C	0.55	0.48	0.72	0.36	0.31
2 (used for calibration)	°C	0.52	0.33	0.33	0.27	0.22
Site				**Population standard deviation**		
1 (used for validation)	°C	0.43	0.48	0.36	0.30	0.30
2 (used for calibration)	°C	0.49	0.33	0.32	0.27	0.22

Table 5.8: Values of calibrated parameters, using the optimisation by division method, and their relevant RMSE and population standard deviation values for urban sewers in the periods between March 2012 and July 2012. Highlighted rows indicate site data used for calibration.

Parameter	**Unit**	**March**	**April**	**May**	**June**	**July**
Heat transfer calibrated parameter, f_{hwa}	-	420	230	35	0.10	0.10
In-sewer air velocity, u_a	m/s	0.20	0.18	0.28	0.28	0.28
Penetration depth, d_s	m	0.01	10.00	0.01	0.41	0.21
Soil thermal conductivity, k_s	W/m.K	0.24	0.24	2.50	2.50	1.38
Site		**RMSE**				
1 (used for validation)	°C	0.83	0.48	0.74	0.40	0.31
2 (used for calibration)	°C	0.39	0.33	0.33	0.28	0.22
Site		**Population standard deviation**				
1 (used for validation)	°C	0.77	0.48	0.40	0.31	0.30
2 (used for calibration)	°C	0.39	0.33	0.33	0.27	0.22

Table 5.9: Values of calibrated parameters, using the Matlab optimisation function 'fmincon' code, and their relevant RMSE and population standard deviation values for large sewers in the periods between February 2013 and May 2013. Highlighted rows indicate site data used for calibration.

Parameter	**Unit**	**February**	**March**	**April**	**May**
Heat transfer calibrated parameter, f_{hwa}	-	415	239	256	194
In-sewer air velocity, u_a	m/s	0.25	0.07	0.23	0.30
Penetration depth, d_s	m	10.00	10.00	10.00	1.00
Soil thermal conductivity, k_s	W/m.K	0.24	0.24	0.24	2.50
Site		**RMSE**			
3 (used for calibration)	°C	0.15	0.12	0.13	0.14
4 (used for validation)	°C	0.35	0.33	0.29	0.16
Site		**Population standard deviation**			
3 (used for calibration)	°C	0.14	0.11	0.13	0.14
4 (used for validation)	°C	0.14	0.15	0.15	0.16

Table 5.10: Values of calibrated parameters, using the optimisation by division method, and their relevant RMSE and population standard deviation values for large sewers in the periods between February 2013 and May 2013. Highlighted rows indicate site data used for calibration.

Parameter	**Unit**	**February**	**March**	**April**	**May**
Heat transfer calibrated parameter, f_{hwa}	-	456	280	280	196
In-sewer air velocity, u_a	m/s	0.22	0.10	0.22	0.36
Penetration depth, d_s	m	10.00	2.00	10.00	0.01
Soil thermal conductivity, k_s	W/m.K	0.24	1.00	0.24	2.50
Site		**RMSE**			
3 (used for calibration)	°C	0.14	0.12	0.13	0.14
4 (used for validation)	°C	0.28	0.25	0.20	0.15
Site		**Population standard deviation**			
3 (used for calibration)	°C	0.14	0.12	0.13	0.14
4 (used for validation)	°C	0.14	0.15	0.15	0.15

Key findings from the calibrated parameter values

The calibrated parameter values were found to be changing depending on the period at which the data was measured as can be observed from Tables 5.7 to 5.10. In particular the heat transfer calibrated parameter (f_{hwa}) was found to be higher in colder months (i.e. February, March and April) than those in warmer months (May, June July) for urban and large sewers. The large sewers have generally shown slightly higher f_{hwa} values in March and April than those attained for the urban sewers, while using May data presented much higher f_{hwa} value than that in urban sewer, as shown by Table 5.7 and Table 5.9. One exception was the value of f_{hwa}, in March obtained from the optimisation by division method (Table 5.8) using urban sewer data (Site 2), which was higher than that of March obtained from large sewer data using both calibration methods. The value of calibrated in-sewer air velocity was generally stable at different months using both calibration methods, and was mostly between around 0.2 and 0.3 m/s. It was noticed that the calibrated soil thermal conductivity and penetration depth vary depending on the measuring period and calibration method. The seasonal variation of the calibrated parameters, particularly $f_{hwa,}$ suggests that heat transfer mechanism varies depending on the weather of the local area as will be explained in Section 5.3. In general, both calibration methods provided close calibrated parameter, RMSE and standard deviation values. The next section discusses, in details, the values of calibrated parameters, their corresponding RMSE and standard deviation values obtained using the four sites' data from both calibration methods.

5.3 Discussion of the Calibration and Validation Results

Calibrating the heat transfer parameters, identified in Table 5.3, through the Matlab optimisation function 'fmincon' code, which is also known as the 'optimisation by constrained nonlinear programming' has shown calibrated parameter values close to those calibrated through the 'optimisation be division' method in most cases. In particular, both methods obtained very close values for heat transfer calibrating parameter (f_{hwa}) and in-sewer air velocity (u_a) using the large sewer data as shown by Tables 5.7 to 5.10. The difference in the soil thermal conductivity (k_s) values, obtained from both calibration methods, can be neglected since the impact of k_s on root mean square error (RMSE) was insignificant, as demonstrated by Figures 5.45, 5.49, 5.53 and 5.57. This

suggests that k_s may vary within its range (0.24 to 2.5W/m.K), identified in Table 5.6, causing negligible impacts on the modelling error. Although the sensitivity analysis, presented in Figure 5.2 and Figure 5.3, indicated that the sewer pipe model is sensitive to k_s, other parameters (i.e. f_{hwa} and u_a) had larger impacts on the modelling error. This was also the case in urban sewers where specifically colder months (i.e. March and April) showed negligible impacts on RMSE when k_s was varied within its range as demonstrated by Figure 5.25 and Figure 5.29. Since the soil penetration depth (d_s) is closely associated with the soil thermal conductivity, when computing the soil thermal resistivity (explained by Equation 3.29), it is worth discussing the impact of varying d_s values when analysing the values of soil thermal conductivity. Assuming steady state conditions, it is expected that d_s varies depending on the scale of wastewater flow rates. Higher values for the product of mass flow rate and the specific heat capacity ($\dot{m} \times c_p$) create more thermal energy and hence require deeper d_s to dissipate this energy. This may explain the reason behind the large sewer (Site 3) obtaining relatively higher d_s than that of the urban sewer in the majority of the months, using both calibration methods, as shown by Table 5.11.

Table 5.11: Monthly averaged wastewater flow rates (L/s) and calibrated values of soil penetration depths (d_s) in large and urban sewers using both calibration methods. Opt. and Fun. stand for optimisation and function respectively. Sites 2 and 3 datasets were utilised for calibration.

Month	**Flow (L/s)**	**Site 2 (urban)**		**Average Flow (L/s)**	**Site 3 (large)**	
		d_s (m)			**d_s (m)**	
		Matlab Opt. Fun.	**Opt. by division**		**Matlab Opt. Fun.**	**Opt. by division**
February	-	-	-	433	10	10
March	12	0.01	0.01	308	10	2
April	14	10	10	281	10	10
May	13	0.1	0.01	339	1	0.01
June	20	0.48	0.41	-	-	-
July	18	0.20	0.21	-	-	-

Referring back to Equation 3.29, thermal resistivity in soil is expressed by $(\frac{d_s}{k_s \times wet.p})$. Therefore, when both d_s and soil thermal conductivity (k_s) were calibrated, Matlab optimises the ratio of d_s to k_s $(\frac{d_s}{k_s})$. This was the case using both calibration methods i.e. the Matlab optimisation function and the optimisation by division method. Although both calibration methods obtained low d_s values for high flow rates in June and July of urban sewers, as shown by Table 5.11, the ratios of $\frac{d_s}{k_s}$ were high to accommodate the larger flows. A relation between wastewater urban sewer flow rates and $(\frac{d_s}{k_s})$ ratios may be developed, using the values obtained from both calibration methods. Figure 5.60 and Figure 5.61 illustrate this relation using the Matlab optimisation function 'fmincon' and optimisation by division methods respectively. The large sewers have generally shown larger yet similar $\frac{d_s}{k_s}$ values at all flows and therefore, plotting $\frac{d_s}{k_s}$ in large sewers was not considered in this section.

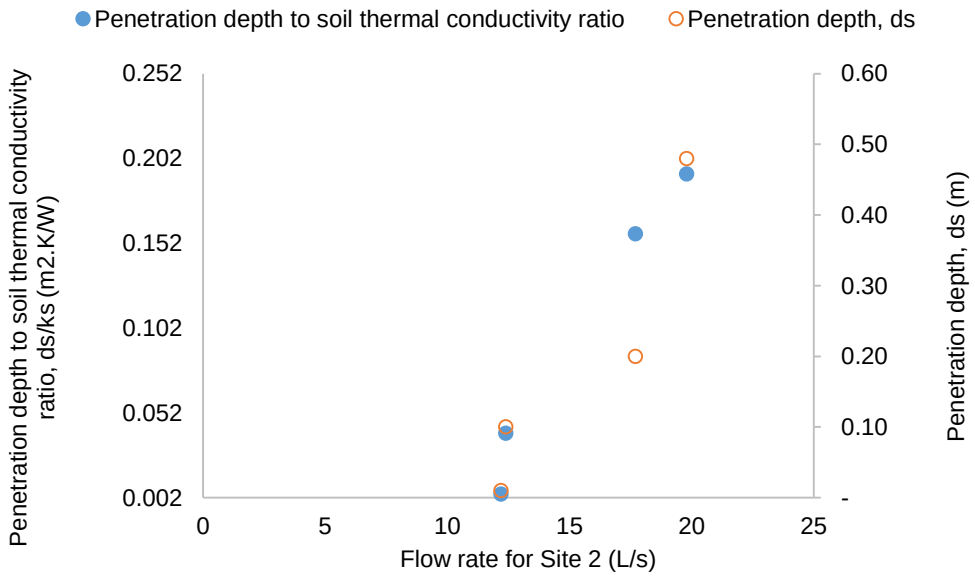

Figure 5.60: Impact of Site 2 wastewater flow rate on the calibrated penetration depth and on the ratio of penetration depth to the soil thermal conductivity using Matlab optimisation function. April period values were avoided in this graph as the $\frac{d_s}{k_s}$ ratio was 42 which is too high to plot among other ratios.

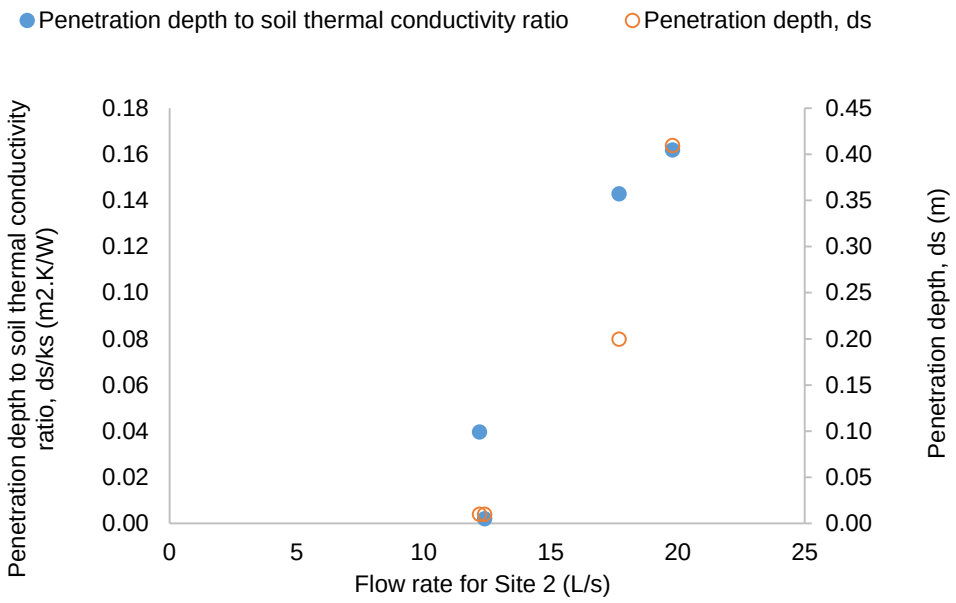

Figure 5.61: Impact of Site 2 wastewater flow rate on the penetration depth and on the ratio of penetration depth to the soil thermal conductivity using optimisation by division method. April period values were avoided in this graph as the $\frac{d_s}{k_{soil}}$ *ratio was also 42 which is too high to plot among other ratios.*

One can observe, from Figure 5.60 and Figure 5.61, the relation between wastewater flow rate and d_s, which indicates that the increase in flow rate results in deeper penetration depths. This relation, between flow rate and d_s, becomes even clearer when d_s is divided by the soil thermal conductivity to form the $\frac{d_s}{k_s}$ ratio. This suggests that higher flow rates require deeper d_s to dissipate more thermal energy, yet lower calibrated d_s values may be obtained when the calibrated k_s shows lower values. Therefore, one shall consider the ratio of $\frac{d_s}{k_s}$ as a whole when studying the soil thermal resistivity. The ratio of $\frac{d_s}{k_s}$ obtained through both calibration methods in April 2012 of urban sewers is much higher than those obtained in other months at the same site. Referring to the optimisation by division method, it can be noticed from Figure 5.30 that the range of d_s shows close RMSE values. This indicates that varying the values of d_s in April 2012 of Site 2 may cause an insignificant impact on the RMSE. For example, if d_s and k_s in March 2012 from Site 2 were used in April 2012 for the same site, i.e. the $\frac{d_s}{k_s}$ ratio in April 2012 becomes 0.004 instead of 42, the RMSE would increase by an insignificant amount (less than 0.01 °C). More detailed work is required to

investigate the calibration of soil penetration depth and soil thermal conductivity. This may be achieved by fixing the soil thermal conductivity values using either default or measured values. Although measuring k_s for the soil surrounding the sewer pipe may prove challenging, examining the Thermo-physical properties of the local soil under different climatic conditions can provide fair estimates of the soil thermal conductivities.

The greatest difference in the calibrated parameter values, obtained using the different calibration methods, was in urban sewers using March data, where f_{hwa}, obtained from the Matlab optimisation function, was almost the fourth of that obtained through the optimisation by division method. The value of f_{hwa} obtained from the latter method fits well with the pattern of f_{hwa} variation across all months in both sites. It is clear that f_{hwa} decreases in warmer months as can be noticed from Tables 5.7 to 5.10 except in urban sewer at March when Matlab optimisation function was implemented. This suggests that the latter calibration method has presented a rather unusual value for f_{hwa} which explains its corresponding high RMSE in March. The pattern of f_{hwa} variation across all months suggests that the heat transfer process between wastewater and in-sewer air is season dependent. Site 2, which was used to calibrate the urban sewer model, has particularly shown low f_{hwa} values in the months of May, June and July. These summer months presented generally higher in-sewer air temperatures than those of wastewater as demonstrated by Figure 5.62. Wastewater temperature variation along a sewer pipe profile is a balance of heat transfer processes between wastewater and in-sewer air and between wastewater and the surrounding soil, through pipe wall, as described by Equation 3.31. These two processes are governed by the in-sewer air and soil temperatures and are influenced by the thermal resistivity components between wastewater and in-sewer air (R_{wa}) and between wastewater and soil (R_{ws}). Rearranging Equation 3.31, which is the main formula used to model wastewater temperature variation along the sewer pipe profile, Equation 5.14 can be developed to show the wastewater temperature difference between up and down streams.

$$T_m - T_{m+n} = \frac{\frac{1}{R_{wa}} \times (T_m - T_{air}) + \frac{1}{R_{ws}} \times (T_m - T_{soil})}{\rho \times Q \times c_p} \times \Delta L \quad (5.14)$$

Referring to the numerator of Equation 5.14, values of the temperature differences between wastewater along the pipe ($T_{m+1,2...}$) and the soil or the in-sewer air (T_{soil} or T_{air} respectively) can change the overall numerator sign from positive to negative. An overall positive sign for the numerator of Equation 5.14 indicates a heat loss from the sewerage wastewater, which results in wastewater temperature drop streamwise. On the other hand, an overall negative numerator sign in Equation 5.14 means an overall heat gain to the sewerage wastewater which causes a wastewater temperature increase streamwise. The measured wastewater temperature was greater than that of soil during all months in Site 2 as illustrated by Figure 5.62, and therefore the multiplication product associated with thermal resistivity between wastewater and soil ($\frac{1}{R_{ws}} \times (T_m - T_{soil})$) in Site 2 stayed positive in all months. Conversely, the in-sewer air temperatures in Site 2 summer months (May, June and July of 2012) were higher than those of wastewater which results in a negative value for the multiplication product associated with the thermal resistivity between wastewater and in-sewer air ($\frac{1}{R_{wa}} \times (T_m - T_{air})$). Therefore, balancing the wastewater temperature variation along Site 2 sewer pipe, in summer months, requires higher R_{wa} values (i.e. lower f_{hwa}). Balancing in this context means that the predicted wastewater temperature variation along the sewer pipe profile, $(T_{m+n} - T_m)$ in Equation 5.14, shall match the measured streamwise temperature change by varying R_{wa} and R_{ws}. For example, higher R_{wa} (i.e. lower f_{hwa}) values result in obtaining lower values of $(\frac{1}{R_{wa}} \times (T_m - T_{air}))$ than those of $(\frac{1}{R_{ws}} \times (T_m - T_{soil}))$ during the summer months in Site 2. Accounting for the signs caused by the measured wastewater temperature differences between wastewater and in-sewer air and soil, the numerator of Equation 5.14 turns to a positive value in Site 2 during summer months, which matches the measured wastewater temperature variation streamwise in Figure 5.63. Hence, lower f_{hwa} were obtained in summer months.

While Figure 5.62 shows Site 2 measured temperature differences between wastewater and in-sewer air and between wastewater and soil, Figure 5.63 shows measured wastewater temperature variation streamwise in Site 2.

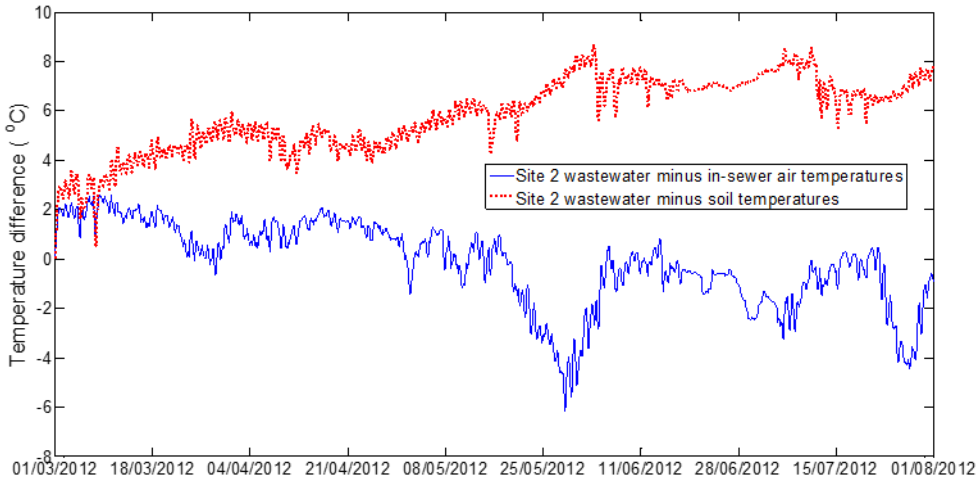

Figure 5.62: Temperature differences between wastewater and in-sewer air and the surrounding soil in Site 2.

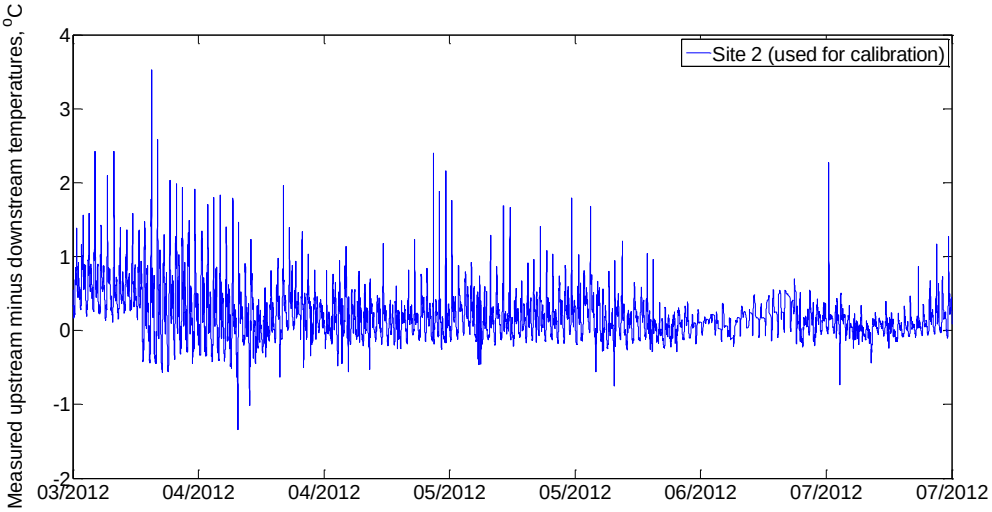

Figure 5.63: Measured wastewater temperature variation along the sewer pipe of Site 2. Considering streamwise direction, positive vertical axis values indicate temperature drop while negatvie values mean temperature increase. Data plotted for the measurement period between 1st March 2012 to the end of July 2013.

The heat transfer coefficient between a liquid and gas is ultimately dependent on thermal conductivities of the fluid and the gas. Therefore, explaining the physical reasons behind the lower f_{hwa} values in summer months requires the understanding of the molecular behaviours in both wastewater and in-sewer air and how this may impact on their thermal conductivities. Wastewater, and in-sewer air, as in any fluid have large intermolecular spacing that makes them less

thermally conductive than solids (Incropera *et al.*, 2007). Hence, the increase in temperature during summer months (May, June and July) may result in increasing these large intermolecular spacing which can eventually result in reducing the thermal conductivities of wastewater and in-sewer air. However, the thermal conductivity of a fluid (e.g. wastewater and in-sewer air) also depends on other factors such as the molecular average speed (Incropera *et al.*, 2007), which can also increase when temperature increases and hence, may result in higher thermal conductivity. Therefore, it is difficult to fully understand the physics behind the lower f_{hwa} obtained for the summer months period. Further work needs to be held to observe the impact of temperature on the thermal conductivity of wastewater and in-sewer air. It was noticed that June 2012 in Site 2 experienced the lowest absolute difference between wastewater and in-sewer air temperatures as shown by Figure 5.62 and hence, the scale of heat transferred between wastewater and in-sewer air was relatively low. Therefore, this may be another reason behind low f_{hwa} value in June 2012.

Values of the large sewer f_{hwa} were generally greater than those of the urban sewers obtained through both calibration methods. This may suggest that the behaviour of heat transfer, between wastewater and in-sewer air, in large sewers is different to that of urban sewers which was concluded in Section 4.3 and was also the findings of Abdel-Aal *et al.* (2015), who used predictive modelling techniques to estimate wastewater temperatures in urban and large sewers. The difference in heat transfer behaviours for urban and large sewers is expected as the wastewater flow rate differ greatly depending on the sewer type. Equation 5.14 interprets wastewater temperature variation along the pipe profile mathematically, which clearly shows that higher wastewater flow rates result in lower temperature variation streamwise. Higher wastewater flow rates mean more energy is required to dissipate in order to drop the wastewater temperature by 1 °C. This is based on the heat capacity of wastewater, which is the multiplication product of the specific heat capacity (c_p) and the wastewater mass flow rate. For example, consider the DWF for Sites 2 and 3 of 0.01 and 0.36 m^3/s respectively (Table 5.1), Site 3 would require 36 times the energy required by Site 2 to drop its temperature by 1 °C. This means the scale of heat transfer, in large sewers, between wastewater and in-sewer air and between wastewater and soil is less than that in urban sewers. Therefore the large sewer model is less

sensitive, to the calibrated parameters, than that of urban sewers which was also shown by Section 5.1.1. This explains why the large sewers have generally presented lower RMSE than that of the urban sewers which also resulted in better distribution of errors, in large sewers, as demonstrated by the PDF figures in Section 5.2.

The calibrated in-sewer air velocity (u_a) varied from 0.06 to 0.5 m/s in the urban and large sewers, using both calibration methods, which is higher than that measured by Madsen, Hvitved-Jacobsen and Vollertsen (2006). The latter authors used a 0.5m diameter sewer pipe with average dry weather flows close to that of urban sewers in this work (i.e. 13 to 16 L/s). However, Madsen's 54 measurements were carried out only during dry weather flow and did not cover different seasons. Therefore, u_a may vary at different climates when calibrated through larger datasets. The lowest u_a value was obtained in March at Site 3 which is likely due to the relatively large drop in wastewater velocity in this period, as observed from Figure 4.21. This relation between the velocity of wastewater and that of in-sewer air was also found by Pescod and Price (1981) who carried out early experimental studies on sewer ventilation to find that in-sewer air velocities are usually slightly less than that of wastewater. Other external factors may influence the in-sewer air velocity too, such as the local wind speed and atmospheric pressure (Pescod and Price, 1981), which were unfortunately not measured in this work. Calibration of u_a has not shown any negative values which suggests that in-sewer air flows in a streamwise direction.

The probability density function (PDF) for those sites used for calibration (i.e. sites 2 and 3) illustrated good distribution, in most cases, compared with those used for validation (Sites 1 and 4). Good PDF distributions mean that the probability density function plot is close to be symmetric around the zero value of the model error. March and May of urban sewers have particularly presented more skewed PDF plots in Site 1, which was used for validation, as shown by Figure 5.27 and Figure 5.35 . This is also reflected in the RMSE values for these months in Site 1. It was noticed that colder months (March and April) showed slightly poorer PDF distribution in all sites, which suggests that there is a systematic error in these months. A poor PDF in this context is identified by PDF distribution being non-Gaussian or having larger skewness around the zero model error. This systematic error in winter months requires further work to investigate its possible

causes. The large sewers have generally shown better model error distribution than that of the urban sewers, as well as lower RMSE values which was explained earlier in this section.

This section has shown that both calibration methods i.e. Matlab optimisation function 'fmincon' and optimisation by division provide close calibrated parameter values. The overall average RMSE obtained from each method at all sites during all months was 0.32°C. The overall average population standard deviation (σ), for all months at all sites was 0.24°C when Matlab optimisation function was implemented, while the optimisation by division method showed an overall average σ of 0.27°C. This suggests that minor differences in the results obtained from both methods are negligible when considering a number of sites at different periods. One advantage of the optimisation by division method was the ability to observe the changes in RMSE caused by each calibrating parameter through the contour plots and soil thermal conductivity figures. However, the process of implementing the Matlab optimisation function was much less time consuming than that of applying the optimisation by division method. Although both methods were implemented using Matlab, the optimisation by division is not a built in technique and therefore an independent Matlab code was written specifically for the purpose of this calibration. Furthermore, computational time was also much larger when the optimisation by division was implemented in Matlab using four 'for loop' codes. For example, the Matlab optimisation function 'fmincon' took eight seconds to run the April 2012 data in urban sewers while the optimisation by division code required two minutes to run using the same data. Optimisation by division requires larger amount of RAM to calibrate all the parameters simultaneously and the number of iteration points was limited to 11 points for each parameter. An additional advantage of the Matlab optimisation function 'fmincon' is the consistency in the obtained RMSE values among each site category. For example, Matlab optimisation function obtained a RMSE in March 2012 for Site 1 (used for validation) that is close to that of Site 2 (used for calibration). On the other hand, the RMSE for Site 2 in March, obtained through the optimisation by division method, was more than the double of that for Site 1.

Therefore, it was decided to use the calibrated parameters obtained through the Matlab optimisation function 'fmincon' when modelling wastewater temperature variations in sewer networks.

Before moving into the next section, the following part of this section shows modelled wastewater temperatures, in all sites, using the calibrated parameters. The modelled wastewater temperature is compared with the measured temperatures from all sites. Modelled wastewater temperatures from this point refers to those modelled using the calibrated parameters obtained from the Matlab optimisation function 'fmincon'. Figure 5.64 and Figure 5.65 show the modelled and measured wastewater temperature variations in Sites 1 and 2 respectively. Figure 5.66 and Figure 5.67 show the modelled and measured wastewater temperature variations in Sites 3 and 4 respectively.

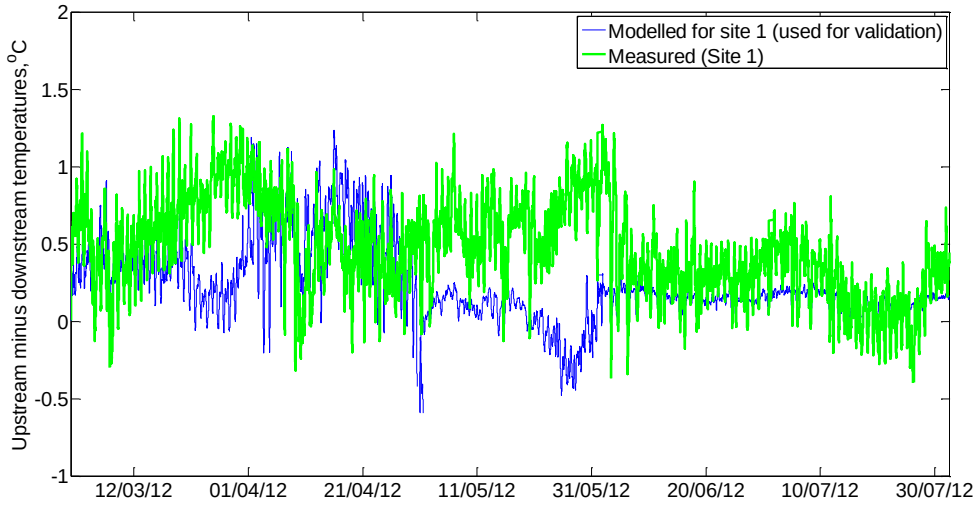

Figure 5.64: Wastewater temperature variation in Site 1 which was used for validating the urban sewer model using calibrated parameters obtained from Matlab optimisation function 'fmincon'. Data plotted for the measurement period between 1st March 2012 and the end of July 2012.

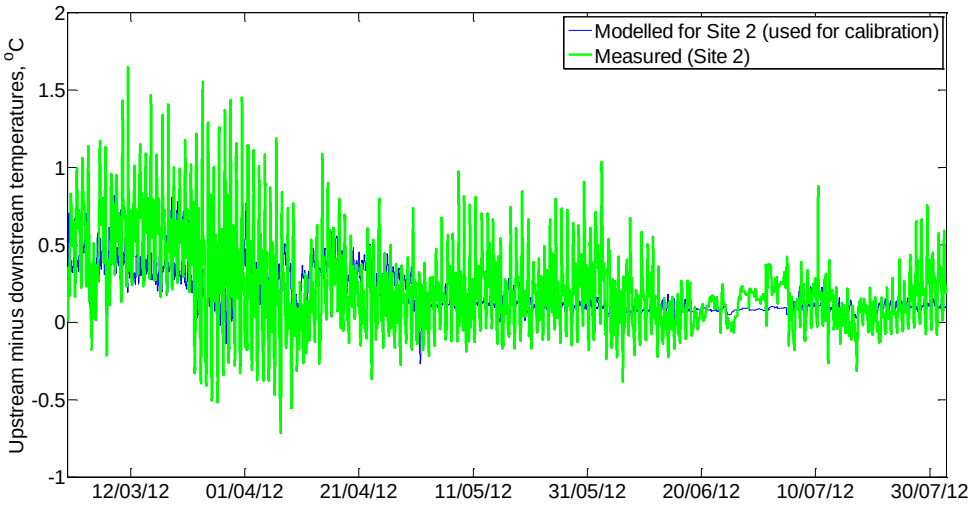

Figure 5.65: Wastewater temperature variation in Site 2 which was used for calibrating the urban sewer model using parameters obtained from Matlab optimisation function 'fmincon'. Data plotted for the measurement period between 1st March 2012 and the end of July 2012.

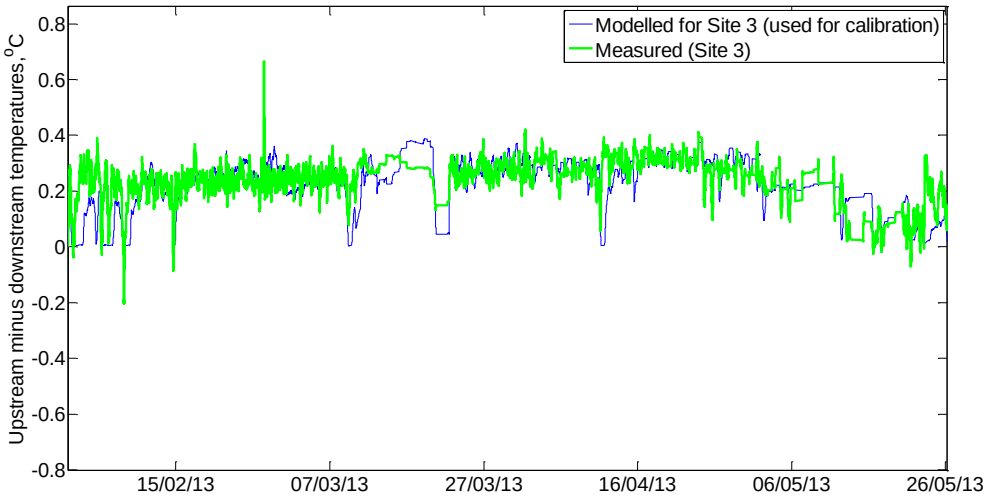

Figure 5.66: Wastewater temperature variation in Site 3 which was used for calibrating the large sewer model using calibrated parameters obtained from Matlab optimisation function 'fmincon'. Data plotted for the measurement period between 1st February 2013 and the end of May 2013.

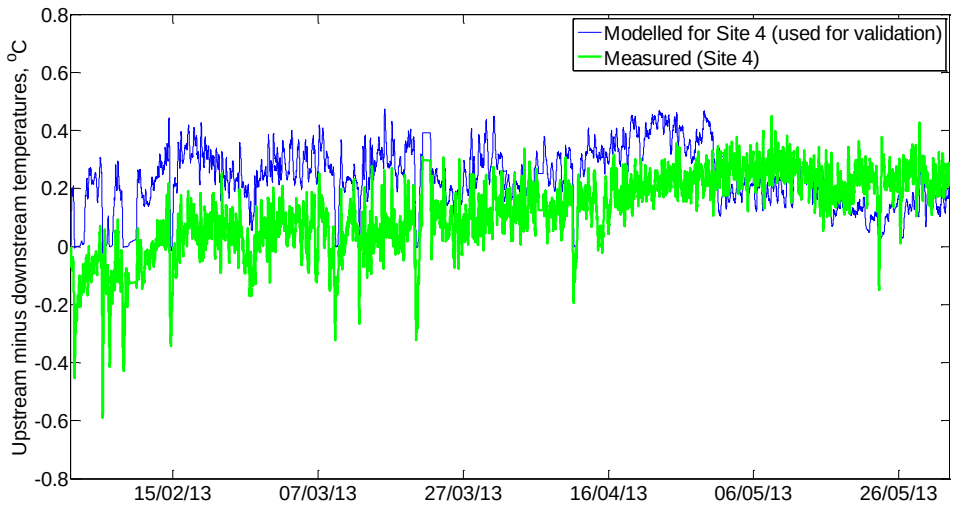

Figure 5.67: Wastewater temperature variation in Site 4 which was used for validating the large sewer model using calibrated parameters obtained from Matlab optimisation function 'fmincon'. Data plotted for the measurement period between 1st February 2013 and the end of May 2013.

It is clear that Figures 5.64 to 5.67 reflect the obtained RMSE in Table 5.7 and Table 5.9, where those sites used for calibration (i.e. Sites 2 and 3) presented good match between modelled and measured values. Sites 1 and 4 showed some periods where measured temperatures were slightly different to those modelled using the calibrated model. This is not unusual as the sites used for validation (i.e. Sites 1 and 4) have independent measured datasets to those used for calibration. Large sewers have shown better match, between measured and modelled temperatures, when the model was validated using Site 4 data which was expected since the RMSE values for large sewers were generally lower than those of urban sewers as explained earlier in this section. Validating the urban and large sewer models reconfirms their validity to utilise their calibrated parameters for modelling wastewater temperatures in sewer pipes and in sewer networks.

5.4 Impact of Measurement Errors on Modelled Wastewater Temperatures

Measured values may vary within their relevant sensor accuracies mentioned in Table 4.2. Therefore, the root mean square error (RMSE) values, obtained through calibration and validation using the urban and large sewers' data, may be affected. This is because the RMSE is based on the difference between measured and modelled wastewater temperatures at the downstream ends of the

sewer as shown by Equation 5.1. In order to observe this effect on RMSE, measured parameters were varied within their relevant sensor accuracies (i.e. between the most negative and positive values) and RMSE values were obtained accordingly. This was achieved for the Matlab optimisation function method since it is the one considered in this work for modelling wastewater temperature variations in sewers. Therefore, same steps followed in Section 5.1 were followed here, yet some of the measured parameters were varied within their relevant sensor accuracies.

Referring to Table 4.2, wastewater depth sensors were shown to have relatively high accuracy (+/-0.003m) and were regularly checked onsite. Thus, the wastewater depth measurements were not varied in this process of investigating the impact of sensor accuracy on the RMSE. The temperature of soil was measured few kilometres from each sewer site and therefore, temperature for the soil surrounding the sewer pipe was not available. This means that the soil temperature sensors were utilised to provide an estimation of the soil surrounding the sewer pipe. Hence, for the sake of investigating the impact of sensor accuracy on RMSE, it was decided to neglect the impact of varying soil temperatures and instead consider those parameters that were measured at the field sites and directly affect the RMSE values. Therefore, these parameters are wastewater velocity (u_w), wastewater temperatures at upstream (T_{US}) and downstream (T_{DS}) and in-sewer air temperature (T_{air}). Each of these parameters was varied from the most negative to the most positive value of their relevant sensor accuracy. This would show the impact of varying the four measured parameters to their sensor accuracy limits (+ and -) on RMSE values. Four measured parameters with negative and positive values create 16 combinations (2^4) that are shown by Table 5.12.

Table 5.12: Combinations of positive and negative sensor accuracy values for wastewater velocity (u_w), wastewater temperature at upstream (T_{US}) and at downstream (T_{DS}) and in-sewer air temperature (T_{air}). Each row (combination) is used for investigating the impact of the sensor accuracy values on RMSE.

Combination	Sign for sensor accuracy value			
	u_w	T_{US}	T_{DS}	T_{air}
1	+	+	+	+
2	+	+	+	-
3	+	+	-	+
4	+	+	-	-
5	+	-	+	+
6	+	-	+	-
7	+	-	-	+
8	+	-	-	-
9	-	+	+	+
10	-	+	+	-
11	-	+	-	+
12	-	+	-	-
13	-	-	+	+
14	-	-	+	-
15	-	-	-	+
16	-	-	-	-

The procedure of implementing the Matlab optimisation function 'fmincon', as explained in Section 5.1, was followed while values of u_w, T_{US}, T_{DS} and T_{air} were varied according to the 16 combinations in Table 5.12. For example, assume values of u_w, T_{US}, T_{DS} and T_{air} were 0.22m/s, 20.04°C, 19.06°C and 18.06°C respectively for a particular sewer at a specific time step, while sensor accuracies for u_w and temperature sensors are 0.03m/s (Section 4.2) and 0.06°C (Section 4.1) respectively. Therefore, implementing a combination from Table 5.12 (say combination 2), u_w, T_{US}, T_{DS} and T_{air} would change to 0.25m/s, 20.10°C, 19.12°C and 18.00°C respectively for this particular time step. All 16 combinations in Table 5.12 were implemented in urban and large sewer sites for the measurement periods using the 'fmincon' method. Although wastewater flow rate monitored by measuring the wastewater depth and velocity, flow rate values were obtained from the measured data as flow rates in m^3/s. This means that varying the wastewater velocity (u_w) would not impact on the measured wastewater flow rate as the model formulae used in calibration and validation considered the final readings of the flow rates in m^3/s. Therefore, and since the final reading of the flow rate (Q) was a function of u_w while depth measurement was considered to

be accurate, testing the impact of varying u_w on the measured flow rates may be achieved by implementing Equation 5.15.

$$Q = Q \frac{u_w}{1 \pm Accuracy\ of\ u_w\ sensor} \tag{5.15}$$

Figure 5.68 and Figure 5.69 show the results of varying the measured u_w, T_{US}, T_{DS} and T_{air} for urban and large sewers respectively. This was achieved using combinations from Table 5.12 along with the sensor accuracy values of 0.03m/s and 0.06°C, given in Table 4.2, for wastewater velocity and temperatures respectively in Sites 1 and 2. Accuracy values for sites 3 and 4 were similar to those of Sites 1 and 2 except that temperature sensors have +/-0.1°C accuracy in Sites 3 and 4 as shown by Table 4.2.

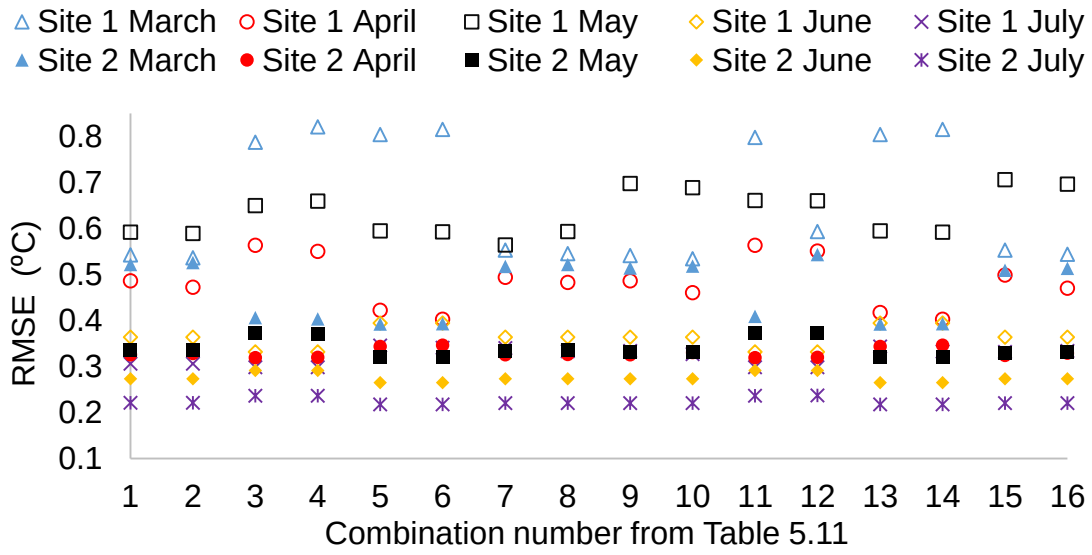

Figure 5.68: Variation of RMSE under different u_w, T_{US}, T_{DS} and T_{air} values obtained from the combinations of Table 5.12 in Site 1 (data used for validation) and Site 2 (data used for calibration). Sensor accuracies are +/- 0.03m/s and +/-0.06°C for u_w and temperatures respectively.

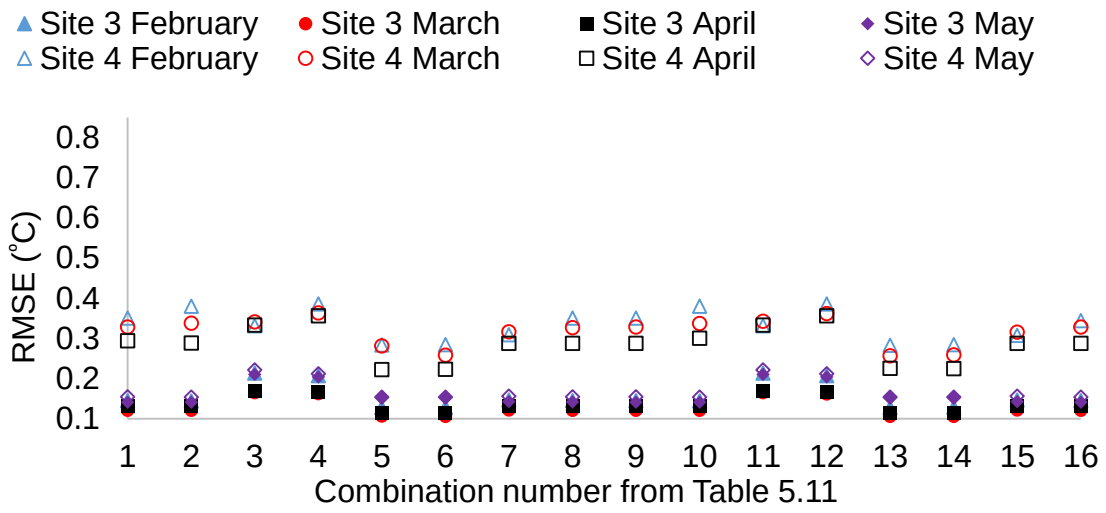

Figure 5.69: Variation of RMSE under different u_w, T_{US}, T_{DS} and T_{air} values obtained from the combinations of Table 5.12 in Site 3 (data used for calibration) and Site 4 (data used for validation). Sensor accuracies are +/- 0.03m/s and +/-0.1°C for u_w and temperatures respectively.

The RMSE values obtained from calibration and validation using 'fmincon' and considering sensor accuracies were shown to be between 0.10°C and 0.82 °C in all sites. Average RMSE values were 0.41°C and 0.21°C for urban and large sewers respectively. It is clear from Figure 5.68 and Figure 5.69 that RMSE values were mostly below 0.80°C. The maximum RMSE (0.82°C) was that of March 2012 in Site 1, which was expected as explained in Section 5.3. The values of RMSE obtained in this section is considered to be reasonable, for the purpose of this work, when considering the conditions at which the data was measured. For example, adding a margin of +/-0.82°C on the modelled wastewater temperature of the WWTP influent can provide useful information for the model user regarding uncertainty due to sensor accuracy when considering the viability of recovering heat from a sewer network. This is because the wastewater temperature varies continuously without heat being recovered and hence, a slight change in the WWTP influent temperature is unlikely to result in major treatment problems.

The impact of measurement errors on the calibrated parameters (f_{hwa}, u_a, d_s and k_s) was also studied in this section. This was achieved by recalibrating the four parameters mentioned above, using Matlab optimisation function, while accounting for the combinations identified in Table 5.12, in a similar manner followed to obtain Figure 5.68 and Figure 5.69. Using urban and large sewer data,

to obtain the calibrated parameters, presented close values to those obtained in Table 5.7 and Table 5.9. However, it was found that the impacts of measurement errors was the highest when combinations 3 to 6 and 11 to 14 (Table 5.12) were implemented. Table 5.13 and Table 5.14 show the values of calibrated parameters with significant differences, compared with their equivalents in Table 5.7 and Table 5.9, for urban and large sewers respectively. Significant differences in this context means that calibrated values that are more than 150% larger or smaller than those obtained in Table 5.7 and Table 5.9.

Table 5.13: Impact of measurement errors on the values of calibrated parameters for urban sewers.

Month	Combination from Table 5.12	Calibrated parameters			
		f_{hwa}	u_a	d_s	k_s
March	3	392	0.23	0.07	2.50
	4	381	0.23	0.16	2.01
	5	333	0.23	10.00	0.24
	6	312	0.23	10.00	0.24
	7	375	0.23	0.32	1.74
	11	417	0.17	0.05	2.50
	13	354	0.17	10.00	0.24
	14	331	0.17	10.00	0.24
April	4	59	0.23	0.01	2.50
	10	190	0.16	2.13	0.24
May	3	0.10	-0.50	0.01	2.50
	4	0.10	-0.50	0.01	2.50
	11	0.10	-0.49	0.01	2.50
	12	0.10	-0.49	0.01	2.50
	14	0.16	0.50	9.35	2.50
June	5	0.10	0.30	10.00	0.24
	6	0.10	0.30	10.00	0.24
	13	0.11	0.24	10.00	0.24
	14	0.10	0.24	10.00	0.24

Table 5.14: Impact of measurement errors on the values of calibrated parameters for large sewers.

Month	Combination from Table 5.12	Calibrated parameters			
		f_{hwa}	u_a	d_s	k_s
February	3	774	0.33	10.00	0.24
	4	607	0.26	10.00	0.24
	5	78	-0.50	0.01	2.50
	6	63	-0.45	0.01	2.50
	11	822	0.27	10.00	0.24
	12	644	0.20	10.00	0.24
	13	83	-0.50	0.01	2.50
	14	66	-0.50	0.01	2.50
March	3	407	0.10	10.00	0.24
	4	350	0.09	10.00	0.24
	5	71	0.10	8.52	2.50
	6	66	0.10	0.01	2.50
	11	429	0.04	10.00	0.24
	13	77	0.06	8.08	2.50
	14	71	0.05	0.01	2.50
April	3	407	0.24	10.00	0.24
	5	90	0.26	0.99	0.24
	6	78	0.25	10.00	0.24
	11	445	0.20	10.00	0.24
	13	95	0.19	10.00	0.24
	14	83	0.19	10.00	0.24
May	3	460	0.38	0.01	2.50
	5	0.1	0.50	10.00	0.24
	6	0.1	0.50	10.00	0.24
	11	468	0.29	0.01	2.50
	12	404	0.29	0.01	2.50
	13	0.1	0.50	10.00	0.24
	14	0.1	0.50	10.00	0.24

It is clear from Table 5.13 and Table 5.14 that accounting for measurement errors presented by combinations 3 to 6 and 11 to 14, results in significant variations in the calibrated parameters. This is because the overall variation in wastewater temperature streamwise is the highest, at the above combinations, compared with the other combinations shown in Table 5.12. Therefore, a key heat transfer calibrated parameter such as f_{hwa} change significantly in both urban and large

sewers. This is expected as the measured wastewater temperature variation streamwise influences the heat transfer process between wastewater and in-sewer air. This influence can be clearly noticed from Equation 3.31 and was found to be the most influential parameter in the predictive model developed by Abdel-Aal *et al.* (2015). Variation of f_{hwa} is closely associated with u_a as explained in Section 5.1.1. Therefore, one can realise from Table 5.13 and Table 5.14 that the calibrated u_a is varied in accordance with the variation of f_{hwa}. In a similar manner, k_s and d_s are also associated as discussed in Section 5.3. The complicity of heat transfer processes in sewers creates a noticeable deal of uncertainty. Therefore, a way to minimise this uncertainty, is to consider sensors with higher accuracy (e.g. 0.01 °C) particularly when measuring sensitive parameters such as wastewater temperatures.

6 The Large Network Model

This chapter presents an implementation example of modelling wastewater temperature variations in a real sewer network. The aim of this chapter is to investigate the impact of recovering heat from a large sewer network consisting of 3093 links (referred to as the 3000 pipe network). Section 6.1 describes the method followed for modelling wastewater temperature in the 3000 pipe network while Section 6.2 demonstrates three potential scenarios of heat recovery in the same sewer network. Summary of the results obtained from modelling the three scenarios and discussion of heat recovery from the sewer network are presented in Table 6.4 and Section 6.2.6 respectively.

6.1 Process of Designing the Large Sewer Network Model

This section introduces the 3000 pipe network that was used for modelling wastewater temperatures. The same network was utilised to demonstrate heat recovery scenarios. This section also explains how the sewer network model, developed in Section 3.3.3, is adapted to enable the modelling of wastewater temperatures in the 3000 pipe network.

The sewer network used in this work consists of 3093 links, 3048 of which are sewer pipes while the rest of the links are valves, pumps, and other connectors that can all be categorised as ‘not pipes’. The network covers a part of the sewerage system in Antwerp, Belgium serving a population equivalent of 79500. The required hydraulic model input data was retrieved from an existing hydrodynamic model created in Infoworks CS. This data includes wastewater hydraulic information (i.e. flow rate, velocity and depth) in each sewer pipe, data from sub-catchments connected to the main network, geometric specifications of sewer pipes, the surrounding soil details and sewer pipe linkages in the network. The data was collected for one year with a time step of 2 minutes. The same manner explained in Section 3.3.3 was followed to develop the large network model. Wastewater from sub-catchments is sourced from foul, trade and surface runoff (rainfall), and is discharged to the main network. Therefore, the impact of flow and temperatures of these sub-catchments, on the temperature variations along the sewer pipes in the network, ought to be considered. Hence, steps shown in Section 3.3.3 were adapted to fit the large network model needs as will be explained in this section. The process of modelling wastewater temperature variation in the 3000 pipe network is illustrated briefly in Figure 6.1. Explanation

of the steps followed to design the large network model is shown later in this section. More details and value ranges of the input parameters are shown in Table 6.1 which was organised in a similar manner to that of Table 3.3.

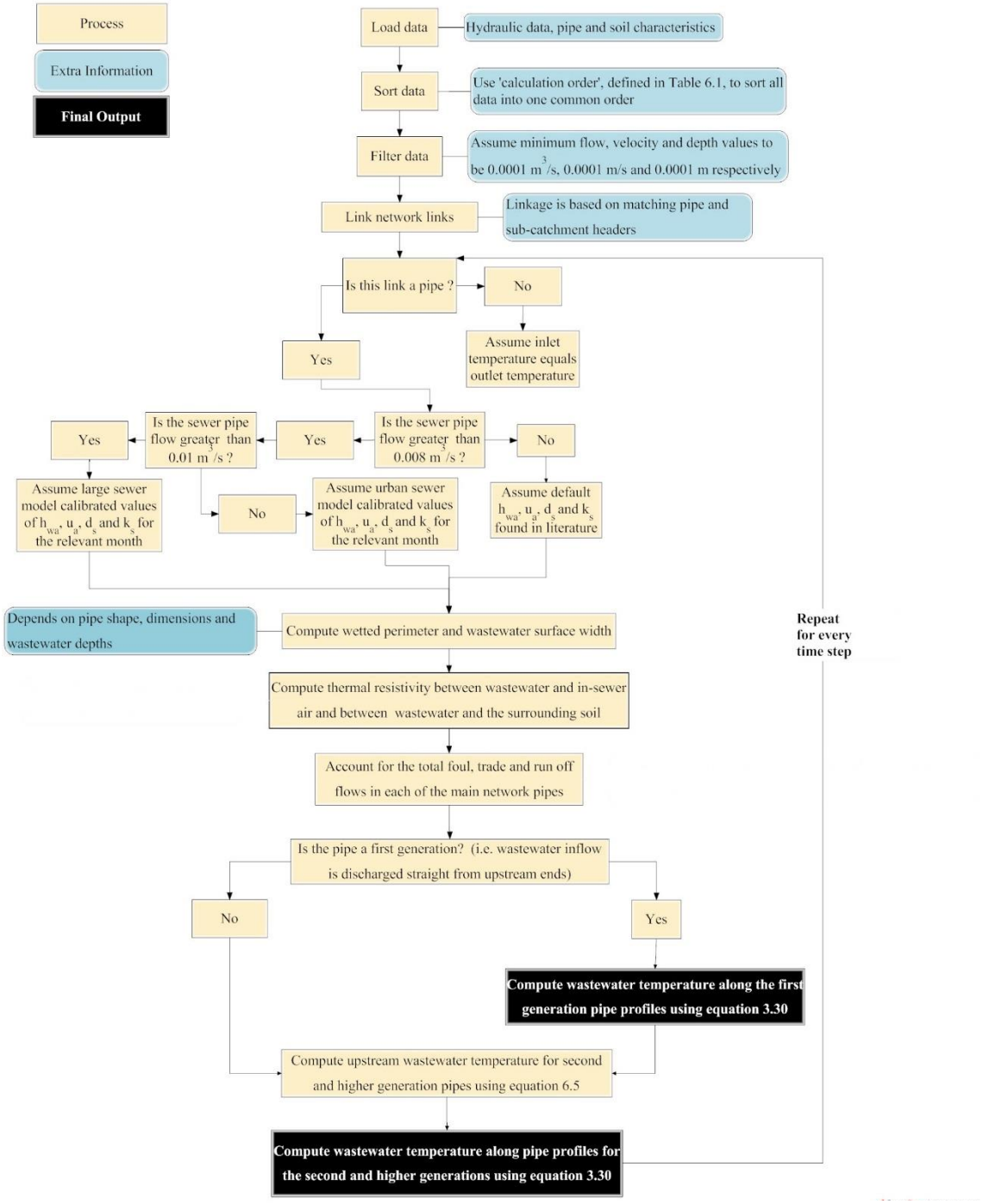

Figure 6.1: Process followed to design the large network model.

Table 6.1: Input parameters for the large network model.

Category	Input parameter	Value / Range	Unit	Notes /assumptions
Sewer temperatures	Upstream wastewater temperature of the first generation pipes, i.e. temperature of wastewater discharged from the very upstream end of the network.	24-27	°C	Assumed based on measurements by Schilperoort (2011).
	In-sewer air temperature.	9 to 25	°C	Assumed, based on measured temperatures (Section 4.1).
Hydraulic data in each pipe	Wastewater flow rate	0.0001 to 10.6	m^3/s	Retrieved from Infoworks CS data for a year at 2 minutes time step. Low (negative and zero) values were filtered. Assumed one streamwise flow direction.
	Wastewater velocity	0.0001 to 2	m/s	
	Wastewater depth	0.0001 to 4.3	m	
Data for sub-catchments connected to the sewer network	Flow of wastewater discharged from trade	0.0001 to 0.007	m^3/s	Retrieved from Infoworks CS data for a year at 2 minutes.
	Flow of wastewater discharged from foul	0.0001 to 1.85	m^3/s	
	Flow of runoff	0.0001 to 0.55	m^3/s	
	Trade wastewater temperature	24-27	°C	Assumed based on measurements by Schilperoort (2011).
	Foul wastewater temperature	24-27	°C	
	Runoff temperature	9 to 15	°C	Assumed based on ambient air temperature.
Specifications of each sewer pipe	Sewer pipe shapes	Circle, egg or rectangular		All retrieved from Infoworks CS
	Sewer pipe materials	Concrete, steel, reinforced concrete, clay, brick, polyvinyl chloride, high density poly ethylene or unknown.		
	Sewer length	1 to 801	m	
	Sewer diameter	0.08 to 5.25	m	
	Sewer wall thickness	0.053 to 0.3	m	
Soil details	Soil type surrounding each pipe	Sand & sand cement mix		Aquafin.
	Soil temperature	7 to 15	°C	Assumed based on measured data.
Pipe linkages	Pipe headers linking sewer pipes, in the network, according to their generations	3048 pipes are connected to each other. This section organises the pipes according to their streamwise position.		Retrieved from Infoworks CS.
	Pipe headers linking sub-catchment pipes to their connected pipes in the network	Flow, from a total of 2296 pipes from trade, foul and surface runoff, is discharged to the 3048 pipe network.		
Calculation order	A 3093 vector showing pipe numbers sorted in order of calculation	Pipe numbers interpret pipe headers in the network.		Infoworks CS

The algorithms used for the large network model can be divided into the following steps in order;

1. Load hydraulic and pipe data from Infoworks CS and define assumed variables (e.g. upstream temperatures for 1st generation pipes at the given time steps)

2. Sort all data according to the 'calculation order' vector defined in Table 6.1. Data loaded in matrices, including hydraulic information, temperatures, pipe dimensions, materials and shapes, soil types, and sub-catchments are all sorted so each column represents a sewer pipe. Rows of each data matrix represent the number of time steps. Data is available for a full year in 263521 time steps, yet the model offers the option to run for a chosen number of time steps, i.e. between different dates and times within the year.

3. Filter data to ensure that there is no negative or zero values in the Infoworks CS data. Wastewater flow rate, velocity and depth values less than or equal to zero were replaced by 0.0001m^3/s, 0.0001m/s and 0.0001m respectively. This assumes that wastewater flows in one direction only streamwise.

4. Link pipes and sub-catchments. Pipes are linked to their corresponding upstream pipes, generation wise, through matching upstream and downstream pipe headers that were supplied by Infoworks CS. The 2296 sub-catchments are also linked to their corresponding pipes in the main network through matching upstream headers with those of the sub-catchments.

5. Determine pipes' thermal conductivities depending on their types and materials supplied by Infoworks CS.

6. Relate to the relative calibrated parameters, f_{hwa}, u_a, d_s and k_s, depending on the modelling period and on the scale of the pipe flow. Relevant calibrated parameters were considered to be those obtained from Matlab

optimisation function shown by Table 5.7 (for urban sewers) and Table 5.9 (for large sewers). As can be noticed from Table 5.1, the urban sewer model was calibrated and validated using data with flow rates between 0.008 and 0.01 m^3/s while the large sewer model was calibrated and validated using data with flow rates between 0.09 and 0.36 m^3/s. Therefore, for sewer pipes with flow rates below 0.008m^3/s, default f_{hwa}, u_a, d_s and k_s values were used and assumed to be the averages found in literature. For sewer pipes with flow rates between 0.008 and 0.01 m^3/s, urban sewer model calibrated parameters (Table 5.7) were used for the relevant month while the large sewer model calibrated parameters were used for pipes with flow rates higher than 0.01 m^3/s.

7. Calculate the dimensions of wastewater flowing in the 3000 pipe network. Three main shapes were found in the network; circle, egg and rectangular. Hence, wetted perimeter and wastewater surface widths for the three shapes were computed based on the wastewater depths and sewer pipe diameters or widths.

8. Compute thermal resistivity between wastewater and in-sewer air and between wastewater and the surrounding soil (R_{wa} and R_{ws}) using Equations 3.27 and 3.29 respectively for each pipe in the 3000 pipe network while accounting for values obtained in the step above. Utilising the measured wastewater velocity, provided in Table 6.1, and considering the in-sewer air velocity (u_a), determined in step 6 of this section, Equation 5.12 can be implemented to estimate the heat transfer coefficient between wastewater and in-sewer air (h_{wa}).

9. Account for temperatures of wastewater discharged from sub-catchments. Discharge from sub-catchments contains flows from trade, foul and surface runoff (rainfall). These flows impact on the modelled wastewater temperatures in the sewer network and therefore, their influences should be quantified. Since exact determination of such influences is almost impossible, the large network model estimates them by accounting for the sub-catchment flow rates and temperatures in a similar manner to that used in the sewer network model which was explained in step 5 of Section

3.3.3. Therefore, Equations 6.1 and 6.2 were developed to account for the impact of wastewater temperatures from sub-catchments.

$$\mathrm{Q_{Subcatchments}} = \mathrm{Q_{foul}} + \mathrm{Q_{trade}} + \mathrm{Q_{runoff}} \quad (6.1)$$

$$T_{subcatchments} = \frac{T_{foul} \times Q_{foul} + T_{trade} \times Q_{trade} + T_{runoff} \times Q_{runoff}}{Q_{Subcatchments}} \quad (6.2)$$

Q and T are flow (m^3/s) and temperature (K) of wastewater for the relevant sewer pipe. $Q_{Subcatchments}$ is the total flow from the relevant sub-catchments.

10. Compute the wastewater temperature variation along each 1st generation pipe. This is achieved in a similar manner to that explained in step 4 of Section 3.3.3 using Equation 3.31 (duplicated below). Values of upstream wastewater temperatures shown in Table 6.1 is utilised for computing wastewater temperature variation along the 1st generation pipe profiles.

$$T_{m+1} = T_m - \left(\frac{\frac{1}{R_{wa}} \times (T_m - T_{air}) + \frac{1}{R_{ws}} \times (T_m - T_{soil})}{\rho \times Q \times c_p} \times \Delta L \right) \quad (3.31)$$

T_m is the wastewater temperature at the very first node of the pipe profile followed by T_{m+1} (second node), T_{m+2} (third node) and so on until reaching the final point which is the downstream wastewater temperature T_{m+n}. Each node is separated by a mesh size of 10 points while $\Delta L = \frac{Pipe\ lenght}{number\ of\ mesh\ points}$. This technique is explained in Section 3.2 and illustrated by Figure 3.2. R is the thermal resistivity (m.K/W) between either wastewater and air (wa) or wastewater and the surrounding (ws). ρ, Q, c_p are wastewater density (kg/m^3), wastewater flow rate (m^3/s) and specific heat capacity for wastewater (J/kg.K) respectively. The units of thermal conductivity and specific heat capacity stay valid for temperatures in Celsius as explained at the end of Section 3.3.2.

11. Compute the wastewater temperature variation along the 2nd and higher generation pipes. This can be achieved in a similar manner to that explained by step 5 of Section 3.3.3 using Equation 3.33. However, sub-catchments in the 3000 pipe network may also be connected with pipes in a geometry similar to that illustrated by Figure 6.2. Therefore, Equations 3.32 and 3.33 can be adapted to account for the impact of wastewater temperatures from pipes and sub-catchments. Hence, Equations 6.3 and

6.4 were developed to compute the upstream wastewater temperatures in cases where there are more than one pipe and or sub-catchments connected to one or more pipes.

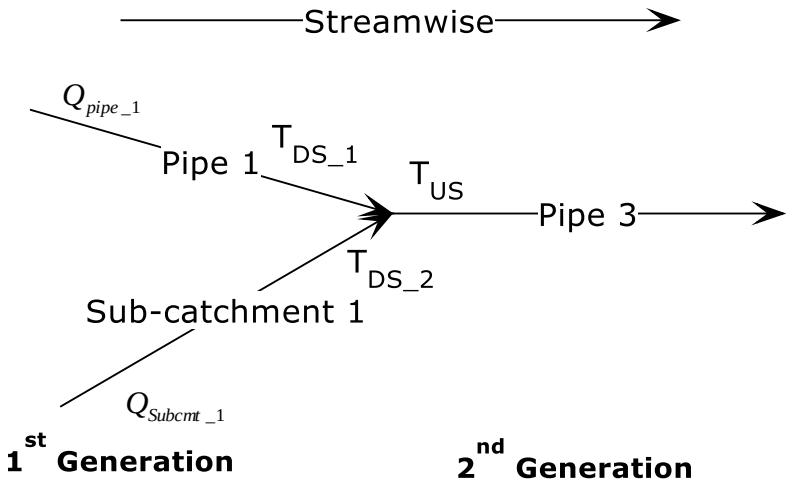

Figure 6.2: Arrangement example of multiple pipes connection in a sewer network.

$$Q_{network\ pipes} = Q_{pipe\_1} + Q_{Subcmt\_1} + Q_{pipe_{np}} + Q_{subcmt_{ns}} \quad (6.3)$$

$$T_{SP} = \frac{T_{DS\_1} \times Q_{pipe\_1} + T_{DS\_2} \times Q_{Subcmt\_1} + T_{DS\_np} \times Q_{DS\_np} + T_{DS\_ns} \times Q_{subcmt_{ns}}}{Q_{network\ pipes}} \quad (6.4)$$

Therefore, accounting for the temperature of wastewater discharged from a number of sub-catchments, explained in step 9 of this section using Equation 6.2, the upstream wastewater temperature of the second and higher generation pipes can be expressed by Equation 6.5.

$$T_{US} = T_{SP} + T_{subcatchments} \quad (6.5)$$

T and Q are temperature (°C) and flow (m^3/s) respectively of relevant wastewater types (i.e. sub-catchment or pipe). SP is the case of sub-catchments and pipes joined together, US and DS denote for upstream and downstream ends of a pipe respectively. Subcmt denotes for sub-catchment while np and ns stand for number of connected pipes and number of connected sub-catchments respectively.

The hydraulic data was considered to be that of the previous time step. This is to account for the time taken before wastewater reaches the point at which the wastewater temperature was modelled, since flow rates correspond to that of the upstream end. The temperature of wastewater at

the upstream of a sewer pipe at all generations can therefore be computed using Equation 3.31. The term 'T_m' which represents the wastewater temperature at the very upstream end of the network is replaced by T_{US} when considering the second and higher generation pipes in the network.

6.2 Implementation of the Large Network Model

This section shows three heat recovery scenarios and their impacts on wastewater temperatures in the 3000 sewer pipes network described in Section 6.1. The scenarios were based on different weather conditions to include dry weather flow (DWF) in cold (March) and relatively warm (May) conditions. Temperature of foul discharge was varied from 24 to 27 °C in March to observe the impact of changing some of the boundary conditions. The three heat recovery scenarios were compared with a 'business as usual' case, where there is no heat recovery taking place in the 3000 pipe network.

6.2.1 Methodology of Incorporating Heat Recovery

The main formula used for estimating wastewater temperature variation along a sewer pipe profile (i.e. Equation 3.31), was based on the principles of energy balance. This means that the temperature drop along the sewer pipe profile is caused by heat transferred to the in-sewer air and to the surrounding soil through the pipe wall. For implementing a heat recovery (HR) scenario, it can be assumed that the amount of heat recovered is an additional heat loss in the sewer pipe. Therefore, referring to Equations 3.31 and 6.5, and assuming heat is recovered near the upstream end of a pipe, Equation 6.6 can be developed for heat recovery applications.

$$T_{m+1} = T_m - \left(\frac{HR}{\rho \times Q_{total} \times c_p}\right) \quad (6.6)$$

T_{m+1} is the wastewater temperature at the second node in the sewer pipe profile (°C), HR is heat recovery in Watts at the first node of a pipe (m), T_m is the wastewater temperature at the upstream (1st node) of 1st generation pipes which is replaced by T_{US} (Equation 6.5) for second and higher generation pipes.

Each of the three scenarios studied in this section comprises of 250 kW heat recovered in each compliant pipe of the 3048 pipes in cold and warm days. A scale of 250kW was assumed based on a study carried out by Vlario in Belgium to find that conventional radiator heat output capacity for 93 flats was approximately between 200 to 300 kW for low and medium heating regimes

respectively. Therefore, an average value of 250kW was considered to be recovered from compliant sewer pipes in the 3000 pipe network. A compliant pipe is controlled by the large network model user and is determined by the pipe's minimum wastewater flow rate and minimum wastewater temperature. The selection of the compliant pipe criteria adds the advantage of restricting heat recovery to pipes with adequate wastewater flow rates and temperatures for the specified heat recovery scale as will be discussed later in this chapter.

6.2.2 Description of the Three Heat Recovery Scenarios

The aim of this section is to develop different scenarios that show the impact of recovering heat from the 3000 pipe network under different conditions. The impact of recovering heat from the network is usually measured by the wastewater influent temperature at the WWTP. This is because some wastewater treatment processes (e.g. nitrification) are largely influenced by the WWTP influent temperature (Wanner *et al.*, 2005). Recovering heat from a sewer network may also be constrained by the wastewater temperature in the sewer pipes. This is to avoid significant wastewater temperature drops that can potentially cause wastewater to freeze in the pipes. Therefore the heat recovery scenarios in this work represent heat recovery from sewer pipes with wastewater temperature of 9°C and above. Another heat recovery case presents a less risky option that restricts heat recovery to be extracted from pipes with wastewater temperatures of 20°C and above.

Data chosen from working days (Monday to Friday) at dry weather flow conditions in March 2012 and May 2012 shows typical characteristics (e.g. flow rate, soil and in-sewer air temperatures) for these months. Therefore, calibrated parameters from the Matlab optimisation function were used from Table 5.7 (urban sewers) and Table 5.9 (large sewers) in March and May. Working days with dry weather flow (DWF) were considered as they represent a more common phenomenon in the Belgian sewer network in Antwerp as shown by measured data in sections 4.2 and 4.3. It was assumed that heat is mostly demanded in the morning (i.e. 7:00 AM) and hence, the three scenarios examined heat recovery at this time during March (Scenarios 1 & 3) and May (Scenario 2). Since there is no abundancy of measured foul temperatures in the literature, it was assumed to be 24°C (Scenarios 1 & 2) and 27°C for the third scenario to observe the impact of increasing foul temperatures. Both foul temperatures are within the range

measured by Schilperoort (2011). Therefore, Scenarios 1 and 2 assume foul temperature of 24°C in March and May respectively while Scenario 3 assumes foul temperature of 27°C in March. Temperature of soil and in-sewer air were assumed to be the relevant averages of those measured in the nearby area of Antwerp. Table 6.2 shows a summary of the assumed boundary condition values used in the three scenarios. A cumulative distribution function (CDF) of the average flow rates in the 3000 pipe network, during the hours between 7:00 and 8:00 AM on Friday 4th May 2012, is shown by Figure 6.3. It was found that 12th March 2012 presented similar CDF for flow rate data and therefore it was not plotted in this section. Each scenario is divided into two cases as described in more details in Table 6.3.

It was assumed that the foul temperature is constant at all time steps. The size of a time step for the hydraulic data retrieved from Infoworks CS is 2 minutes. This means that the sewer network is continuously, i.e. every 2 minutes, recharged with the same foul temperature identified as a boundary condition. The implementation of heat recovery scenarios considers the average hydraulic data over one hour (30 time steps) to minimise the effects of any errors in any of the time steps. This section uses probability density functions (PDF), plots of total heat recovered against the minimum required flow rates and tables showing the predicted WWTP influent temperatures, to interpret the impact of recovering heat from the 3000 pipe network.

Table 6.2: Boundary condition parameters used for March and May heat recovery scenarios.

Parameter	Values in		Unit	Notes
	March	May		
Foul temperature	24 and 27	24	°C	Assumed based on measurements by Schilperoort (2011).
Trade temperature	24	24	°C	Assume to be equal to foul temperature.
Runoff temperature	9	15	°C	Assumed to be equal to ambient temperature.
In-sewer air temperature	9	15	°C	Assumed to be equal to ambient temperature.
Soil temperature	11	11	°C	Assumed based on measured data (Figure 4.10).
Flow rates (pipe, foul, trade, and runoff)	0.1 – 340	0.1 – 340	L/s	Supplied by Infoworks CS. See Figure 6.3.

Table 6.3: Details of the three heat recovery scenarios implemented using the 3000 pipe network. Min. denotes for minimum, HR stands for heat recovery while WW and temp. denote for wastewater and temperature respectively.

Scenario	Case	Day	HR from pipes with		HR	Temperatures					Network flow
			Min. Flow	Min. WW temp.		Foul	Trade	Runoff	In-sewer air	Soil	
			L/s	C	kW			C			L/s
1	1.1	Monday 12th March 2012	25, 50, 100 & 200	9	250	24	24	9	9	11	0.1 to 340
	1.2	Monday 12th March 2012		20		24	24	9	9		
2	2.1	Friday 4th May 2012		9		24	24	15	15		
	2.2	Friday 4th May 2012		20		24	24	15	15		
3	3.1	Monday 12th March 2012		9		27	27	9	9		
	3.2	Monday 12th March 2012		20		27	27	9	9		

Figure 6.3 shows cumulative distribution function (CDF) of the average flow rates in the 3000 pipe network, during the hours between 7:00 and 8:00 AM on Friday 4th May 2012.

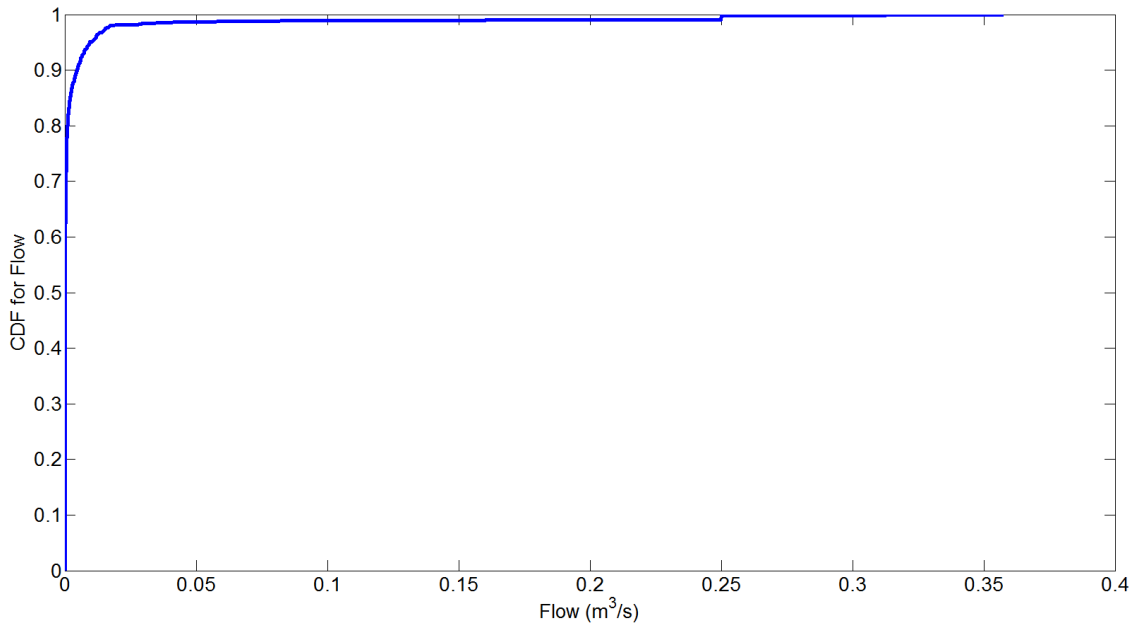

Figure 6.3: Cumulative distribution function of the flow rates in the 3000 pipe network during 4th May 2012 (7:00 to 8:00 AM).

6.2.3 Scenario 1 Results: Heat Recovery in March 2012

Figure 6.4 shows the flow rate data, obtained by Infoworks CS during March 2012, which is used to observe periods of DWF events in working days.

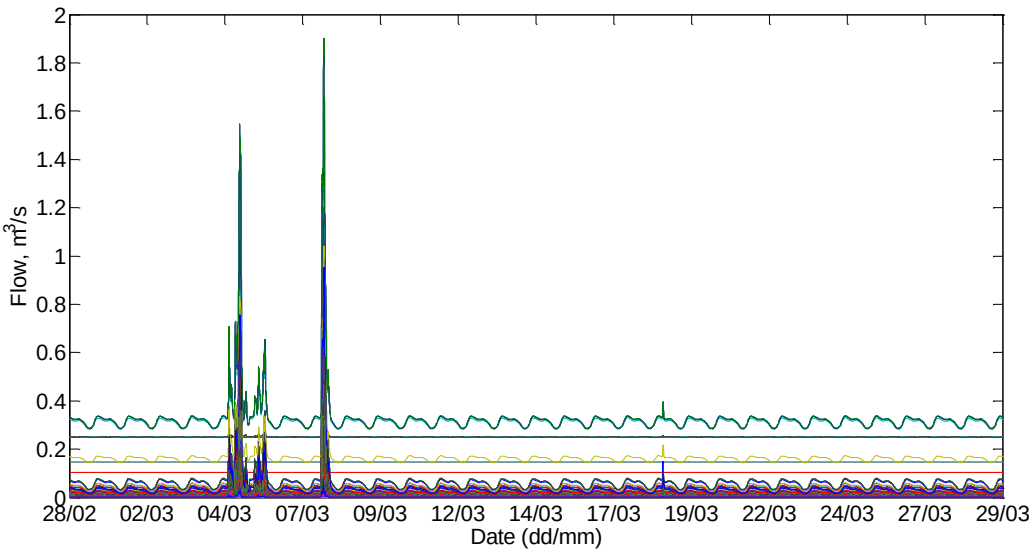

Figure 6.4: Wastewater flow rates in randomly selected 2800 pipes of the 3000 pipe network during March 2012. Each line represents a pipe in the network.

The dry weather flow (DWF) was noticed, from Figure 6.4, by observing flow rates on the days with no rainfall events. Peaks shown by Figure 6.4 were assumed to represent rainfall events. Therefore, avoiding these peaks, one can notice that DWF is approximately below 0.35m^3/s. This can be used to identify working days with DWF for implementing heat recovery scenarios. Therefore, Figure 6.5 was obtained to show a dry weather flow during Monday 12th March 2012, which will be considered for March heat recovery scenarios during the hours between 7:00 and 8:00 AM.

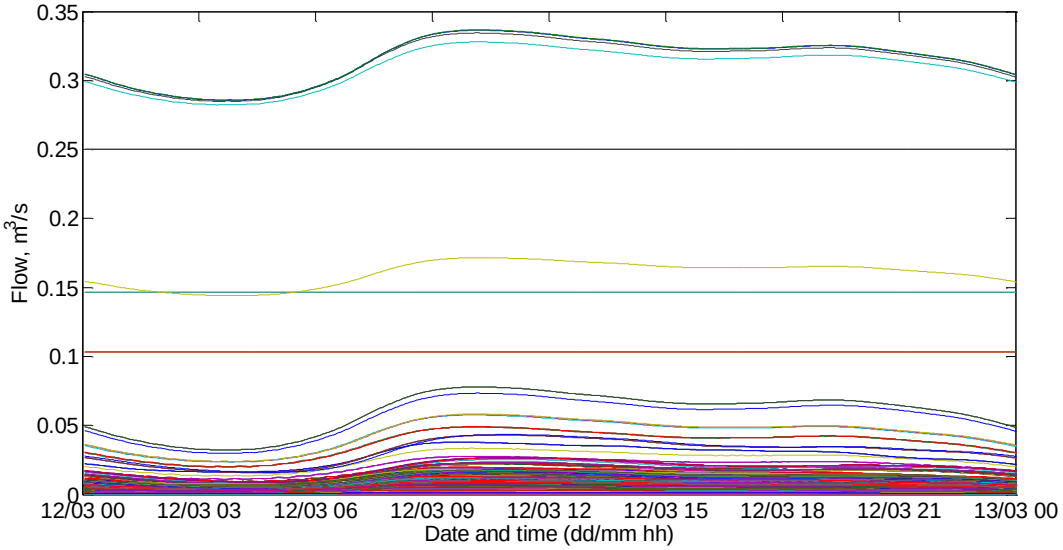

Figure 6.5: Wastewater dry weather flow variation in randomly selected 2800 pipes of the 3000 pipe network on Monday 12th March 2012. Each line represents a pipe in the network.

Figure 6.6 shows the probability density function (PDF) for heat recovery and business as usual cases using pipes with minimum wastewater temperatures of 9°C and minimum flow rates of 25, 50, 100, 200 L/s. Heat recovered is assumed to be 250kW/pipe on Monday 12th March 2012 while the number of pipes involved varies depending on the minimum required flow rate as shown by Table 6.4 and Figure 6.8

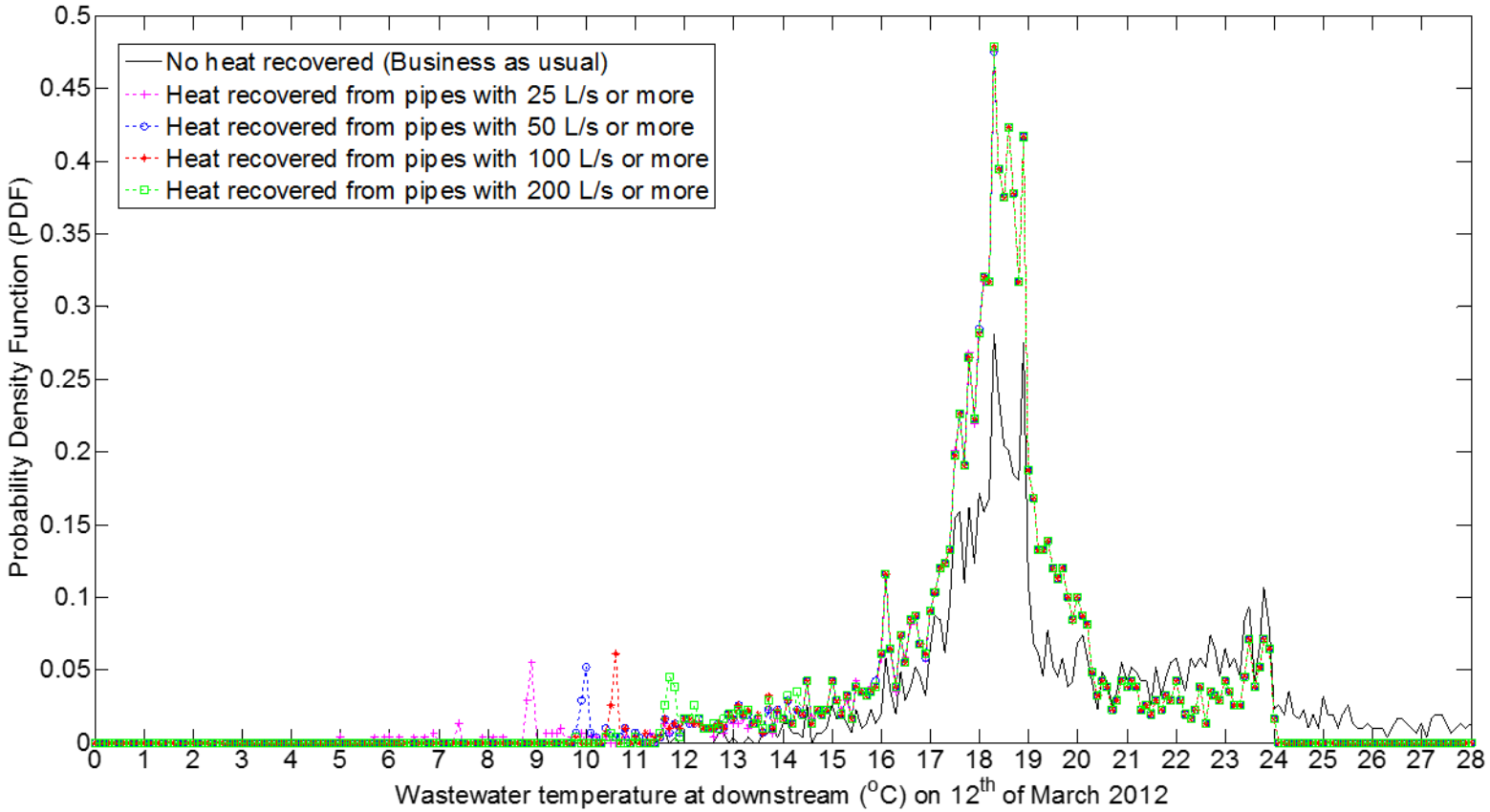

Figure 6.6: Case 1.1 Probability distribution function (PDF), for wastewater temperatures on 12th March 2012 before and after heat (250kW/pipe) is recovered. Pipes with minimum wastewater temperatures of 9°C were considered for heat recovery. Total heat recovered for this case is shown in Table 6.4 .

Another heat recovery case on Monday 12th March 2012 assumes similar scale of heat recovery (250kW/pipe) using pipes with minimum wastewater temperatures of 20°C. Figure 6.7 shows the probability density function (PDF) for heat recovery and business as usual cases using pipes with minimum wastewater temperatures of 20°C and minimum flow rates of 25, 50, 100, 200 L/s. The number of pipes involved varies depending on the minimum required flow rate as shown by Table 6.4 and Figure 6.8.

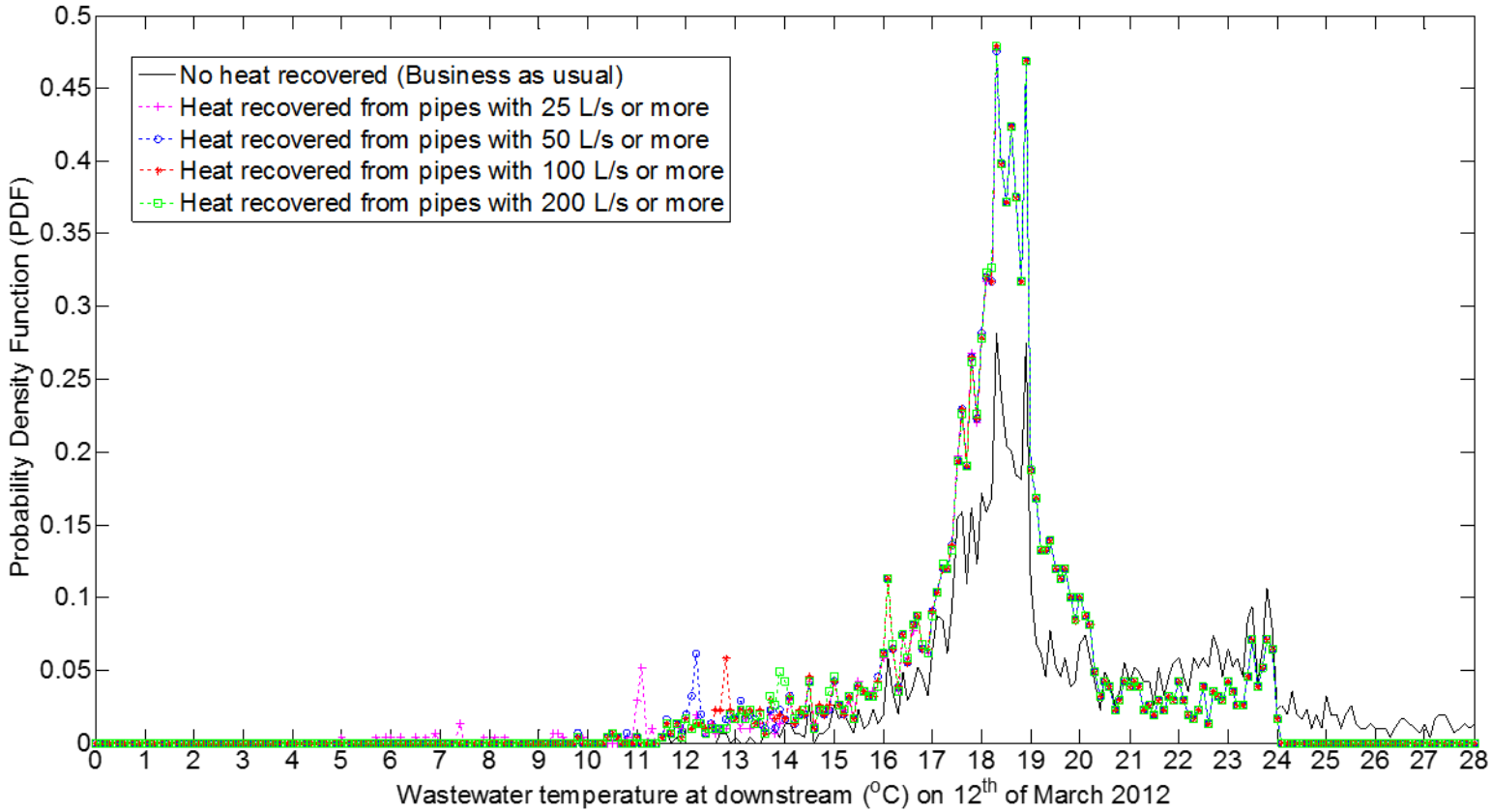

Figure 6.7: Case 1.2 Probability distribution function (PDF), for wastewater temperatures on 12th March 2012 before and after heat (250kW/pipe) is recovered. Pipes with minimum wastewater temperatures of 20°C were considered for heat recovery. Total heat recovered for this case is shown in Table 6.4.

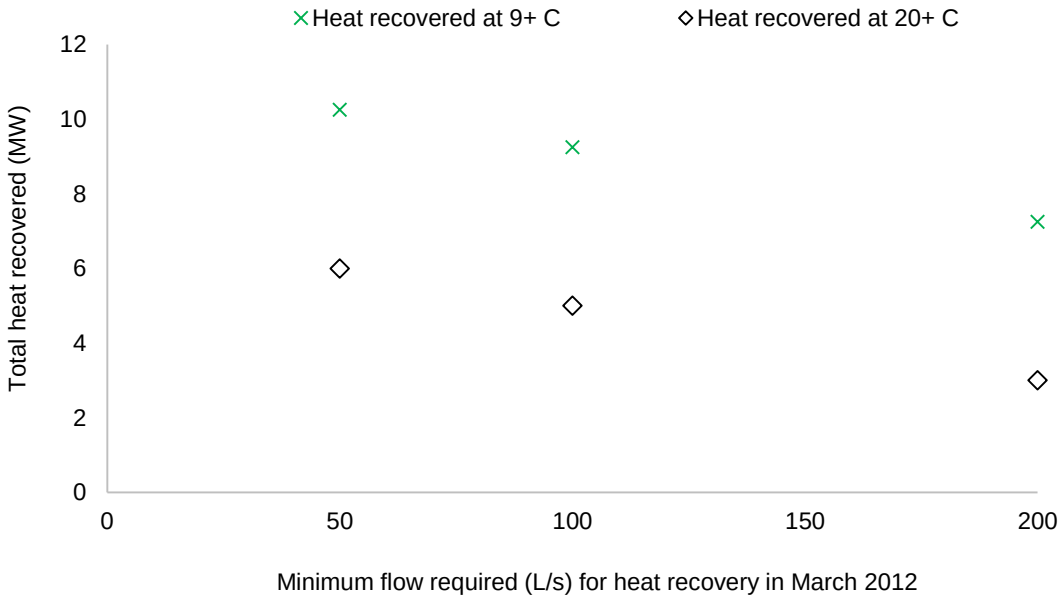

Figure 6.8: Potential of 250kW/pipe heat recovery on 12th March 2012 using pipes with minimum wastewater temperatures of 9 and 20°C under flow rates of 25, 50, 100 & 200 L/s. The number of pipes used is shown in Table 6.4.

6.2.4 Scenario 2 Results: Heat Recovery in May 2012

Findings of the May 2012 scenario was also represented in a similar manner to that of March 2012. Observing DWF events was achieved by illustrating the flow variation during May 2012, found from Infoworks CS, as shown by Figure 6.9.

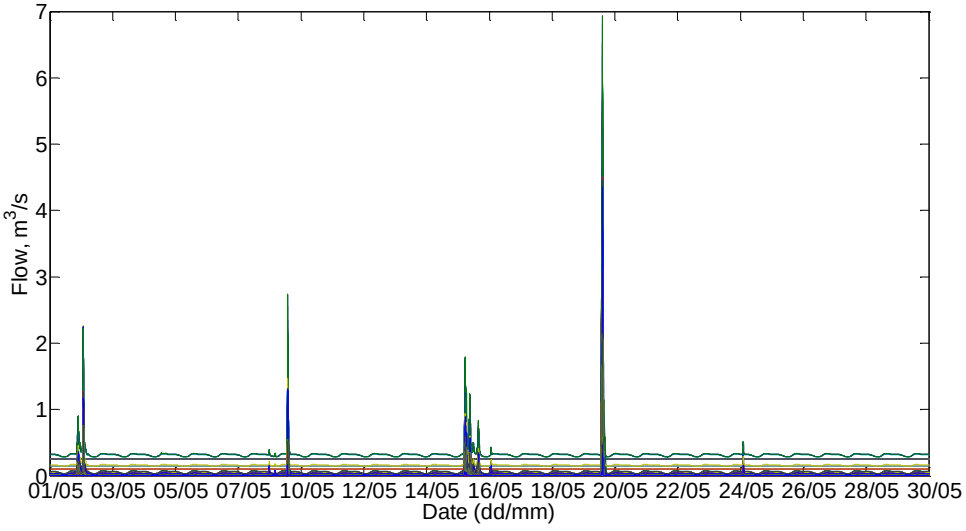

Figure 6.9: Wastewater flow rates in randomly selected 2800 pipes of the 3000 pipe network during May 2012. Each line represents a pipe in the network.

Dry weather flow in May 2012 was observed to be similar to that in March 2012 which was below 0.35m^3/s. Figure 6.10 shows the dry wastewater flow variation during a working day (Friday 4th May 2012).

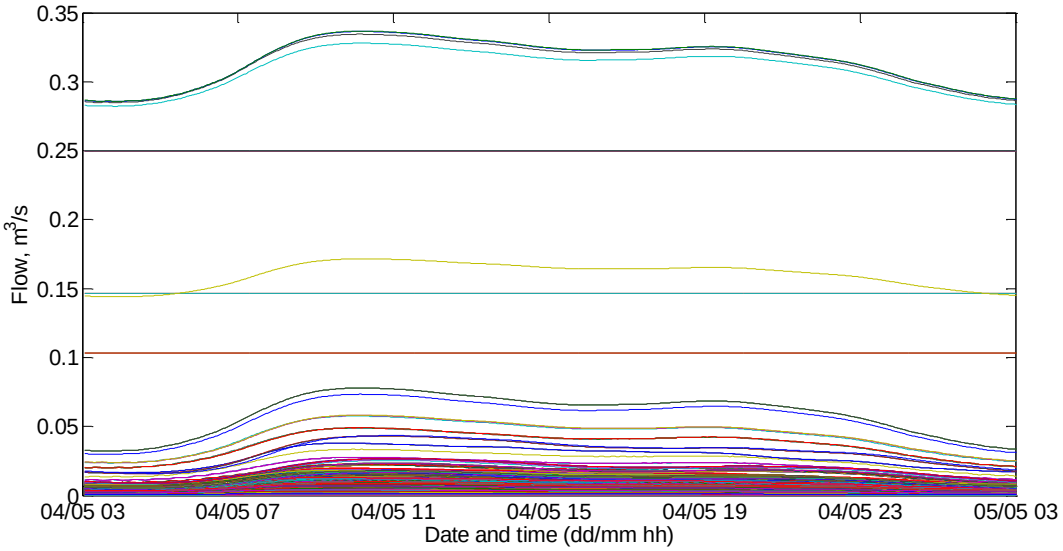

Figure 6.10: Wastewater dry weather flow variation on Friday 4th May 2012. Each line represents a pipe in the network.

Figure 6.11 shows the probability density function (PDF) for heat recovery and business as usual cases using pipes with minimum wastewater temperatures of 9°C and minimum flow rates of 25, 50, 100, 200 L/s. Heat recovered is assumed to be 250kW/pipe on Friday 4th May 2012 while the number of pipes involved varies depending on the minimum required flow rate as shown by Table 6.4 and Figure 6.13.

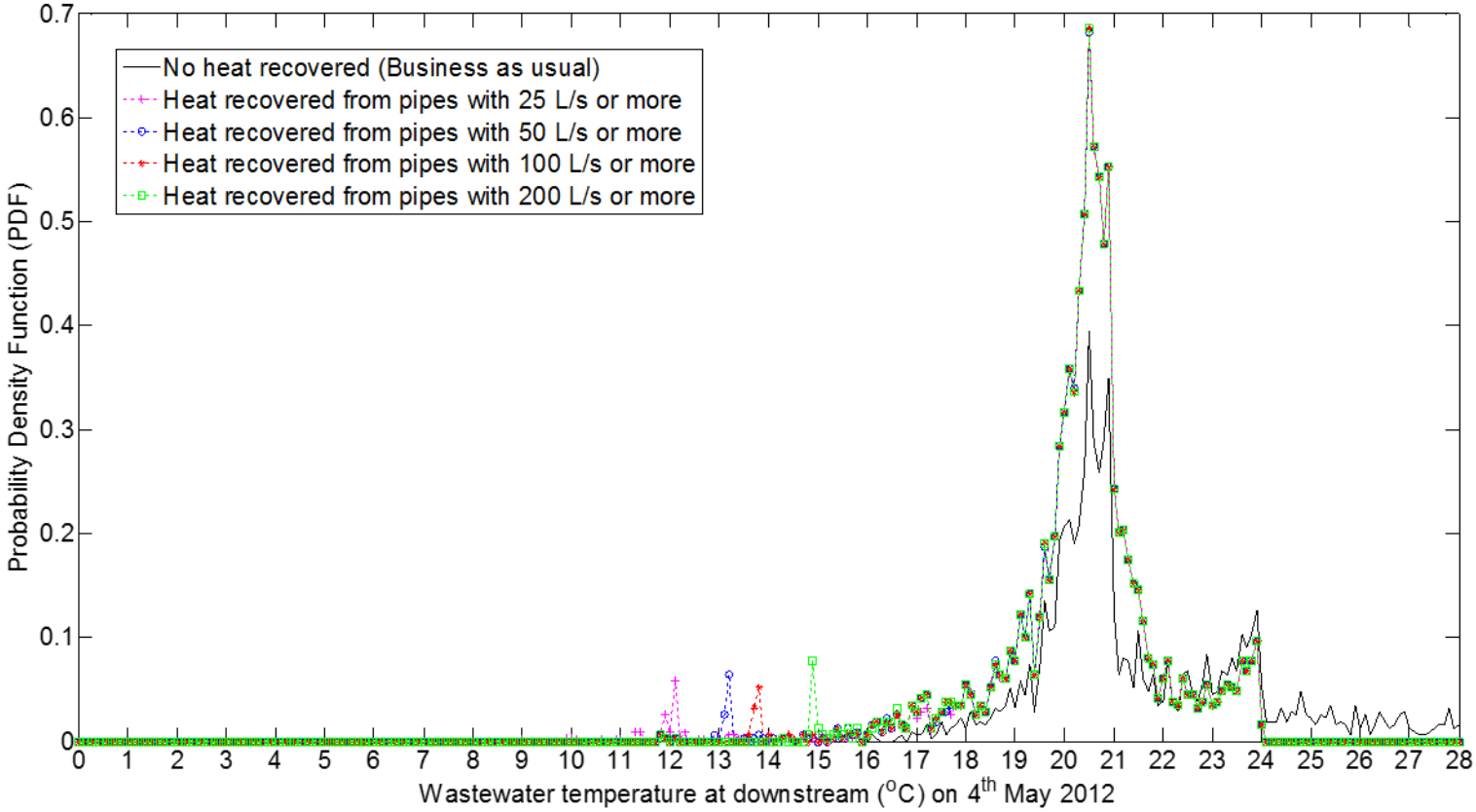

Figure 6.11 : Case 2.1 Probability distribution function (PDF), for wastewater temperatures on 4th May 2012 before and after heat (250kW/pipe) is recovered. Pipes with minimum wastewater temperatures of 9°C were considered for heat recovery. Total heat recovered for this case is shown in Table 6.4.

Another heat recovery on Friday 4th May 2012 assumes the same scale of heat recovery (250kW/pipe) using pipes with minimum wastewater temperatures of 20°C. Figure 6.12 shows the probability density function (PDF) for heat recovery and business as usual cases using pipes with minimum wastewater temperatures of 20°C and minimum flow rates of 25, 50, 100, 200 L/s. The number of pipes involved varies depending on the minimum required flow rate as shown by Table 6.4 and Figure 6.13.

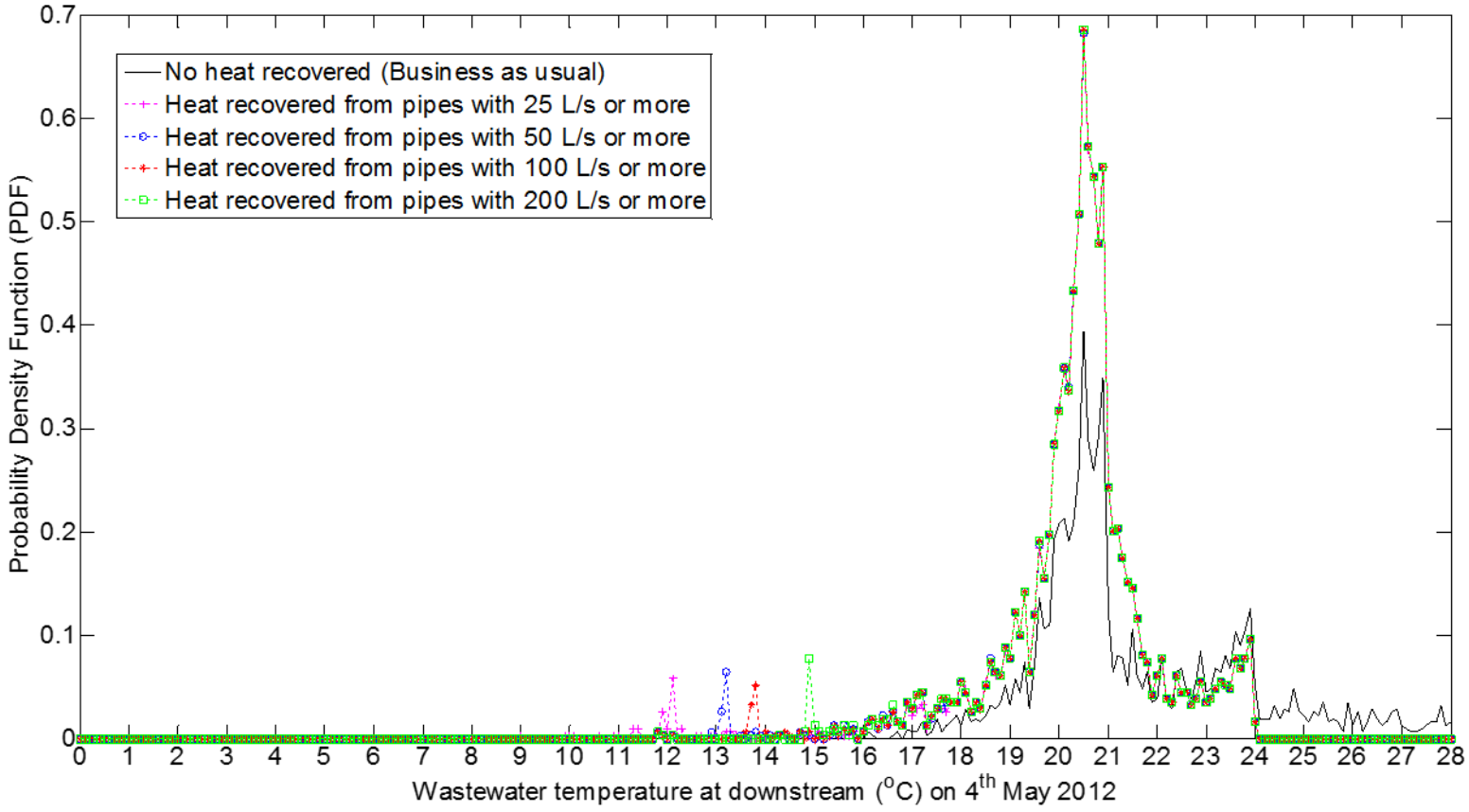

Figure 6.12: Case 2.2 Probability distribution function (PDF), for wastewater temperatures on 4th May 2012 before and after heat (250kW/pipe) is recovered. Pipes with minimum wastewater temperatures of 20°C were considered for heat recovery. Total heat recovered for this case is shown in Table 6.4.

The total heat recovered in Scenario 2 at different flow rates is shown by Figure 6.13.

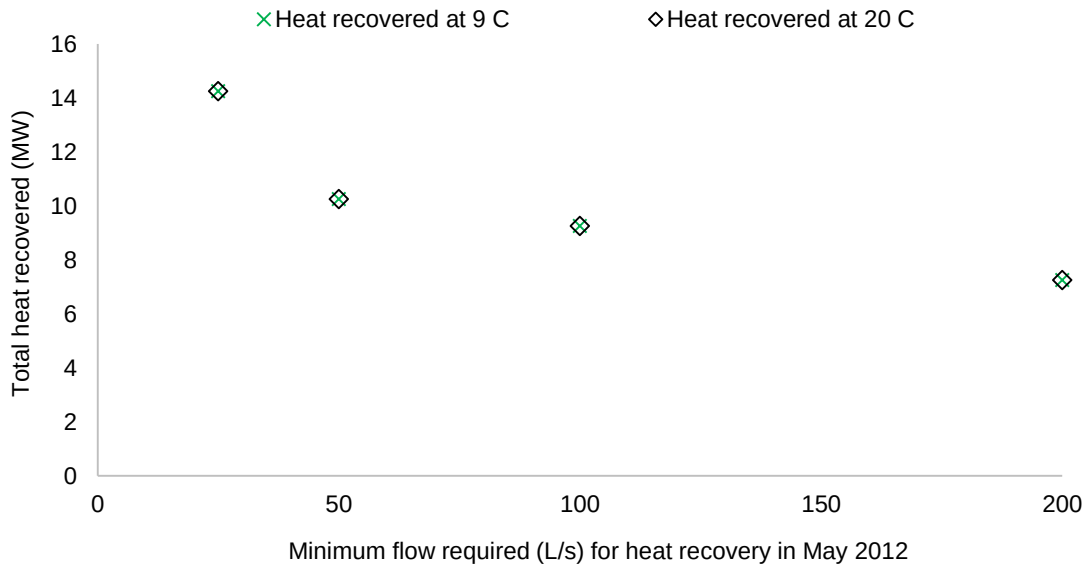

Figure 6.13: Potential of 250kW/pipe heat recovery in May 2012 using pipes with minimum wastewater temperatures of 9 and 20°C under flow rates of 25, 50, 100 & 200 L/s. The number of pipes used is shown in Table 6.4.

6.2.5 Scenario 3 Results: Heat Recovery in March 2012 with Higher Foul Temperature

This section presents two heat recovery cases similar to those in March 2012 (Section 6.2.3), yet assuming higher foul temperatures. A 250kW/pipe was assumed to be recovered from sewerage wastewater with foul temperature of 27°C on Monday 12th March 2012. Figure 6.14 shows the probability density function (PDF) for heat recovery and business as usual cases, assuming foul temperature of 27°C, using pipes with minimum wastewater temperatures of 9°C and minimum flow rates of 25, 50, 100, 200 L/s. The number of pipes involved varies depending on the minimum required flow rate as shown by Table 6.4 and Figure 6.16.

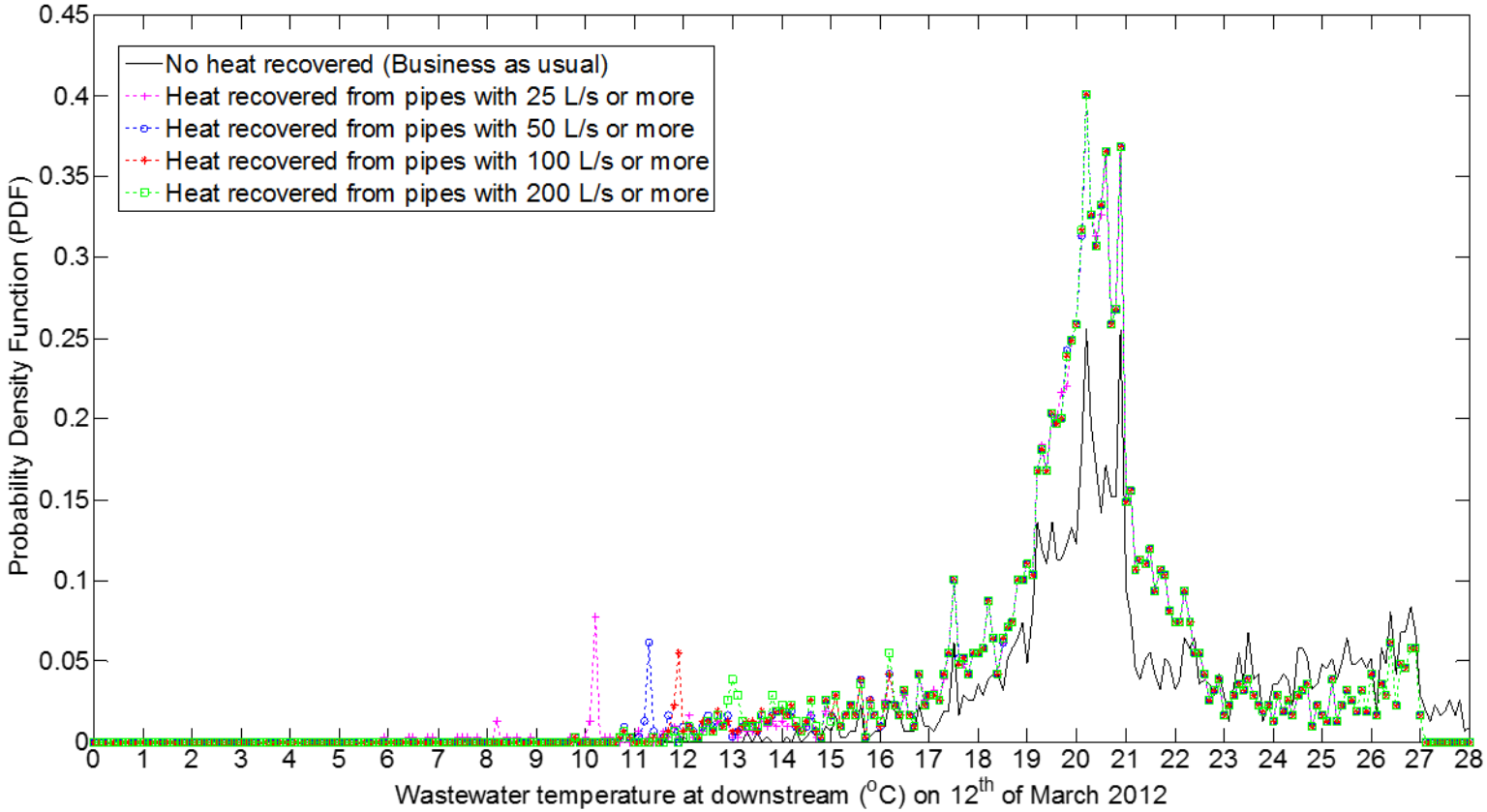

Figure 6.14: Case 3.1 Probability distribution function (PDF), for wastewater temperatures on Monday 12th March 2012 before and after heat (250kW/pipe) is recovered assuming foul temperature of 27°C. Pipes with minimum wastewater temperatures of 9°C were considered for heat recovery. Total heat recovered for this case is shown in Table 6.4.

The probability density function (PDF) for heat recovery and business as usual cases, assuming foul temperature of 27°C, using pipes with minimum wastewater temperatures of 20°C and minimum flow rates of 25, 50, 100, 200 L/s is illustrated by Figure 6.15. The number of pipes involved varies depending on the minimum required flow rate as shown by Table 6.4 and Figure 6.16.

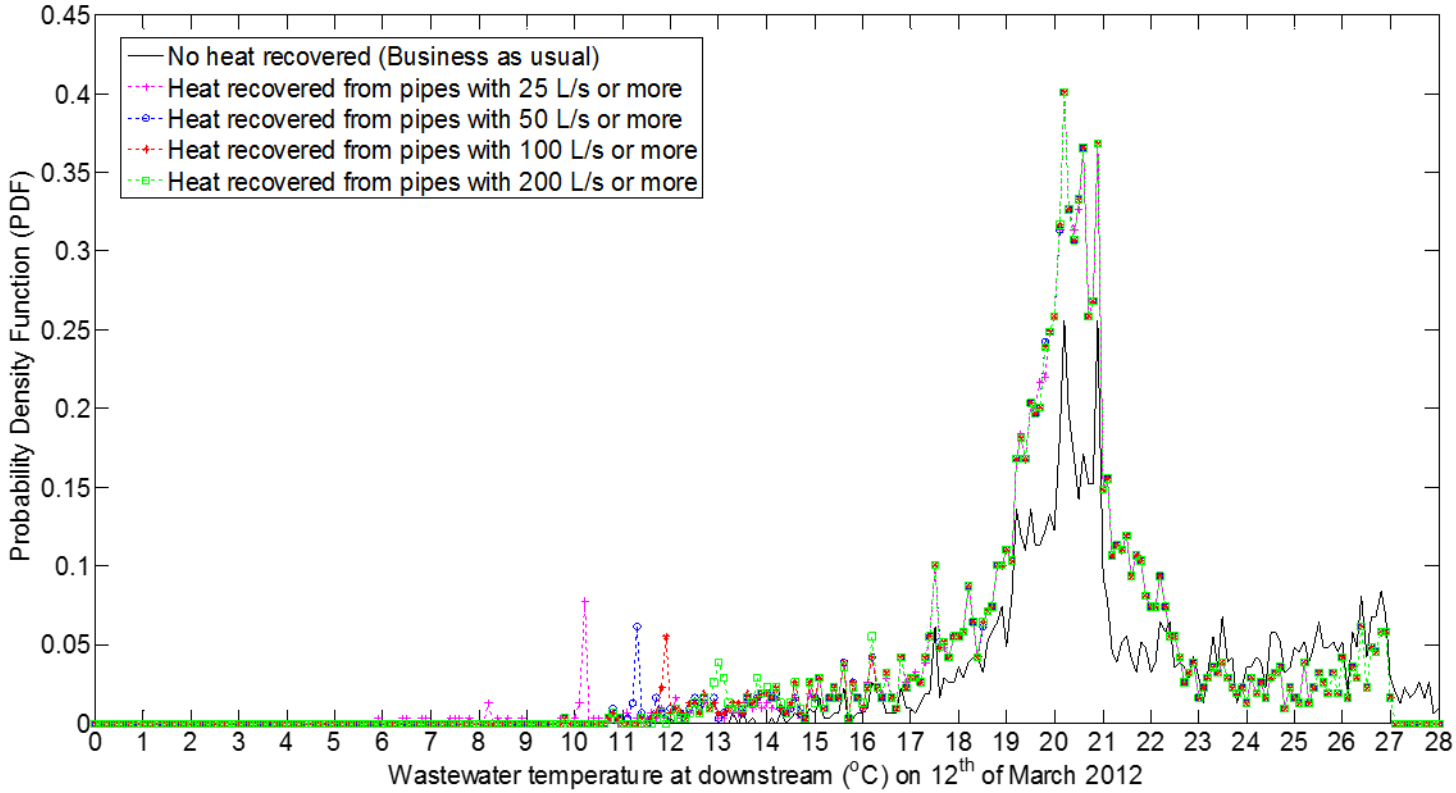

Figure 6.15: Case 3.2 Probability distribution function (PDF), for wastewater temperatures on Monday 12th March 2012 before and after heat (250kW/pipe) is recovered assuming foul temperature of 27°C. Pipes with minimum wastewater temperatures of 20°C were considered for heat recovery. Total heat recovered for this case is shown in Table 6.4.

The total heat recovered in Scenario 3 at different flow rates is shown by Figure 6.16.

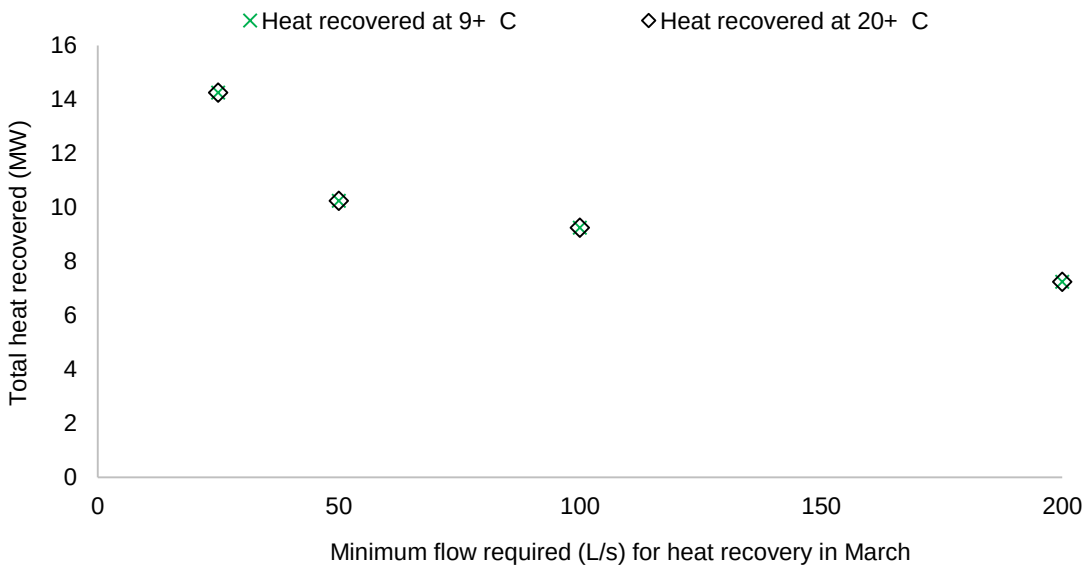

Figure 6.16: Potential of 250kW/pipe heat recovery on 12th March 2012 using pipes with minimum wastewater temperatures of 9 and 20°C under flow rates of 25, 50, 100 & 200 L/s. Foul temperature was assumed to be 27 °C. The number of pipes used is shown in Table 6.4.

The results of modelling the three heat recovery scenarios under all cases are summarised in Table 6.4.

Table 6.4: Summary of the results obtained from modelling the three heat recovery (HR) scenarios.

Scenario	Condition	Case	Minimum required flow	Minimum required wastewater temperature	No. of pipes involved	Total HR (250kW/pipe)	Influent temperature	Minimum wastewater temperature in the network
			L/s	°C		MW	°C	°C
1	March with foul temperature = 24°C	1.1	25	9	57	14	9	5
			50	9	41	10	10	10
			100	9	37	9	11	10
			200	9	29	7	12	10
		1.2	25	20	40	10	11	5
			50	20	24	6	12	10
			100	20	20	5	13	10
			200	20	12	3	14	10
2	May with foul temperature = 24°C	2.1	25	9	57	14	12	9
			50	9	41	10	13	12
			100	9	37	9	14	12
			200	9	29	7	15	12
		2.2	25	20	57	14	12	9
			50	20	41	10	13	12
			100	20	37	9	14	12
			200	20	29	7	15	12
3	March with foul temperature = 27°C	3.1	25	9	57	14	10	6
			50	9	41	10	11	10
			100	9	37	9	12	10
			200	9	29	7	13	10
		3.2	25	20	57	14	10	6
			50	20	41	10	11	10
			100	20	37	9	12	10
			200	20	29	7	13	10

6.2.6 Discussion of the Network Implementation Scenarios

Recovering heat from sewer pipes, in Scenario 1 at cases 1.1 and 1.2, results in an increase in the number of sewer pipes that obtained wastewater temperatures below 15°C, compared with that before recovering heat (business as usual scenario). This is illustrated by the probability density functions in Figure 6.6 and Figure 6.7. However, heat recovery in Scenario 1 using sewer pipes with wastewater temperatures of 20 °C and above (case 1.2), demonstrated less pipes with wastewater temperature below 11 °C compared with that of case 1.1. This may indicate that case 1.2 is more viable than case 1.1. Nevertheless, case 1.1 results in more total heat recovery from the 3000 pipe network than that of case 1.2, as shown by Figure 6.8, while the WWTP influent temperatures in cases 1.1 and 1.2 are close (1 or 2°C difference). Therefore, one may consider case 1.1 to be more attractive than case 1.2. It can be noticed from Table 6.4 that minimum Scenario 1 wastewater temperature in the sewer network was 5°C which is lower than the minimum measured in March (around 7°C) as shown by Figure 4.6 and Figure 4.7. However, wastewater flowing in the 3000 pipe network at 5°C recovers some of the heat losses by extracting heat from the surrounding soil (11°C) and in-sewer air (9°C). Therefore, WWTP influent temperatures obtained in Scenario 1 were 9°C and above, as shown by Table 6.4, which was close to that minimum temperature measured in Antwerp WWTP (Figure 4.14). Scenario 2 has shown larger wastewater temperature values in the sewer network and for the WWTP influent as shown by Table 6.4. This wax expected since the relatively high in-sewer air temperature (15°C) results in heat being transferred from in-sewer air to wastewater and hence, wastewater temperature in the network does not drop below the soil temperature (11°C) before heat is recovered. It was noticed that Scenario 2 presented similar PDF graphs for cases 2.1 and 2.2 (Figure 6.11 and Figure 6.12). This indicates that recovering heat from pipes with wastewater temperatures of 9°C (case 2.1) or above and 20°C or above (case 2.2), results in having a very similar number of sewer pipes with wastewater temperatures between 11 and 15°C. This is because the number of pipes involved (presented in Table 6.4) in cases 2.1 and 2.2 is the same and therefore the total heat recovered from the network is also the same as shown by Figure 6.13. The number of pipes involved is the compliant pipes, i.e. pipes with the minimum required flow rates (25, 50, 100 & 200 L/s) and minimum required

wastewater temperatures, set by the model user, for heat recovery (9 and 20°C for cases 2.1 and 2.2 respectively).

Recovering heat in March while assuming higher foul and trade temperatures in case 3.1 (i.e. 27°C instead of 24°C) showed close results to that of case 1.1 as can be noticed from Table 6.4. However, case 3.2 presented a more attractive heat recovery option than that of case 1.2 since the total heat recovered in case 3.2 was more than that of case 1.2 while wastewater temperatures (in the network and of the WWTP influent) were close to that of case 1.2. This is due to the larger number of pipes with 20°C and above available for heat recovery in case 3.2. Therefore, heat recovery may prove attractive for catchments with higher foul and trade temperatures. Referring to Equations 6.3 to 6.6, it is obvious that increasing foul and trade temperatures result in less wastewater temperature drop along the pipe profile which consequently causes higher WWTP influent temperature. Scenario 3 showed similar PDF for cases 3.1 and 3.2, as can be noticed from Figure 6.14 and Figure 6.15. This was expected at such high foul and trade temperatures, where the number of pipes with wastewater temperatures above 9°C is equal to that of pipes with wastewater temperatures above 20°C. Hence, Figure 6.16 shows similar potential heat recovery scales for cases 3.1 and 3.2. The number of pipes involved in Scenarios 2 and 3 were also similar and hence the scales of total heat recovered were the same in both scenarios. However, despite the higher foul temperature in Scenario 3 (27°C), Scenario 2 showed higher WWTP influent temperatures (Table 6.4) than that of Scenario 3. This is due to the higher in-sewer air temperature in Scenario 2 (15°C) than that of Scenario 3 (9°C). Therefore, heat is transferred from in-sewer air to wastewater, along the 3000 pipe network to increase its temperature at the WWTP influent in Scenario 2. This indicates that higher foul temperature does not necessarily result in higher WWTP influent temperature, yet the temperature of in-sewer air influences the variation of wastewater temperature along the sewer network which results in varying the WWTP influent temperature.

All the PDF graphs (i.e. Figures 6.6, 6.7, 6.11, 6.12, 6.14, and 6.15) presented similar characteristics in terms of the shift in PDF caused by varying the minimum required flow rates. Lower flow rates result in larger number of pipes with lower wastewater temperatures which was expected as discussed earlier using Equation 6.6. These PDF graphs mentioned above have also illustrated how the

‘business as usual’ case showed more pipes with high wastewater temperatures (i.e. greater than 15°C) than any of the heat recovery scenarios which was predictable. Although, recovering heat in all scenarios results in obtaining more pipes with lower wastewater temperature (i.e. 15°C and less), the above mentioned PDF graphs demonstrate that the majority of the pipes have high wastewater temperatures (i.e. between 20 and 22 °C).

Viability of a heat recovery option may vary from one environment to another. For example the minimum measured influent temperature in this work was around 9°C, and hence one may assume this value to be the threshold for WWTP influent temperatures. Some European countries allow a maximum drop of 1°C, from the usual WWTP influent temperature, despite the potential drops in wastewater temperatures in the network. Therefore, this large network model presented a number of potential heat recovery scenarios. The model was designed to be flexible so that the end users may vary the boundary conditions according to their relevant preferred values. Other parameters such as the minimum wastewater flow rates and temperatures that designate the compliant pipes (from which heat is recovered) can also be altered by the end user. Therefore, varying these parameters in the large network model estimates the impact of recovering heat (at any scale) on the wastewater temperatures in the network and of the WWTP influent.

6.3 Aquafin Hydraulic Model (Infoworks CS) Build up and Validation Process Summary

This section describes the specifications of the flow survey, explains how velocity and discharge were measured and explains the guidelines followed for setting up the measurement campaign. The section then shows how the model was validated. The Infoworks CS hydraulic model created by Aquafin (2014) is built and validated based on “Hydronaut procedure 6.5 version June 2014”.

Flow survey:

Rainfall is measured in the urban catchment using a standard tipping bucket rain gauge which is placed on a flat surface with no objects placed in the surrounding area that may disturb the measurements. The distance from any object should be at least twice the height of the object, with a minimum distance of 4.5 m. Thiessen polygons are used to convert ‘points of rainfall’ as measured by the rain gauges, to a spatial rainfall estimate used as a model input. Hence, an adequate number of rain gauges are required to cover the area of interest. The Aquafin (2014) procedure assumes that at least 1 rain gauge per 5 km^2 is necessary. In extended rural areas this is not always practically possible, instead at least 1 rain gauge is placed in a significant centre of habitation. The number of rain gauges usually varies between 3 and 8, whereby each Section of a sewer system has to be covered by at least 1 rain gauge. Rainfall radar data has not been used for the building of the Antwerp Infoworks CS model. Parameters such as evaporation and infiltration are not measured as part of the Hydronaut procedure. Hence the net precipitation entering the system is calculated within the selected runoff models.

Areas sensitive to sedimentation should be avoided for installing flow monitoring devices, since wastewater depth is generally measured by pressure transducers that are sensitive to sedimentation. Ageing of the membrane in the pressure transducer can lead to a drift from zero control measurements, and hence, calibration of the sensor can be used to check this. The pressure transducers generally used for flow surveys as described in the Hydronaut procedure measures up to 3.5 m pressure-level, and need a minimum water depth of 5 cm.

Velocity measurements and flow calculations:

Velocity is usually measured by Doppler velocity sensors that are fitted in the sewer without causing large amount of dirt accumulation and or disruption of the wastewater flow. The velocity sensors are less reliable for wastewater flowing at less than 0.1 m/s. The Hydronaut procedure recommends the use of bidirectional velocity sensors, in order to account for wastewater flowing forward and backward.

Flow is derived from the velocity and the wetted area, which varies as a function of the water level and the conduit cross-section shape. Hence the accuracy of the discharge is dependent on the accuracy of the measured depth and velocity as shown by Table 6.5.

Table 6.5: Summary of the reliability of the discharge based on the depth and velocity measurements.

Wastewater depth (m)	**Wastewater velocity (m/s)**	**Reliability of flow rate (Q) measurement (m^3/s)**
>= 0.05	> = 0.1	Reliable for subcritical flow, measurement error possible in supercritical flow
<0.05	>=0.1	Large error on Q in subcritical regime.
>=0.05	<0.1	Error in Q gets larger the more the velocity gets smaller than 0.1
<0.05	<0.1	Q is not reliable

The number of flow sensors employed depends on the size of the study. A general guideline is that 5 depth and velocity sensors are placed, plus an extra sensor to be placed for every 50 nodes. For studies smaller than 500 nodes, this total can be increased or decreased by 5 sensors, while for studies larger than 500 nodes, the total number can be increased or decreased by 10 sensors.

Modelled results

Maximum modelled flow peak values can be missed or significantly ‘smoothed out’ if the result time step is selected too large, hence time-steps are checked against pumping regime (time taken for switching on and off pumps). Data for

model validation should be selected from 2 dry weather flow with minimum 3 consecutive days without precipitation, and also from 3 days of rainfall events. The criteria of selecting rainfall events for model validation is shown by Table 6.6.

Table 6.6: Criteria for selection of rainfall events for model validation.

Criteria	Parameter	Value
Hydraulic	Degree of system filling	>50%
	Ratio of water depth during rainfall events to that during dry weather flow	≥3
Hydrological	Rainfall amount	> 5 mm
	Rainfall intensity during 2x2 minutes	> 5 mm/hr
	Rainfall duration	> 30 minutes

The validation process consists of 4 formal steps:

1. Evaluate the measured data.
2. Compare the basic model with measured data.
3. Add necessary changes to the basic model so modelled results meet the measured data as best as possible. Changes to the model may not be made based on the hydraulic model results alone, any proposed changes need to be accompanied by evidence from field observations. (For example, a concrete conduit can only be allocated a significantly higher hydraulic roughness coefficient if field visit shows the conduit is in a bad state due to for example serious concrete corrosion.) The Hydronaut (2014) illustrates several examples of reasons why the hydraulic model can deviate from the flow measurements.
4. Compare the behaviour of the validated model results with the measured data.
5. Steps 3 and 4 are an iterative process and can be repeated several times, these steps need to be carried out by an experienced hydraulic modeller.

7 Overall Discussions

The literature has shown that recovering heat from wastewater running in combined or foul sewer pipes presents a good opportunity due to the relatively high wastewater temperatures that have been observed to reach 22 and 27°C in different European countries (Chapter 1 and Section 2.2). This potential opportunity was also reconfirmed by the data measured and shown in Section 4.1 where wastewater in combined sewers reached 22 °C (Figure 4.6 and Figure 4.7). The literature has also reported a great potential of heat recovery in some European countries like Switzerland where Hanspeter (2008) predicted a potential of an annual 2 TWh heat recovery from the Swiss sewerage system. The recovery of heat from sewers is associated with some potential technical risks in terms of wastewater treatment. Biological wastewater treatment processes are temperature dependant as explained in Chapter 2 and in Shammas (1986), Metcalf and Eddy (2004) and Wanner *et al.* (2005). Shammas (1986) carried out experimental work to test the impact of varying wastewater temperature, from 4 to 33°C, in an activated sludge, on nitrification and found that the nitrification rate increases as wastewater temperature increases. This is because the depth of oxygen penetration in the floc increases as wastewater temperature decreases, since oxygen is not consumed rapidly at the surface of the floc (Company, 2009). Therefore, the temperature drop in wastewater, caused by heat recovered from wastewater in sewer pipes, may impact negatively on the wastewater treatment process. This creates the need for modelling wastewater temperature, along the sewer pipe profiles, in order to investigate the impact of recovering heat from sewerage wastewater on the end-of-system WWTP. The TEMPEST model was developed for similar purposes (Sections 2.2 and 2.3), however it was found to be an over complex mainly due to the incorporation of some parameters, such as sewer slope, friction coefficient and chemical oxygen demand degradation rate, which have negligible effects on the modelled wastewater temperature. The negligible effect was estimated, by Dürrenmatt (2006), to be less than 0.2% on modelled wastewater temperatures. TEMPEST was not being implemented for large sewers in published works. Therefore, there was a gap for developing a simpler computationally efficient model that estimates wastewater temperature along the sewer pipe profiles for large combined sewer networks. Simpler model in this perspective implies that

the model incorporates the key input parameters that are sensitive to heat transfer processes and the values for which are available to the end user. The purpose of a simpler model is to save computational time when estimating wastewater temperatures for a large number of time steps and pipes. This becomes critical when developing the computational model for a large sewer network such as the 3093 links network (referred to as the 3000 pipe network) used in this study. As far as the author is aware, no computational models have been developed for estimating wastewater temperature variation in large sewer networks.

Modelling wastewater temperature variation in sewer pipes requires the measurements of key heat transfer related parameters in the wastewater. This is to understand and analyse the heat transfer processes in the sewer pipes and also to utilise the data for the sewer pipe model calibration and validation. Considering the sewer pipe to be a partially filled pipe, it was concluded from Section 3.3.2, that heat in sewers is transferred between wastewater and the in-sewer air and between wastewater and the surrounding soil through the pipe wall. These heat transfer processes are dominated by the local temperature of wastewater, in-sewer air and the surrounding soil and also rely on thermal resistivity values between wastewater and in-sewer air and between wastewater and soil (Section 3.3.2). The hydraulics of wastewater flowing in the sewer pipes also play a major part in the heat transfer processes as shown by Equation 3.31. Therefore, the key heat transfer parameters that were measured in this work are temperatures of wastewater, in-sewer air and the surrounding soil along with wastewater velocity, depth and flow rate.

The upstream and downstream temperatures of wastewater and in-sewer air were measured, every 15 or 20 minutes, for a full year in two “urban” and two “large” sewer pipes. As far as the author is aware, such wastewater and in-sewer air temperature measurements are not available in published literature. The measured wastewater and in-sewer air temperatures, presented in Chapter 4, have shown patterns (e.g. Figure 4.6) that relate to the regional ambient temperature (Figure 4.3). It was also observed from Chapter 4 that the daily wastewater temperature and flow rate variations match the predicted demands of water consumption during a working day (e.g. Figure 4.4). The latter graph for example demonstrated how water consumption increases during the morning of a working day which was also associated by an increase in wastewater

temperatures. One can also observe that soil temperatures measured at deeper depths (3.7m) were less influenced by the ambient temperature than those measured closer to the surface at 1.5m depth (e.g. Figure 4.10). These patterns of measured data variations suggest that the data is realistic and can be utilised for understanding the heat transfer processes in sewer pipes. It was also noticed, from measured data in Chapter 4, that wastewater temperature drops streamwise in cold weather (September to May), which is expected since in-sewer air temperatures are lower than that of wastewater during cold weather periods. Heat is always transferred from higher to lower temperatures. However, in-sewer air temperatures were higher in warmer weather days (May to August) than that of wastewater, yet a wastewater temperature drop streamwise was also observed. This is due to the soil temperature being lower than that of wastewater during warm periods. For example, Figure 4.6 shows higher in-sewer air temperatures, in Site 1, than that of wastewater during July, while Figure 4.10 demonstrates lower local soil temperatures than that of Site 1 wastewater during July. Hence the wastewater temperature drop in July at Site 1 is caused by the lower soil temperatures. Therefore, wastewater temperature variation is mainly due to heat being transferred to in-sewer air and to the soil through the pipe wall. This reconfirms the theoretical behaviour of heat transfer in sewers mentioned in Section 3.3.2 and discussed earlier in this section. It was noticed that there is more heat flux taking place in the urban sewers than that in the large sewers which suggests that heat transfer in sewers is dependent on the scale of the wastewater flow rate. This was expected theoretically when applying Equation 5.14, which shows that the higher the wastewater volumetric flow rate (Q), the less temperature drop streamwise (T_m - T_{m+n}) takes place along sewer pipe profile. This is the case when assuming the impacts of thermal resistivity between wastewater and in-sewer air (R_{wa}) and between wastewater and soil (R_{ws}) are relatively close for urban and large sewers. The different heat transfer mechanisms in urban and large sewers was also noticed by Abdel-Aal *et al.* (2015), who employed predictive modelling techniques to estimate wastewater temperatures at the downstream ends of urban and large sewers.

Heat transfer in sewer pipes is a complex process, compared with that in fully filled pipes, since the sewer pipe is an unconfined environment in which the hydraulics of the wastewater change continuously. This is caused by different

factors such as storm water, infiltration and the daily production of wastewater from residential and industrial areas. Furthermore, some thermal resistivity parameters associated with the computation of thermal resistivity values are difficult to measure, not available in literature or may require extensive laboratory work to determine. These parameters were found to be heat transfer coefficient calibrating parameter (f_{hwa}), in-sewer air velocity (u_a), penetration depth (d_s) and soil thermal conductivity (k_s) as explained in Section 5.1.1. Therefore, these four parameters (f_{hwa}, u_a, d_s and k_s) were calibrated, based on the sewer pipe model (Equation 3.31), for urban and large sewers using measured data from Sites 2 and 3 respectively (Chapter 5). The sewer pipe model was then validated for urban and large sewers using independent measured data from Sites 1 and 4 respectively. Calibration and validation of the sewer pipe model were mainly based on calculating the root mean square error (RMSE) of the difference between measured and modelled wastewater temperatures at the downstream ends of the sewer pipes as given by Equation 5.1. This RMSE (Equation 5.1) was utilised to account for the effects of measurement errors generated by sensor accuracies as explained in Section 5.4.

The heat transfer calibrated parameter (f_{hwa}) was proven to be a crucial parameter, yet can usually be determined empirically. The calibrated in-sewer air velocity (u_a) and f_{hwa} showed different values for different calendar months which suggests that the heat transfer process between wastewater and in-sewer air varies seasonally. These two calibrated parameters (f_{hwa} and u_a) are important for modelling heat transfer in sewer pipes and can be used for urban and large sewers, using the values given by Table 5.7 and Table 5.9 respectively. Calibrated u_a values (0.07 to 0.50m/s) were within the range found in literature, yet u_a was mostly shown to be between 0.1 and 0.2m/s. There is an increasing interest in the area of estimating in-sewer air velocity since it is a critical parameter for other areas in the wastewater industry. For example, there has been some research in the areas of odour control (Camarillo *et al.*, 2013), sewer ventilation (Wang *et al.*, 2012) and gaseous emissions (Edwini-Bonsu and Steffler, 2006) where the knowledge of in-sewer air velocity is needed. The calibrated ratio of penetration depth to soil thermal conductivity ($\frac{d_s}{k_s}$) provided realistic values that relate to the scale of thermal energy dissipated to soil depending on the wastewater flow rate as shown by Figure 5.60 and Figure 5.61.

However, further work needs to be carried out to investigate methods of calibrating k_s and d_s separately, i.e. by fixing k_s to its default value while calibrating d_s. This may provide more accurate values for each parameter (i.e. d_s and k_s) than those obtained using the ratio of $\frac{d_s}{k_s}$ in the calibration process.

The calibrated sewer pipe model, which was validated on independent datasets, was further developed to model wastewater temperature variation along sewer pipe profiles in a large sewer network. This is a real Belgian sewer network with 3093 links, 3048 of which are sewer pipes. The adapted sewer network model is named the large network model (Chapter 6). Such a large sewer network (of 3000 pipes) demands substantial adaptation to the sewer pipe model and created some challenges that were tackled by making critical assumptions. For example, in a sewer network a number of upstream (1st generation) sewer or sub-catchment pipes may be connected to a downstream pipe (2nd generation), as shown by Figure 6.2. Therefore, it was assumed that the temperature of wastewater entering the 2nd generation pipes is a function of wastewater temperatures and flow rates of the lower generation pipes as given by Equation 6.5. It was assumed that wastewater temperature stays the same along the profile of a sewer network link. The sewer network studied in this work included 45 links that varied from valves to pumps or others and hence, more details is required to enable the modelling of wastewater temperature profiles in these links. Data from Infoworks CS was supplied by Aquafin (a Belgian wastewater utility) for the 3093 links sewer network and was utilised for the implementation of the sewer network model. Apart from the hydraulic data (wastewater flow rate, velocity and depth), pipe details were also available from Aquafin and were utilised to determine the relevant thermal conductivity. The calibrated parameters obtained by the Matlab optimisation function 'fmincon' in Table 5.7 for "urban" sewers and in Table 5.9 for "large" sewers were utilised in the large network model. This was achieved by categorising the sewer network pipes into urban sewers (flow rates between 0.008 and 0.01 m^3/s) and large sewers (flow rates greater than 0.09 m^3/s). Average default values found in literature were used instead of the calibrated parameters for sewer network pipes with flow rates less than 0.008 m^3/s. This is because the measured data used for calibration and validation was only available for sewer pipes with flow rates greater than 0.008m^3/s. The large network model was designed by developing a Matlab code that can be incorporated in other

software packages (e.g. Infoworks CS). Although the model was tested on the 3000 pipe network, it was designed to be applied on any network that has similar data parameters to those of the 3000 pipe network. Future work may be carried out to test the sewer network model on other real sewer networks.

Implementation of the three heat recovery scenarios (Section 6.2) was based on the simulation of 1 hour duration. The hydraulic data was obtained from Infoworks CS, which uses a time step of 2 minutes. Therefore, data from 30 time steps were averaged to implement the heat recovery model using the scenarios described in Section 6.2. The total computational time for each case scenario, of those described in Section 6.2, is around five minutes. This is considered to be a reasonable computational time for such a large sewer network. Being a steady state model is a major factor behind this relatively short computational time.

A viable heat recovery option is assessed by considering the minimum allowable influent sewage temperature at the WWTP and the minimum wastewater temperature in the sewer network. The critical values for these two temperatures may be determined by the end-user of the large network model depending on their preferences or on the local regulations. In this work, it is assumed that heat recovery with a minimum WWTP influent temperature of 10^0 C and a minimum wastewater temperature in the sewer network of 9°C can be considered to be the criteria of a viable option. This was assumed based on the nature of wastewater temperatures, with no heat being recovered, in the Belgian sewers where the WWTP influent temperature was shown to be varying between around 9 and 20 °C (Figure 4.14) while wastewater temperature in sewers varied between 7 and 22°C (Section 4.1). For example, 250 kW/pipe heat recovered during March 2012 on a working day, shown by case 1.1 of Table 6.4, from wastewater flow rates of 100L/s or more, is considered to be a viable option. Accounting for the highest RMSE of 0.82°C, obtained from validating the sewer pipe model in March 2012 while considering sensor accuracies (Figure 5.68), the modelled WWTP influent temperature may vary between 10.18 and 11.82°C. Hence, this heat recovery case is considered to stay viable since the modelled influent temperature at the WWTP and wastewater temperature in sewers stay above 10°C and above 9°C respectively when accounting for modelling errors. The 250kW/pipe was estimated to be recovered from 37 pipes while each location of the heat recovery is adequate for meeting the required radiator heat output capacity for 93 flats.

This was based on a heat recovery project delivered by Vlario in Belgium as mentioned in Section 6.2.1. Assuming a 100% efficient heat recovery system, 3400 flats in this catchment may potentially benefit from heat recovered in case 1.1 (Table 6.4) at wastewater flow rates of 50L/s and above. It is worth highlighting that heat recovery was assumed to be processed in a sewer network that is recharged every 2 minutes, based on Infoworks CS data, with discharges from foul, trade and surface runoff. These discharges were assumed to have constant temperatures at all time steps.

Due to the same reasons that result in less wastewater temperature variation along the large sewer pipe profiles (described earlier in this section), the large sewer pipes (i.e. flow rate is high) have generally shown more potential of heat recovery. Potential in this context means that heat can be recovered while keeping the wastewater temperature profile relatively high (e.g. greater than 10 °C). Referring to Equation 6.6, and assuming constant heat recovery (HR), one can notice that the increase in volumetric wastewater flow rate (Q_{total}) results in keeping the wastewater temperature variation along the sewer pipe profile ($T_{m+1,2..}$) high. Therefore, when comparing the urban with the large sewers, the measured upstream temperature (T_{US}) is relatively close for both site categories, however, the large sewers have much larger DWF than that of urban sewers. Hence, and as observed from the heat recovery scenarios in Section 6.2, recovering heat from wastewater while keeping wastewater temperatures relatively high is mainly governed by upstream wastewater temperatures, in-sewer air temperatures and flow rates. Therefore, heat recovery from high industrial wastewater temperatures may present great viable potentials. Some industries (e.g. oil refineries) discharge high temperature wastewater that may reach 50°C at the activated sludge stage of the treatment. Some biological processes such as nitrification is unfeasible at temperatures higher than 40°C (Lopez-Vazquez *et al.*, 2014). Therefore, this type of wastewater needs to be cooled down to reach an acceptable temperature of 35°C (Metcalf and Eddy, 2004 and Grady *et al.*, 2011). Hence, heat recovery in this case may prove to be even more attractive since it can save the costs of cooling down the temperature of wastewater in addition to the usual benefits of utilising recovered heat.

The current climate change and global warming may increase the future potential of heat recovery from sewers assuming wastewater temperature increases

accordingly. However, with modern smart metering systems along with targets to cut energy and water consumptions, water usage may prove to be more efficient in the future. This is more likely to be the case in the new built cities or when substantial developments in the infrastructures of the wastewater sewerage take place. Therefore, a reduction in water consumption may result in less potential for heat recovery from sewers. Nevertheless, current and future improvements in thermal insulations and radiator efficiencies can also reduce the overall demand on heating.

Heat recovery in sewers can be utilised for further applications beyond heating. Recovering heat from sewers can be utilised for electricity generation using thermocouple technology. This is based on the thermoelectric effect which was discovered by Thomas Seebeck in 1821. In an electric circuit with two dissimilar metals connected at their ends, if the junction of each metal is at different temperature to the other, an electric current would flow in the circuit. The temperature difference between the metal junctions influences the magnitude of the flowing current and hence electricity can be generated. This opens more doors for utilising thermal energy stored in wastewater, yet modelling the viability of these applications is crucial.

8 Overall Conclusions

This work has presented wastewater temperatures for the four seasons in urban and large sewers. Measured data was utilised to understand the process of heat transfer in sewers. It was found that heat in sewerage wastewater is mainly transferred to in-sewer air and to the surrounding soil through the pipe wall.

A computationally efficient model was developed to estimate wastewater temperature along sewer pipe profiles. The developed model was calibrated and validated using independent measured datasets. Main heat transfer parameters that were calibrated are; heat transfer coefficient factor between wastewater and in-sewer air, in-sewer air velocity, soil thermal conductivity and soil penetration depth. Values of root mean square error (RMSE) were computed based on the difference between measured and modelled wastewater temperatures at the downstream ends of individual sewer pipes. Calibration and validation showed RMSE between 0.10 and 0.82°C when accounting for sensor accuracies. This is considered to be reasonable for such sewerage environment and for the purpose of investigating the viability of heat recovery from sewers. The computational model was further developed and implemented on a real 3000 pipe network (79500 PE). Applications of heat recovery on such large network was presented, and viable options showed the potential of meeting the residential heat demands of 10% of the 79500 PE catchment.

Increasing interest in the field of heat recovery from sewers requires such computational efficient models for assessing the viability of implementing these applications.

9 Recommended Future Work

- Investigate the mechanism of heat transfer between wastewater and in-sewer air during summer time (May, June and July).
- Develop experimental techniques to determine the soil penetration depths for sewer pipes. Utilise these techniques to understand and model soil penetration depths.
- Examine the impact of pipe gradients on flow directions (i.e. positive and negative wastewater velocities) and on the overall performance of the large network model.
- Develop modelling techniques (e.g. predictive methods) to estimate diurnal variation of ambient air, foul, trade and runoff temperatures. Integrate these techniques in the large network model assuming ambient air temperature is similar to that of in-sewer air.
- Integrate the large network model into hydraulic modelling software packages such as Infoworks CS and SWMM.
- Implement a modelled heat recovery scenario from a sewer network and monitor wastewater temperature variations at random pipes in the network and of the WWTP influent. Validate the large network model by this implementation.

10 References

Abdel-Aal, M., Mohamed, M., Smits, R., Abdel-Aal, R., De Gussem, K., Schellart, A. & Tait, S. (2015) 'Predicting wastewater temperatures in sewer pipes using abductive network models', *Water Science & Technology,* 71**,** pp. 89-96.

Abdel-Aal, M., Smits, R., Mohamed, M., De Gussem, K., Schellart, A. & Tait, S. (2014) 'Modelling the viability of heat recovery from combined sewers', *Water Science & Technology,* 70**,** pp. 297-306.

Aquafin (2014) *Hydronaut procedure 6.5 versie Juni 2014 (In Dutch, Specifications for monitoring campaigns and model validation: Internal report by Aquafin).* Translated from Dutch to English by Alma Schellart. Aartselaar: Aquafin.

Camarillo, M.K., Stringfellow, W.T., Hanlon, J.S. & Basha, E. (2013) 'Performance of sanitary sewer collection system odour control devices operating in diverse conditions', *Water Science and Technology,* 68**,** pp. 2527-2533.

Cengel, Y.A. (2003) *Heat transfer: A practical approach. 2nd edn.* New York: MacGraw Hill.

Cipolla, S. & Maglionico, M. (2014) 'Heat recovery from urban wastewater: Analysis of the variability of flow rate and temperature', *Energy and Buildings,* 69**,** pp. 122-130.

Company, N. (2009) *The nalco water handbook. 3rd edn.* New York: McGraw Hill.

De Gussem, K.R.L., Donckels Mr., B. & Weemaes, M. (2013) 'Impact of sewage heat extraction on waste water treatment plant performance and greenhouse gas emission', *The 7th International Conference on Sewer Processes and Networks***,** Sheffield, 28 – 30 August 2013. International Water Association (IWA). Available at:
http://www.shef.ac.uk/polopoly_fs/1.336418!/file/Donckels_presentation_session 10.pdf (Accessed: 2 October 2014).

Demir, H., Koyun, A. & Temir, G. (2009) 'Heat transfer of horizontal parallel pipe ground heat exchanger and experimental verification', *Applied Thermal Engineering,* 29**,** pp. 224-233.

Durrenmatt, D.J. (2006) *Berechnung des verlaufs der abwassertemperatur im kanalisationsrohr. (Calculation of wastewater temperature profiles in sewers).* Diploma thesis. Swiss Federal Institute of Technology (ETH).

Dürrenmatt, D.J. & Wanner, O. (2008) 'Simulation of the wastewater temperature in sewers with TEMPEST', *Water Science & Technology,* 57**,** pp. 1809-1815.

Dürrenmatt, D.J. & Wanner, O. (2014) 'A mathematical model to predict the effect of heat recovery on the wastewater temperature in sewers', *Water Research,* 48**,** pp. 548-558.

Edwini-Bonsu, S., A.M.ASCE & Steffler, P.M. (2006) 'Dynamics of air flow in sewer conduit headspace', *Journal of Hydraulic Engineering,* 132**,** pp. 791-799.

Escalas-Cañellas, A., Ábrego-Góngora, C.J., Barajas-López, M.G., Houweling, D. & Comeau, Y. (2008) 'A time series model for influent temperature estimation: Application to dynamic temperature modelling of an aerated lagoon', *Water Research,* 42**,** pp. 2551-2562.

Esen, H., Inalli, M. & Esen, M. (2007) 'Numerical and experimental analysis of a horizontal ground-coupled heat pump system', *Building and Environment,* 42**,** pp. 1126-1134.

Flinspach, D. (1973) *Wärmelastplan neckar plochingen bis mannheim stand. (Heat Loading Plan for Neckar Plochingen in Mannheim).* Stuttgart: Ministerium für Ernährung.

Grady Jr, C.L., Daigger, G.T., Love, N.G. & Filipe, C.D. (2011) *Biological wastewater treatment. 3rd edn.* London: CRC Press.

Hanspeter, E. (2008). *Abwasserwärmenutzung: Potenzial, wirtschaftlichkeit und förderung. (Potential and feasibility of the heat recovery from wastewater).* Translated from German by Maxence Carrel. Available at: http://www.news.admin.ch/NSBSubscriber/message/attachments/13220.pdf (Accessed: 17 November 2012).

Hoes, O.A.C., Schilperoort, R.P.S., Luxemburg, W.M.J., Clemens, F.H.L.R. & van de Giesen, N.C. (2009) 'Locating illicit connections in storm water sewers using fiber-optic distributed temperature sensing', *Water Research,* 43**,** pp. 5187-5197.

Howe, A. (2009). *Renewable energy potential for the water industry: Environment agency report: Sc070010/r5.* Available at: https://www.gov.uk/government/uploads/system/uploads/attachment_data/file/291637/scho1209brof-e-e.pdf (Accessed: 14 August 2014).

Incropera, F.P., DeWitt, D.P., Bergman, T.L. & Lavine, A.S. (2007) *Fundamentals of heat and mass transfer. 6th edn.* Hoboken: J. Wiley & Sons.

Kelly, N. & Thomson, M. (2012). *Future energy demand in the domestic sector.* Available at: http://www.topandtail.org.uk/publications/N.Kelly.WP2%201ReportFutureEnergyDemand.pdf (Accessed: 12 August 2014).

Khan, S., Wilkes, E. & Prime, J. (2014). *Energy consumption in the UK (2014): Overall energy consumption in the UK since 1970.* Available at: www.gov.uk/government/uploads/system/uploads/attachment_data/file/337452/ecuk_chapter_1_overall_factsheet.pdf (Accessed: 11 August 2014).

Lohani, S. & Schmidt, D. (2010) 'Comparison of energy and exergy analysis of fossil plant, ground and air source heat pump building heating system', *Renewable Energy,* 35**,** pp. 1275-1282.

Lopez-Vazquez, C., Kubare, M., Saroj, D., Chikamba, C., Schwarz, J., Daims, H. & Brdjanovic, D. (2014) 'Thermophilic biological nitrogen removal in industrial wastewater treatment', *Applied microbiology and biotechnology,* 98**,** pp. 945-956.

MacLeay, I., Harris, K. & Annut, A. (2014). *Digest of united kingdom energy statistics 2014.* Available at: file:///C:/MAA%20150514/LR/Energy/DIGEST%20OF%20UNITED%20KINGDOM%202014.pdf (Accessed: 10 August 2014).

Madsen, H.I., Hvitved-Jacobsen, T. & Vollertsen, J. (2006) 'Gas phase transport in gravity sewers: A methodology for determination of horizontal gas transport and ventilation', *Water Environment Research***,** pp. 2203-2209.

Metcalf & Eddy (2004) *Wastewater engineering treatment and reuse. 4th edn.* New York: Mcgrow Hill.

Mitchell, J.K. & Soga, K. (1993) *Fundamentals of soil behavior. 2nd edn.* New York: John Wiley & Sons, Inc.

Met Office (2014). *Temperature, rainfall and sunshine time-series*. Available at: http://www.metoffice.gov.uk/climate/uk/actualmonthly/ (Accessed: 20 August 2014).

Mohamed, M., Kezza, O.E., Abdel-Aal, M., Schellart, A. & Tait, S. (2015) 'Effects of coolant flow rate, groundwater table fluctuations and infiltration of rainwater on the efficiency of heat recovery from near surface soil layers', *Geothermics,* 53**,** pp. 171-182.

Ngo, C.C. & Lai, F.C. (2009) 'Heat transfer analysis of soil heating systems', *International Journal of Heat and Mass Transfer,* 52**,** pp. 6021-6027.

Osborn, L. (2014). *Sunniest places and countries in the world.* Available at: http://www.currentresults.com/Weather-Extremes/sunniest-places-countries-world.php (Accessed: 14 August 2014).

Ozisik, N. (1994) *Finite difference methods in heat transfer.* Boca Raton: CRC press.

Parker, W.J. & Ryan, H. (2001) 'A tracer study of headspace ventilation in a collector sewer', *Journal of the Air & Waste Management Association,* 51**,** pp. 582-592.

Pescod, M. & Price, A. (1981) 'Fundamentals of sewer ventilation as allied to the Tyneside sewerage scheme', *Water Pollution Control,* 80**,** pp. 17-33.

Peters, C. (2007) *Potenziale von Regenwasserversickerung, Speicherung, Urinseparation und Pumpwerkssteuerung für den Gewässerschutz (Potentials of stormwater infiltration, storage, urine separation and real time control to minimize river impacts dynamic long time simulation of sewer network and waste water treatment plant and multi-criteria analysis).* PhD. Berlin Technical University.

Piechowski, M. (1998) 'Heat and mass transfer model of a ground heat exchanger: Validation and sensitivity analysis', *International Journal of Energy Research,* 22**,** pp. 965-979.

Piechowski, M. (1999) 'Heat and mass transfer model of a ground heat exchanger: Theoretical development', *International Journal of Energy Research,* 23**,** pp. 571-588.

Schilperoort, R. (2011). *Monitoring as a tool for the assessment of wastewater quality dynamics*. PhD Thesis. TU Delft.

Schilperoort, R. & Clemens, F. (2009) 'Fibre-optic distributed temperature sensing in combined sewer systems', *Water Science and Technology,* 60**,** pp. 1127-1134.

Schmid, F. (2008) *Sewage water: Interesting heat source for heat source for heat pumps and chillers,* Zürich: Swiss Energy Agency for Infrastructure Plants.

Shammas, N.K. (1986) 'Interactions of temperature, ph, and biomass on the nitrification process', *Water Pollution Control Federation,* 58**,** pp. 52-59.

Shizas, I. & Bagley, D.M. (2004) 'Experimental determination of energy content of unknown organics in municipal wastewater streams', *Journal of Energy Engineering,* 130**,** pp. 45-53.

Wang, Y.C., Nobi, N., Nguyen, T. & Vorreiter S, L. (2012) 'A dynamic ventilation model for gravity sewer networks', *Water Science and Technology,* 65**,** pp. 60-68.

Wanner, O., Panagiotidis, V., Clavadetscher, P. & Siegrist, H. (2005) 'Effect of heat recovery from raw wastewater on nitrification and nitrogen removal in activated sludge plants', *Water Research,* 39**,** pp. 4725-4734.

Wu, Y., Gan, G., Verhoef, A., Vidale, P.L. & Gonzalez, R.G. (2010) 'Experimental measurement and numerical simulation of horizontal-coupled slinky ground source heat exchangers', *Applied Thermal Engineering,* 30**,** pp. 2574-2583.